KU Leuven
Biomedical Sciences Group
Faculty of Pharmaceutical sciences
Department of Pharmaceutical and Pharmacological sciences

BROADENING THE SCOPE OF AMORPHOUS SOLID DISPERSIONS:

ALTERNATIVE MANUFACTURING AND FORMULATION APPROACHES

Aswin Dereymaker

Jury:

Promoter:	Prof. dr. Guy Van den Mooter
Co-promoter:	Prof. dr. Johan Martens
Chair:	Prof. dr. Ann Van Schepdael
Jury members:	Prof. dr. Véronique Préat
	Prof. dr. Juergen Siepmann
	Dr. Ivo Van Assche
	Prof. dr. Chris Vervaet

Dissertation presented in partial fulfilment of the requirements for the degree of Doctor in Pharmaceutical Sciences

February 2017

Acknowledgements

This thesis is the result of four years of dedication to the field of solid dispersions and has come to existence after some hard work, long days (sometimes nights), successful experiments interspersed with some failed ones, some cheering and some frustrations. In other words, research in a nutshell. However, the most important point to stress out at this point, is that all of this work would not have been made possible without the help of a few people, and it is only right that I can express my gratitude for their contributions in this section.

In the first place, I would like to thank my supervisor, Prof. dr. Guy Van den Mooter. First of all, for giving me all these great opportunities, with the Denali project and the PhD project. Secondly, for his excellent guidance and mentoring during all this time. It has been a tremendous joy and pleasure working with you. I would also like to thank Prof. dr. Johan Martens as my co-supervisor.

My gratitude also goes out to the jury members - Prof. dr. Véronique Préat, Prof. dr. Juergen Siepmann, Dr. Ivo Van Assche, Prof. dr. Ann Van Schepdael and Prof. dr. Chris Vervaet- for carefully reading and correcting my thesis and providing me with helpful advice during the course of my PhD.

This thesis would also not have been the same if not for some valuable collaborations which lifted the entire research to a higher level. I would like to thank Prof. dr. Jan Van Humbeeck of the Department of Materials Engineering for being able to use his thermal analysis and SEM equipment, and to Danny Winant for helping me carry out TGA and DSC experiments. Furthermore, I would like to thank Prof. dr. Guy Van Assche of Physical Chemistry and Polymer Science of the University of Brussels (VUB) for his help in trying to carry out micro-TA experiments on my uncooperative beads, and his expert advice in TGA methodology. Prof. dr. Peter Adriaensens of the Institute for Materials Research of Hasselt University is kindly acknowledged for performing and analysing solid state NMR experiments which helped me a lot in my research. Last, but not least, I also had the immense pleasure to visit the University of Nottingham during my PhD, and more specifically the lab of Prof. dr. Clive Roberts (Advanced Materials and Healthcare Technologies). I am very grateful to Clive for opening up his lab to me and allowing me to perform experiments on the very specialized equipment (AFM, ToF-SIMS), which in the end, together with his expert advice, proved to be invaluable for this thesis. I would also like to thank Dr. Xinyong Chen for his training and guidance in the

AFM experiments and Dr. David Scurr for performing the ToF-SIMS experiments for me, and guiding me all the way through the pretty elaborate analysis of the data. Thank you very much for all the time, effort and follow-up spent on all my experiments.

Being part of Drug Delivery and Disposition for these five years has been a true pleasure and a huge honour for me. This is why I would also like to thank all former and current colleagues of the lab for all the nice moments spent. A special mention goes out to the 'lunch' group (with varying members) which always provided a welcome distraction around noon. A special mention here as well to Patrick and Bernard who were always there to provide some brainstorming and practical assistance for all my experiments, and who took care of the general well-being of the people and the machines residing in the lab. Also thanks to Jenny and Sonia for tackling the more practical stuff and lifting our burden. I also would like to thank Sandra, who expertly supervised me during my master internship and introduced me to solid dispersions specifically, and research work in general.

During my PhD, I also had to honour to supervise students during their internships in the lab. This has been a very enriching experience for me and I hope all of you learned as much from me as I learned from you. A very special thank you to Shari, Frederik, Jirka and Giulia.

I would also like to thank all my family and friends for providing some welcome distraction during these years as a PhD student and for helping me whenever possible. A special thanks goes out to Benny for designing the cover of this thesis. I would also like to give a special place in this acknowledgment section to Vicky, who has been there for me for the past year and a half and who has given me courage, strength, love and compassion along this journey.

Last, but certainly not least, I would also like to thank my parents and my sister, who have always been there for me. Not only these past four years, but for a good thirty already. Without you all of this would have not been possible and I would not be the person I am today. Thank you for everything.

List of Abbreviations

ACN: acetonitrile

ANOVA: analysis of variance

API: active pharmaceutical ingredient

BCS: biopharmaceutics classification system

CINN: cinnarizine

CP/MAS NMR: cross polarization/magic angle spinning nuclear magnetic resonance

DCM: dichloromethane

DLS: dynamic light scattering

DSC: differential scanning calorimetry

EC: ethyl cellulose

ERL: Eudragit® RL

ERS: Eudragit® RS

EtOH: ethanol

FDA: (U.S.) food and drug administration

HPLC: high-performance liquid chromatography

INDO: indomethacin

KETO: ketoconazole

mDSC: modulated differential scanning calorimetry

NSAID: non-steroidal anti-inflammatory drug

NAP: naproxen

PVP: polyvinylpyrrolidone

SEM: scanning electron microscopy

ss-NMR: solid-state nuclear magnetic resonance

stdev: standard deviation

TEC: triethyl citrate

Tg: glass transition temperature

ToF-SIMS: time-of-flight secondary ion mass spectrometry

XRPD: X-ray powder diffraction

Table of Contents

Chapter 1: General Introduction

1.1 Drug discovery evolution leading to an abundance of poorly soluble drugs

People have been using drugs since the dawn of mankind. Some historians believe the first indications of drug use can be seen on prehistorical cave paintings [1]. The first written record of medical therapy has been found on a papyrus scroll describing treatments used in Ancient Egypt. This scroll has been dated back to about 1500 BC [2]. Until 150 years ago, humans still solely relied on natural resources to provide pharmacologically active substances, but mind you, until today this source still provides a significant source for new drug leads [3]. By the second half of the nineteenth century, organic chemistry and pharmacology had evolved in such a way, that it laid a platform for a whole new class of molecules: synthetic drugs. The origin of synthetic drug development can be traced back to the textile industry, and more specifically to the emerge of synthetic dye development. The first synthetic dyes were derived from coal-tar, a by-product formed after coal distillation. Coal-tar is rich in aromatic molecules, including naphthalene and acetanilide, which are among the first developed synthetic drugs [2, 4].

In the twentieth century, drug discovery evolved from active compound identification of traditional medicines or serendipitous discovery to a more systematic approach, namely the discovery and development of combinatorial chemistry and high throughput screening [5, 6]. Combinatorial chemistry allows for the synthesis of hundreds or thousands of structural analogue molecules, hereby creating a compound library which is then up for screening [7]. which is performed in a high throughput set-up that allows for these large numbers molecules to be tested for their biological or pharmacological activity. Ultimately and ideally this will lead to the discovery of chemical structures (so-called leads) which can be further developed into marketable drugs [8].

Despite the massive growth in the number of compounds and the highly efficient screening methods to generate leads, this has not been translated into a higher number of marketed drug compounds [9]. So, despite the generation of these highly specific, highly potent drug candidates that work well in the early stages of drug development, drug attrition rates are still high. Drug attrition is caused by various factors: clinical safety, commercial reasons, patent issues, but also formulation, pharmacokinetic and bioavailability issues [10]. Some data suggests that an estimated 50% of drug candidates display poor absorption, distribution, metabolism,

elimination or toxicity (ADMET) properties. The number of drugs on the market having ADMET problems is also estimated being half [11]. Circumventing ADMET problems can be achieved by screening compound libraries and drug candidates for potentially disadvantageous ADMET properties. An example to address the absorption part of ADMET is Lipinski's 'rule of five', where compounds can be screened for properties which have an adverse influence on solubility and permeability. These properties are: more than 5 hydrogen bond donors, more than 10 hydrogen bond acceptors, a molecular weight in excess of 500 Da, a calculated log P greater than 5 [12]. Still today new improved methods are developed for rapid drug candidate screening on solubility and permeability characteristics for absorption estimation [13]. Solubility and permeability are of utmost importance in oral drug delivery. After all, if drugs don't dissolve they are unable to permeate, and if they are unable to permeate, they are not taken up by the systemic circulation, which is important for drugs with the ambition to display systemic effects.

To establish a firm grip on solubility and permeability problems, first, a clear definition of poor solubility and/or permeability needs to be defined. In 1995, Amidon et al. introduced the biopharmaceutics classification system (BCS) to correlate in vitro drug dissolution and in vivo bioavailability [14]. Four classes have been defined in this classification system. Class 1 drugs exhibit high solubility and high permeability, class 2 drugs combine poor solubility with high permeability, class 3 drugs high solubility with poor permeability and class 4 drugs show poor solubility and poor permeability. Poor solubility is defined as the inability of the highest dose of the drug to dissolve in less than 250 ml of a medium with pH 1-7.5. A drug displays poor permeability when less than 90% of the highest dose strength is absorbed in humans [15]. A classification of the top 200 drug products on the market in several countries showed that around 70% can be classified as class 2, 3 or 4, and thus showed solubility and/or permeability issues [16].

1.2 Gastro-intestinal absorption and solubility/dissolution rate promoting formulation strategies

Another path can be gone down when trying to tackle absorption and solubility/dissolution rate problems in drug candidates. Instead of screening and removing candidates displaying disadvantageous physicochemical properties, different formulation strategies can be applied to enhance drug permeability or solubility. Permeability of drugs can be increased by creating a

pro-drug which has increased permeability (e.g. valacyclovir or tenofovir diisoopropyl fumarate)[17] or formulating the drug together with so-called 'absorption enhancers'. These are functional excipients that can enhance membrane permeation by dilating tight junctions in cell membranes (paracellular penetration enhancement) or increase penetration inside cell membranes (transcellular penetration enhancement). An example of an excipient which can perform both action mechanisms, is sodium caprate [18].

Over the last few decades, numerous strategies have been developed to enhance drug solubility and/or dissolution rate. What follows is a non-exhaustive summary of the main mechanisms:

- ***Salt formation:*** often seen as the primary approach in enhancing dissolution rate and solubility of weakly acidic and basic poorly soluble drugs. The solubility of these drugs as function of pH dictates whether salt formation might be suitable [19].
- ***Pro-drug formation:*** a pro-moiety, enhancing drug solubility, is covalently linked to the drug. After the desired effect, a pro-drug can be chemically or enzymatically converted to the native drug substance [20].
- ***Particle size reduction:*** drug particles, preferably in nanometre size scale, exhibit increased dissolution rate due to higher surface area and increased solubility under critical particle size. Addition of a stabilizer is needed to prevent spontaneous aggregation [21].
- ***Lipid-based systems:*** from simple lipid solutions to more advanced self-emulsifying drug delivery systems, lipid based systems can enhance drug solubilisation, reach the systemic circulation via lymphatic drug transport and/or interact with enterocyte based transport [22, 23].
- ***Cocrystals:*** crystal composed of a drug and a coformer. Solubility of cocrystals is determined by a range of coformer properties and possible interactions with the drug crystal [24].
- ***Cyclodextrins:*** cyclic oligosaccharides, able to form inclusion complexes with poorly soluble drugs, thus enhancing apparent drug solubility [25].
- ***Mesoporous silica:*** inert mesoporous material which can confine single drug molecules inside of its pores. Upon contact with release medium, the drug molecules exit the pores displaying a higher apparent solubility and release rate [26, 27].

- ***Amorphous systems:*** exploitation of the higher energy state and lack of long range order of amorphous drugs, compared to their crystalline counterparts. Formulations comprising drugs in the amorphous state will be discussed in more detail in the next paragraph.

1.3 Drug amorphisation

The amorphisation of a substance, drug or otherwise, can be envisioned as the freezing of a liquid into the solid state. Contrary to their crystalline counterpart, amorphous solids only possess short range order, whereas crystalline solids show three-dimensional long range order of molecules into repeating patterns (the crystal lattice). The smallest molecular groups exhibiting these repeating patterns are called a unit cell. Because of this higher disorder, amorphous solids (or glasses) show higher molecular mobility and increased enthalpy, entropy and volume compared to the corresponding crystalline solid but these same thermodynamic properties are lower compared to the liquid state. This phenomenon is visualized in Figure 1.1, where enthalpy, entropy or volume is plotted in function of temperature at constant pressure.

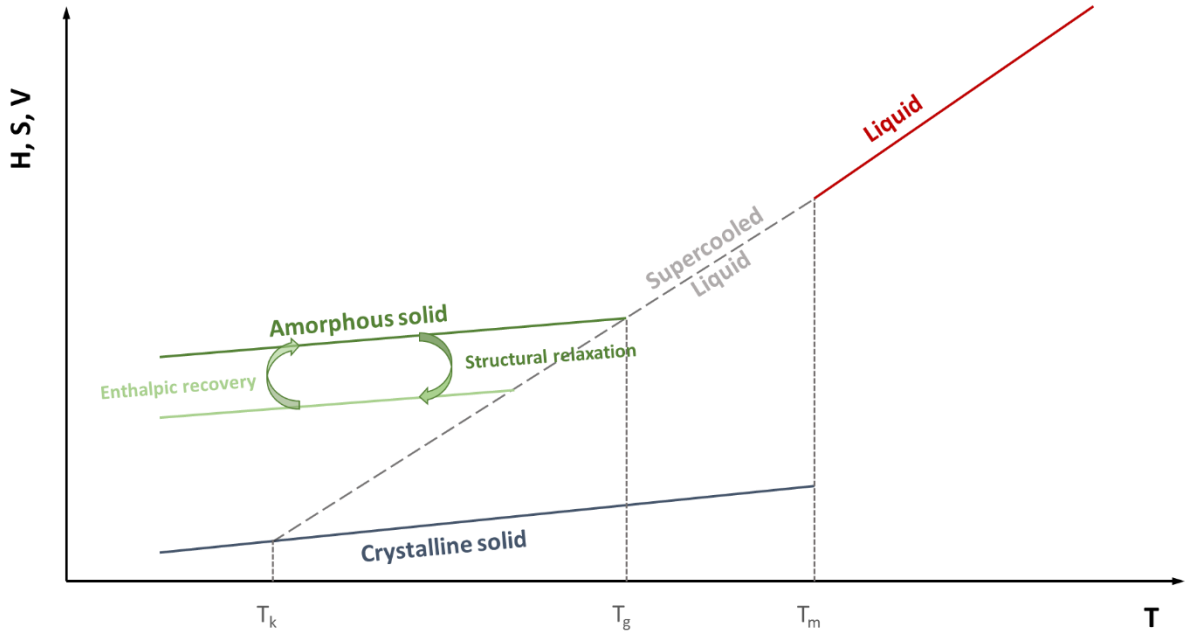

Figure 1.1: Schematic plot of enthalpy (H), entropy (S) or free volume (V) in function of temperature (T) for molecular substances at constant pressure.

When a crystalline solid is heated, it will melt and become a liquid at T_m which is the melting temperature. Melting is a first order transition and the liquid state is reached by a jump in H, S and V values compared to the crystalline state. When this liquid is cooled slowly, it will allow for sufficient time for the molecules to rearrange into a crystal. But if this liquid is cooled fast

enough to bypass the rearrangement into a crystal, the liquid can be cooled below T_m and go to the supercooled liquid state, which is in equilibrium with the liquid state. When further cooled, the molecules in the supercooled liquid will exhibit a sudden loss in translational motion, fall out of equilibrium and will transform into an amorphous solid at the glass transition temperature (T_g). The supercooled liquid is 'frozen' into a disordered state, which is thermodynamically unstable, nonequilibrium state and displays a higher viscosity compared to the liquid state. Since crystalline solids are the lowest energy state, molecules will strive to this state. This makes amorphous solids inherently unstable. Not only are the thermodynamic parameters of the amorphous solid higher than that of the crystalline solid, also the molecular mobility is enhanced. This is also responsible for the higher instability of the amorphous form. Nucleation is a result of localized faster molecular mobility [28].

Certain conditions like elevated temperature or humid environments for an extended period of time can provoke 'structural relaxation' to amorphous solids. Here, the amorphous solid loses energy, gains order and may approach the energy values of the crystalline state. Ultimately, structural relaxation can lead to a conversion to the crystalline state. There is also a phenomenon opposite to structural relaxation which is called 'enthalpic recovery', here energy is added to the system (e.g. in the form of heat) converting it again to its original energetic state. It can also be argued that the glass transition is a thermodynamic prerequisite for supercooled liquids, since otherwise they could reach enthalpy values equal or lower than the crystalline state. The temperature at which this would happen is called the Kauzmann temperature (T_k). It is practically impossible for glass transition temperatures to reach the Kauzmann temperature, since the cooling rate would have to be infinitesimally fast. The glass transition is also not a fixed value since it can vary due to different heating and cooling rates, molecular mass, history, geometry or purity of the sample [29].

Amorphous solids can not only be prepared by melt quenching (as described above), but also from a solution by rapid solvent evaporation, crystal lattice disruption or vapor condensation (some of these methods will be discussed when introducing preparation methods for solid dispersions).

To avoid crystallization of the amorphous form, this last can be stored at temperatures well below T_g. An empirical rule, known as the 'T_g-50'-rule, stipulates that when an amorphous material is stored at 50°C below the glass transition temperature, molecular mobility values have dropped low enough to provide acceptable stability [30].

As shown in the previous paragraph, amorphous solids have higher free energy compared to a crystal and lack the highly-ordered crystal lattice. This gives them a benefit in solubility since they don't have to overcome lattice energy. However, due to their inherent instability and propensity to crystallize, amorphous forms of drugs are rarely formulated as such.

1.4 Solid dispersions

The first step towards the notion of solid dispersions was made in 1961 by Sekiguchi and Obi [31]. In their study, eutectic mixtures were made up of sulfathiazole and urea, showing higher absorption compared to sulfathiazole as such. Since urea doesn't display any solubilizing action or enhances absorption , it was concluded that the physical state of sulfathiazole in the eutectic mixture was responsible for the accelerated absorption. 10 years later, a first definition and classification of solid dispersions was formulated by Chiou and Riegelman [32]. A solid dispersion was defined as 'the dispersion of one or more active ingredients in an inert carrier or matrix at solid state prepared by the melting (fusion), solvent, or melting-solvent method'. A classification was also constructed, depending on the crystalline, amorphous or molecularly dispersed state of the drug and the crystalline or amorphous state of the carrier [32, 33]. An overview is provided in Table 1.1.

Table 1.1: classification of solid dispersions, adapted from Dhirendra et al. 34.

Type of solid dispersion	*Drug*	*Carrier*	*# Phases*
Eutectic mixtures	*Crystalline*	*Crystalline*	*2*
Amorphous precipitate in a crystalline carrier	*Amorphous*	*Crystalline*	*2*
Solid solutions	*Molecularly dispersed*	*Crystalline*	*1*
Glass suspensions	*Crystalline or amorphous*	*Amorphous*	*2*
Glass solutions	*Molecularly dispersed*	*Amorphous*	*1*

As mentioned previously, the first solid dispersion created was a eutectic mixture. In this mixture, two compounds are miscible in the liquid state, but not in the solid state. At the eutectic composition, both compounds will simultaneously crystallize from the melt and form a very fine dispersion. If one compound is a poorly soluble drug and the other a highly soluble carrier, this will increase the surface area of the drug improving dissolution rate and ultimately the bio-availability. An amorphous precipitate in a crystalline carrier is seldomly created and has no value to the solid dispersion research.

Solid solutions are characterized by the presence of a molecularly dispersed drug in the crystal lattice of the carrier. This can be achieved by replacing a molecule in the lattice (substitutional solid solution) or occupying the space within the crystal lattice structure (interstitial solid solution). A solid solution can be continuous (unlimited miscibility) or discontinuous (limited miscibility). All in all, the role of solid solutions in solid dispersions is also limited. The most relevant examples of eutectic mixtures/solid solutions created, are combinations of a drug with the semi-crystalline polymers polyethylene glycol (PEG)[35-37] or Pluronic [38].

Glass suspensions combine an amorphous carrier with an amorphous (or crystalline) drug compound. The advantage of using amorphous carriers is that a greater extent of miscibility with an amorphous drug can be achieved. Finally, in a glass solution, there is solid solubility or miscibility between drug and carrier, resulting in a molecularly dispersed drug phase in an amorphous carrier forming a one phase system. These amorphous carriers are for the most part hydrophilic polymers. Nowadays in almost all solid dispersion formulations, there is a strive for the creation of glass solutions, where the drug particle size is reduced to the absolute minimum, resulting in a maximized dissolution rate. This can be evidenced by the Nernst-Brunner (or modified Noyes-Whitney) equation [39]:

$$\frac{dC}{dt} = \frac{DS}{Vh}(C_s - C) \qquad \text{Eq.1.1}$$

In this equation, $\frac{dC}{dt}$ (mol/(l.s)) is the dissolution rate, *C* (mol.l) the concentration at time t, *Cs* (mol/l) the saturation solubility, *D* (cm²/s) the diffusion coefficient, *S* (cm²) the surface area, *V* (ml) the volume of the dissolution medium and *h* (cm) the thickness of the diffusion layer. This equation shows that the surface area is proportional to the dissolution rate. A molecularly dispersed system has a minimized particle size, and thus ultimately a maximized surface area. As mentioned before, the creation of a stable glass solution requires the equilibrium or thermodynamic solid solubility of the drug in the carrier not to be exceeded. In practice, however, this thermodynamic solid solubility is often exceeded, which can be because of energy intensive processing, creating glass solutions which are unstable over time. Note that thermodynamically unstable glass solutions will turn into glass suspensions, with either amorphous or crystalline separated phases being formed [40]. Although long term stability has always been the main concern of formulation scientists concerning amorphous solid dispersions, a recent publication has shown a kinetically stabilized amorphous solid dispersion

of nifedipine to remain fully amorphous for 25 years [41]. Specific drug-polymer interactions like van der Waals, dipolar, hydrogen bonding or Coulomb interactions can enhance the miscibility and solid solubility [42]. Miscibility is the tendency of an active pharmaceutical ingredient (API) in its supercooled or glassy state, to mix with the carrier. Solid solubility can be described as the carrier acting as a solvent to dissolve the crystalline API. Presence of crystalline API does not necessarily point to immiscibility of the drug-polymer system [43, 44].

To avoid the creation of unstable glass solutions, a lot of efforts have been put into theoretical or experimental determination of the thermodynamic solid solubility and miscibility of poorly soluble drugs and amorphous carriers [45-48]. Miscibility determination can be assessed with qualitative methods like glass transition measurement, solubility parameter determination, computational data mining and micro-Raman, or with quantitative methods like computational analysis of X-ray diffraction measurements, solid-state nuclear magnetic resonance, Flory-Huggins interaction parameter and a combination of techniques (atomic force microscopy, electron microscopy…). For a more complete overview of these different possibilities, the reader is referred to a mini-review by Meng *et al.* [49]. As intermolecular interactions can have a beneficial effect and solubility and miscibility, factors like humidity (plasticization effect of water) and heat (elevated molecular mobility) can have a negative influence on the stability of glass solutions [50, 51].

1.5 Carriers used in the formulation of solid dispersions

Carriers for solid dispersions have evolved to a great extent since urea was used to make the first solid dispersion [31]. Whereas in the early stages of solid dispersion development, crystalline carriers were predominantly used, nowadays the focus has almost entirely shifted to amorphous (polymeric) carriers [52].

1.5.1 Crystalline carriers

The disuse of crystalline carriers was the result of their inability to contain drugs in the amorphous or molecularly dissolved state, their lower drug loading and the inferior stabilizing effect compared to amorphous carriers, due to less availability of interaction sites [53]. The exception here is the use of the semi-crystalline carrier polyethylene glycol (PEG), due to its hydrophilic nature and slight surface active properties. However, the very diverse influence of

PEG on the stability (crystallization) of drugs [35], or of drugs on the stability of PEG [54], make it currently still a very unpredictable and therefore less used polymer.

1.5.2 (hydrophilic) Amorphous carriers

Amorphous polymers are, generally considered, the most suitable option for glass solution formulation. Because of the amorphous nature, full miscibility with amorphous drugs can be achieved. Polymers with a high glass transition temperature can have an anti-plasticization effect on the amorphous drug, effectively avoiding crystallization of the drug by reducing molecular mobility and thus increasing stability [55]. This can be seen as an application of the T_g-50 rule, where the T_g is increased to allow stability near room temperature. The T_g-50 is a rule of thumb, rather than universally applicable in this situation, since some exceptions have been observed [56]. This stable glass transition temperature of a drug-polymer mixture can be predicted using the Gordon-Taylor equation [57]:

$$T_g = \frac{w_1 T_{g1} + k_{GT}(1-w_1) T_{g2}}{w_1 + k_{GT}(1-w_1)} \qquad \text{Eq. 1.2}$$

Since $T_{g1} \leq T_{g2}$, the former usually represents the T_g of the drug and the latter the T_g of the polymer. w is the weight fraction and k_{GT} is a constant equalling $\frac{\rho_1 \Delta\alpha_1}{\rho_2 \Delta\alpha_2}$. Here, ρ is the density of the components and $\Delta\ \alpha$ the change in thermal expansivity. When applying the Simha-Boyer rule [58], this constant can be approached as $\frac{\rho_1 T_{g1}}{\rho_2 T_{g2}}$. Other, less used, equations to predict the resultant mix-T_g of a drug-polymer system are the Fox, Couchman-Karasz or Kwei equations [55]. Deviations from the calculated T_g can point to presence of a plasticizer (residual solvent or water) or to a decrease in density of the mixture in case of a decreased experimental T_g Strong interactions between drug and polymer result in an increased experimental T_g. These strong interactions like ionic interactions or hydrogen bonding can also play an important role in the formation of stable solid dispersions [59].

Amorphous polymers used in the formulation of solid dispersions are mostly hydrophilic polymers, capable of rapidly dissolving in the entire (or part of the) pH range. Per their chemical structure, 3 main groups can be identified. The names and abbreviations of the most important polymers of each group are shown in Table 1.2 together with their T_g, molecular weight (Mw) and the pH range in which they are soluble.

Table 1.2: Different groups of amorphous polymers used as carriers for solid dispersions, adapted from Newman [60]

Group	Name	Abbreviation	T_g (°C)	Mw (kDa)	Soluble pH
Cellulose derivatives	*Hydroxypropylmethylcellulose*	*HPMC*	*160-180*	*10-1500*	*1-10*
	Hydroxypropylcellulose	*HPC*	*100-150*	*50-1250*	*1-10*
	Hydroxypropylmethylcellulose acetate succinate	*HPMCAS*	*113*	*55-93*	*> 5.5-6.5*
Polyvinyl polymers	*Polyvinylpyrrolidone*	*PVP*	*120-174*	*2,5-3000*	*1-10*
	Polyvinyl alcohol	*PVA*	*180-190* 228*	*20-200*	*1-10*
	Polyvinylpyrrolidone – polyvinyl acetate	*PVPVA*	*106*	*45-70*	*1-10*
	Polyvinyl caprolactam – polyvinyl acetate grafted on PEG	*Soluplus®*	*60-70*	*64*	*1-10*
Methacrylate polymers**	*Basic Butylated Methacrylate Copolymer*	*E100*	*57*	*47*	*< 5.0*
	Methacrylic Acid - Methyl Methacrylate Copolymer (1:1)	*L100*	*195*	*125*	*> 6.0*
	Methacrylic Acid - Ethyl Acrylate Copolymer (1:1) Type A	*L100-55*	*111*	*320*	*> 5.5*
	Methacrylic Acid - Methyl Methacrylate Copolymer (1:2)	*S100*	*173*	*125*	*> 7.0*

*depending on partial (180-190°C) or full (228°C) hydrolyzation **T_g and Mw based on [61]

The choice of carrier depends on several carrier and drug properties. First, an acceptable miscibility and solid solubility between drug and carrier should be achievable, allowing the formation of stable glass solutions. Preferably, there is also a possibility of drug-polymer interactions such as hydrogen bonding or ionic interactions. The carrier should be able to release the drug from its matrix at the preferred target site. Depending on the production method of the formulation, the carrier should possess either thermal stability or acceptable solubility in an array of organic solvents. Another critical quality of a good carrier is its ability to maintain supersaturated drug concentrations. It has been stipulated that a polymeric carrier can do this by forming solute-polymer interactions which hinders the reorganization of a cluster of solute molecules into an ordered crystal structure [62]. Once a suitable carrier is

found, different grades of the same polymer can have an influence on stability or release. For example: the hydrolyzation of PVA, different molecular weight or substitution grades of cellulose derivates [63], or different chain lengths (Mw) of PVP [64, 65].

The success of hydrophilic amorphous polymers as carriers for solid dispersions is reflected in the amount applied in marketed solid dispersions. Table 1.3 represents a compilation of marketed products using solid dispersion technology. As can be seen, all of these products use hydrophilic amorphous polymers, except for Gris-PEG, which uses the semi-crystalline PEG as a carrier.

Table 1.3: List of marketed solid dispersion products, adapted from Williams et al. [66]

Product	Drug	Carrier	Company
Gris-PEG	*griseofulvin*	PEG	Pedinol Pharmacal Inc.
Certican	*everolimus*	HPMC	Novartis Pharmaceuticals
Intelence	*etravirine*	HPMC	Tibotec
Nivadil	*nilvadipine*	HPMC	Fukisawa Pharmaceutical Co., Ltd
Prograf	*tacrolimus*	HPMC	Astellas Pharma US, Inc
Sporanox	*itraconazole*	HPMC	Janssen Pharmaceuticals
Isoptin-SRE	*verapamil*	HPC/HPMC	Abbott Laboratories
Incivek	*telaprevir*	HPMCAS	Vertex Pharmaceuticals
Zelboraf	*vemurafenib*	HPMCAS	Roche
Cesamet	*nabilone*	PVP	Valeant Pharmaceuticals
Kaletra	*lopinavir/ritonavir*	PVPVA	Abbott Laboratories
Norvir	*ritonavir*	PVPVA	Abbott Laboratories

1.5.3 New carrier approaches

In recent years, different strategies have been reported to address some of the drawbacks in using hydrophilic amorphous polymers in solid dispersion technology.

- ***Co-Amorphous drug formulations:*** combination of two low molecular weight components that form a single phase amorphous system. This can be either a combination of two drugs or a drug combined with a low molecular weight excipient such as an amino acid. This approach tries to reduce the amount of excipient to stabilize the formulation. It also reduces the hygroscopic nature of many 'classic' solid dispersions [67].

- ***'in-situ'-amorphisation:*** drugs are converted to the amorphous state upon contact with dissolution medium, vapour or lipolysis thus conveniently avoiding storage related instability [68].
- ***Controlled release of solid dispersions:*** sometimes labelled as fourth generation carriers for solid dispersions. Controlled release formulations of poorly soluble drug compounds can offer similar advantages to other controlled or sustained formulations, like improved compliance by reduced dosing frequency, decreased side effects, and prolonged therapeutic effects [69]. Polymers frequently used in the controlled release of solid dispersions include cellulose derivates like ethyl cellulose (EC), hydroxpropylmethylcellulose acetate phthalate (HPMC-AP) and some grades of HPMC and HPC, polyethylene oxide (PEO, high Mw PEG) and methacrylates like Eudragit RL and RS grade. These polymers release the drug by diffusion rather than by dissolution. Controlled release polymers can be applied as (part of) the matrix or as an outer layer through which the drug has to diffuse before being released [70, 71]. Moreover, it has been observed that although rapidly dissolving polymers lead to fast generation of high supersaturated drug concentration levels, it does not always result in an optimal enhancement of bio-availability [72]. Hence controlled release polymers could slow down this fast increase and prolong the supersaturated drug concentrations. This has been demonstrated by Sun and Lee and their results are bundled in an interesting commentary about the interplay between dissolution and precipitation [73].

1.6 Manufacturing techniques of solid dispersions

Of the four techniques to render drugs amorphous named earlier on, three are actively used in solid dispersion manufacturing. The choice of a manufacturing technique is dependent upon drug and polymer properties and can have a vast impact on the stability and pharmaceutical performance of the solid dispersion.

1.6.1 Crystal lattice disruption

The disruption of the crystal lattice of drugs, also called mechanical activation is performed by high-intensity milling. Although the fundamental aspects of the amorphisation processes are still not fully understood, this technique has been shown to be effective in amorphisation of drugs as such [74]. This method has been successful in the creation of co-amorphous systems[67] and only very recently, some successful efforts in making polymeric solid dispersions have

been reported [75-77]. Some benefits of using milling for the creation of solid dispersions include the omission of possibly toxic or destabilizing solvents, and its potential for thermolabile compounds.

1.6.2 Melt quenching

Melt fusion with subsequent quenching was the technique used in the creation of the first solid dispersion [31]. Since then, optimized techniques have been developed to produce amorphous solid dispersions. Hot melt extrusion is the most investigated technique applying the melting method [78]. In hot melt extrusion, a physical mixture of drug and polymer are introduced into a heated barrel. One or multiple screws provide propulsion and mixing of the molten mixture. Finally, this melt is pushed out of the extruder via a dye, which allows to produce extrudates of different diameters. The temperature decrease out of the dye allows for solidification. The barrel temperature, screw speed, screw design and feed rate are process parameters which can influence the quality of the end product [79]. The main advantages of hot melt extrusion are solvent free production and the possibility for continuous processing. Disadvantages are inability to use thermally degradable products and, often, the need for post processing operations like milling or pelletizing (which can have a disadvantageous effect on solid dispersion stability). Although it has to be noted that these post processing steps can be avoided by shaping the extrudates into tablets via calendering [80]. Different products manufactured with hot melt extrusion are on the market today, not only solid dispersions but also sustained delivery products like eye implants or contraceptives [81]. A variation on this technique is co-extrusion, which can provide a multi-layered extrudate suitable for fixed dose combinations or controlled release drug delivery [82].

In recent years, two additional melting methods have come to the forefront. The first technique is thermal injection moulding. A technique which is already established for a long time in the plastics industry and medical device manufacturing, has now been proposed for the proposed for the production of immediate release tablets [83].

A second method is fused deposition modelling (extrusion based 3D printing technique) to produce oral drug formulations. This technique has a tremendous potential in the application for personalized medicine, with possibilities of individual doses, amounts, release properties,… Contemporary hurdles include compatibility of drugs and excipients with the 3D printing technique and regulatory challenges that need to be overcome [84, 85].

1.6.3 Rapid solvent evaporation

When formulating solid dispersions through rapid solvent evaporation, the well-established go-to method is spray drying. In this technique, a drug-polymer solution is fed through a nozzle and mixed with pressurized air to form fine droplets (atomization). Other nozzle types, using centrifugal, pressure, kinetic or vibration energy for atomization are available as well. These droplets are further transported and dried along a heated air flow or carrier gas through a drying chamber and a cyclone, where particles within a desirable size range fall out of the air stream in a collector. Extensive reviews have been written about the formulation of solid dispersions through spray drying with considerable attention to the influence of process and formulation variables on the final product [86, 87]. The subsequently formed powder can be processed in a wide array of drug delivery systems (capsules, tablets, dispersible powders…). Spray drying is also a suitable method for thermally degradable compounds since the temperature during spray drying is less high compared to hot melt extrusion. The presence of residual solvent, which can act as a plasticizer or is potentially toxic, is seen as one of the techniques' main disadvantages.

Recently developed or introduced solvent removal techniques for producing solid dispersions include inkjet printing[88, 89], electrospinning and electrospraying [83, 89]. Scaling-up challenges currently form the biggest pitfall for the further implementation of these techniques of solid dispersion research.

1.6.4 Fluid bed coating

A manufacturing technique using the solvent method, which has been long overlooked in solid dispersion research, is fluid bed coating. Although there is a drug formulation on the market that uses this technique, Sporanox (Janssen Pharmaceuticals) which is a solid dispersion of itraconazole and HPMC layered on inert sugar spheres and this has been used as a reference in some comparative studies[90-92], there has not been done a lot of research on the technique itself, or on what makes it suitable for solid dispersion exploitation. Fluid bed coating, on the other hand, can be considered an established technique in controlled drug release formulation with numerous articles being published on the layering of controlled release polymers like ethylcellulose[93], poly(meth)acrylates[94], polyvinylacetate[95] or blends thereof [96, 97]Fluid bed coating uses the constant patterned movement of starter cores to apply a cyclic layering of a

drug polymer solution. Figure 1.2 shows a schematic representation of a fluid bed coating device.

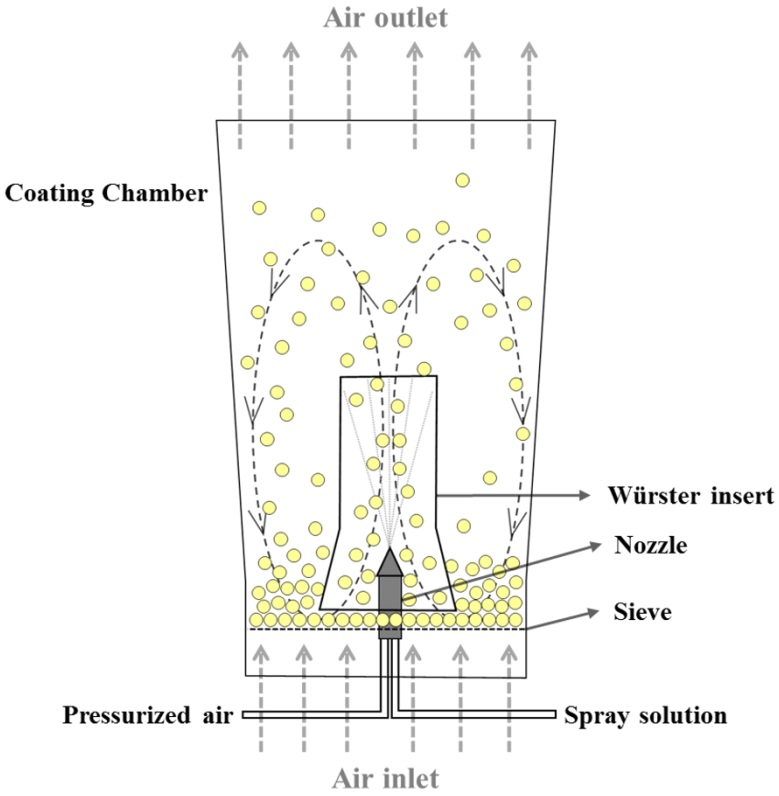

Figure 1.2: Schematic representation of bottom spray fluid bed coating using a Würster insert.

The movement of the inert particles is provided by fluidization through an inlet air stream. In fluidization, particles are suspended in fluidizing air, which moves upwards and thereby counteracts gravitational forces. This inlet air stream should be accurately selected since the superficial velocity of the air should exceed the minimum fluidization velocity of the particles, but cannot exceed their terminal velocity. For this reason, a small particle size range is preferred[98].

Fluid bed coating can consist of 3 set-ups. In a top spray configuration, the nozzle is place above the fluidized bed, resulting in opposed directions of sprayed liquid and air flow. This set-up is mainly used for granulation purposes. The set-up displayed in Figure 2 is a bottom spray configuration with an optional Würster insert (conical cylinder placed over the nozzle with a slightly decreasing diameter). In this set-up sprayed liquid and air flow are unidirectional, which increases contact between droplets and particles, and increases droplet drying time compared to top spray and this generally results in more efficient and homogenous coating. A third set-up consists of a rotary disk at the bottom equipped with slits where the air flow enters. The

nozzle or nozzles are located on the side of the coating chamber. This gives rise to a tangential spray on the fluidized particles, hence the name 'tangential spray' set-up. This set-up gives rise to a particular 'rope-like' particle motion, which results in dense and spherical shapes. The high agitation in the equipment is seen as the most important drawback to the system [99]. It must be noted that coating and granulation processes share some similar equipment, the difference is that process and formulation parameters in granulation are chosen so agglomeration is promoted, while in coating this must be avoided.

In a bottom spray set-up with a Würster insert, which is the most common configuration for coating purposes, inert pellets are fluidized and make a circular movement (as indicated with arrows on Figure 1.2). This made possible by the air plate configuration which directs air flow to the centre of the plate, near the nozzle. Furthermore, the bead movements benefit from the narrowing diameter of the Würster insert to accelerate through acceleration of the air flow on one hand, and the increasing diameter of the coating chamber causing deceleration of air flow and beads on the other hand. The Würster insert has additional benefits in the fact that it separates and directs the upward moving beads away from the downward falling beads. In this way, a more effective coating can be achieved. The nozzle atomizes the spraying liquid and these fine droplets hit the surface of the beads. After the beads have been wetted they move upwards and fall back down at the side of the coating chamber, this allows for a sufficient drying time and they are redirected to the centre of the coating chamber where the entire coating process can restart. This circular movement of the beads allows for repeated layering of a sprayed solution or dispersion onto these beads until the desired coating level is achieved, this process is schematically shown in Figure 1.3.

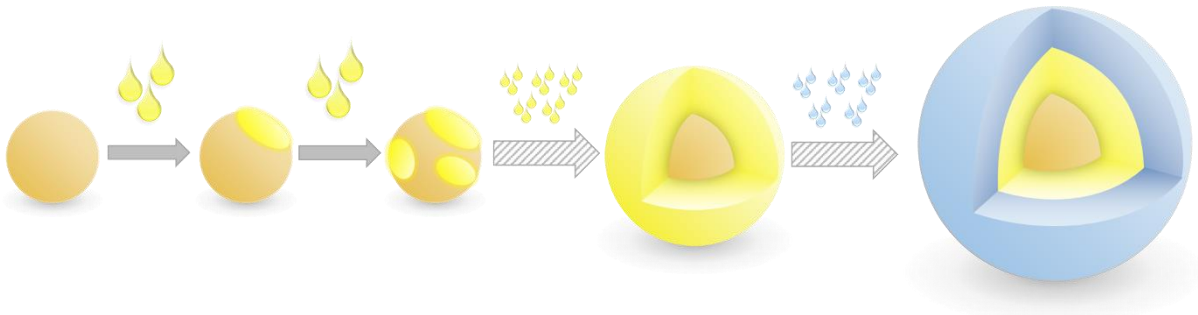

Figure 1.3: Schematic representation of the cyclic layering of inert beads. The beads are wetted by droplets from the spraying solution and subsequently dried. This process is repeated until a desired coating level is applied to the bead. Fluid bed coating allows for the application of multiple layers to be coated consecutively.

Adjustable process parameters for fluid bed coating include:

- ***Air flow rate:*** allows for fluidization, optimal particle movement and drying (time) of the wetted particles
- ***Air flow temperature***: adjusted for optimal solvent or water evaporation
- ***Air flow humidity:*** humidity control can influence the air drying capacity
- ***Atomizing air flow:*** adjustment of droplet size of the supplied liquid
- ***Feed rate:*** needs to be adjusted for optimal film formation around the bead

Suboptimal process parameters can result in agglomeration, when the wetted beads are not dried fast enough, or spray drying, when the sprayed liquid solidifies before hitting a substrate.

Fluid bed coating can address some issues encountered in solid dispersion research. First, drying of the layered beads can be performed within the coating device itself, omitting additional drying steps, minimizing residual solvent levels, and thus increasing stability. Secondly, it has been shown that post processing steps can have a negative influence on the stability of solid dispersions. Ayenew *et al.* for example showed demixing of naproxen-PVP solid dispersion upon compression [100]. By applying fluid bed coating, compressional forces can be avoided since coated beads can be immediately filled into capsules. Thirdly, it has been shown that API crystallization happens faster at the surface of solid dispersion particles as compared to the bulk [101]. This issue can be addressed by applying a second protective coating on top the solid dispersion (see Figure 1.3). Application of the second coating also does not require transfer and handling steps as it can be performed in the same device. This multi-layering approach is also an ideal prerequisite for controlled release coating. A controlled release coating can be applied immediately after the solid dispersion coating without extra handling steps. Coating multiparticulates also provides benefits over tablet coating like: a better spread over the gastrointestinal tract, reduced risk of dose dumping and transit times are more predictable [102].

1.7 Characterization techniques for solid dispersions

1.7.1 Bulk characterization

Due to the (potentially) complex physicochemical properties of solid dispersions, an in-depth characterization of these systems is required. The primary indicator of a glass solution

is its glass transition temperature. The most widespread method to detect the glass transition is through thermal analytical techniques, and more specifically differential scanning calorimetry (DSC) analysis. DSC can differentiate between glass solutions, displaying a single T_g and phase separated systems displaying a double T_g. Single T_g's of glass solution can be compared with theoretical T_g's from the Gordon-Taylor equation (Eq. 2). Furthermore, crystallization into and melting of crystalline fractions are also detectable. In case of small heat capacity changes or solvent loss in the region of interest, modulated temperature differential scanning calorimetry (mDSC) can be used. Here, a sinusoidal waveform is superimposed on the heating rate, allowing for a separation into heat capacity related (or thermodynamic) phenomena and kinetic phenomena. Baird and Taylor described the full potential of using of thermal analysis techniques in solid dispersions in an interesting review [103].

X-ray powder diffraction (XRPD) is a powerful method to identify crystal species in solid dispersions which become apparent by their Bragg peaks. It has been used extensively in tandem with (m)DSC to identify polymorphic transitions or exclude crystallization or amorphisation induced by heating. Recent advances in instrumentation and insights in amorphous structures have enabled the use of XRPD in the characterization of amorphous materials as well [104].

Other techniques used for bulk characterization of solid dispersions:

- ***Thermogravimetric analysis (TGA):*** investigation into solvent/water content of formulations and assessment of drying kinetics. It can be coupled (so-called hyphenated set up) with gas chromatography, infrared spectroscopy or mass spectrometry to identify volatile compounds.
- ***Infrared (IR) and Raman spectroscopy:*** application for the detection of different crystalline or amorphous phases, also a preferred technique in molecular interaction identification. Their non-invasive nature also allows for quality control and process analytical technology purposes [105]. Some comparative studies between XRPD, Raman and IR spectroscopy have been performed [106].
- ***Dielectric spectroscopy (DES):*** molecular mobility investigation in glasses and supercooled liquids, insight into the different relaxation processes and crystallization kinetics [107].

- ***Terahertz spectroscopy:*** relatively novel analytical technique depicting fast molecular dynamics of molecules determining the onset and strength of molecular mobility to predict stability of the amorphous state [108].
- ***Solid-state nuclear magnetic resonance (ssNMR):*** very powerful, but also very complex tool to determine molecular dynamics and phase compositions of solid dispersions [109].

1.7.2 Spatially resolved (or imaging) characterization

As powerful and detailed the bulk characterizing techniques may be, sometimes there is a need for spatially resolved information of solid dispersions. These characterization techniques allow for the separation into different parts or regions of interest within a drug delivery system which can be of interest in complex systems, differentiation between bulk and surface properties or during dissolution.

Lots of the spectroscopic techniques mentioned in the previous paragraph can be used for imaging purposes as well. Infrared[110], Raman[105] or Terahertz[111] spectroscopy have all been successfully applied in imaging set-ups. Raman imaging has also been successfully applied for real time and in situ investigation of the dissolution mechanisms in solid dispersions [112].

Scanning electron microscopy (SEM) has been very useful for the topographical investigation of drug delivery systems. Also, crystal identification and form can be observed through SEM. This technique is unable to distinguish between different amorphous phases within one system. The detection of crystal structures can also be performed using polarized light microscopy (PLM) which is an ideal platform (fast, inexpensive) for initial screening studies of solid dispersions.

Atomic force microscopy is a probe based surface analysis technique, which uses a nanometre scaled tip to raster scan a sample surface. The sharper the probe tip, the higher the resolution that can be achieved. Adhesion and repulsion forces on the probe provide topographical, morphological and phase distribution information. AFM has been shown to be able to determine drug-excipient miscibility in solid dispersions [113]. AFM probes have also been used for nanoscale thermal analysis purposes. Here, the tip of the AFM probe is heated and deflection of the tip can be measured in function of temperature. This technique allows the determination of glass transition temperatures on a nanometer scale [114]. AFM can also be coupled to infrared spectroscopy to obtain chemical information of a sample at the high spatial resolutions obtained by AFM [115].

Special emphasis should be put here on Time of Flight Secondary Ion Mass Spectrometry (ToF-SIMS) as a surface analysis technique capable of chemical identification and distribution (mapping). ToF-SIMS is based upon the bombardment of a sample surface with primary ions which will detach, among other structures, ion fragments from the surface. These are the secondary ions. The secondary ions are accelerated and injected into a Time-of-Flight analyser where the positive or negative ions (depending on the set polarity of the equipment) will be separated, depending on their mass-to-charge ratio. The spectra can lead to a complete identification of chemical structures present on the surface with a very low detection limit (ppb range). Because the primary ion beam can be focused, a sample can be raster scanned, providing spatial distribution information with a very high spatial resolution (0.2 μm). Because of the non-penetrating nature of the primary ion beams, sample information from the upper few nanometres of the sample is acquired. By using less destructive primary ion beams like C_{60}^{+} ions, depth profiling of the surface can be performed with an in-depth resolution of a few nanometers [116]. A disadvantage of ToF-SIMS is that it can only provide semi-quantitative information on the chemical composition of the sample surface, therefore the analysis is sometimes performed together with X-ray photoelectron scattering (XPS) which can allow quantitative analysis through information on atomic concentrations and chemical bonding [114].

1.8 References

1. Sneader, W., The Prehistoric Period. In *Drug Discovery*, John Wiley & Sons, Ltd: 2005; pp 6-11.

2. Jones, A. W., Early drug discovery and the rise of pharmaceutical chemistry. *Drug Testing and Analysis* **2011,** *3* (6), 337-344.

3. Atanasov, A. G.; Waltenberger, B.; Pferschy-Wenzig, E.-M.; Linder, T.; Wawrosch, C.; Uhrin, P.; Temml, V.; Wang, L.; Schwaiger, S.; Heiss, E. H.; Rollinger, J. M.; Schuster, D.; Breuss, J. M.; Bochkov, V.; Mihovilovic, M. D.; Kopp, B.; Bauer, R.; Dirsch, V. M.; Stuppner, H., Discovery and resupply of pharmacologically active plant-derived natural products: A review. *Biotechnology advances* **2015,** *33* (8), 1582-1614.

4. Drews, J., Drug Discovery: A Historical Perspective. *Science* **2000,** *287* (5460), 1960.

5. Pina, A. S.; Hussain, A.; Roque, A. C. A., An Historical Overview of Drug Discovery. In *Ligand-Macromolecular Interactions in Drug Discovery: Methods and Protocols*, Roque, A. C. A., Ed. Humana Press: Totowa, NJ, 2010; pp 3-12.

6. Ng, R., Appendix 1: History of Drug Discovery and Development. In *Drugs*, John Wiley & Sons, Inc.: 2008; pp 391-397.

7. Van Hijfte, L.; Marciniak, G.; Froloff, N., Combinatorial chemistry, automation and molecular diversity: new trends in the pharmaceutical industry. *Journal of Chromatography B: Biomedical Sciences and Applications* **1999,** *725* (1), 3-15.

8. An, W. F.; Tolliday, N. J., Introduction: Cell-Based Assays for High-Throughput Screening. In *Cell-Based Assays for High-Throughput Screening: Methods and Protocols*, Clemons, P. A.; Tolliday, N. J.; Wagner, B. K., Eds. Humana Press: Totowa, NJ, 2009; pp 1-12.

9. Bleicher, K. H.; Bohm, H.-J.; Muller, K.; Alanine, A. I., Hit and lead generation: beyond high-throughput screening. *Nat Rev Drug Discov* **2003,** *2* (5), 369-378.

10. Waring, M. J.; Arrowsmith, J.; Leach, A. R.; Leeson, P. D.; Mandrell, S.; Owen, R. M.; Pairaudeau, G.; Pennie, W. D.; Pickett, S. D.; Wang, J.; Wallace, O.; Weir, A., An analysis of the attrition of drug candidates from four major pharmaceutical companies. *Nat Rev Drug Discov* **2015,** *14* (7), 475-486.

11. Gershell, L. J.; Atkins, J. H., A brief history of novel drug discovery technologies. *Nat Rev Drug Discov* **2003,** *2* (4), 321-327.

12. Lipinski, C. A.; Lombardo, F.; Dominy, B. W.; Feeney, P. J., Experimental and computational approaches to estimate solubility and permeability in drug discovery and development settings. *Advanced Drug Delivery Reviews* **1997,** *23* (1), 3-25.

13. Miyaji, Y.; Fujii, Y.; Takeyama, S.; Kawai, Y.; Kataoka, M.; Takahashi, M.; Yamashita, S., Advantage of the Dissolution/Permeation System for Estimating Oral Absorption of Drug Candidates in the Drug Discovery Stage. *Molecular Pharmaceutics* **2016,** *13* (5), 1564-1574.

14. Amidon, G. L.; Lennernas, H.; Shah, V. P.; Crison, J. R., A theoretical basis for a biopharmaceutic drug classification: the correlation of in vitro drug product dissolution and in vivo bioavailability. *Pharm Res* **1995,** *12* (3), 413-20.

15. Food and Drug, A., Guidance for industry: waiver of in vivo bioavailability and bioequivalence studies for immediate-release solid oral dosage forms based on a biopharmaceutics classification system. *Food and Drug Administration, Rockville, MD* **2000**.

16. Takagi, T.; Ramachandran, C.; Bermejo, M.; Yamashita, S.; Yu, L. X.; Amidon, G. L., A Provisional Biopharmaceutical Classification of the Top 200 Oral Drug Products in the United States, Great Britain, Spain, and Japan. *Molecular Pharmaceutics* **2006,** *3* (6), 631-643.

17. Maag, H., Overcoming poor permeability – the role of prodrugs for oral drug delivery. *Drug Discovery Today: Technologies* **2012,** *9* (2), e121-e130.

18. Aungst, B. J., Absorption Enhancers: Applications and Advances. *The AAPS Journal* **2012,** *14* (1), 10-18.

19. Serajuddin, A. T. M., Salt formation to improve drug solubility. *Advanced Drug Delivery Reviews* **2007,** *59* (7), 603-616.

20. Rautio, J.; Kumpulainen, H.; Heimbach, T.; Oliyai, R.; Oh, D.; Jarvinen, T.; Savolainen, J., Prodrugs: design and clinical applications. *Nat Rev Drug Discov* **2008,** *7* (3), 255-270.

21. Peltonen, L.; Strachan, C., Understanding Critical Quality Attributes for Nanocrystals from Preparation to Delivery. *Molecules* **2015,** *20* (12).

22. Porter, C. J. H.; Trevaskis, N. L.; Charman, W. N., Lipids and lipid-based formulations: optimizing the oral delivery of lipophilic drugs. *Nat Rev Drug Discov* **2007,** *6* (3), 231-248.

23. Mu, H.; Holm, R.; Müllertz, A., Lipid-based formulations for oral administration of poorly water-soluble drugs. *International Journal of Pharmaceutics* **2013,** *453* (1), 215-224.

24. Thakuria, R.; Delori, A.; Jones, W.; Lipert, M. P.; Roy, L.; Rodríguez-Hornedo, N., Pharmaceutical cocrystals and poorly soluble drugs. *International Journal of Pharmaceutics* **2013,** *453* (1), 101-125.

25. Kurkov, S. V.; Loftsson, T., Cyclodextrins. *International Journal of Pharmaceutics* **2013,** *453* (1), 167-180.

26. Xu, W.; Riikonen, J.; Lehto, V.-P., Mesoporous systems for poorly soluble drugs. *International Journal of Pharmaceutics* **2013,** *453* (1), 181-197.

27. Vialpando, M.; Martens, J. A.; Van den Mooter, G., Potential of ordered mesoporous silica for oral delivery of poorly soluble drugs. *Ther Deliv* **2011,** *2* (8), 1079-91.

28. Graeser, K. A.; Patterson, J. E.; Zeitler, J. A.; Rades, T., The Role of Configurational Entropy in Amorphous Systems. *Pharmaceutics* **2010,** *2* (2), 224-244.

29. Hancock, B. C.; Zografi, G., Characteristics and significance of the amorphous state in pharmaceutical systems. *J Pharm Sci* **1997,** *86* (1), 1-12.

30. Surikutchi, B. T.; Patil, S. P.; Shete, G.; Patel, S.; Bansal, A. K., Drug-excipient behavior in polymeric amorphous solid dispersions. *J. Excipients Food Chem.* **2013,** *4* (3), 70-94.

31. Sekiguchi, K.; Obi, N., Studies on Absorption of Eutectic Mixture. I. A Comparison of the Behavior of Eutectic Mixture of Sulfathiazole and that of Ordinary Sulfathiazole in Man. *Chemical & pharmaceutical bulletin* **1961,** *9* (11), 866-872.

32. Chiou, W. L.; Riegelman, S., Pharmaceutical Applications of Solid Dispersion Systems. *Journal of Pharmaceutical Sciences* **1971,** *60* (9), 1281-1302.

33. Leuner, C.; Dressman, J., Improving drug solubility for oral delivery using solid dispersions. *Eur J Pharm Biopharm* **2000,** *50* (1), 47-60.

34. Dhirendra, K.; Lewis, S.; Udupa, N.; Atin, K., Solid dispersions: a review. *Pak J Pharm Sci* **2009,** *22* (2), 234-46.

35. Zhu, Q.; Harris, M. T.; Taylor, L. S., Modification of Crystallization Behavior in Drug/Polyethylene Glycol Solid Dispersions. *Molecular Pharmaceutics* **2012,** *9* (3), 546-553.

36. Zhu, Q.; Toth, S. J.; Simpson, G. J.; Hsu, H.-Y.; Taylor, L. S.; Harris, M. T., Crystallization and Dissolution Behavior of Naproxen/Polyethylene Glycol Solid Dispersions. *The Journal of Physical Chemistry B* **2013,** *117* (5), 1494-1500.

37. Chen, Z.; Liu, C.; Zhang, L.; Qian, F., Dissolution Characteristics of Fast-Crystallizing β - Lapachone within Different Semicrystalline Microstructures of Polyethylene Glycol or Poly(ethylene oxide)–Poly(propylene oxide)–Poly(ethylene oxide) Triblock Copolymer. *Crystal Growth & Design* **2016,** *16* (9), 5367-5376.

38. Qian, F.; Tao, J.; Desikan, S.; Hussain, M.; Smith, R. L., Mechanistic Investigation of Pluronic® Based Nano-crystalline Drug-polymer Solid Dispersions. *Pharmaceutical Research* **2007,** *24* (8), 1551-1560.

39. Dokoumetzidis, A.; Macheras, P., A century of dissolution research: From Noyes and Whitney to the Biopharmaceutics Classification System. *International Journal of Pharmaceutics* **2006,** *321* (1–2), 1-11.

40. Huang, Y.; Dai, W.-G., Fundamental aspects of solid dispersion technology for poorly soluble drugs. *Acta Pharmaceutica Sinica. B* **2014,** *4* (1), 18-25.

41. Theil, F.; Anantharaman, S.; Kyerematen, S. O.; van Lishaut, H.; Dreis-Kühne, S. H.; Rosenberg, J.; Mägerlein, M.; Woehrle, G. H., Frozen in Time: Kinetically Stabilized Amorphous Solid Dispersions of Nifedipine Stable after a Quarter Century of Storage. *Molecular Pharmaceutics* **2016**.

42. Yang, Z.; Han, C. D., Rheology of Miscible Polymer Blends with Hydrogen Bonding. *Macromolecules* **2008,** *41* (6), 2104-2118.

43. Marsac, P. J.; Shamblin, S. L.; Taylor, L. S., Theoretical and Practical Approaches for Prediction of Drug–Polymer Miscibility and Solubility. *Pharmaceutical Research* **2006,** *23* (10), 2417.

44. Qian, F.; Huang, J.; Hussain, M. A., Drug-polymer solubility and miscibility: Stability consideration and practical challenges in amorphous solid dispersion development. *J Pharm Sci* **2010,** *99* (7), 2941-7.

45. Mahieu, A.; Willart, J. F.; Dudognon, E.; Danede, F.; Descamps, M., A new protocol to determine the solubility of drugs into polymer matrixes. *Mol Pharm* **2013,** *10* (2), 560-6.

46. Sun, Y.; Tao, J.; Zhang, G. G.; Yu, L., Solubilities of crystalline drugs in polymers: an improved analytical method and comparison of solubilities of indomethacin and nifedipine in PVP, PVP/VA, and PVAc. *J Pharm Sci* **2010,** *99* (9), 4023-31.

47. Altamimi, M. A.; Neau, S. H., Use of the Flory-Huggins theory to predict the solubility of nifedipine and sulfamethoxazole in the triblock, graft copolymer Soluplus. *Drug Dev Ind Pharm* **2016,** *42* (3), 446-55.

48. Marsac, P. J.; Li, T.; Taylor, L. S., Estimation of drug-polymer miscibility and solubility in amorphous solid dispersions using experimentally determined interaction parameters. *Pharm Res* **2009,** *26* (1), 139-51.

49. Meng, F.; Dave, V.; Chauhan, H., Qualitative and quantitative methods to determine miscibility in amorphous drug–polymer systems. *European Journal of Pharmaceutical Sciences* **2015,** *77*, 106-111.

50. Zhu, D.; Zografi, G.; Gao, P.; Gong, Y.; Zhang, G. G. Z., Modeling Physical Stability of Amorphous Solids Based on Temperature and Moisture Stresses. *Journal of Pharmaceutical Sciences* **2016,** *105* (9), 2932-2939.

51. Marsac, P. J.; Rumondor, A. C.; Nivens, D. E.; Kestur, U. S.; Stanciu, L.; Taylor, L. S., Effect of temperature and moisture on the miscibility of amorphous dispersions of felodipine and poly(vinyl pyrrolidone). *J Pharm Sci* **2010,** *99* (1), 169-85.

52. Vasconcelos, T.; Sarmento, B.; Costa, P., Solid dispersions as strategy to improve oral bioavailability of poor water soluble drugs. *Drug Discov Today* **2007,** *12* (23-24), 1068-75.

53. Van Duong, T.; Van den Mooter, G., The role of the carrier in the formulation of pharmaceutical solid dispersions. Part I: crystalline and semi-crystalline carriers. *Expert Opinion on Drug Delivery* **2016,** *13* (11), 1583-1594.

54. Duong, T. V.; Van Humbeeck, J.; Van den Mooter, G., Crystallization Kinetics of Indomethacin/Polyethylene Glycol Dispersions Containing High Drug Loadings. *Mol Pharm* **2015,** *12* (7), 2493-504.

55. Baghel, S.; Cathcart, H.; O'Reilly, N. J., Polymeric Amorphous Solid Dispersions: A Review of Amorphization, Crystallization, Stabilization, Solid-State Characterization, and Aqueous Solubilization of Biopharmaceutical Classification System Class II Drugs. *Journal of Pharmaceutical Sciences* **2016,** *105* (9), 2527-2544.

56. Chokshi, R. J.; Shah, N. H.; Sandhu, H. K.; Malick, A. W.; Zia, H., Stabilization of low glass transition temperature indomethacin formulations: impact of polymer-type and its concentration. *J Pharm Sci* **2008,** *97* (6), 2286-98.

57. Gordon, M.; Taylor, J. S., Ideal copolymers and the second-order transitions of synthetic rubbers. i. non-crystalline copolymers. *Journal of Applied Chemistry* **1952,** *2* (9), 493-500.

58. Simha, R.; Boyer, R. F., On a General Relation Involving the Glass Temperature and Coefficients of Expansion of Polymers. *The Journal of Chemical Physics* **1962,** *37*, 1003-1007.

59. Kothari, K.; Ragoonanan, V.; Suryanarayanan, R., The role of drug-polymer hydrogen bonding interactions on the molecular mobility and physical stability of nifedipine solid dispersions. *Mol Pharm* **2015,** *12* (1), 162-70.

60. Newman, A., *Pharmaceutical Amorphous Solid Dispersions*. Wiley: 2015; p 504.

61. Parikh, T.; Gupta, S. S.; Anuprabha, M.; Serajuddin, A. T., Investigation of thermal and viscoelastic properties of polymers relevant to hot melt extrusion - III: Polymethacrylates and polymethacrylic acid based polymers (PDF Download Available). *Journal of Excipients and Food Chemicals* **2014,** *5* (1), 56-64.

62. Ilevbare, G. A.; Liu, H.; Edgar, K. J.; Taylor, L. S., Maintaining Supersaturation in Aqueous Drug Solutions: Impact of Different Polymers on Induction Times. *Crystal Growth & Design* **2013,** *13* (2), 740-751.

63. Siepmann, J.; Peppas, N. A., Modeling of drug release from delivery systems based on hydroxypropyl methylcellulose (HPMC). *Advanced drug delivery reviews* **2001,** *48* (2), 139-157.

64. Paudel, A.; Van Humbeeck, J.; Van den Mooter, G., Theoretical and Experimental Investigation on the Solid Solubility and Miscibility of Naproxen in Poly(vinylpyrrolidone). *Mol Pharm* **2010**, *7* (4), 1133-1148

65. Van Duong, T.; Van den Mooter, G., The role of the carrier in the formulation of pharmaceutical solid dispersions. Part II: amorphous carriers. *Expert Opinion on Drug Delivery* **2016**, 1-14.

66. Williams, H. D.; Trevaskis, N. L.; Charman, S. A.; Shanker, R. M.; Charman, W. N.; Pouton, C. W.; Porter, C. J. H., Strategies to Address Low Drug Solubility in Discovery and Development. *Pharmacological Reviews* **2013,** *65* (1), 315.

67. Dengale, S. J.; Grohganz, H.; Rades, T.; Lobmann, K., Recent advances in co-amorphous drug formulations. *Adv Drug Deliv Rev* **2016,** *100*, 116-25.

68. Priemel, P. A.; Grohganz, H.; Rades, T., Unintended and in situ amorphisation of pharmaceuticals. *Adv Drug Deliv Rev* **2016,** *100*, 126-32.

69. Vo, C. L.; Park, C.; Lee, B. J., Current trends and future perspectives of solid dispersions containing poorly water-soluble drugs. *Eur J Pharm Biopharm* **2013,** *85* (3 Pt B), 799-813.

70. Giri, T. K.; Kumar, K.; Alexander, A.; Badwaik, H.; Tripathi, D. K., A novel and alternative approach to controlled release drug delivery system based on solid dispersion technique. *Bulletin of Faculty of Pharmacy, Cairo University* **2012,** *50* (2), 147-159.

71. Tran, P. H.-L.; Tran, T. T.-D.; Park, J. B.; Lee, B.-J., Controlled Release Systems Containing Solid Dispersions: Strategies and Mechanisms. *Pharmaceutical Research* **2011,** *28* (10), 2353-2378.

72. Augustijns, P.; Brewster, M. E., Supersaturating Drug Delivery Systems: Fast is Not Necessarily Good Enough. *Journal of Pharmaceutical Sciences* **2012,** *101* (1), 7-9.

73. Sun, D. D.; Lee, P. I., Haste Makes Waste: The Interplay Between Dissolution and Precipitation of Supersaturating Formulations. *The AAPS Journal* **2015,** *17* (6), 1317-1326.

74. Descamps, M.; Willart, J. F., Perspectives on the amorphisation/milling relationship in pharmaceutical materials. *Adv Drug Deliv Rev* **2016,** *100*, 51-66.

75. Nart, V.; Franca, M. T.; Anzilaggo, D.; Riekes, M. K.; Kratz, J. M.; de Campos, C. E.; Simoes, C. M.; Stulzer, H. K., Ball-milled solid dispersions of BCS Class IV drugs: Impact on the dissolution rate and intestinal permeability of acyclovir. *Mater Sci Eng C Mater Biol Appl* **2015,** *53*, 229-38.

76. Kang, N.; Lee, J.; Choi, J. N.; Mao, C.; Lee, E. H., Cryomilling-induced solid dispersion of poor glass forming/poorly water-soluble mefenamic acid with polyvinylpyrrolidone K12. *Drug Dev Ind Pharm* **2015,** *41* (6), 978-88.

77. Wlodarski, K.; Tajber, L.; Sawicki, W., Physicochemical properties of direct compression tablets with spray dried and ball milled solid dispersions of tadalafil in PVP-VA. *Eur J Pharm Biopharm* **2016,** *109*, 14-23.

78. Tiwari, R. V.; Patil, H.; Repka, M. A., Contribution of hot-melt extrusion technology to advance drug delivery in the 21st century. *Expert Opin Drug Deliv* **2016,** *13* (3), 451-64.

79. Thiry, J.; Krier, F.; Evrard, B., A review of pharmaceutical extrusion: critical process parameters and scaling-up. *Int J Pharm* **2015,** *479* (1), 227-40.

80. Vynckier, A. K.; Lin, H.; Zeitler, J. A.; Willart, J. F.; Bongaers, E.; Voorspoels, J.; Remon, J. P.; Vervaet, C., Calendering as a direct shaping tool for the continuous production of fixed-dose combination products via co-extrusion. *European Journal of Pharmaceutics and Biopharmaceutics* **2015,** *96*, 125-131.

81. Stankovic, M.; Frijlink, H. W.; Hinrichs, W. L., Polymeric formulations for drug release prepared by hot melt extrusion: application and characterization. *Drug Discov Today* **2015,** *20* (7), 812-23.

82. Vynckier, A. K.; Dierickx, L.; Voorspoels, J.; Gonnissen, Y.; Remon, J. P.; Vervaet, C., Hot-melt co-extrusion: requirements, challenges and opportunities for pharmaceutical applications. *J Pharm Pharmacol* **2014,** *66* (2), 167-79.

83. Qi, S.; Craig, D., Recent developments in micro- and nanofabrication techniques for the preparation of amorphous pharmaceutical dosage forms. *Adv Drug Deliv Rev* **2016,** *100*, 67-84.

84. Alhnan, M.A.; Okwuosa, T. C.; Sadia, M.;Wan, K.W.; Ahmed, W.; Arafat, B., Emergence of 3D Printed Dosage Forms: Opportunities and Challenges. *Pharm Res* **2016,** *33* (8), 1817-1832

85. Long, J.; Gholizadeh, H.; Lu, J.; Bunt, C.; Seyfoddin, A., Review: Application of Fused Deposition Modelling (FDM) Method of 3D Printing in Drug Delivery. *Curr Pharm Des* **2016**.

86. Paudel, A.; Worku, Z. A.; Meeus, J.; Guns, S.; Van den Mooter, G., Manufacturing of solid dispersions of poorly water soluble drugs by spray drying: Formulation and process considerations. *International Journal of Pharmaceutics* **2013,** *453* (1), 253-284.

87. Singh, A.; Van den Mooter, G., Spray drying formulation of amorphous solid dispersions. *Adv Drug Deliv Rev* **2016,** *100*, 27-50.

88. Kolakovic, R.; Viitala, T.; Ihalainen, P.; Genina, N.; Peltonen, J.; Sandler, N., Printing technologies in fabrication of drug delivery systems. *Expert Opin Drug Deliv* **2013,** *10* (12), 1711-23.

89. Nguyen, D. N.; Clasen, C.; Van den Mooter, G., Pharmaceutical Applications of Electrospraying. *J Pharm Sci* **2016,** *105* (9), 2601-20.

90. Six, K.; Daems, T.; de Hoon, J.; Van Hecken, A.; Depre, M.; Bouche, M.-P.; Prinsen, P.; Verreck, G.; Peeters, J.; Brewster, M. E.; Van den Mooter, G., Clinical study of solid dispersions of itraconazole prepared by hot-stage extrusion. *European Journal of Pharmaceutical Sciences* **2005,** *24* (2–3), 179-186.

91. Mellaerts, R.; Mols, R.; Jammaer, J. A. G.; Aerts, C. A.; Annaert, P.; Van Humbeeck, J.; Van den Mooter, G.; Augustijns, P.; Martens, J. A., Increasing the oral bioavailability of the poorly water soluble drug itraconazole with ordered mesoporous silica. *European Journal of Pharmaceutics and Biopharmaceutics* **2008,** *69* (1), 223-230.

92. Van Eerdenbrugh, B.; Van Speybroeck, M.; Mols, R.; Houthoofd, K.; Martens, J. A.; Froyen, L.; Van Humbeeck, J.; Augustijns, P.; Van den Mooter, G., Itraconazole/TPGS/Aerosil®200 solid dispersions: Characterization, physical stability and in vivo performance. *European Journal of Pharmaceutical Sciences* **2009,** *38* (3), 270-278.

93. Muschert, S.; Siepmann, F.; Cuppok, Y.; Leclercq, B.; Carlin, B.; Siepmann, J., Improved long term stability of aqueous ethylcellulose film coatings: importance of the type of drug and starter core. *Int J Pharm* **2009,** *368* (1-2), 138-45.

94. Nollenberger, K.; Albers, J., Poly(meth)acrylate-based coatings. *International Journal of Pharmaceutics* **2013,** *457* (2), 461-469.

95. Kolter, K.; Dashevsky, A.; Irfan, M.; Bodmeier, R., Polyvinyl acetate-based film coatings. *International Journal of Pharmaceutics* **2013,** *457* (2), 470-479.

96. Siepmann, F.; Siepmann, J.; Walther, M.; MacRae, R. J.; Bodmeier, R., Polymer blends for controlled release coatings. *Journal of Controlled Release* **2008,** *125* (1), 1-15.

97. Gallardo, D.; Skalsky, B.; Kleinebudde, P., Controlled release solid dosage forms using combinations of (meth)acrylate copolymers. *Pharm Dev Technol* **2008,** *13* (5), 413-23.

98. Szafran, R. G., Fluid-Bed Technology for Encapsulation and Coating Purposes. In *Encapsulation Nanotechnologies*, John Wiley & Sons, Inc.: **2013**; pp 71-105.

99. Dixit, R.; Puthli, S., Fluidization technologies: Aerodynamic principles and process engineering. *J Pharm Sci* **2009,** *98* (11), 3933-60.

100. Ayenew, Z.; Paudel, A.; Van den Mooter, G., Can compression induce demixing in amorphous solid dispersions? A case study of naproxen-PVP K25. *Eur J Pharm Biopharm* **2012,** *81* (1), 207-13.

101. Yang, Z.; Nollenberger, K.; Albers, J.; Craig, D.; Qi, S., Molecular indicators of surface and bulk instability of hot melt extruded amorphous solid dispersions. *Pharm Res* **2015,** *32* (4), 1210-28.

102. Garbacz, G.; Klein, S., Dissolution testing of oral modified-release dosage forms. *Journal of Pharmacy and Pharmacology* **2012,** *64* (7), 944-968.

103. Baird, J. A.; Taylor, L. S., Evaluation of amorphous solid dispersion properties using thermal analysis techniques. *Advanced Drug Delivery Reviews* **2012,** *64* (5), 396-421.

104. Thakral, S.; Terban, M. W.; Thakral, N. K.; Suryanarayanan, R., Recent advances in the characterization of amorphous pharmaceuticals by X-ray diffractometry. *Advanced Drug Delivery Reviews* **2016,** *100*, 183-193.

105. Paudel, A.; Raijada, D.; Rantanen, J., Raman spectroscopy in pharmaceutical product design. *Advanced Drug Delivery Reviews* **2015,** *89*, 3-20.

106. Croker, D. M.; Hennigan, M. C.; Maher, A.; Hu, Y.; Ryder, A. G.; Hodnett, B. K., A comparative study of the use of powder X-ray diffraction, Raman and near infrared spectroscopy for quantification of binary polymorphic mixtures of piracetam. *Journal of Pharmaceutical and Biomedical Analysis* **2012,** *63*, 80-86.

107. Grzybowska, K.; Capaccioli, S.; Paluch, M., Recent developments in the experimental investigations of relaxations in pharmaceuticals by dielectric techniques at ambient and elevated pressure. *Advanced Drug Delivery Reviews* **2016,** *100*, 158-182.

108. Sibik, J.; Zeitler, J. A., Direct measurement of molecular mobility and crystallisation of amorphous pharmaceuticals using terahertz spectroscopy. *Advanced Drug Delivery Reviews* **2016,** *100*, 147-157.

109. Paudel, A.; Geppi, M.; Van den Mooter, G., Structural and Dynamic Properties of Amorphous Solid Dispersions: The Role of Solid- State Nuclear Magnetic Resonance Spectroscopy and Relaxometry. *Journal of pharmaceutical sciences* **2014,** *103* (9), 2635-2662.

110. Kazarian, S. G.; Ewing, A. V., Applications of Fourier transform infrared spectroscopic imaging to tablet dissolution and drug release. *Expert Opin Drug Deliv* **2013,** *10* (9), 1207-21.

111. Haaser, M.; Gordon, K. C.; Strachan, C. J.; Rades, T., Terahertz pulsed imaging as an advanced characterisation tool for film coatings--a review. *Int J Pharm* **2013,** *457* (2), 510-20.

112. Tres, F.; Treacher, K.; Booth, J.; Hughes, L. P.; Wren, S. A. C.; Aylott, J. W.; Burley, J. C., Real time Raman imaging to understand dissolution performance of amorphous solid dispersions. *Journal of Controlled Release* **2014,** *188*, 53-60.

113. Lauer, M. E.; Grassmann, O.; Siam, M.; Tardio, J.; Jacob, L.; Page, S.; Kindt, J. H.; Engel, A.; Alsenz, J., Atomic force microscopy-based screening of drug-excipient miscibility and stability of solid dispersions. *Pharm Res* **2011,** *28* (3), 572-84.

114. Meeus, J.; Chen, X.; Scurr, D. J.; Ciarnelli, V.; Amssoms, K.; Roberts, C. J.; Davies, M. C.; van Den Mooter, G., Nanoscale surface characterization and miscibility study of a spray-dried injectable polymeric matrix consisting of poly(lactic-co-glycolic acid) and polyvinylpyrrolidone. *J Pharm Sci* **2012,** *101* (9), 3473-85.

115. Van Eerdenbrugh, B.; Lo, M.; Kjoller, K.; Marcott, C.; Taylor, L. S., Nanoscale mid-infrared imaging of phase separation in a drug-polymer blend. *J Pharm Sci* **2012,** *101* (6), 2066-73.

116. Barnes, T. J.; Kempson, I. M.; Prestidge, C. A., Surface analysis for compositional, chemical and structural imaging in pharmaceutics with mass spectrometry: A ToF-SIMS perspective. *International Journal of Pharmaceutics* **2011,** *417* (1–2), 61-69.

Chapter 2: Objectives

After more than fifty years of extensive research into solid dispersions, the enabling strategy for poorly soluble drugs still faces tough challenges. Despite its tremendous potential to enhance solubility and dissolution rate, a limited number of solid dispersions are on the market today. Amongst the primary reasons for this restricted output are poor stability and the inability to maintain supersaturated drug concentrations for extended periods of time.

Some of the known causes for instability can be bypassed by using fluid bed coating. This solid dispersion production method has long been overlooked in solid dispersion research, despite being used in the successful production of one marketed solid dispersion (Sporanox®). This manufacturing technique has some advantages over other solvent methods: efficient drying post production inside the device, no additional stress inducing processing steps and protection from surface crystallization by adding a protective coating layer.

Although the dissolution behaviour of coated solid dispersions on inert carriers has been investigated, very few research efforts have been put into the investigation of its phase behaviour. For this reason, the **first objective** of this thesis is the development of an mDSC method for the characterization of indomethacin-PVP glass solutions layered on inert carriers.

In order to control and optimize the drug release behaviour of these coated glass solutions, an additional controlled release coating layer was added. The **second objective** was to investigate the phase behaviour of these complex coated systems, which make use of two different controlled release polymers. Additionally, the influence of a pore former and coating from a solution or a dispersion on the phase behaviour was investigated. A complete phase behaviour analysis is made possible by combining surface characterization (ToF-SIMS) and bulk characterization (mDSC and XRPD).

The **third objective** focused on the pharmaceutical performance of these multilayer coatings. The influence of the aforementioned formulation changes and the controlled release coating thickness on the drug release behaviour was investigated and special emphasis was put on the role of a charge interaction between drug and controlled release polymer on the release rate.

Controlled release polymers are not only investigated as a rate controlling membrane on top of glass solutions, their potential role as a solid dispersion carrier is assessed as well. So, in the **fourth objective** of this thesis, Eudragit® RL is tested as an alternative carrier for solid dispersions, either alone or in combination with a hydrophilic polymer in order to enhance drug bio-availability. For the manufacturing of these drug delivery systems, spray drying will be used. The phase behaviour of the solid dispersions will be investigated together with the dissolution rate, with special attention to the generation of supersaturation.

Throughout this work different model drugs have been used. The main API, recurring in all chapters, is indomethacin, which is a non-steroidal anti-inflammatory drug (NSAID) which is poorly soluble (in acidic media), weakly acidic, and has the potential to form interactions with solid dispersion carriers through its carboxyl function. Results obtained with indomethacin are compared with naproxen (NSAID, poorly soluble, weak acid) and ketoconazole (anti-fungal, poorly soluble, weak base) in Chapter 3, and with naproxen and cinnarizine (anti-histaminic drug, poorly soluble, weak base) in Chapter 6.

Chapter 3: The peculiar behavior of the glass transition temperature of amorphous drug-polymer films coated on inert sugar spheres

Results of this chapter are based on:

Dereymaker, A.; Van den Mooter, G. The Peculiar Behavior of the Glass Transition Temperature of Amorphous Drug–Polymer Films Coated on Inert Sugar Spheres. J. Pharm. Sci. ***2015****, 104, 1759-1766.*

3.1 Abstract

Fluid bed coating has been proposed in the past as an alternative technology for manufacturing of drug-polymer amorphous solid dispersions, or so-called glass solution. It has the advantage of being a one step process, and thus omitting separate drying steps, addition of excipients or manipulation of the dosage form. In search of an adequate sample preparation method for mDSC analysis of beads coated with glass solutions, glass transition broadening and decrease of the glass transition temperature was observed with increasing particle size of crushed coated beads and crushed isolated films of indomethacin and polyvinylpyrrolidone. Substituting indomethacin with naproxen gave comparable results. When ketoconazole was probed or the solvent in INDO-PVP films was switched to DCM or a methanol-DCM mixture, two distinct T_g regions were observed. Particles with small sizes had a glass transition in the high T_g region, large sized particles in the low T_g region. This particle size dependent glass transition was ascribed to different residual solvent amounts in the bulk and at the surface of the particles. A correlation was observed between the deviation of the glass transition temperature from that calculated from the Gordon-Taylor equation and the amount of residual solvent at the glass transition temperature of particles with different sizes.

3.2 Introduction

Solid dispersions are considered to be one of the promising formulation strategies to increase the solubility and bioavailability of poorly soluble active pharmaceutical ingredients (API).[1] Despite being reported for the first time over 40 years ago[2], only a limited number of approved drug formulations are on the market today.[3] While there are many subdivisions of solid dispersions, attention nowadays is focused on glass solutions where the drug is molecularly dispersed into an amorphous carrier (mostly polymers), resulting in a one phase system.[4,5] Because solid dispersion manufacturing often leads to supersaturated glass solutions which are in thermodynamical non-equilibrium, risks of phase separation into drug rich and polymer rich regions are constantly present, which can ultimately lead to crystallization of the API and the subsequent loss of its solubility advantage.[6] Phase separation risk can even be increased by absorption or adsorption of water from the environment, residual solvent or manipulations of the glass solutions into final dosage forms.

In addition to spray drying as a well-established manufacturing procedure for glass solutions via the solvent method, fluid bed coating can be proposed as a viable alternative. As compared to spray drying, fluid bed coating is a largely unexplored manufacturing method and has numerous potential advantages. It allows the formulation to be dried immediately into the coating device. This is very important to remove residual solvents from the system, because these are often toxic and can cause unwanted plasticization of the system. Also, the coating of beads omits any additional processing steps, like milling or compression, to acquire a final dosage form. These additional processing steps have been shown to lead to solid state changes, for example compression which induced amorphous-amorphous phase separation in spray dried solid dispersions.[7]

Few studies have been previously reported in literature, mostly emphasizing on the solubility advantage of the solid dispersions prepared by coating in comparison with the pure drug substance. However, a thorough understanding of the physical structure and phase behavior is of the utmost importance for the estimation of the stability of the produced solid dispersions. To analyze this phase behavior, differential scanning calorimetry (DSC) is one of the tools of choice. It is able to detect the most important markers of instability in solid dispersions, namely amorphous-amorphous phase separation, enthalpic recovery of amorphous materials and the presence of crystalline API. Due to solid dispersions being multi-

component systems and the production method, some transitions can overlap in a standard DSC. In modulated differential scanning calorimetry (mDSC), where the total heat flow can be mathematically separated (a deconvolution operation) into a reversing heat flow (a measure of the sample's heat capacity) and a non-reversing heat flow signal (heat flow associated with kinetic or kinetically controlled processes), these overlapping transitions can be clearly distinguished. For example, when preparing solid dispersions using the solvent evaporation method, some residual solvent can remain present in the system, upon evaporation due to heating in the DSC. This will be visible in the thermogram as a broad endotherm masking all other thermal events (glass transition). Due to the kinetic nature of solvent evaporation, this will be explicitly visible into the non-reversing heat flow signal in mDSC, provided a well optimized modulation program.

When glass solutions are produced, they are monophasic systems which will show one single glass transition, showing full miscibility of polymer and API. One of the most commonly used ways to calculate this mix-T_g is by using the Gordon-Taylor equation8:

$$T_g = \frac{w_1 T_{g1} + k_{GT}(1-w_1) T_{g2}}{w_1 + k_{GT}(1-w_1)} \qquad \text{Eq. 3.1}$$

In this equation: $T_{g1} \leq T_{g2}$ so T_{g1} usually represents the glass transition of the drug and T_{g2} the glass transition of the polymer. w is the weight fraction and the constant $k_{GT} = \frac{\rho_1 \Delta\alpha_1}{\rho_2 \Delta\alpha_2} \approx \frac{\rho_1 T_{g1}}{\rho_2 T_{g2}}$ [9], where ρ is the density of the component and Δ α the change in thermal expansivity of the component at T_g .[10]

In previously performed studies involving coated solid dispersions onto inert carriers, a lot of variation is seen in methodology of DSC/mDSC analysis. Hsiu-O et al.[11] and Zhang et al.[12] performed DSC analysis with the coated pellets loaded as such into the aluminium pans. Sun et al. did not analyze the produced solid dispersions with DSC.[13] In the study of Li et al. solid dispersion samples were prepared by spraying into the drying chamber without sugar pellets under the same coating conditions, and then the solid dispersions were peeled off carefully and ground to a fine powder for DSC analysis.[14] Nikowitz et al. did not specify any DSC sample preparation method in their paper about the study of recrystallization in coated pellets.[15] Lastly, in a recent study of Mahmoudi et al. amorphous solid drug dispersions were prepared via either rotary evaporation or fluid bed drug layering. Only powder samples from the rotary evaporation were analyzed by DSC.[16]

The aim of this study is to develop a reliable mDSC method for glass solutions, coated on an inert carrier, and the investigation of an interesting glass transition phenomenon associated with this method development.

Naproxen (NAP), indomethacin (INDO) and ketoconazole (KETO) were used as model drugs. Polyvinylpyrrolidone (PVP) K25 was selected as a model hydrophilic polymer. NAP and INDO both have hydrogen donors which can form hydrogen bonds with PVP, whereas KETO is unable to form hydrogen bonds with the polymer. NAP-PVP and INDO-PVP are well known solid dispersion systems which have been extensively studied in the past.[17-21]

3.3 Materials and methods

3.3.1 Materials

Naproxen and Indomethacin were purchased from FAGRON Ltd. (Waregem, Belgium), ketoconazole was a kind gift from Janssen Pharmaceutica (Beerse, Belgium), polyvinylpyrrolidone K 25 was a generous gift from BASF (Ludwigshafen, Germany). Sugar spheres (diameter 710 - 850 µm) were kindly donated by Hanns G. Werner GmbH (Tornesch, Germany).

3.3.2 Methods

Fluidized bed coating

A 30-70% IND-PVP (1:2 weight ratio to beads) glass solution was coated onto 500g of beads from a 6.67% (w/v) ethanol solution, using bottom spray fluid bed coating. The sugar spheres were loaded into the preheated coating chamber of an Aeromatic MP 1 multiprocessor (GEA, Switzerland). The sugar beads were heated for half an hour. The drug-polymer solution was coated onto the sugar beads using a bottom spray set-up with a Würster insert. When the spraying was finished, the pellets were dried until immobilization due to electrostatic charges. The coated spheres where unloaded, weighed and dried for an additional 48 hours in an oven at 40°C. In the formation of the INDO-PVP beads, the air volume was set at 1566.3L/min, inlet temperature was 50°C, atomizing air pressure 1.5 bar and the feed rate was 6 ml/min. After 48 hours of drying in a hot air oven at 40°C, sugar beads were crushed with a pestle in a mortar and sieved into different particle size ranges.

Film formation by rotary evaporation

Glass solution films were made using a Büchi Rotavapor R-210 (Flawil, Switzerland). API-polymer (30-70% w-w) was dissolved into a common solvent (ethanol, Dichloromethane (DCM) or a 1:1 (v/v) mixture of DCM and methanol) to form a 10% (w/v) solution. The water bath was set to 60°C for ethanol solutions and 40°C for DCM and DCM-methanol solutions. A round bottom flask with the solution was rotated into the water bath under vacuum. After formation of a film, the glass solution was dried for an additional 48 hours in an oven at 40°C. In accordance with the coated beads, the films were crushed and sieved in different particle size ranges for analysis.

Modulated temperature differential scanning calorimetry (mDSC)

mDSC measurements were carried out with a TA instruments Q2000 modulated DSC (Leatherhead, UK) equipped with a refrigerated cooling system (RCS90). During analysis, the DSC cell was purged with a nitrogen flow of 50 ml/min. Mathematical analysis of the data was performed using TA Instruments Universal Analysis software (version 4.4, Leatherhead, UK). TA Instruments standard aluminium pans (Brussels, Belgium) were used for all measurements. Glass transition temperatures were measured at half height in the reversing heat flow. The step jump in heat capacity observed in the reversing heat flow signal was further examined in the corresponding derivative signal after Savitsky-Golay smoothing with points of window set at 20. The first derivative of the reversing heat flow was chosen to visualize the glass transitions because discrete changes are much better visible in the peaks of the derivative reversing heat flow, as compared with the small baseline shifts of the original reversing heat flow. Octadecane and indium were used to calibrate the DSC temperature scale, the enthalpic response was calibrated with indium. The heat capacity was calibrated using sapphire disks. All sample masses were between 4-7 mg (accurately weighed). The samples were kept isothermal at 40°C for 60 minutes, followed by heating from 40°C to 180°C (or 0-200°C depending on the experiment) for the glass solution films and 0°C to 165°C for the coated beads. A heating rate of 2°C/min was applied with a temperature modulation of 0.636°C every 40s. All samples were measured in duplicate.

Thermo gravimetric Analysis

The prepared samples (coated beads and films, crushed and sieved) were analyzed using a TA instruments SDT Q600 (Leatherhead, UK) to determine moisture and volatile contents. The samples were heated at 5°C/min from 25 °C to 150 °C in a continuous mode in a first type of experiment. In the second type of experiment, samples were kept isothermal at 50°C for 20 hours, heated to 140°C at 10°C/min and kept isothermal for 2 hours, and finally cooled again to 50°C at 10°C/min and kept isothermal for 1 hour. Finally, in a third experiment samples were kept isothermal at 40°C for 1 hour and subsequently heated at 2°C per minute to 170°C. A dry N_2 purge of 100 mL/min was used to be able to maintain an inert environment. Weight loss due to solvent and moisture evaporation was calculated as percentage weight loss compared to the original sample mass. Sample masses are between 10 and 20 mg (accurately weighed).

3.4 Results and discussion

3.4.1 mDSC analysis of INDO-PVP (30/70% w/w) glass solutions, coated onto sugar beads

As mentioned above, no universally applicable sample preparation method exists for the DSC analysis of coated beads. In search of effective sample preparation for mDSC analysis, the bottom of a DSC pan was filled with coated beads and analyzed. This approach produced no visible signal other than the melting peak of sucrose. It was clear that the contact area between the coating and the bottom of the pan was insufficient. In a second attempt, beads were crushed to improve thermal contact. However, the only visible transition was the melting of the sucrose beads, leading to the observation that there was, proportionally, too much sucrose present. In a next step, beads were crushed gently with a pestle and mortar and sieved to separate different particle sizes in an attempt to find a specific particle size range where more coating was present relative to the sucrose content. This sieving was performed using seven sieves (pore diameter: 32µm, 63µm, 90µm, 150µm, 250µm and 355µm). After sieving for an adequate time the material on top was discarded (larger than 355µm), the other material was collected and stored separately for each particle size range. Subsequently, six different particle size ranges were stored in closed containers: 0-32µm, 32-63µm, 63-90µm, 90-150µm, 150-250µm and 250-355µm. Figure 3.1 shows the first derivate of the reversing heat flow in function of temperature for the different particle sizes of crushed and sieved INDO-PVP beads.

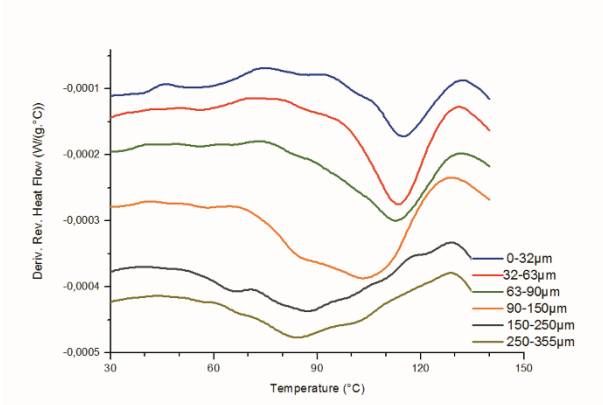

Figure 3.1: Derivative reversing heat flow in function of temperature for different particle size ranges of crushed and sieved INDO-PVP (30/70% w/w) coated sucrose beads.

Surprisingly, the data show a shift and broadening of the glass transition region with increasing particle size. Table 3.1 lists the numerical values of the mean glass transition onset, offset, range and half-height temperature of 3 replicate experiments. There is a difference of

26.2°C between mean glass transition temperature of the smallest and largest particle size range. The glass transition range has also increased with ca. 18°C, which means the mean width has become more than doubled, hence a large broadening of the glass transition region. This glass transition shift is probably also the reason why it only becomes visible in DSC after sieving. When the beads are only crushed, there is a large particle size variety present, so the sample will have multiple small glass transitions which will lead to a very broad signal in the reversing heat flow, which is not detectable by mDSC.

Table 3.1: Mean glass transition onset, offset, range and half-height temperature of different particle size ranges of INDO-PVP coatings onto sucrose beads (n=3).

n=3	***Glass transition temperature (°C)***				
Particle size (µm)	**Onset**	**Offset**	**Range**	**Half Height**	**St dev Half Height**
0-32	105.9	122.6	16.7	**114.2**	0.7
32-63	104.8	121.2	16.4	**113.0**	0.8
63-90	101.8	123.3	21.5	**112.4**	2.9
90-150	84.1	116.0	31.9	**100.0**	0.4
150-250	69.3	108.6	39.3	**89.1**	2.2
250-355	70.4	105.4	34.9	**88.0**	0.2

3.4.2 mDSC analysis of INDO-PVP (30/70% w/w) glass solution films

To confirm this particle size induced glass transition temperature decrease and broadening in a more simple formulation, INDO-PVP films were made by rotary evaporation. In essence, this is the way the glass solutions are formed on the sucrose beads during fluid bed coating. Droplets form miniature films around the inert carrier and are dried during cycling in the fluidized bed. When reentering the Würster insert and being sprayed upon, this process repeats itself. Derivative reversing heat flow signals in function of temperature for the different particle size ranges are shown in Figure 3.2 for a first and second heating cycle. After the first heating cycle is completed, the sample is cooled at maximum capacity of the Q2000 DSC (around 30°C/min). After temperature equilibration at 0°C the second heating cycle is initiated with the same heating rate and modulation parameters used during first heating.

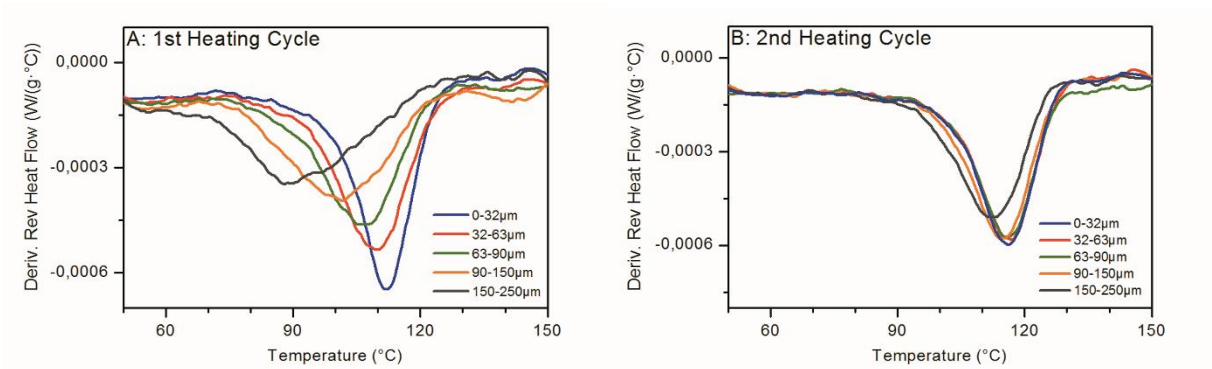

Figure 3.2: Derivative reversing heat flow in function of temperature for INDO-PVP films in the first 5 (A) and second (B) heating cycle for different particle sizes.

All numerical information about the glass transition is given in Table 3.2. From the INDO-PVP films, it's also evident that T_g shifts to lower temperatures and broadens as the particle size increases. There is an 18.4°C difference in temperature shift and a 16.6°C broadening between the values of the smallest and largest particle size. These differences disappear respectively to 3.6°C and 1.9°C when the sample is cooled and reheated.

Table 3.2: Mean glass transition onset, offset, range and half-height temperature of different particle size ranges of INDO-PVP films in first and second heating cycle (n=3).

1st heating cycle	***Glass transition temperature (°C)***				
Particle size (µm)	**Onset**	**Offset**	**Range**	**Half Height**	**St dev Half Height**
0-32	104.0	118.7	14.7	**111.3**	0.1
32-63	101.6	119.6	18.0	**108.9**	1.0
63-90	94.4	116.3	21.8	**105.4**	0.6
90-150	87.3	113.8	26.5	**100.6**	0.3
150-250	77.2	108.5	31.3	**93.0**	0.6
2nd heating cycle	***Glass transition temperature (°C)***				
Particle size (µm)	**Onset**	**Offset**	**Range**	**Half Height**	**St dev Half Height**
0-32	107.3	123.1	15.9	**115.2**	0.6
32-63	107.7	123.2	15.4	**115.5**	0.1
63-90	106.8	122.9	16.0	**114.8**	0.3
90-150	105.9	122.3	16.3	**114.0**	0.4
150-250	102.8	120.5	17.7	**111.6**	0.0

The dependence of the glass transition temperature on the particle size has, to the best of our knowledge, never been reported before. Contrary to the well-known melting point depression related to particle size reduction[22], there is no fundamental physical phenomenon known to explain the dependence of the glass transition temperature on the particle size.[21] The trend observed in the coated beads was thus confirmed and even more pronounced in

the glass solution films. Furthermore, when samples are cooled and reheated in the mDSC, all differences virtually disappear. These observations lead to two possible explanations. First, there can be a difference in mixing for different particle sizes. When a particle with a larger size would have a higher ratio of indomethacin compared to the particles with smaller size, the glass transition would be lower. This could be seen as different phases in different particle sizes. However, this would be highly unlikely because the films are prepared from a solution where drug and polymer are fully dissolved. It is evenly unlikely that these different drug-polymer ratios are induced while crushing the films or beads because the samples are crushed with the same intensity and during the same amount of time. A second hypothesis can be proposed where different particle sizes have different amounts of residual solvents, which can act as a plasticizer and thus cause a decrease in glass transition temperature of the system.

The heat-cool-heat experiment cannot exclude one of the hypotheses. Residual solvent will be completely removed when heating up to 180°C and plasticizing effects of these solvents will be eliminated when the sample is reheated. However heating above the glass transition also increases the mobility of the (amorphous) drug and polymer, which can affect the mixing of drug and polymer, also eliminating the observed differences in the first heating step.

Previous studies provide the data to calculate the glass transition temperature of glass solutions with the Gordon-Taylor equation for this drug-polymer system. Glass transition temperature (430 K) and density (1.14 g/cm³) for PVP K25 are taken from Paudel et al.[17], glass transition temperature (315 K) and density (1.31 g/cm³) of indomethacin from Matsumoto and Zografi[21]. Calculation yielded a glass transition temperature of the glass solution of 118°C. Glass transitions of the second heating cycles are closest to this ideal mixing T_g. The reason is of course that in the second heating cycle most of the residual solvents (which act as plasticizer) are eliminated from the glass solutions and not that the system is approaching ideal behavior (as the values are close to those calculated from the Gordon-Taylor equation in the second heating cycle). When considering the first heating cycle, particles with the smallest size have a glass transition temperature closest to 118°C, which points out that at the glass transition, the smallest particles contain the least residual solvent.

Different observations were made when the same film fragments, divided in different size ranges, were stored at room temperature for 7 weeks and reanalyzed with mDSC. The thermograms of the different particle size ranges are shown in Figure 3.3. The observed glass

transition shift observed in the initial thermogram, has now disappeared. Only the particles with the largest size still show a decrease in T_g.

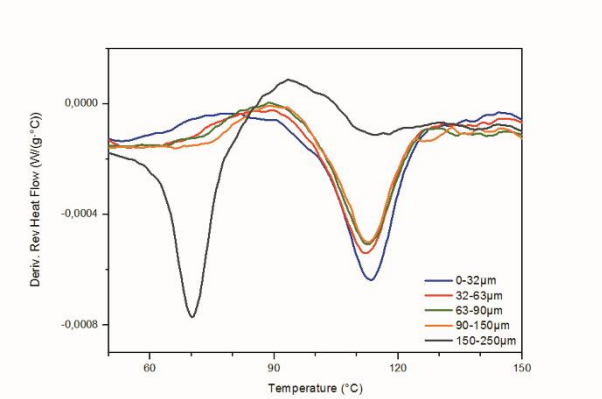

Figure 3.3: Derivative reversing heat flow in function of temperature for different particle size INDO-PVP films after storage at room temperature for 7 weeks.

Storage at room temperature can enable the samples to further dry and get rid of the residual solvents, but storage at room temperature, which is far below the glass transition temperature of the glass solutions, does not provide the necessary mobility to spontaneously induce mixing of the systems. It can be reasonably assumed that larger particles, which have a much smaller surface area to mass ratio, and thus contact surface with the surroundings (air), need a longer time to lose their residual solvent. This is the reason why the particles with the largest size range still have a decreased glass transition temperature. This experiment thus reinforces the residual solvent hypothesis.

3.4.3 mDSC analysis of glass solution films of Naproxen-PVP and Ketoconazole-PVP (30-70% w-w)

In order to confirm the generality of the observed phenomenon, systems with a different API (Naproxen and Ketoconazole) were selected and compared with the same polymer and in the same ratio to solely investigate the influence of changing the active component. Ketoconazole was chosen because, contrary to INDO and NAP, it does not have any hydrogen donor groups and is thus unable to form hydrogen bonds with PVP. Figure 3.4 shows the derivative of the reversing heat flow for NAP-PVP (30-70% w/w) and KETO-PVP (30-70% w/w) in function of temperature for 5 different particle size ranges.

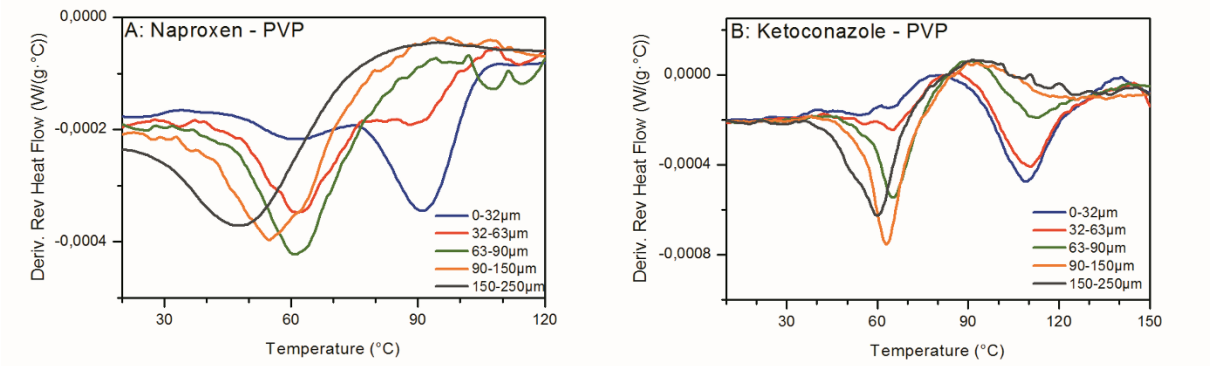

Figure 3.4: Derivative reversing heat flow thermogram of NAP-PVP (A) and KETO-PVP (B) for 5 different particle sizes.

The different particle sizes for the NAP-PVP glass solution again show a distinct glass transition decrease for increasing particle size, although this decrease is mainly observed between the two smallest particle sizes, further decrease is more discrete. KETO-PVP shows a different pattern, as in these glass solution particles, two different glass transition regions can be distinguished. Particles with smaller sizes (0-32µm and 32-63µm) predominantly reside in the high T_g region, around 115-120°C. Particles with larger sizes (150-250µm and 250-355µm) are mainly in the low T_g region, around 60-70°C. The particles with an intermediate size range (between 63-90µm) have two T_g peaks, one in each region.

While the NAP-PVP samples confirmed the trend observed with the INDO-PVP samples, KETO-PVP showed a slightly different behavior, though still a particle size dependent glass transition temperature.

For the calculation of the Gordon-Taylor equation, glass transition temperature (279K) and density (1.25 g/cm³) of naproxen are taken from Paudel et al.[17] and T_g (317.5K) and density (1.30g/cm³) of ketoconazole from Van den Mooter et al.[23] Glass transition temperature for naproxen is calculated at 100°C and for ketoconazole at 119°C. It is again obvious that glass transitions from the smallest particles are closest to the calculated mixing T_g, thus reinforcing again the role of the available surface area for solvent evaporation.

3.4.4 mDSC analysis of INDO-PVP (30/70% w/w) glass solution films from a 10% (w/v) DCM and DCM-methanol (50-50% v-v) solution

To investigate the influence of different solvents on the phase behavior and resulting glass transition decrease with particle size, ethanol as solvent was replaced by dichloromethane and a 1:1 mixture of dichloromethane and methanol. For the pure DCM, 5 particle size ranges up to 250µm were tested, for the DCM-methanol mixture 7 particle size ranges were tested, up

to 425µm. Figure 3.5 represents the derivative reversing heat flow in function of temperature for the different particle size ranges of DCM (A) and DCM-methanol (B).

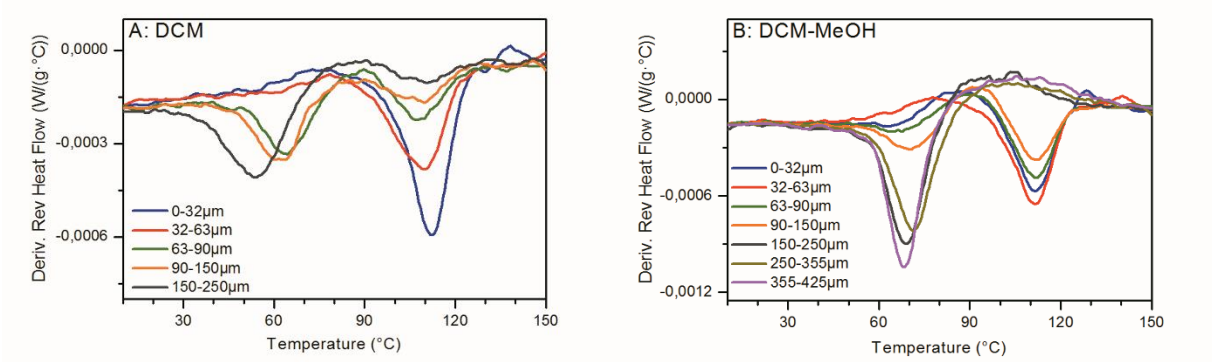

Figure 3.5: Derivative heat flow in function of temperature for the different particle size ranges of a INDO-PVP glass solution film, prepared from a DCM (A) and DCM-Methanol (B) solution.

With the change of solvent, the same phenomenon was observed as in the KETO-PVP glass solutions, produced from an ethanol solution. For DCM as well as DCM-methanol, a distinction can again be made between a high T_g region with predominantly the particles with smaller size ranges on one hand, and a low T_g region with the particles with larger size ranges on the other hand. Intermediate particle size ranges again show a glass transition in the high T_g region as well as in the low T_g region. These experiments show the separation in T_g regions is not a phenomenon that can be solely described to KETO-PVP, but something as simple as a change in solvent can induce this separation.

3.4.5 TGA analysis of INDO-PVP (30-70% w-w) glass solution films

To be able to take into account the role of the residual solvent, present in the film particles, and/or the amount of absorbed water from the environment into the particles, TGA analysis was performed on all of the particle size ranges. Table 3.3 represents the average weight loss of different particle size ranges of INDO-PVP using a heating program of 5°C/min from 25°C to 150°C.

Table 3.3: weight loss (%) for different particle size ranges of INDO-PVP film

INDO-PVP FILMS	**Sample 1**	**Sample 2**	**Mean**
Particle size (µm)	**Weight loss (%)**	**Weight loss (%)**	**Weight loss (%)**
0-32	3.877	4.793	***4.335***
32-63	4.488	4.280	***4.384***
63-90	4.565	4.431	***4.498***
90-150	3.983	4.157	***4.070***
150-250	4.690	4.220	***4.455***

These experiments clearly show a more or less equal amount of solvent in particles of a different size range. This seems to disprove the solvent hypothesis. However, a second TGA analysis was performed on 3 particle sizes of the INDO-PVP films, to differentiate between weight loss sub-T_g (50°C) and above-T_g (140°C). Figure 3.6 represents the weight (%) and temperature (°C) in function of time (min) for 0-32µm, 90-150µm and 250-355µm particles.

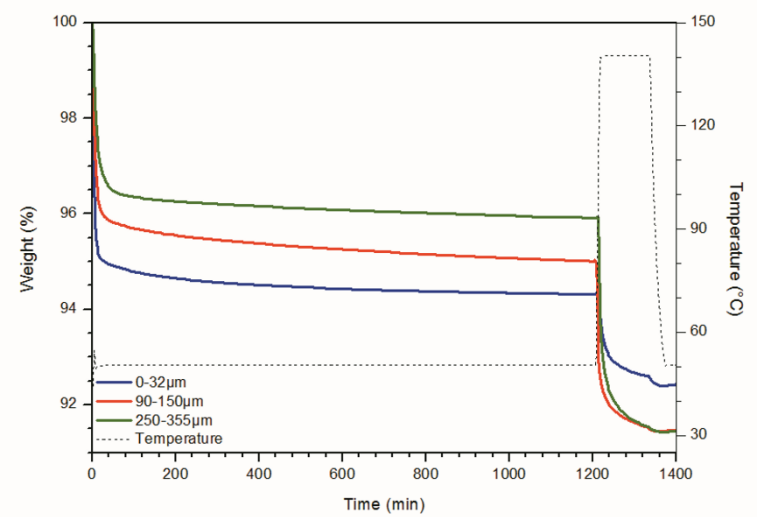

Figure 3.6: Weight (%) and temperature (°C)in function of time (min) for INDO-PVP film particles with a size range of 0-32µm (blue line), 90-150µm (red line) and 250-355µm (green line).

In the first isothermal step at 50°C, the smaller the particles, the more weight is lost due to evaporation of residual solvent, which can be explained by its higher surface area to mass ratio. Despite being dried for 20 hours, all particle size samples still contain residual solvent, which isn't released before heating above the glass transition temperature. After completion of the experiment, particles in the range between 90-150µm and 250-355µm have lost almost exactly the same mass, the 0-32µm particle size range is only slightly higher.

These findings lead to the conclusion that there is a difference in residual solvent amount, but specifications need to be made. The glass transition shift with increasing particle size range is a result of differences in sub-T_g residual solvent evaporation. Due to the much higher surface area to mass ratio of the small particle size ranges, residual solvent can evaporate to a higher extent than from the particles with larger size ranges, where more bulk solvent will be present. When looking at mDSC thermograms with two distinct T_g regions, the high T_g region can be represented by the glass transition of the solvent poor surface of the film particles and the low T_g region by the solvent 'rich' bulk of the film particles. Gradually shifting of the glass transition can be seen as a more discrete transition than separation into two distinct T_g regions. These differences can be achieved during heating in the DSC cell or during the

isothermal step of 40°C for 1 hour, programmed before every run. The fact that this glass transition decrease has disappeared after 7 weeks also supports this hypothesis because here the residual solvent could have had enough time to evaporate, except in the largest particle size range where a T_g decrease is still visible. These findings can shine another light on DSC experiments of solid dispersions, prepared by solvent methods like for instance spray drying, which may contain a very broad range of particle sizes. When only DSC analysis is performed on particles with an intermediate particle size range (see Figures 3.4 and 3.5), two glass transitions may theoretically be observed and falsely interpreted as a phase separated system, which in reality really are particles with different solvent poor surface/solvent rich bulk ratios. The broadening and gradual shift of glass transitions has already been reported before.[24] In this article, this shift and broadening is a result of moisture sorption, which results in a depressed T_g in the outer layers of glassy maltodextrin particles. It can be stated that this effect is in fact a similar phenomenon of what was observed in this article but in the opposite direction.

In an attempt to prove the residual solvent hypothesis, a third TGA experiment was performed where the heating method was equal to the mDSC method, namely an isothermal step at 40°C for 1 hour and subsequently a heating step of 2°C/min to 170°C. When simultaneously performing these TGA and mDSC experiments on a freshly prepared INDO-PVP (30-70% w/w) film (from a 10% ethanol solution w/v), which was crushed and separated into different particle size ranges, it was possible to determine the exact residual solvent amount at the glass transition temperature of the different size ranges. Glass transition temperatures were determined in the mDSC experiment. Previously, the glass transition temperature of INDO-PVP (30-70% w/w) had been calculated using the Gordon-Taylor equation and was 118°C. From this temperature, we can calculate the deviation for each particle size range. This is described in Table 3.4 together with the solvent loss from the glass transition temperature to 170°C for each particle size range.

Table 3.4: Weight loss from the glass transition temperature (%) and Gordon-Taylor T_g temperature depression (%) for the different particle size ranges of INDO-PVP film

INDO-PVP FILM (30-70% w/w)		
Particle size (µm)	**Solvent loss from T_g to 170°C (%)**	**Gordon-Taylor T_g temperature depression (%)**
0-32	1.35	95.29
32-63	1.86	87.40
63-90	2.21	84.54
90-150	2.51	78.07
150-250	2.74	77.65
250-355	3.15	70.77

When the deviation from the Gordon-Taylor temperature is put in function of the solvent loss from T_g to 170°C, a correlation can be found, this is represented in Figure 3.7.

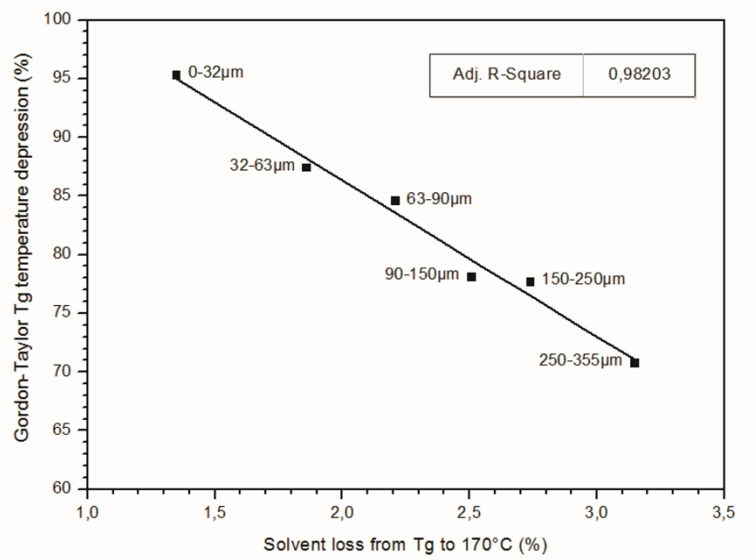

Figure 3.7: Depression on the Gordon-Taylor glass transition temperature in function of solvent loss from the glass transition to 170°C for all different particle size ranges, with trendline and R^2 value.

As can be seen from Figure 3.7, the correlation has a good fit (R^2= 0.983). This indicates that the glass transition temperature decrease with increasing particle size is a result of the presence of the amount of residual solvent at the glass transition temperature, and not of the total amount of residual solvent. The glass transition temperature decrease is not in correspondence with the total amount of residual solvent because of the different evaporation rates, due to the different surface area to mass ratio's, discussed in the previous TGA experiment. This evaporation is an imminent consequence of the manner in which DSC measures the glass transition temperature, namely by heating up the sample. When performing

(m)DSC analysis on glass solutions, prepared by the solvent method, caution is necessary when interpreting glass transitions from particles with wide particle size ranges.

3.5 Conclusions

In search of a suitable mDSC sample preparation method for glass solutions of INDO-PVP, coated on inert carriers, an interesting phenomenon arised. When crushed and sieved into different particle size ranges, glass transitions of the coated beads shifted to lower temperatures and broadened with increasing particle size range. These findings were confirmed for INDO-PVP films prepared by rotary evaporation. Substituting indomethacin with naproxen gave comparable results. When the API was ketoconazole and the solvent in INDO-PVP films was switched to DCM or a methanol-DCM mixture, two distinct T_g regions were observed. Small particle sizes had a glass transition in the high T_g region, large particle sizes in the low T_g region. TGA experiments showed that, while total mass loss due to residual solvent evaporation for all particle sizes are more or less the same, there is a distinct difference for sub T_g and above T_g mass loss, due to huge differences in surface area to mass ratio. Differences in glass transition for different particle size ranges can be ascribed to differences in solvent-free surface and solvent-rich bulk ratios. A correlation was found between the solvent loss from the glass transition temperature on and the deviation from the Gordon-Taylor derived glass transition temperature for the different particle size ranges. This further indicates that the glass transition decrease in glass solution particles with increasing particle size is due to the amount of residual solvent present at the glass transition temperature of the particles.

3.6 References

1. Serajuddin, A. T. M. Solid dispersion of poorly water-soluble drugs: early promises, subsequent problems, and recent breakthroughs. *J Pharm Sci* **1999,** 88, 1058-1066.

2. Sekiguchi, K.; Obi, N. Studies on absorption of eutectic mixture. I. a comparison of the behavior of eutectic mixture of sulfathiazole and that of ordinary sulfathiazole in man. *Chem Pharm Bull* **1961**, 9, 866–872.

3. Huang, Y.; Dai, W. G. Fundamental aspects of solid dispersion technology for poorly soluble drugs. *Acta Pharm Sin B* **2014**, 4, 18-25.

4. Chiou, W.L.; Riegelman, S. Pharmaceutical applications of solid dispersion systems. *J Pharm Sci* **1971**, 60, 1281-1302.

5. Dhirendra, K.; Lewis, S.; Udupa, N.; Atin, K. Solid dispersions: a review. *Pak J Pharm Sci* **2009**, 22, 234-246.

6. Van den Mooter, G. The use of amorphous solid dispersions: a formulation strategy to overcome poor solubility and dissolution rate. *Drug Discov Today Technol* **2012**, 9, e79− e85.

7. Ayenew, Z.; Paudel, A.; Van den Mooter, G. Can compression induce demixing in amorphous solid dispersions? A case study of naproxen-PVP K25. *Eur J Pharm Biopharm* **2012**, 81, 207-213.

8. Gordon, M.; Taylor, J. S. Ideal copolymers and the second-order transitions of synthetic rubbers. I. non-crystalline copolymers. *J Appl Chem* **1952**, 2, 493-500.

9. Simha, R.; Boyer, R. F. On a general relation involving the glass temperature and coefficients of expansion of polymers. *J Chem Phys* **1962**, 37, 1003–1007.

10. Kalogeras, I. M. A novel approach for analyzing glass-transition temperature vs. composition patterns: application to pharmaceutical compound+polymer systems. *Eur J Pharm Sci* **2011**, 42, 470–483.

11. Hsiu-O, H.; Huei-Lin, S.; Tsuimin, T.; Ming-Thau, S. The preparation and characterization of solid dispersions on pellets using a fluidized-bed system. *Int J Pharm* **1996**, 139, 223-229.

12. Zhang, X.; Sun, N.; Wu, B.; Lu, Y.; Guan, T.; Wu, W. Physical characterization of lansoprazole/PVP solid dispersion prepared by fluid-bed coating technique. *Powder Technol* **2008**, 182, 480-485.

13. Sun, N.; Wei, X.; Wu, B.; Chen, J.; Wu, W. Enhanced dissolution of silymarin/polyvinylpyrrolidone solid dispersion pellets prepared by a one-step fluid-bed coating technique. *Powder Technol* **2008**, 182, 72-80.

14. Li, J.; Liu, P.; Zhang, W. L.; Yang, J. K.; Fan, Y. Q. Novel Tanshinone II A ternary solid dispersion pellets by a single-step technique: in vitro and in vivo evaluation. *Eur J Pharm Biopharm* **2012**, 80, 426-432.

15. Nikowitz, K.; Pintye-Hodi, K.; Regdon Jr, G. Study of recrystallization in coated pellets – effect of coating on API crystallinity. *Eur J Pharm Sci* **2013**, 48, 563-571

16. Mahmoudi, Z. N.; Upadhye, S. B.; Ferrizzi, D.; Rajabi-Siahboomi, A. R. In vitro characterization of a novel polymeric system for preparation of amorphous solid drug dispersions. *AAPS J* **2014**, 16, 685-697.

17. Paudel, A.; Van Humbeeck, J.; Van den Mooter, G.; Theoretical and experimental investigation on the solid solubility and miscibility of naproxen in poly(vinylpyrrolidone). *Mol Pharm* **2010**, 7, 1133-1148.

18. Paudel, A.; Van den Mooter, G. Influence of solvent composition on the miscibility and physical stability of naproxen/PVP K25 solid dispersions prepared by cosolvent spray-drying. *Pharm Res* **2012**, 29, 251-270.

19. Paudel, A.; Loyson, Y.; Van den Mooter, G. An investigation into the effect of spray drying temperature and atomizing conditions on miscibility, physical stability, and performance of naproxen-PVP K25 solid dispersions. *J Pharm Sci* **2013**, 102, 1249-1267.

20. Taylor, L. S.; Zografi, G. Spectroscopic characterization of interactions between PVP and indomethacin in amorphous molecular dispersions. *Pharm Res* **1997**, 14, 1691-1698.

21. Matsumoto, T.; Zografi, G. Physical properties of solid molecular dispersions of indomethacin with poly(vinylpyrrolidone) and poly(vinylpyrrolidone-co-vinylacetate) in relation to indomethacin crystallization. *Pharm Res* **1999**, 16, 1722-1728.

22. Xu, Q.; Sharp, I. D.; Yuan, C. W.; Yi, D. O.; Liao, C. Y.; Glaeser, A. M.; Minor, A. M.; Beeman, J. W.; Ridgeway, M. C.; Kluth, P.; Ager, J. W. 3rd; Chrzan, D. C.; Haller, E. E. Large melting point hysteresis of Ge nanocrystals embedded in SiO2. Phys Rev Lett 2006, 97, 155701.

23. Van den Mooter, G.; Wuyts, M.; Blaton, N.; Busson, R.; Grobet, P.; Augustijns, P.; Kinget, R. Physical stabilisation of amorphous ketoconazole in solid dispersions with polyvinylpyrrolidone K25. *Eur J Pharm Sci* **2001**, 12, 261–269.

24. van Sleeuwen, R. M.; Zhang, S.; Normand, V. Spatial glass transition temperature variations in polymer glass: application to a maltodextrin-water system. *Biomacromolecules* **2012**, 13, 787-797.

Chapter 4: Controlling the release of indomethacin from glass solutions layered with a rate controlling membrane using fluid-bed processing. Part 1: Surface and cross-sectional chemical analysis

Results of this chapter are based on:

Dereymaker, A.; Scurr, D. J.; Steer, E. D.; Roberts, C. J.; Van den Mooter, G. Controlling the release of indomethacin from glass solutions layered with a rate controlling membrane using fluid-bed processing. Part 1: Surface and cross-sectional chemical analysis Mol Pharm ***xxxx****, (manuscript submitted).*

4.1 Abstract

Fluid bed coating has been shown to be a suitable manufacturing technique to formulate poorly soluble drugs in glass solutions. Layering inert carriers with a drug-polymer mixture enables these beads to be immediately filled into capsules, thus avoiding additional, potentially destabilizing, downstream processing. In this study fluid bed coating is proposed for the production of controlled release dosage forms of glass solutions by applying a second, rate controlling membrane on top of the glass solution. Adding a second coating layer adds to the physical and chemical complexity of the drug delivery system so a thorough understanding of the physical structure and phase behavior of the different coating layers is needed. This study aimed to investigate the surface and cross-sectional characteristics (employing SEM and ToF-SIMS) of an indomethacin-polyvinylpyrrolidone (PVP) glass solution, top-coated with a release rate controlling membrane consisting of either ethyl cellulose or Eudragit RL. The implications on the addition of a pore former (PVP) and the coating medium (ethanol or water) were also considered. In addition, polymer miscibility and the phase analysis of the underlying glass solution were investigated.

Significant differences in surface and cross-sectional topography of the different rate controlling membranes or the way they are applied (solution vs. dispersion) were observed. These observations can be linked to the polymer miscibility differences. The presence of PVP was observed in all rate controlling membranes, even if it is not part of the coating solution. This could be attributed to residual powder presence in the coating chamber. The distribution of PVP among the sample surfaces depends on the concentration and the rate controlling polymer used. Differences can again be linked to polymer miscibility. Finally, it was shown that the underlying glass solution layer remains amorphous after coating of the rate controlling membrane, whether formed from an ethanol solution or an aqueous dispersion.

4.2 Introduction

Although the potential of solid dispersions to increase the apparent solubility/dissolution rate and consequently the bio-availability of biopharmaceutics classification system (BCS) class II drugs has been widely demonstrated in the last couple of decades, there is still a huge discrepancy in the research input and the commercial output. The main challenges of commercializing solid dispersions remain the long term physical stability of such systems, with the amorphous or molecularly dispersed drug inherently prone to phase separation, crystallization and ultimately a decrease in solubility. Not only can long term stability issues potentially arise, processing solid dispersion powders into their final dosage form can also lead to phase separation, as recently shown by Ayenew *et al.* during the compression of Naproxen polyvinylpyrrolidone (PVP) solid dispersions[1]. This is a hurdle which can be overcome by coating solid dispersions onto inert carriers and thus avoiding the requirement for major additional downstream processing steps.

Coating glass solutions onto inert carriers can also be exploited to transform them into controlled release formulations. Coated pellets in the size range of 100µm-1mm for controlled release purposes have already been demonstrated as beneficial as compared to controlled release coated tablets. This is thought to be as they are less prone to variability in stomach emptying rates in the fasted state[2]. In the fed state there are additional factors to take into consideration including the composition and caloric value of the administered meal and the size and density of the particles. Therefore, no real consensus has been reached yet on stomach residence times of controlled release formulations. Pellets also show a more even spread in the gastrointestinal tract in comparison with a single coated tablet. Having a high number of coated pellets also reduces the risk for dose-dumping[3, 4]. Furthermore, the surface of amorphous materials has also been shown to be more vulnerable to crystallization, it has been shown that an additional coating layer could potentially stabilize these glasses [5].

The first and foremost reason to produce a controlled release formulation from glass solutions is to maximize the absorption window for poorly soluble drugs by allowing an appropriate amount of dissolved drug to be available for absorption at extended time intervals. Moreover, a slower release rate will reduce the precipitate rate of poorly soluble drugs from their supersaturated state. Controlling the release of glass solutions also allows for a decreased dosing scheme, a better patient compliance and a reduced risk of side effects[6]. It could,

however, be argued that poorly soluble drugs already inherently possess a slow release dissolution profile, but this is compound specific, and non-adjustable.

The overarching goal of this study is to investigate the potential of coated glass solutions to control or reduce the release rate of poorly soluble drugs. For this purpose, bilayer coated sucrose carriers (pellets), of which the first layer consists of a glass solution of indomethacin (INDO) in polyvinylpyrrolidone K25 (PVP) in a 30:70 (w:w) ratio were generated. To control the release of indomethacin from this glass solution, a top layer was applied, consisting of the insoluble polymer ethyl cellulose (EC) and the insoluble but swellable polymer Eudragit RL® (ethyl acrylate: methyl methacrylate: trimethylammonioethylmethacrylate co-polymer in a molar ratio of 1:2:0.2) (ERL). One has to keep in mind that applying a top coating will add to the overall pill burden. Hence, in some specific cases, the dose strength will be a limiting factor in the application of this type of dosage form.

Owing to the complex composition of the coated glass solutions, typical solid state analytical techniques such as modulated differential scanning calorimetry (mDSC) [7] or X-ray powder diffraction (XRPD) are inadequate for this specific multi-layer samples because they only provide bulk analysis (no spatial resolution). Thermal analysis by (m)DSC can detect two separate amorphous phases, provided they are larger than the critical length scale of the technique (~30nm)[8]. In conventional wide angle XRPD, transmission geometry doesn't allow depth resolution as incident x-rays go completely through the sample. Also, in reflection geometry, the penetration depth of the x-rays doesn't allow in depth resolution, spatial resolution can only be achieved in combination with other techniques[9]. Glancing angle x-ray techniques can be used to measure varying sample thicknesses since penetration depths are lower and can be calculated according to the incident x-ray beam angle[10, 11]. This leads to conclude that mDSC and/or XRPD don't provide adequate information on the different layers of complex coated systems. It has even been shown recently that the phase behavior study of a single layer glass solution onto an inert carrier is not straightforward[12].

Time of Flight Secondary Ion Mass Spectrometry (ToF-SIMS) has been used as a surface analysis technique in a wide array of research fields; from biological samples (cells, tissues, proteins, lipids) [13-17], over material science[18] to pharmaceutical formulations[19-24]. ToF-SIMS is based upon the bombardment of a sample surface with a primary ion beam (e.g. Ar^+, Cs^+, Bi_3^+) under ultra-high vacuum conditions. The impact of the kinetic energy of these primary ions upon the sample surface will result in desorption of electrons, atoms, molecular fragments and

whole molecules. The ionized molecular fragments are of particular interest for ToF-SIMS. These secondary ions are accelerated and injected into the Time-of-Flight analyzer. For ions with an equal charge, this will result in equal kinetic energy and thus the velocity of these ions will depend on their mass-to-charge ratio (m/z). Hence, the time needed to reach the detector is indicative for the m/z of the detected molecular fragment and will result in a negative or positive mass spectrum, depending on the charge of the collected molecular fragments[19, 20, 25-27] ToF-SIMS has a very low detection limit (ppb range), a high surface sensitivity and high spatial resolution (0.2µm)[28]. Owing to these properties, ToF-SIMS is highly suited for surface chemical identification and surface chemical distribution (mapping) and will therefore be used to analyze the layered beads, and by doing so, elucidate their chemical structure.

The purpose of this study ("part 1") is to investigate the phase behavior of the surface and physical cross-sections of sucrose beads coated with two layers: an inner layer made up of a glass solution of indomethacin in PVP K25 and an outer layer consisting of a rate controlling membrane made up of ethylcellulose or Eudragit RL. In addition, the influence of a pore former (PVP K25) in the outer layer and application of the outer layer from an organic solution or an aqueous dispersion on the phase behavior was investigated. Surface and cross-sectional morphology was investigated by scanning electron microscopy (SEM), the chemical composition and distribution of the bead surfaces and cross-sections was analyzed using ToF-SIMS. Physical structure of the glass solutions was assessed by XRPD, while polymer mixing was tested using mDSC.

4.3 Experimental section

4.3.1 Materials

Indomethacin was purchased from FAGRON Ltd. (Waregem, Belgium). Polyvinylpyrrolidone K 25 was a generous gift from BASF (Ludwigshafen, Germany). Sucrose spheres (diameter 710 - 850 µm) were kindly donated by Hanns G. Werner GmbH (Tornesch, Germany). Ethyl cellulose (ethoxy content 48.0 - 49.5% w/w) powder and triethyl citrate were purchased from Sigma-Aldrich (Zwijndrecht, The Netherlands). Eudragit RL® PO and 30 D were purchased from Evonik Industries (Darmstadt, Germany).

4.3.2 Fluid bed coating

Coated beads were prepared using an Aeromatic MP 1 multiprocessor (GEA, Bubendorf, Switzerland) in a bottom spray setup, equipped with a Würster insert. A 30 : 70 (w:w) INDO-PVP (w/w) glass solution with a total solid content of 250,0 g was coated onto 500,0 g of sucrose beads from a 10% (w/v) ethanol solution. The sucrose spheres were loaded into the preheated coating chamber at 50 °C and heated for 10 minutes. The drug-polymer solution was coated onto the sucrose pellets at a feed rate of 13 cm^3/min and this feed was atomized at an air pressure of 1.5 bar. Meanwhile the heated air stream was passing through the fluid bed coater at a rate of 1.78 m^3 /min. When the spraying was finished, the pellets were dried until immobilization due to electrostatic charge was observed. The coated spheres were unloaded, weighed and dried for an additional 48 hours in an oven at 50 °C. In the case when a top layer (rate controlling membrane) was applied, the feed solution was immediately changed after completion of the glass solution layer. The controlled release top layer consisted of a rate controlling polymer (ERL or EC) which was applied from a 10% w/v ethanolic solution. Additional batches were prepared that contained PVP K25 as a pore former in the rate controlling membrane (in a concentration of 10% or 25% w/w relative to the total solid content) or the plasticizer TEC, added in a concentration of 20% w/w relative to the amount of rate controlling polymer. Finally ERL was also applied as an aqueous dispersion (10% w/v) instead of an ethanolic solution. Controlled release top coating total solid content was 200,0 g. The coating process parameters are the same for the top coating layer as for the glass solution layer, except for the feed rate with the ERL ethanolic solutions. Here the feed rate was reduced to 6.5ml/min because of the electrostatic charges created inside of the fluid bed coater. After completion of the coating, the beads were also dried in the coater for at least

10 minutes, removed from the coater and additionally dried in an oven for at least 48 hours. Ethanolic solutions are dried at 50°C, aqueous dispersions at 60°C to allow for curing of ERL.

4.3.3 Spray drying

The miscibility between PVP K25 and EC or ERL was investigated for spray dried samples. ERL or EC were combined with PVP K25 in different ratios: 100-0, 75-25, 50-50, 25-75 and 0-100 % w/w. Each composition was spray dried from a 10% w/v ethanol solution using a Büchi Mini Spray Dryer B-191 (Büchi, Flawil, Switzerland). The inlet air temperature was 50°C, the heated air flow rate 0,56 m^3/min, the atomizing air flow rate 0.02 m^3/min and the feed rate 4.8 cm^3/min. The obtained polymer mixtures were additionally dried for 48 hours in a vacuum oven at 25°C (Mazzali Systems, Monza, Italy), prior to mDSC analysis to investigate polymer miscibility.

4.3.4 Scanning electron microscopy

The morphology of the coated beads was investigated with SEM using a Philips XL30 ESEM-FEG instrument (Philips, Eindhoven, The Netherlands) equipped with a field emission electron gun. Whole beads and cross-sections (made with a scalpel under an optical microscope) were fixed on an aluminum stub using double-sided carbon tape. The samples were coated with gold by sputtering for 45 s at 20 mA. The SEM was used with an acceleration voltage of 2.00 kV to acquire as much surface detail as possible by minimizing secondary electron loss. This way charge accumulation on the sample is also low. A spot size of 3 and a secondary electron detector were used.

4.3.5 Time-of-flight secondary ion mass spectrometry

For chemical composition and distribution analysis, ToF-SIMS was performed using a ToF-SIMS IV (ION-TOF Gmbh, Münster, Germany). This spectrometer was equipped with a pulsing bismuth liquid metal gun (Bi_3^+) and a single stage reflectron analyzer. A flood gun was applied to produce low energy electrons to compensate surface charging from the primary ion beam (positive charges). For surface analysis, samples were fixed to glass slides using double sided tape prior to analysis. When analyzing whole beads, only the uppermost part of the bead was analyzed due to the shape and size of the beads. This surface analysis comprised of an analysis area of 200 × 200 µm with a raster scanned resolution of 256 × 256 pixels. For cross-sectional analysis, beads were embedded into Epofix™ cold-setting resin , and sliced using a glass knife

on a RMC ultramicrotome PowerTome. For the cross-sectioned beads, an analysis area of 500 × 500 µm was raster scanned with a resolution of 256 × 256 pixels. All samples were analyzed in the negative ion polarity mode and analyzed using SurfaceLab 6 (ION-TOF Gmbh, Münster, Germany). Firstly, controls were analyzed with reference material of all components. Different characteristic ions were chosen as the most selective to the specific compound. The chosen indomethacin marker was $C_7H_{10}O_4$-, the PVP marker was $C_3H_4N_2O^-$, the EC marker was $C_2H_5O^-$, the ERL marker CH_3O- and the sucrose marker $C_{12}H_{21}O_{11}^-$. Marker intensities and ion peaks for the control samples are shown in Figure A of Supporting Information. Measured secondary ion intensities for every component were normalized to total intensity count to allow for a semi-quantitative comparison between samples. It should be noted that the control ion for EC is also formed in the ERL control spectrum. Since there are no samples where both polymers are present at the same time, this didn't pose any interpretation problems.

4.3.6 Modulated differential scanning calorimetry

mDSC analysis of spray dried polymers and polymer mixtures was carried out with a TA instruments Q2000 modulated DSC (Leatherhead, UK) equipped with a refrigerated cooling system (RCS90). The DSC cell was purged with a nitrogen flow of 50 ml/min during analysis. Data processing was performed using TA Instruments Universal Analysis software (version 4.4, Leatherhead, UK). TA Instruments standard aluminium pans (Brussels, Belgium) were used for all measurements. All sample masses were between 5-6 mg (accurately weighed). The samples were heated from 0°C to 180°C. A heating rate of 2°C/min was applied with a temperature modulation of 0.636°C every 40s. All samples were measured in triplicate. Glass transition temperatures were measured at half height in the reversing heat flow. The step jump in heat capacity observed in the reversing heat flow signal was further examined in the corresponding derivative signal after Savitsky-Golay smoothing with points of window set at 10°C. n-Octadecane and indium were used to calibrate and validate the DSC temperature scale. Indium was also used to calibrate and validate the enthalpic response. The heat capacity was calibrated and validated using sapphire disks.

4.3.7 X-ray powder diffraction

Coated beads and reference powders were analyzed at room temperature using an automated X'pert PRO diffractometer (PANalytical, Almelo, the Netherlands). All samples

were placed in the sample holders, clamped between Kapton foil and analyzed in transmission mode using a Cu tube (Kα 1.5418 Angstrom; generator at 45kV and 40mA). Analysis was performed in continuous scan mode in 2θ range from 4° to 40° with a 0.0167° step size and 200 seconds counting time per step. The X'pert Data Collector and the X'pert Data Viewer (PANalytical, Almelo, The Netherlands) were used for data collection and analysis.

4.4 Results

4.4.1 Surface and cross-sectional investigation of the coated beads with SEM

The structures of the outer surface of whole beads with different outer coatings are shown in Figure 4.1.

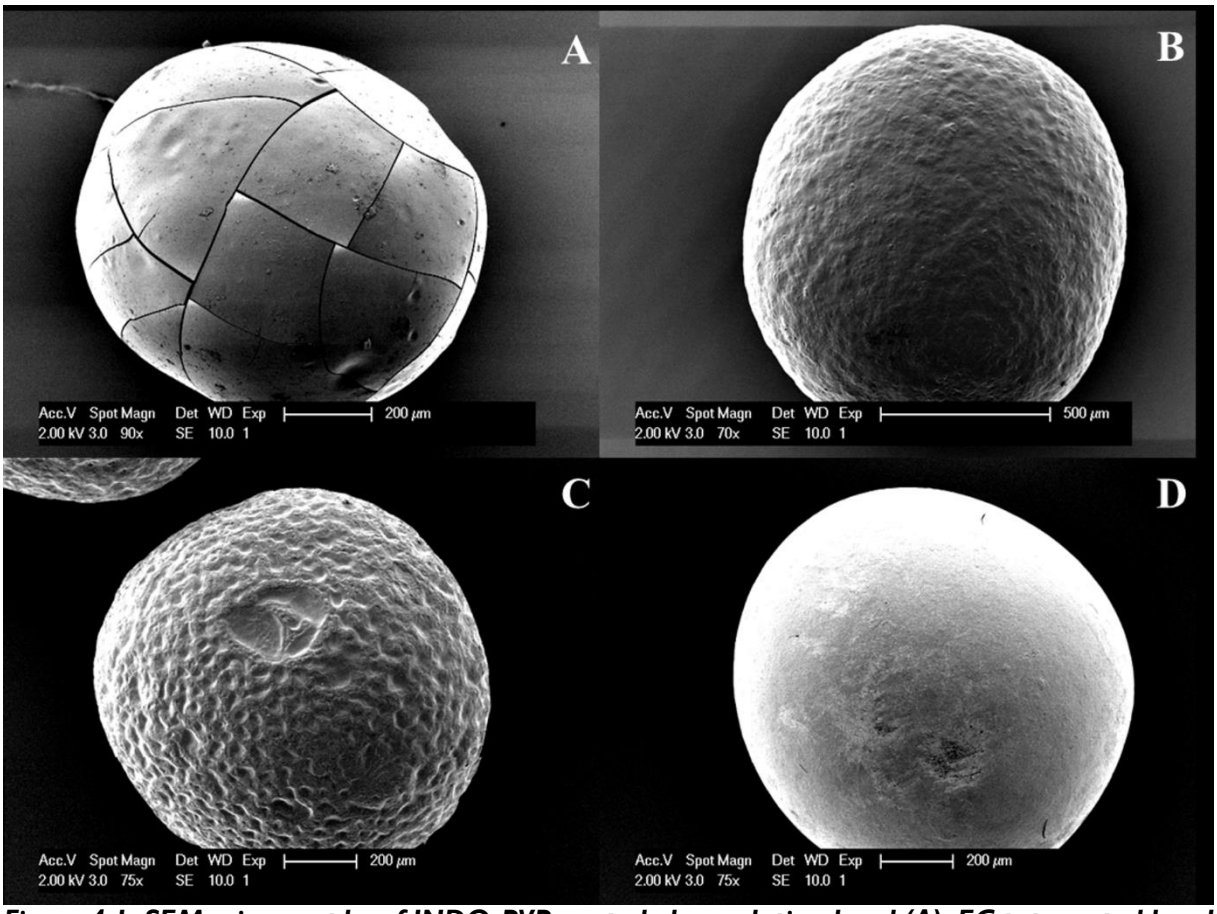

Figure 4.1: SEM micrographs of INDO-PVP coated glass solution bead (A), EC top coated bead (B), ERL top coated bead from an ethanolic solution (C) and ERL top coated bead from an aqueous dispersion (D)

Figure 4.1A shows an INDO-PVP glass solution coated bead which appears spherical in shape with a smooth surface. Such beads exhibit surface cracks with different lengths and depths. In this example there is one major dent in the coating. Figure 4.1B shows beads which

were coated with an inner layer of INDO-PVP and an outer layer of EC. These beads are spherical but and no cracking is observed. The surface appears slightly rougher compared to the INDO-PVP surface. An INDO-PVP glass solution inner layer combined with an ERL outer layer, coated from an ethanol solution, is displayed in Figure 4.1C. No cracks were observed but now the surface is rough and shows pitted 'golf ball-like' surface structure. Finally, Figure 4.1D presents an INDO-PVP glass solution layer with an ERL top coating sprayed from an aqueous dispersion. This resulted in smooth, spherical beads with a few rougher spots. A few very minor cracks or crescent shaped holes can be observed.

The SEM analysis of the cross-sectioned beads revealed the different coating layers and inner morphology of the different formulations as illustrated in Figure 4.2. Figure 4.2A depicts a cross-section of the INDO-PVP coated bead. There is a distinct difference in morphology between the inner sugar core, which has a rough morphology, and the glass solution coating which has a smoother appearance. There are also cracks visible in the cross-sectioned view. Figure 4.2B and 4.2B' show the sugar core, INDO-PVP inner layer and EC outer layer. The sugar core and glass solution layer possess the same features as described in the previous figure. The EC outer coating layer has a distinct 'layered' structure and seems to be loosely attached to the inner glass solution layer with a distinct gap between the two coating layers. Beads with a top coating of EC and 20% w/w of TEC were also analyzed (Figure B of Supporting Information), but no differences were observed when compared to Figure 4.2B and 4.2B'. The EC layers are morphologically very different from the ERL top coating, which is shown in Figures 4.2C and 4.2C', where it is sprayed from an ethanol solution and in Figure 4.2D from an aqueous dispersion. The ERL layer is much smoother compared to the EC layer and equally smooth compared to the glass solution layer but with the absence of cracks. In this case, the two different coating layers are also attached to each other.

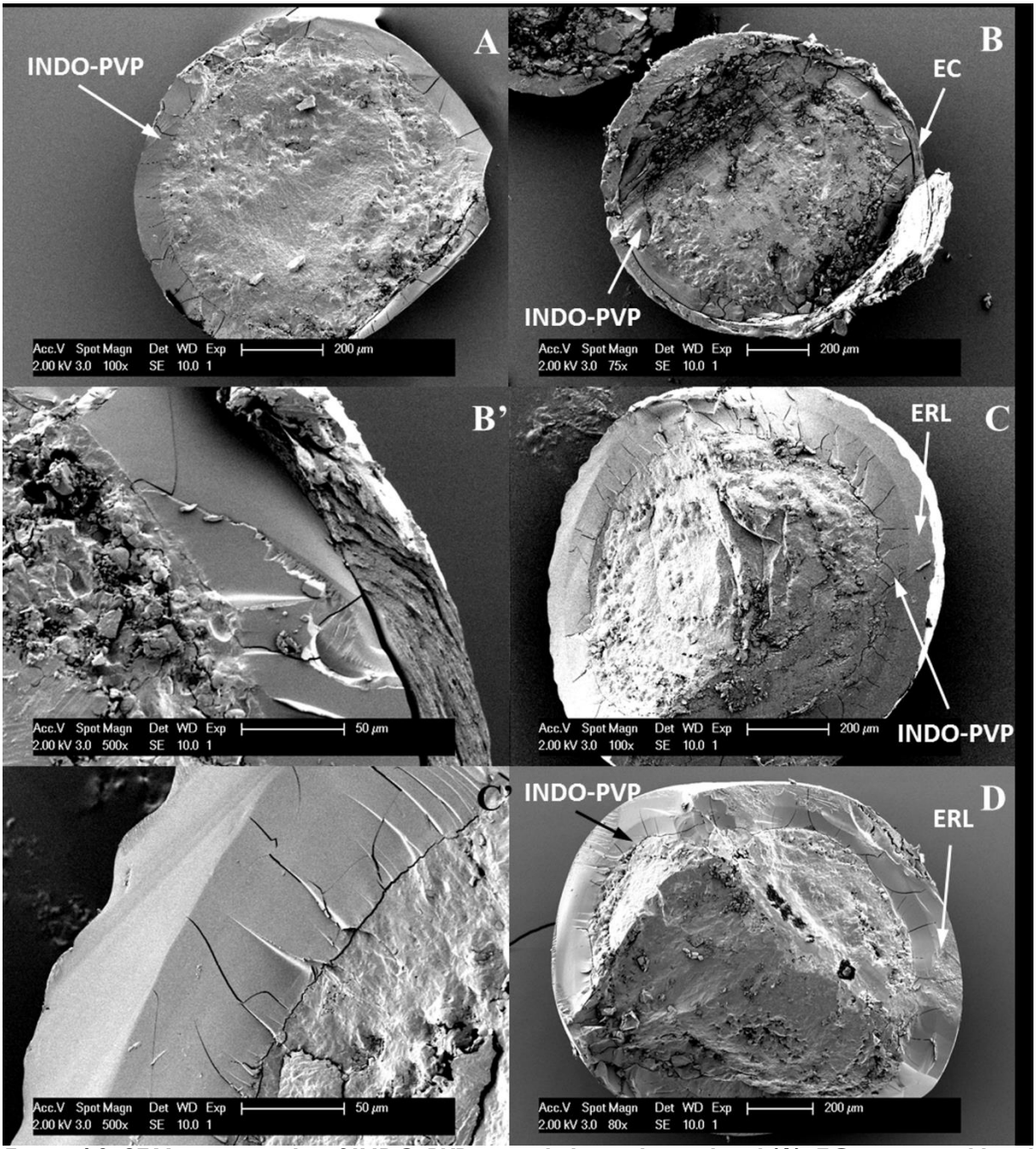

Figure 4.2: SEM micrographs of INDO-PVP coated glass solution bead (A), EC top coated bead (B) and a detailed view on the coating layers (B'), ERL top coated bead from an ethanolic solution (C) with a detailed view on the coating layers (C'), and, an ERL top coated bead from an aqueous dispersion (D).

4.4.2 Chemical surface composition and distribution of the coated beads by ToF-SIMS

Using the data obtained from the control samples, sample spectra were investigated for the presence or absence of each marker upon the samples. Secondary ion images are then constructed for chosen ions. ToF-SIMS secondary ion spectra and images of the surface of the INDO-PVP glass solution layer are shown in Figure 4.3. Figure 4.3a Shows the presence of ion peaks at the marker positions of PVP (left) and INDO (right), Figure 4.3b shows, from left to

right, the total ion image, the PVP marker ion ($C_3H_4N_2O^-$) image, the INDO ion marker ($C_7H_{10}O_4^-$) image and the overlay of the PVP (green) and INDO (blue) marker ion. The total ion image shows the presence and intensity of (any) detectable ions, this shows where different components can be present. The PVP marker ion image shows where the ions, which have been determined to be specific for PVP are present on the sample surface. The same observations can be made for the INDO ion marker image. To easily detect distributional differences between different marker ions (and thus the distribution of different components of the system), overlays can be created where different marker ions are assigned to a different colour.

From the ion spectra (Figure 4.3a), it is apparent that both molecules are present in the glass solution coating. From the total ion image, the cracks in the surface are also visible. In terms of distribution, by observing the markers of INDO, PVP and the overlay of both, it is clear that the presence of both molecules along the entire surface shows a homogeneous distribution.

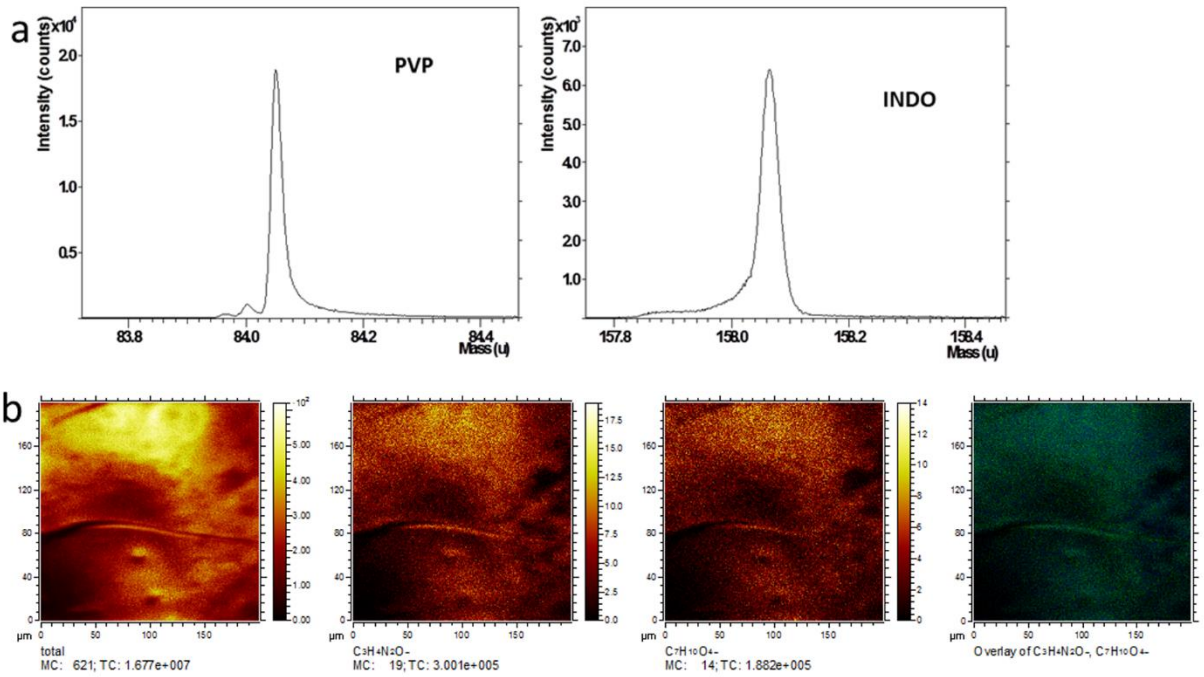

Figure 4.3: ToF-SIMS ion spectra of INDO-PVP coated glass solution (a) at PVP and INDO marker positions. ToF-SIMS ion images of INDO-PVP coated glass solution (b) with the total ion image, the PVP marker image, the INDO marker image and an overlay of PVP marker image (green) and INDO marker image (blue).

Secondary ion images of ERL coated formulations are provided in Figure 4.4. Figure 4.4a-d show ion images of ERL 100%, ERL-PVP 90-10%, ERL-PVP 75-25% and ERL latex 100% respectively. Secondary ion spectra are provided in Figure C of Supporting Information. All

ERL top coated formulations show presence of PVP marker ion on the sample surface, as can be seen in in the secondary ion spectra. The presence of PVP is expected for the ERL-PVP 90-10% and ERL-PVP 25% coatings, because PVP is used here as a pore former in the rate controlling membrane, but it was not anticipated in coatings made up of pure ERL. Although all of the formulations show PVP presence at the surface, the distribution is different. From the ion images in Figure 4.4 it can be seen that in the formulations where PVP is used as a pore former, the distribution of PVP is more homogeneous throughout the surface. In both ERL 100% samples, which contained no pore former, the secondary ion images show PVP 'hot spots', i.e. local areas with a high marker intensity of PVP (column 3 of Figure 4.4a and 4.4d) and a low marker intensity of ERL (column 2 of Figure 4.4a and 4.4d). Secondary ion spectra of ERL based samples also show a very small INDO marker intensity for ERL 100% and ERL 100% latex. For ERL-PVP 90-10% and ERL-PVP 75-25%, no clearly defined peaks could be observed in the spectra. This is also shown in the INDO marker ion images of Figure 4.4 where only very few localized INDO spots can be observed in ERL 100% and ERL 100% latex. ERL-PVP 90-10% and ERL-PVP 75-25% only show background noise. It has to be remarked that not the entire surface is represented in the ion images of the sample as it was not possible to obtain data from the full 200 × 200 μm range. The system seems to cope with the topography but not with the curvature of the sample as it progressively goes out of focus. The loss of SIMS data due to the sample curvature is illustrated for each sample in the effect upon the total ion image which is provided for each system in column 1 of Figure 4.4.

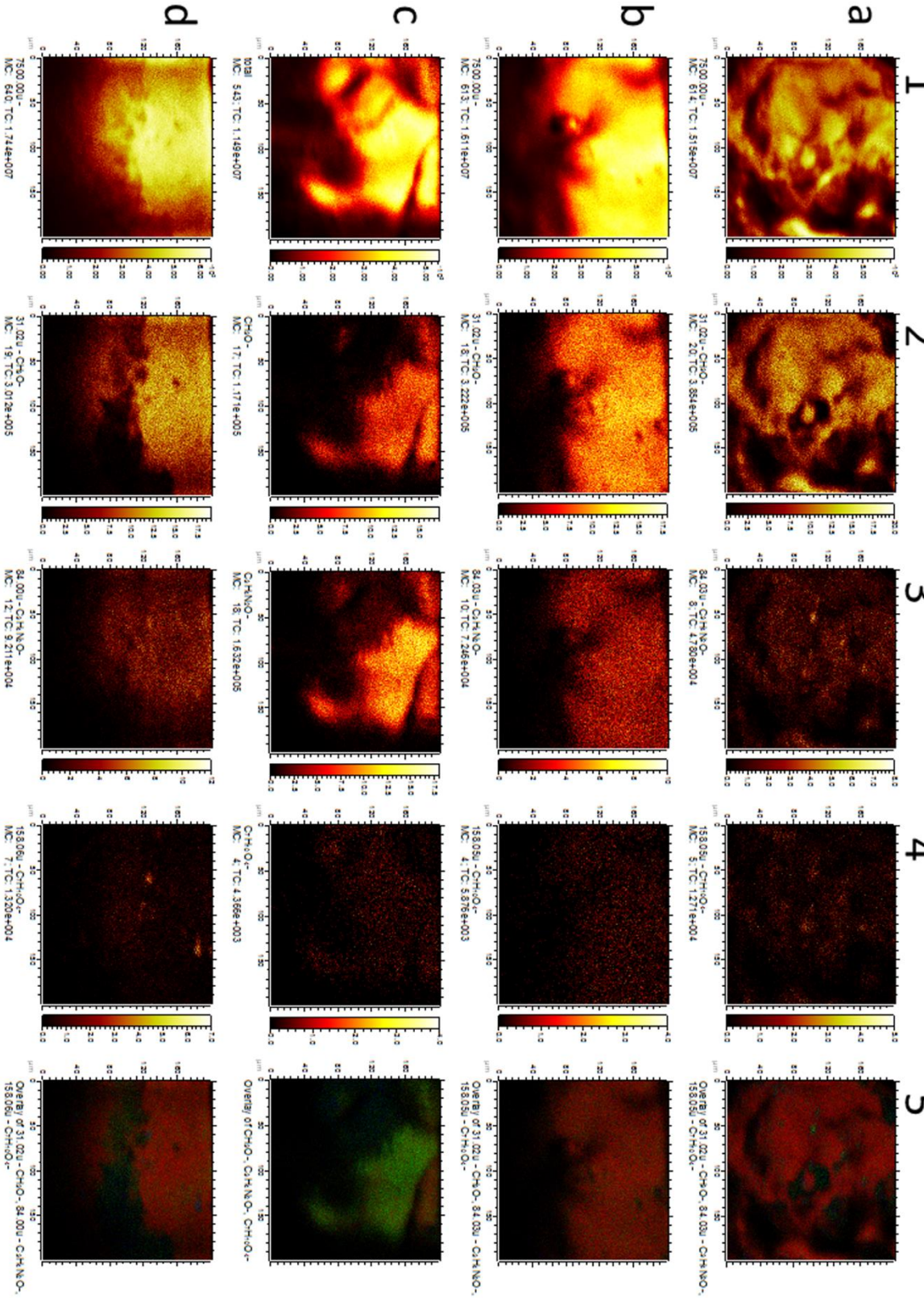

Figure 4.4: ToF-SIMS ion images of ERL coated formulations, 100% ERL (row a), ERL-PVP 90-10% (row b), ERL-PVP 75-25% (row c) and 100% ERL latex (row d). Column 1 represents the total ion images of all formulations, column 2 the ERL marker images, column 3 the PVP marker images, column 4 the INDO marker images and column 5 an overlay image of ERL marker (red), PVP marker (green) and INDO marker (blue).

As the ToF-SIMS is a semi-quantitative analysis method, only trends can be derived from the ion intensities obtained. To be able to compare different measurements and different formulations, the ion intensities presented were normalized by total ion intensity. Figure 5 illustrates the intensities for the PVP and ERL diagnostic ions. Although the ERL ion intensity decreases with decreasing ERL content in the outer layer, the same cannot be said of the PVP marker intensity. Surprisingly, there seems to be a similar PVP marker intensity in both 100% ERL outer layers, either sprayed from an ethanol solution or aqueous dispersion, and ERL-PVP 90-10%. Additionally, when PVP is added to the formulation as a pore former, a large variation between three independent measurements was observed. ERL-PVP 75-25% shows the highest PVP marker intensity. Since no INDO marker peaks can be observed in ion spectra of ERL-PVP 90-10% and ERL-PVP 75-25%, the marker intensities for INDO in Figure 4.5 represent background noise, INDO marker intensities for ERL 100% and ERL 100% latex are barely larger than this background noise intensities.

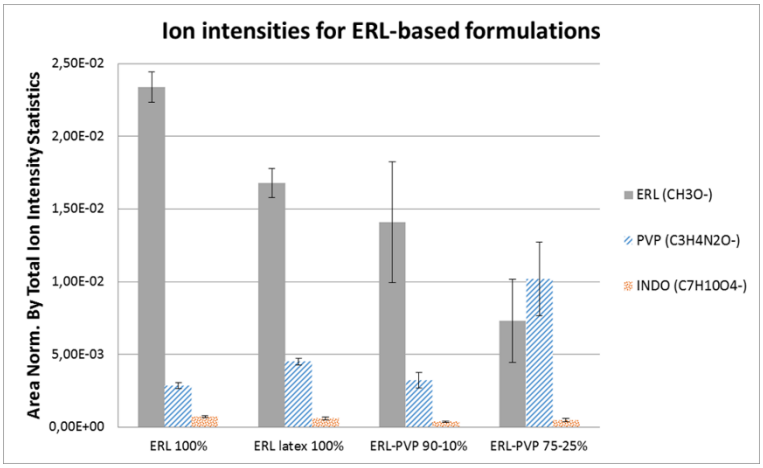

Figure 4.5: Ion intensities for the different formulations containing an ERL-based outer coating layer. ERL marker intensities are represented in filled grey bars, PVP marker intensities are striped blue bars and INDO marker intensities are orange dotted bars. Ion intensities are measured as a mean of 3 surfaces and the area is normalized by total ion statistics.

Secondary ion spectra from the EC coated samples were also analyzed for marker ion intensities. The ion spectra of EC coated samples are shown in Figure D of Supporting Information. Secondary ion images were constructed from these spectra. These images are shown in Figure 4.6. In this figure, rows A, B, C and D represent the EC 100% coated sample, EC-PVP 90-10%, EC-PVP 75-25% and EC 100% with the addition of 20% TEC as a plasticizer (EC 100% - TEC) respectively. Once again, from the ion spectra, the presence of PVP can be observed in every sample, even in those samples that would not be anticipated to contain PVP in their outer layer, namely EC 100% and EC 100% - TEC. Local PVP regions are again visible, but this time they are even more pronounced and spread out diffusely along a large area of

the analyzed surface. From the overlay ion images of the samples with PVP as a pore former (Figure 4.6b and 4.6c, column 3), it can be observed that the distribution of PVP is more heterogeneous, compared to both EC 100% samples and also compared to ERL samples with identical pore former amounts. Ion peaks for the INDO marker ion can be distinguished in all EC samples (Figure D of Supporting Information), although they have very small intensities (10^{-5} range). Only in the EC-PVP 90-10% sample, one specific INDO spot can be observed (Figure 4.6b, column 3).

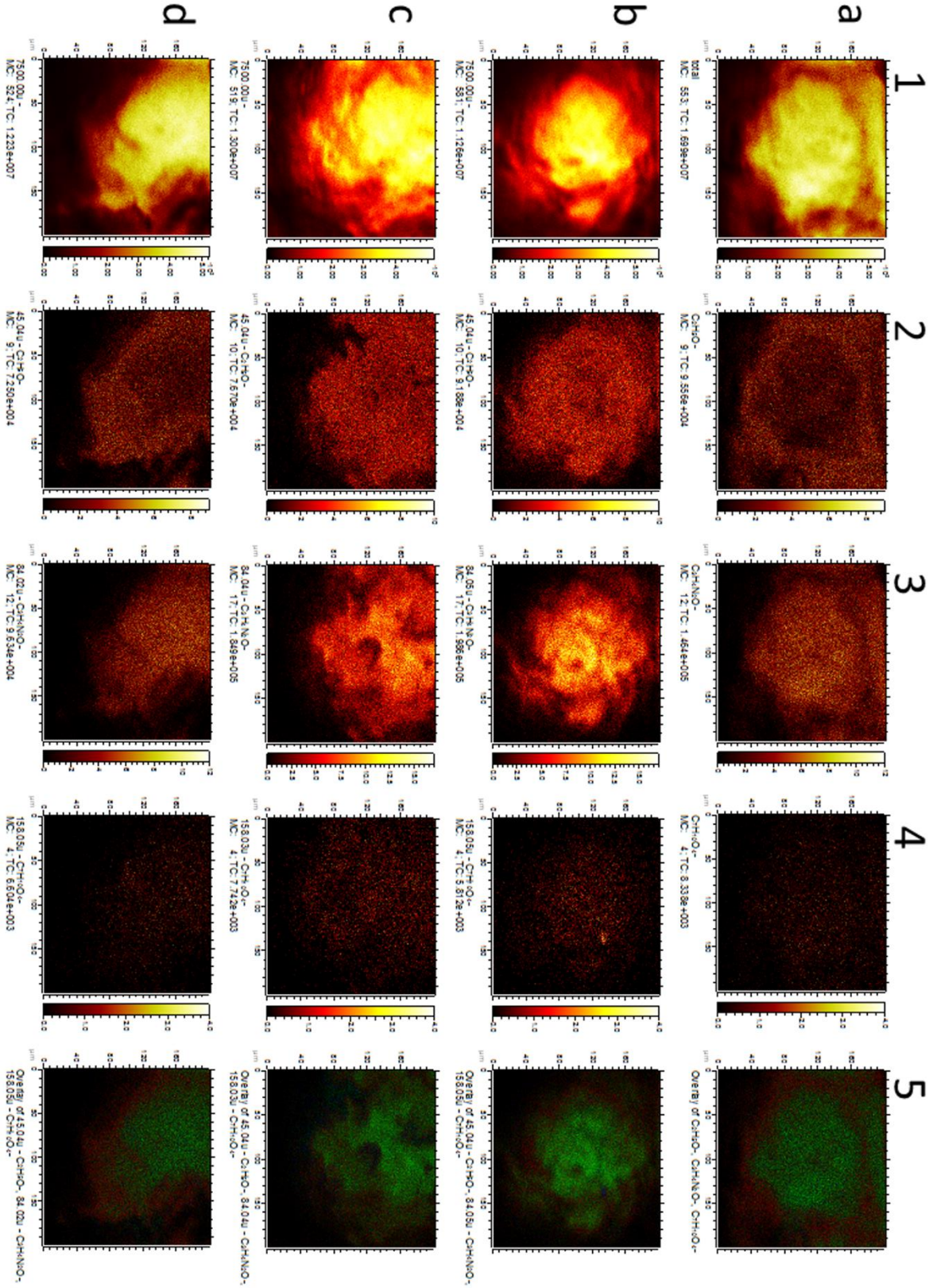

***Figure 4.6:** ToF-SIMS ion images of EC coated formulations, 100% EC (row a), EC-PVP 90-10% (row b), EC-PVP 75-25% (row c) and EC 100% - TEC (row d). Column 1 represents the total ion images of all formulations, column 2 the EC marker images, column 3 the PVP marker images, column 4 the INDO marker images and column 5 an overlay image of EC marker (red), PVP marker (green) and INDO marker (blue).*

For the marker ion intensities of EC samples in Figure 4.7, the EC marker intensity is similar for EC 100%, EC 100% - TEC, and EC-PVP 90-10%. EC-PVP 75-25% has a decreased EC marker intensity. Contrary to ERL top layer samples, samples containing PVP as a pore former also have higher ion intensities for the PVP marker as compared to the 100% EC coated formulations. However, the ion intensity for the PVP marker is higher for the EC-PVP 90-10% sample, compared to the EC-PVP 75-25% sample. Similar to ERL samples, INDO marker intensity is very low and is for the most part background noise.

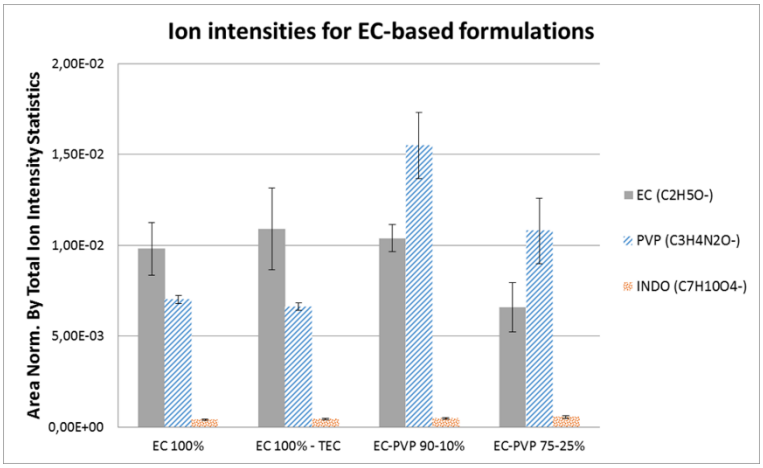

Figure 4.7: Ion intensities for the different formulations containing an EC-based outer coating layer. EC marker intensities are represented in filled grey bars, PVP marker intensities are striped blue bars and INDO marker intensities are orange dotted bars. Ion intensities are measured as a mean of 3 surfaces and the area is normalized by total ion statistics.

4.4.3 Chemical cross-sectional composition and distribution of the coated beads by ToF-SIMS

Physical cross-sections of each bead formulation were also analyzed with ToF-SIMS. The same markers for all components were used plus an additional sucrose bead marker ion. Presence of all marker ion peaks was checked and secondary ion images are then constructed for these marker ions. ToF-SIMS secondary ion spectra are shown in Figure E of Supporting Information and images of the INDO-PVP glass solution cross-section are shown in Figure 4.8. From the distribution of the different marker ions, a well-defined INDO-PVP glass solution layer can be observed as an outer layer on top of the sucrose bead. It is interesting to note here that inside the sucrose bead core, there seems to be presence of INDO and PVP marker. This was also observed when a control sample was analyzed, as seen in the sucrose control sample ion intensities (Supporting Information Figure F). This shows that the presence of INDO and PVP marker ions is inherent to the sucrose bead, which molecular constitution is not fully known, as they were purchased as such. Furthermore, the glass solution layer does

not show a homogeneous distribution of INDO and PVP across the diameter of the bead. INDO seems to be more present at the inner part of the glass solution layer, while PVP is more present at the outer part of the glass solution layer. This observation in particular is observed in one specific sample since the cross sections are not measured in triplicate. Since this inhomogeneous distribution is also not observed in top-coated glass solutions, no general claims can be made about this observation. The presence of two sugar spots in the glass solution layer is probably due to chipping during cross-sectioning.

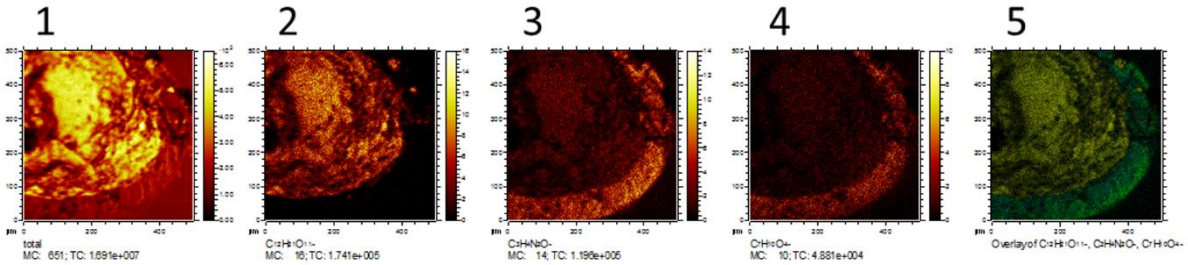

Figure 4.8: ToF-SIMS ion images of a cross-section of an INDO-PVP glass solution coated bead. Column 1 represents the total ion images of all formulations, column 2 the sucrose marker images, column 3 the PVP marker images, column 4 the INDO marker images and column 5 an overlay image of sucrose marker (yellow), PVP marker (green) and INDO marker (blue).

Secondary ion images of the cross-sections of ERL based outer layer formulations are provided in Figure 4.9. Figure 4.9a-d show ion images of cross-sections of sugar cores, coated with an INDO-PVP glass solution and outer coating of ERL 100%, ERL-PVP 90-10%, ERL-PVP 75-25% and ERL latex 100% respectively. Secondary ion spectra are provided in Figure G of the Supporting Information and show, not surprisingly ion peaks for all ion markers in every formulation. From the ion images it can be seen that INDO and PVP show a well-defined glass solution layer on top of the sucrose core. This glass solution layer in turn is again separated from the ERL top layers. PVP distribution along the ERL 100% layer is not seen and is very diffuse along the ERL 100% latex layer. As PVP is incorporated as a pore former, its intensity along the outer layer increased (Figure 4.9 column 3). In all formulations, INDO marker intensity is noticed solely in the glass solution layer, except for the ERL 100% latex layer where an INDO marker presence is observed right above the glass solution layer (Fig. 4.9d, Column 4). ERL marker presence is limited to the outer coating layer.

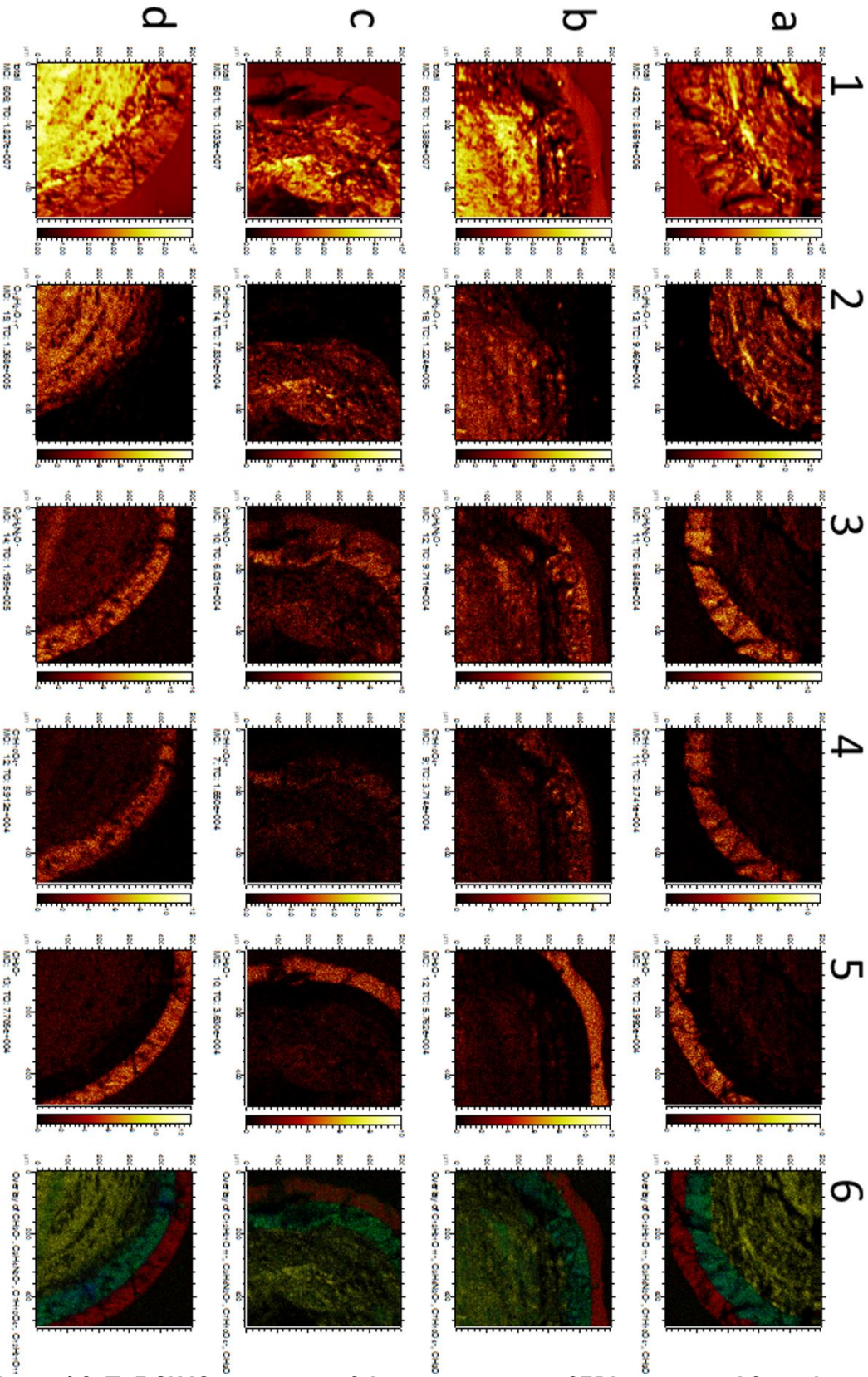

Figure 4.9: ToF-SIMS ion images of the cross-sections of ERL top coated formulations, ERL100% (row a), ERL-PVP 90-10% (row b), ERL-PVP 75-25% (row c) and ERL 100% latex (row d). Column 1 represents the total ion images of all formulations, column 2 the sucrose marker images, column 3 the PVP marker images, column 4 the INDO marker images, column 5 the ERL marker images and column 6 an overlay image of ERL marker (red), PVP marker (green), INDO marker (blue) and sucrose marker (yellow).

Cross-sections of EC based outer layer formulations were analyzed similarly to the ERL based outer layer formulations. Figure 4.10a-d provides ion images of the cross-sections of all different formulations, while all ion spectra are provided in Figure H of Supporting Information. Again, presence of all ion markers of the different components of the formulation was observed. Ion images show clearly defined INDO-PVP glass solution and EC based coating layers. PVP marker ion presence is observed in all EC coating layers, but is becoming more intense when applied as a pore former. This minor presence is attributed to the EC itself as can be seen from the control intensities (Supporting Information Figure I), and is similar to the sucrose control mentioned earlier. A similar phenomenon is not observed for the INDO marker and has no visible marker intensity in the EC based top layer. The smearing of the outer EC 100% layer (Figure 4.10a, column 5) is a result of physical damage during the bead cross-sectioning process.

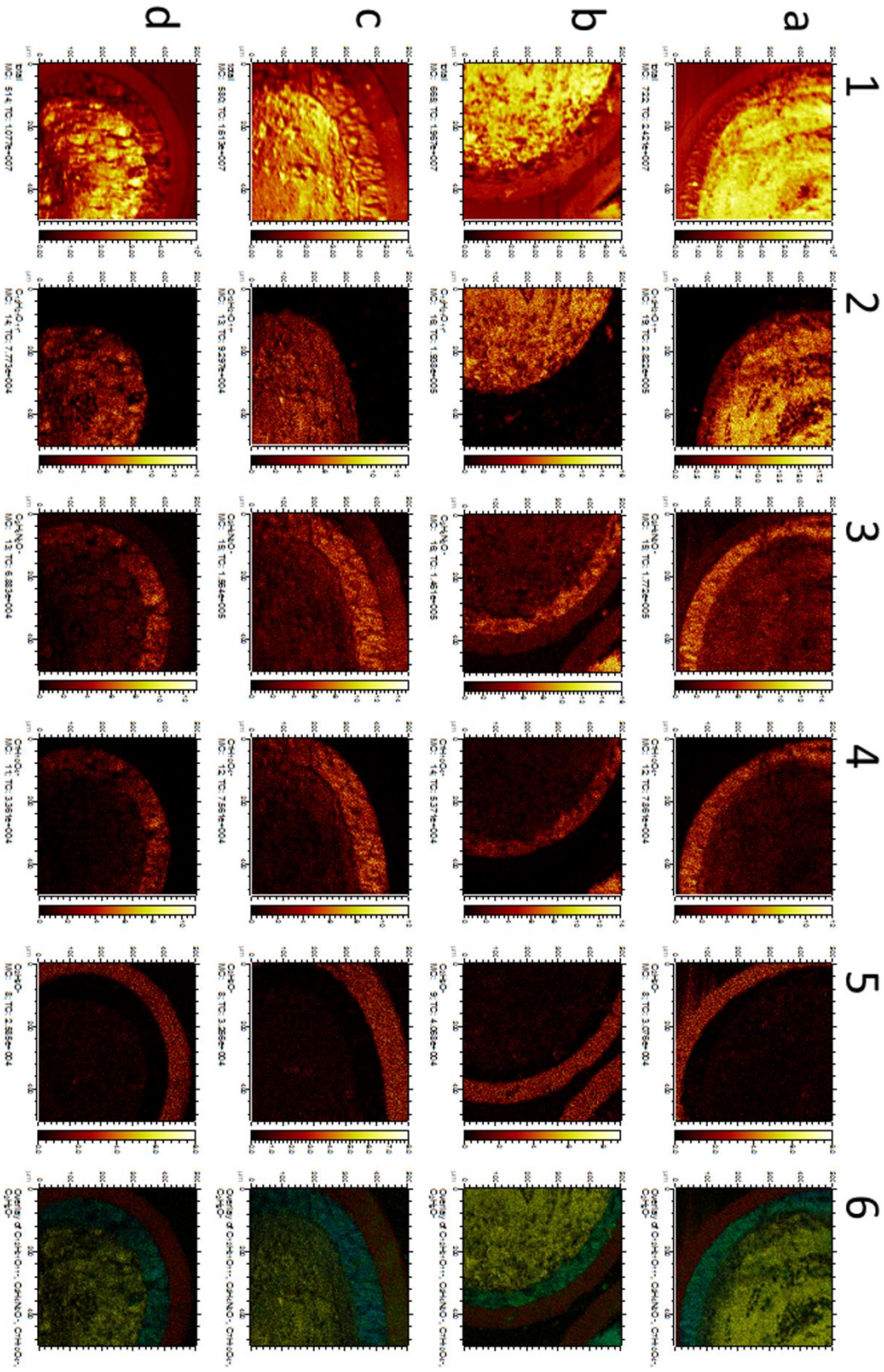

Figure 4.10: ToF-SIMS ion images of the cross-sections of EC top coated formulations, EC 100% (row a), EC-PVP 90-10% (row b), EC-PVP 75-25% (row c) and EC 100% - TEC (row d). Column 1 represents the total ion images of all formulations, column 2 the sucrose marker images, column 3 the PVP marker images, column 4 the INDO marker images, column 5 the ERL marker images and column 6 an overlay image of ERL marker (red), PVP marker (green), INDO marker (blue) and sucrose marker (yellow).

In order to investigate if INDO or PVP can migrate into the outer ERL or EC based coating, this coating layer is divided into several regions of interest, forming an inner, middle and outer layer of the top coatings (One example of the EC 100% sample is given in Figure J of Supporting Information). The different regions of interest intensities and total intensity of the INDO and PVP ion markers of the ERL top coatings are shown in Figure 4.11. Figure 4.11a represents PVP marker intensities and Figure 4.11b shows INDO marker intensities.

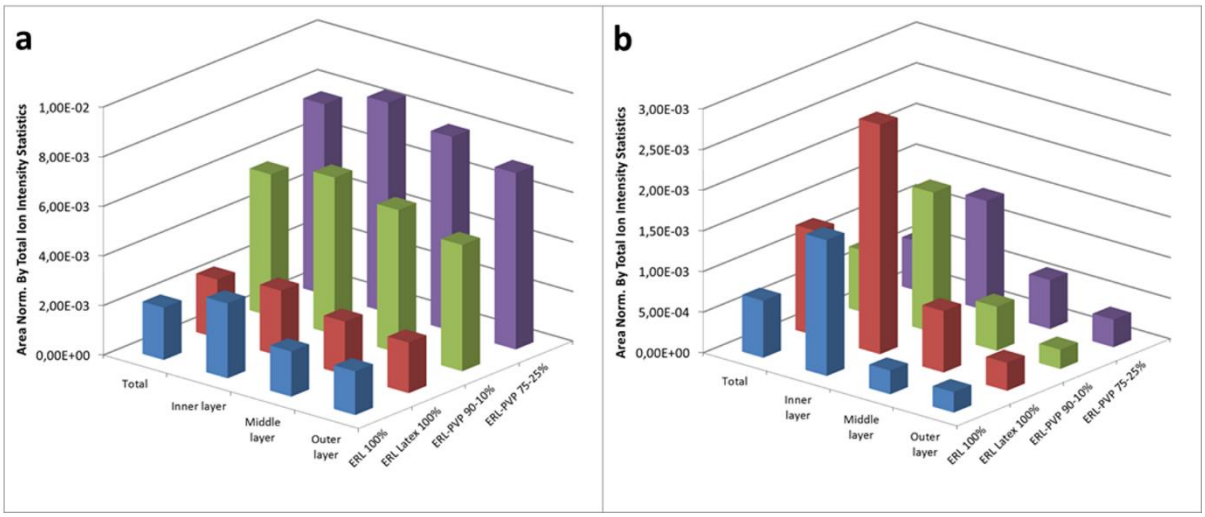

Figure 4.11: Total, inner layer, middle layer and outer layer intensities of the PVP (a) and INDO (b) ion markers of ERL top coatings. ERL 100% intensities are shown in blue bars, ERL 100% latex intensities in red bars, ERL-PVP 90-10% intensities in green bars and ERL-PVP 75-25% intensities in purple bars.

Identical intensity plots for EC top coatings are represented in Figure 4.12, where Figure 4.12a shows PVP marker intensities and Figure 4.12b represents INDO marker intensities. PVP marker intensities are higher in ERL (Fig. 4.11a) and EC (Fig.4.12a) coatings where PVP was used as a pore former, which confirms previous results from the ToF-SIMS surface analysis. All ERL top coating formulations show a PVP intensity gradient from the inner to the outer layer. INDO marker total intensity (Fig. 4.11a) is largest in ERL 100% latex top coating. ERL 100%, ERL-PVP 90-10% and ERL-PVP 75-25% show similar INDO marker intensities. Similar to PVP marker intensities, there is an intensity gradient from the inner to the outer layer of all ERL based top coatings. A PVP marker intensity gradient is also observed in all EC formulations, except for EC-PVP 75-25%. This gradient is less pronounced than the one in ERL formulations. An INDO marker gradient is also observed for all EC top coatings (Fig. 4.12b), except EC-PVP 75-25%, but INDO marker intensities are slightly lower compared to ERL top coatings. The intensity difference is also most pronounced between the inner and middle layer of the EC based top coatings. The INDO marker intensity of the EC or ERL top coatings are

still considerably small when compared to the marker intensity of the glass solution layer. This ranges from 4.5% for EC-PVP 75-25% to 14% for ERL-PVP 75-25% and ERL 100% latex.

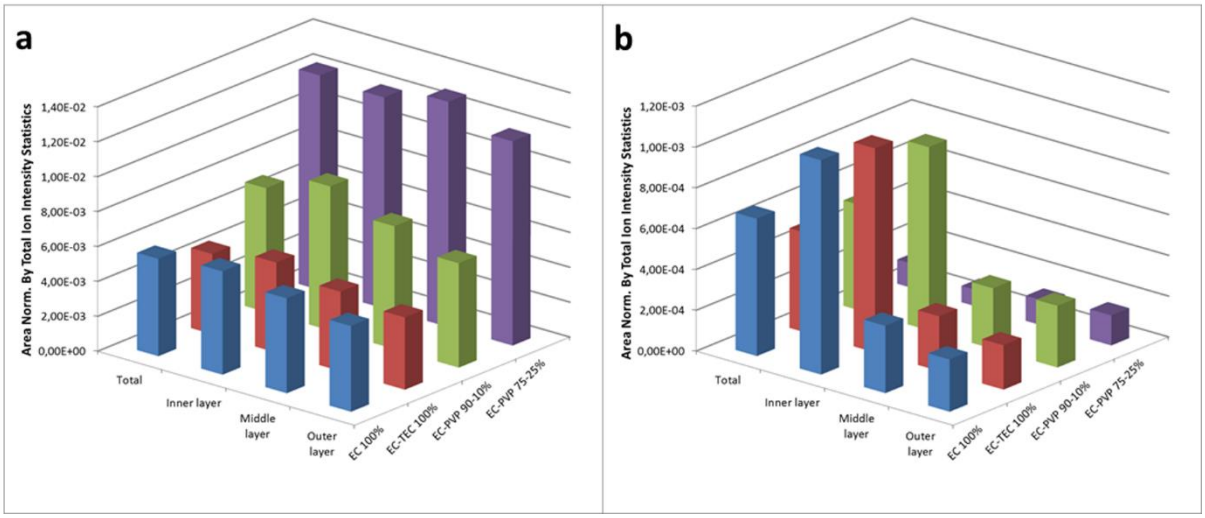

Figure 4.12: Total, inner layer, middle layer and outer layer intensities of the PVP (a) and INDO (b) ion markers of EC top coatings. EC 100% intensities are shown in blue bars, EC 100% - TEC intensities in red bars, EC-PVP 90-10% intensities in green bars and EC-PVP 75-25% intensities in purple bars.

4.4.4 Polymer miscibility

Polymer blends were prepared by spray drying from an ethanol solution and analyzed by mDSC to investigate polymer miscibility. Miscibility was evaluated based on the position and number of glass transition (T_g) events. The glass transition temperature was measured in the reversing heat flow (half height in the heat capacity step change) and first derivative of the reversing heat flow (peak value). mDSC thermograms with these signals are presented in Figure 4.13 with ERL based samples in figure 4.13a and EC based samples in figure 4.13b.

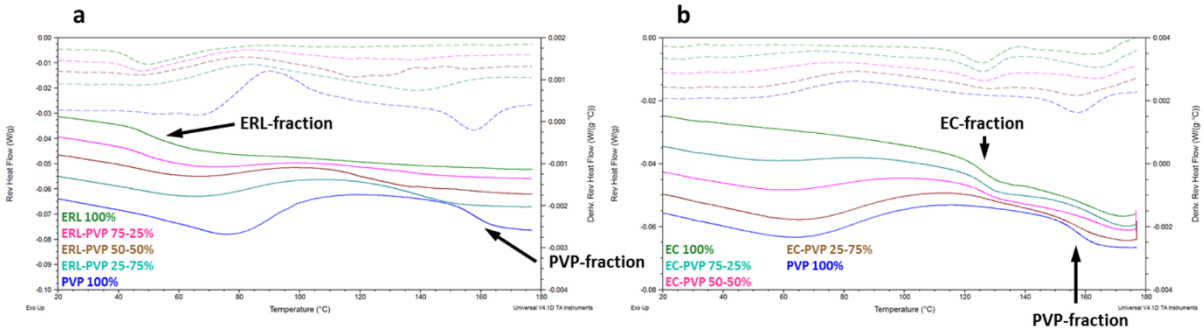

Figure 4.13: mDSC thermogram overlay of the reversing heat flow (full lines) and the first derivative of the reversing heat flow (dotted lines) of the different spray dried ERL-PVP (a) and EC-PVP (b) polymer mixtures.

The glass transition temperatures of all analyzed samples are given in Table 4.1 (EC-based samples) and Table 4.2 (ERL-based samples). The mean glass transition temperature of spray

dried pure PVP, EC and ERL is 156.8°C, 125.1°C and 53.5°C respectively. Two T_g's can be observed in the spray dried polymer blends, indicating that PVP is not miscible (or only to a certain extent) with ERL or EC. The major difference between EC-PVP mixtures and ERL-PVP relates to the fact that in the EC-PVP systems both T_g's remain more or less at the same temperature, while in coatings consisting of ERL-PVP the Tg of PVP decreases with increasing ERL content. No glass transition event due to the PVP fraction could be observed in the ERL-PVP 75-25 blend, while no clear ERL Tg can be observed in ERL-PVP 50-50% and ERL-PVP 25-75%.

Table 4.1: Glass transition temperatures of the different spray dried EC-PVP polymer mixtures.

EC/PVP ratio (%)	Glass transition temperature (C°)			
	EC-fraction		*PVP-fraction*	
	Mean	SD	Mean	SD
100/0	125.1	0.8		
75/25	125.0	0.7	161.1	1.0
50/50	125.1	0.1	162.2	1.0
25/75	125.5	0.6	156.9	0.4
0/100			156.8	0.2

All formulations are measured in triplicate with the mean and standard deviation.

Table 4.2: Glass transition temperatures of the different spray dried ERL-PVP polymer mixtures.

ERL/PVP ratio (%)	Glass transition temperature (C°)			
	ERL-fraction		*PVP-fraction*	
	Mean	SD	Mean	SD
100/0	53.5	0.7		
75/25	52.0	1.3	-	-
50/50	-	-	123.7	2.2
25/75	-	-	137.5	1.1
0/100			156.9	0.7

All formulations are measured in triplicate with the mean and standard deviation.

4.4.5 Physical structure of the glass solution layer

Different reference materials and coated beads were investigated by XRPD to investigate the stability of the solid state properties of the glass solution when applying a rate controlling membrane. Figure 4.14 shows the diffractograms of the reference materials, an INDO-PVP glass solution coating and different ERL based membrane top layers.

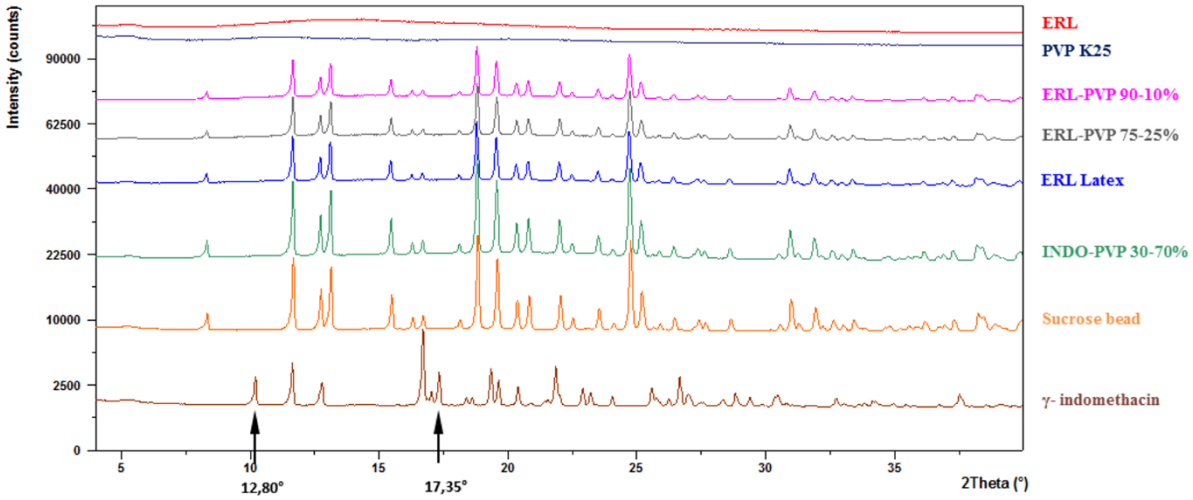

Figure 4.14: XRPD diffractogram of reference substances (ERL, PVP K25, sucrose pellet and γ -indomethacin), INDO-PVP glass solution coating and different ERL based coatings (ERL-PVP 90-10%, ERL-PVP 75-25% and ERL latex coating). Characteristic peaks of γ -indomethacin are marked with arrows at 12.80° and 17.35°

All coated samples show the Bragg peaks from the sucrose pellets, but none of them show the typical Bragg peaks of γ -indomethacin, which is the most stable crystalline form. Representative indomethacin Bragg peaks are indicated with arrows at 2θ angles of 12.80° and 17.35°. EC based samples were also analyzed and neither showed indomethacin Bragg peaks (data not shown).

4.5 Discussion

4.5.1 Coated bead surface and cross-sectional topography

The SEM image of the INDO-PVP coated bead (Figure 4.1A) shows a smooth surface with cracks of different sizes running all along the surface. These cracks are proposed to be a result of the drying of the glass solution. The spraying solvent, in this case ethanol, acts as a plasticizer of the INDO and PVP mixture, and as this solvent evaporates, the drug polymer mixture becomes more brittle as a result of an increasing glass transition temperature. This, together with contraction forces due to solvent evaporation from the spherical bead surface, could result in a cracked INDO-PVP glass solution layer. A cross-sectional image (Figure 4.2A) of these glass solution beads demonstrate that these cracks can extend from the outer surface to the sucrose core of the bead. These cracks also remain present when the INDO-PVP glass solution is top coated with an EC or ERL membrane (Figure 4.2B, 4.2B', 4.2C and 4.2C'). No cracks are present in any of the EC or ERL membranes themselves due to the probable higher flexibility of these films, which solely exist of polymer (or polymer mixtures). The topography of these coatings varies from very rough (ERL solution layer), over mildly rough (EC layer), to generally smooth (ERL dispersion layer). It is clear that the same polymer, sprayed from a solution or an aqueous dispersion generates vastly different surface morphologies. This is not unexpected as the film forming process from an aqueous dispersion is significantly different from that of a solution. The beads coated with the dispersion were also additionally cured to further optimize polymer inter-diffusion and coalescence, and this probably contributes to the generation of a smooth surface.

Although the cross-sectioning procedure applied induced specific features (artifacts) on the surface of the cross-section, like an unremoved part of the EC layer at the bottom part of Figure 4.2B or cutting traces observed in the glass solution layer of Figure 4.2B', the difference between the glass solution layer with an additional ERL top layer or an EC top layer is very clear. Firstly, the EC membrane shows a layered structure along the coated layer, while the ERL membrane shows a smooth topography along the cross-section more resembling the glass solution layer. A second main difference lies in the attachment of the top layers to the glass solution layer. While the border between the ERL coating and the glass solution can only be observed through a change in grey tone, the border between the EC layer and the glass solution layer is indicated by the presence of a discernible delamination. It is impossible to

know if this opening already existed before the cross-sectioning or if it was created during cross-sectioning. However, the fact that all samples were cut in the same way, suggests that the EC layer is, at the least, much more loosely attached compared to the ERL layer. The miscibility data, shown in the mDSC experiments, provide further arguments for this observation.

4.5.2 Composition of coated bead surfaces

ToF-SIMS surface analysis showed a clear determination of the composition and polymer distribution along the surface of the coated beads. We recently reported that INDO-PVP coated beads (30-70% w/w) form a glass solution, i.e. one phase systems characterized by a single T_g where the drug is molecularly dispersed into the polymer matrix[12]. The homogeneous distribution observed along the surface of INDO and PVP ions in the present study suggests the same excellent miscibility of both components. ToF-SIMS was able to clearly discriminate chemically between the four potential components (ERL, EC, PVP and INDO) in samples which can contain up to three of these components. This was demonstrated by the components marker ions which showed a high specificity. In contrast to the expected presence and distribution of INDO and PVP in the glass solutions, EC and ERL layers showed unexpected results. Where its presence would not be anticipated, PVP markers are clearly observed in pure ERL or EC top coatings (Fig. 4.4a,d and 4.6a,d Column 3 respectively). Two possibilities are proposed to explain the presence of PVP in these layers, the first one being a contamination with residual PVP, that became attached to the coating processor wall or Würster insert from the prior glass solution coating step. This is possible because the two coating layers are applied consecutively during the coating process, so there is always a fraction of droplets which are not sprayed on the beads and stick to the inner walls of the fluid bed coater or Würster insert and dry, or which dry before impinging on the beads. The second possibility is that PVP could migrate through the controlled release layer to the surface of the bead. Prior to drying of the sprayed polymer in the processor, the wetted particle could give rise to enhanced polymer mobility, leading to migration. It must be noted that while there is a clear presence of the PVP marker ion, very limited marker ion intensity of INDO was observed in the outer layer (only in ERL 100%, ERL 100% latex and EC surfaces). As the sprayed solution contains both INDO and PVP, there is no reason why INDO should not be present on the coater wall or should not migrate through the ERL layer together with the PVP. Firstly the specific ion for INDO has a much higher mass compared to the PVP marker

ion, making it more specific but less intense. Secondly, the glass solution only contains 30% (w/w) of INDO opposite to 70% (w/w) PVP. These two reasons could account for the smaller INDO marker intensities observed on ERL and EC surfaces.

When PVP is added as a pore former, it is more evenly distributed on the outer surface compared to the spots observed in the pure ERL or EC surfaces. For ERL based surfaces, a higher PVP marker intensity was observed in coatings containing 25% of PVP compared to those containing only 10% of pore former (Figures 4.5). The opposite was observed in EC based surfaces (Figure 4.7), but here, the high variability of the PVP marker intensities point to high variability in surface distribution and constitution. This could also be concluded when taking into account the distribution of PVP along the surface. Whereas in the ERL coated samples, the PVP is more evenly spread and present over the entire surface of the coated beads (Fig. 4.4b,c Column 3), in the EC coated samples a more localized PVP presence could be observed (Fig. 4.6b,c Column 3). This further points to more heterogeneity of EC-PVP surfaces compared to ERL-PVP surfaces.

4.5.3 Composition of coated bead cross-sections

Although an additional component was introduced in the coated bead cross-sections, the sucrose starting core, it was still possible to distinguish all compounds, i.e. finding marker ions for all chemical entities despite very similar structural compositions (both sucrose and EC are complex carbohydrates). All investigated samples show very distinct layering, namely a glass solution layer on top of the sugar core and an ERL or EC based layer on top of the glass solution. Consecutively coating both layers, even from an identical solvent did not result in some kind of transition layer between both coatings.

The presence of the PVP ion marker in pure ERL layers is not as pronounced as it was with the surface analysis, as only a diffuse presence along the ERL 100% latex layer is observed. When PVP is used as a pore former, there is an even distribution along the top coating layers. In pure EC layers, the diffuse presence of PVP can be attributed to the properties of the control sample. Again, when PVP is added as a pore former, the PVP marker intensity is significantly more pronounced along the top coating layer.

Analyzing cross-sections allowed for the investigation of potential INDO and/or PVP migration into the top coating ERL or EC layer. An inner, middle and outer layer was created for all samples by defining different regions of interest. The ERL based coating showed

decreasing PVP and INDO marker intensities along the top coating membrane, irrespective of the membrane constitution. This intensity gradient was higher for INDO marker intensities as opposed to PVP marker intensities, pointing to an increased INDO presence in the inner layer of the top coating membrane. This was most pronounced in ERL 100% latex membrane. Because this membrane is formed from an aqueous dispersion, the water used as a spraying vehicle, is not removed from the system as easily as ethanol, despite the higher coating chamber temperature (60°C versus 50°C). This in turn can enhance molecular mobility of INDO and cause a migration into this outer membrane. Another explanation can be the curing step of the latex formulation where beads are stored at higher temperature compared to the beads coated from an ethanol solution. Similar intensity gradients are observed at EC top coated membranes, although less pronounced. EC-PVP 75-25% is the only membrane not showing this gradient. The reason for this is unknown. It has to be remarked that the migration of INDO and PVP is very limited along the top coating membranes. INDO for example, has an intensity of maximum 15% in the entire EC or ERL top coatings compared to glass solution marker intensity. This limited migration of INDO and PVP cannot explain the presence of PVP spots, observed along the pure ERL or EC surfaces. Because there isn't a clear distributional evidence for this in the secondary ion images (no or very small and homogeneous marker presence), it can be concluded that these PVP spots at the surface are a result of contaminations during coating (collisions with dried powder particles on the coating walls). When small enough, this could generate spots on the surface which are not visible in cross-sections of the outer membranes.

4.5.4 Polymer miscibility

The mDSC study of miscibility between the rate controlling polymers EC or ERL on one hand and the pore former PVP on the other hand, shows a different phase behavior of these polymer mixtures. The EC-PVP system does not mix, which is apparent by the presence of two T_g's. Both glass transition temperatures stay fairly constant in all ratios, indicating immiscibility between both components. In case of the ERL-PVP blends we can observe an increase in the T_g of PVP with increasing PVP content. This shows that both polymers seem to be at least partially miscible. In ERL-PVP 50-50% and ERL-PVP 25-75% no ERL T_g could be determined because it was either masked by solvent or water evaporation, or because ERL was mixed with the PVP fraction. The poor miscibility of both polymer blends corresponds with previously made observations with ToF-SIMS, which showed separate PVP domains in

EC or ERL based layers. The partial miscibility between ERL and PVP can also explain why the ERL top coating is better attached to the glass solution layer. This is in contrast with the EC coating, which shows complete immiscibility with PVP, which is, at the most, only loosely connected. This immiscibility between EC and PVP can also be the explanation for the more localized PVP domains, when PVP is used as a pore former in EC coatings, as observed in ToF-SIMS surface images.

4.5.5 Glass solution phase analysis

It has been previously shown that an INDO-PVP 30-70% (w/w) coating surrounding a sucrose pellet forms a glass solution, i.e. a molecularly dispersed drug in a polymeric carrier, resulting in a one phase system[12]. It remains, however, possible that the application of a rate controlling membrane on top of this glass solution could potentially cause instability to the glass solution through crystallization of indomethacin. This could be especially true when the rate controlling membrane was applied from an aqueous dispersion, because it is well known that the presence of water, even in the form of water vapor, can potentially result in drug crystallization. From the results of the XRPD analysis of the coated beads it became apparent that this is not the case. As the measurements were performed in transmission mode, all different layers of the beads were scanned which is evidenced by the presence of the characteristic Bragg peaks of the sucrose pellets in all diffractograms. However, no characteristic Bragg peaks of crystalline indomethacin were present in any of the samples, indicating that indomethacin remains X-ray amorphous after the application of a rate controlling membrane, whether this is from an ethanol solution or an aqueous dispersion.

4.6 Conclusions

In this study, the composition and polymer distribution of complex coated systems was elucidated by combining complementary solid state analytical techniques. Sucrose cores were coated with an INDO-PVP glass solution layer and on top of this, a rate controlling membrane was applied. These membranes consisted of EC or ERL with or without a pore former (PVP), coated from a solution or an aqueous dispersion, and with or without plasticizer (TEC) added.

SEM images revealed vastly different topography of the surface of the different coated beads with a cracked surface for INDO-PVP glass solution, a rough surface for ERL coating from a solution and smooth surface for ERL coated from a dispersion. This difference can be appointed to the different film formation process and an additional curing step for the dispersion. Cross-sections revealed a difference in structure between ERL and EC based layers being smooth and well attached to the glass solution substrate or presenting a more layered structure loosely attached to substrate respectively. The difference in attachment can be attributed to the fact that ERL is partially miscible with PVP and that EC is immiscible.

ToF-SIMS analysis showed to be an excellent method to provide details regarding the chemical composition of the surfaces and the distribution of the different components. The ToF-SIMS analysis showed the unexpected presence of PVP in layers made up of pure ERL or EC, originating from residual presence in the fluid bed coater. INDO and PVP show very limited migration into the outer membranes. Furthermore, there is a different localization in the samples containing PVP as a pore former. In the ERL-PVP coatings, the PVP seems to be more evenly distributed throughout the surface, whereas in the EC-PVP coatings, the presence of PVP seems to be more localized. This difference can be explained by the miscibility differences shown in mDSC and can have a significant effect on drug diffusion through this layer.

XRPD analysis revealed that the application of a rate controlling membrane does not affect the solid state properties of the underlying glass solution, even when coated from an aqueous dispersion.

This study reveals a unique insight into complex coated systems (glass solution + controlled release layer) on inert carriers. Rate controlling polymer selection, pore former selection and concentration can all have major consequences for the resulting phase behavior, and

deposition onto the carrier. This in turn will have a significant impact on the performance of this type of drug delivery system.

4.7 References

1. Ayenew, Z.; Paudel, A.; Van den Mooter, G. Can compression induce demixing in amorphous solid dispersions? A case study of naproxen-PVP K25. *Eur. J. Pharm. Biopharm*. **2012**, 81, 207-213.

2. Varum, F. J. O.; Merchant, H. A.; Basit, A. W. Oral modified-release formulations in motion: The relationship between gastrointestinal transit and drug absorption. *Int. J. Pharm*. **2010**, 395, 26-36.

3. Garbacz, G.; Klein, S. Dissolution testing of oral modified-release dosage forms. *J. Pharm. Pharmacol*. **2012**, 64, 944-968.

4. Lopez, F. L.; Ernest, T. B.; Tuleu, C.; Gul, M. O. Formulation approaches to pediatric oral drug delivery: benefits and limitations of current platforms. *Expert. Opin. Drug Deliv*. **2015**, 12, 1727-1740.

5. Yu, L. Surface mobility of molecular glasses and its importance in physical stability. *Adv. Drug Deliv. Rev*. **2016**, 100, 3-9.

6. Tran, P. H. L.; Tran, T. T. D.; Park, J. B.; Lee, B. J. Controlled release systems containing solid dispersions: strategies and mechanisms. *Pharm. Res.* **2011**, 28, 2353–2378.

7. Baird, J. A.; Taylor, L. S. Evaluation of Amorphous Solid Dispersion Properties Using Thermal Analysis Techniques. *Adv. Drug Deliv. Rev.* **2012**, 64, 396-421.

8. Newman, A.; Engers, D.; Bates, S.; Ivanisevic, I.; Kelly, R. C.; Zografi, G. Characterization of amorphous API : Polymer mixtures using X-ray powder diffraction. *J. Pharm. Sci.* **2008**, 97, 4840-4856.

9. Yun, Y.; Zou, X.; Hovmöller, S.; Wan, W. Three-dimensional electron diffraction as a complementary technique to powder X-ray diffraction for phase identification and structure solution of powders. *IUCrJ* **2015**, 2, 267-282.

10. Liu, J.; Saw, R. E.; Kiang, Y. H. Calculation of effective penetration depth in X-ray diffraction for pharmaceutical solids. *J. Pharm. Sci.* **2010**, 99, 3807-3814.

11. Thakral, N. K.; Yamada, H.; Stephenson, G. A.; Suryanarayanan R. Spatial Distribution of Trehalose Dihydrate Crystallization in Tablets by X-ray Diffractometry. *Mol. Pharm.* **2015**, 12, 3766-3775.

12. Dereymaker, A.; Van den Mooter, G. The Peculiar Behavior of the Glass Transition Temperature of Amorphous Drug–Polymer Films Coated on Inert Sugar Spheres. *J. Pharm. Sci.* **2015**, 104, 1759-1766.

13. Fletcher, J. S.; Rabbani, S.; Henderson, A.; Blenkinsopp, P.; Thompson, S. P.; Lockyer, N. P.; Vickerman, J. C. A New Dynamic in Mass Spectral Imaging of Single Biological Cells. *Anal. Chem.* **2008**, 80, 9058-9064.

14. Touboul, D.; Halgand, F.; Brunelle, A.; Kersting, R.; Tallarek, E.; Hagenhoff, B.; Laprévote, O. Tissue Molecular Ion Imaging by Gold Cluster Ion Bombardment. *Anal. Chem.* **2004**, 76, 1550-1559.

15. Kraft, M. L.; Klitzing, H. A. Imaging lipids with secondary ion mass spectrometry *Biochim. Biophys. Acta* **2014**, 1841, 1108-1119.

16. Passarelli, M. K.; Winograd, N. Lipid imaging with time-of-flight secondary ion mass spectrometry (ToF-SIMS) *Biochim. Biophys. Acta* **2014**, 1811, 976-990.

17. Bodzon-Kulakowska, A.; Suder, P. Imaging mass spectrometry: Instrumentation, applications, and combination with other visualization techniques. *Mass Spectrom. Rev.* **2016**, 35, 147–169.

18. McPhail, D. S. Applications of Secondary Ion Mass Spectrometry (SIMS) in Materials Science. *J. Mater. Sci.* **2006**, 41, 873–903.

19. Belu, A. M.; Davies, M. C.; Newton, J. M.; Patel, N. ToF-SIMS characterization and imaging of controlled-release drug delivery systems. *Anal. Chem.* **2000**, 72, 5625–5638.

20. Barnes, T. J.; Kempson, I. M.; Prestidge, C. A. Surface analysis for compositional, chemical and structural imaging in pharmaceutics with mass spectrometry: a ToF-SIMS perspective. *Int. J. Pharm.* **2011**, 417, 61–69.

21. Meeus, J.; Chen, X.; Scurr, D. J.; Ciarnelli, V.; Amssoms, K.; Roberts, C. J.; Davies, M. C.; Van den Mooter, G. Nanoscale surface characterization and miscibility study of a spray-dried injectable polymeric matrix consisting of poly(lactic-co-glycolic acid) and polyvinylpyrrolidone. *J. Pharm. Sci.* **2012**, 101, 3473–3485.

22. Meeus, J.; Scurr, D. J.; Chen, X.; Amssoms, K.; Davies, M. C.; Roberts, C. J.; Van den Mooter, G. Combination of (M)DSC and Surface Analysis to Study the Phase Behaviour and Drug Distribution of Ternary Solid Dispersions. *Pharm. Res.* **2015**, 32, 1407-1416.

23. Meeus, J.; Lenaerts, M.; Scurr, D. J.; Amssoms, K.; Davies, M. C.; Roberts, C. J.; Van den Mooter, G. The Influence of Spray-Drying Parameters on Phase Behavior, Drug Distribution, and In Vitro Release of Injectable Microspheres for Sustained Release. *J. Pharm. Sci.* **2015**, 104, 1451-1460.

24. Meeus, J.; Scurr, D. J.; Appeltans, B.; Amssoms, K.; Annaert, P.; Davies, M. C.; Roberts, C. J.; Van den Mooter, G. Influence of formulation composition and process on the characteristics and in vitro release from PLGA-based sustained release injectables. *Eur. J. Pharm. Biopharm*. **2015**, 90, 22-29.

25. Brown, A.; Vickerman, J. C. Static SIMS for applied surface analysis. *Surf. Interface Anal.* **1984**, 6, 1–14.

26. Jesson, D. A.; Watts, J. F. The Interface and Interphase in Polymer Matrix Composites: Effect on Mechanical Properties and Methods for Identification. *Polym. Rev.* **2012**, 52, 321–354.

27. Lietz, C. B.; Gemperline, E.; Li, L. Qualitative and quantitative mass spectrometry imaging of drugs and metabolites. *Adv. Drug Deliv. Rev.* **2013**, 65, 1074–1085.

28. Prestidge, C. A.; Barnes, T. J.; Skinner, W. Time-of-flight secondary-ion mass spectrometry for the surface characterization of solid-state pharmaceuticals. *J. Pharm. Pharmacol.* **2007**, 59, 251-259.

Chapter 5: Controlling the release of indomethacin from glass solutions layered with a rate controlling membrane using fluid-bed processing. Part 2: The influence of formulation parameters on drug release

Results of this chapter are based on:

Dereymaker, A.; Pelgrims, J.; Engelen, F.; Adriaensens, P.; Van den Mooter, G. Controlling the release of indomethacin from glass solutions layered with a rate controlling membrane using fluid-bed processing. Part 2: The influence of formulation parameters on drug release Mol Pharm ***xxxx****, (manuscript submitted).*

5.1 Abstract

This study aimed to investigate the pharmaceutical performance of an indomethacin-polyvinylpyrrolidone (PVP) glass solution applied using fluid bed processing as a layer on inert sucrose spheres, and subsequently top-coated with a release rate controlling membrane consisting of either ethyl cellulose or Eudragit RL. The implications of the addition of a pore former (PVP) and the coating medium (ethanol or water) on the diffusion and release behavior were also considered. In addition, the role of a charge interaction between drug and controlled release polymer on the release was investigated.

Diffusion experiments pointed to the influence of pore former concentration, rate controlling polymer type and coating solvent on the permeability of the controlled release membranes. This can be translated to drug release tests, which show the potential of diffusion tests as a preliminary screening test and that diffusion is the main factor influencing release. Drug release tests also showed the effect of coating layer thickness. A charge interaction between INDO and ERL was demonstrated, but this had no negative effect on drug release. The higher diffusion and release observed in ERL-based rate controlling membranes was explained by a higher hydrophilicity, compared to EC.

5.2 Introduction

Research on solid dispersions has been spanning for over half a century. Since being first described in 1961 by Sekiguchi and Obi [1] , over being defined and classified 10 years later by Chiou and Riegelman [2], to ultimately being a widespread concept as a poorly soluble drug formulation strategy, solid dispersions have gathered some attention over time [3]. Typically, solid dispersions are formulated in combination with hydrophilic polymers as immediate release formulations. A lot of hydrophilic polymers (semi-crystalline and amorphous) have been tested for their potential use in solid dispersions [4, 5], but only few have been successfully utilized into marketed solid dispersions [6]. When using these polymers, which show good water solubility, supersaturated gastrointestinal drug concentrations occur relatively fast after administration. However, supersaturation is not always maintained for a sufficient period of time leading to sub-optimal bioavailability enhancement. Even in vitro-in vivo comparisons cannot be readily made, as was reported in a study by Six *et al.* [7]. Transforming rapidly dissolving but fast-precipitating solid dispersions into slow-release formulations might therefore improve their absorption enhancing potential [8].

Different techniques have been proposed and used to prepare controlled release formulations for solid dispersions, like hot melt extrusion, powder compression, granulation and emulsion methods, or more recently electrospraying [9]. Hot-melt extrusion, for example, has been one of the well explored systems to make slow-release drug-polymer systems. The drugs incorporated are mainly water soluble compounds that are combined with a controlled release polymer [10, 11] that can be part of the matrix or used as a rate controlling membrane [12]. In the current study, fluid bed coating is proposed as an alternative and relatively unexplored technique. Beten *et al.* showed the feasibility of loading controlled release drug-polymer coevaporates of dipyridamole and enteric Eudragit polymers using an industrial scale fluid bed coating system [13]. One of the main advantages of this process is that additional or multiple steps in the preparation process like milling, sieving, compression or additional tablet coating can be omitted. The ability of fluid bed coating to produce multiple layered systems is ideal for the preparation of controlled release solid dispersions. The solubilization can be maximized by choosing an appropriate (polymeric) carrier for the solid dispersion (or, ideally, the glass solution) layer. Subsequently, an additional rate controlling membrane can be applied on top of the glass solution layer to optimize the release during a well-defined time frame.

The feasibility of this approach is described in the companion paper ('Controlling the release of indomethacin from glass solutions layered with a rate controlling membrane using fluid-bed processing. Part 1: Surface and cross-sectional chemical analysis'). Two clearly defined coating layers were observed. The surface properties of different rate controlling membranes applied could be explained to a large extent by the polymer mixing behavior. The physical structure of the underlying glass solution layer was also shown not being affected by the slow-release top coating, even when this last was sprayed from an aqueous dispersion.

The focus of the current paper is the investigation of the pharmaceutical performance of these formulations, i.e. their release behavior and the effect of formulation changes on the drug release. The glass solution layer is always made up of indomethacin (INDO) in polyvinylpyrrolidone K25 (PVP) in a 30:70 % w/w ratio. Two different rate controlling polymers will be tested, ethyl cellulose (EC) and Eudragit RL (ERL). PVP will also be used as a pore former and triethyl citrate (TEC) will be used as a plasticizer. Special emphasis in this study will be put on the possible charge interaction between negatively charged INDO (above pH 4.5) and the positively charged ERL, which is a water insoluble polymer, but the presence of quaternary ammonium groups in ERL is responsible for pH-independent swelling [14, 15]. Drug release from ERL systems however, can be sensitive to the presence of other anionic species like buffer components or organic acids [16-18]. This charge interaction has also been reported with other NSAID's in the past [19-21]. This possible charge interaction will be studied using Solid State Nuclear Magnetic Resonance (ss-NMR) and the implications of this interaction will be studied in sorption, permeability and drug release tests.

5.3 Experimental section

5.3.1 Materials

Indomethacin was purchased from FAGRON Ltd. (Waregem, Belgium). Polyvinylpyrrolidone K 25 was a generous gift from BASF (Ludwigshafen, Germany). Sucrose spheres (diameter 710 - 850 µm) were kindly donated by Hanns G. Werner GmbH (Tornesch, Germany). Ethyl cellulose (ethoxy content 48.0-49.5% w/w) powder and triethyl citrate (TEC) were purchased from Sigma-Aldrich (Zwijndrecht, The Netherlands). Eudragit RS® PO (ERS), Eudragit RL® PO and Eudragit RL® 30D were purchased from Evonik Industries (Darmstadt, Germany).

5.3.2 Fluid bed coating

Coated beads were prepared using an Aeromatic MP 1 multiprocessor (GEA, Bubendorf, Switzerland) in a bottom spray setup, equipped with a Würster insert. A 30:70 (w:w) INDO-PVP (w/w) glass solution with a total solid content of 250,0g was coated onto 500,0g of sucrose beads from a 10% (w/v) ethanol solution. The sucrose spheres were loaded into the preheated coating chamber at 50°C and heated for 10 minutes. The drug-polymer solution was coated onto the sucrose pellets, using a feed rate of 13cm^3/min. This feed was atomized at an air pressure of 1.5 bar. Meanwhile the heated air stream was passing through the fluid bed coater at a rate of 1.78 m^3 /min. When the spraying was finished, the pellets were dried until immobilization due to electrostatic charges was observed. The coated spheres were unloaded, weighed and dried for an additional 48 hours in an oven at 50°C. In the case when a top layer (rate controlling membrane) was applied, the feed solution was immediately changed after completion of the glass solution layer. The controlled release top layer consisted of a rate controlling polymer (ERL or EC) with an added pore former (PVP K25) in a 10% or 25% ratio to the total solid content and the plasticizer TEC, added in a concentration of 20% w/w relative to the amount of rate controlling polymer. The rate controlling membrane was applied from a 10% w/v ethanolic solution. Also, ERL-PVP 90-10% (w-w) was applied as an aqueous dispersion (10% w/v) instead of an ethanolic solution. The coating process parameters are the same for the top coating layer as for the glass solution layer, except for the feed rate with the ERL ethanolic solutions, where the feed rate was reduced to 6.5cm^3 /min) because of the electrostatic charges created inside of the fluid bed coater. After completion of the coating, the beads were dried in the coater for at least 10 minutes, followed by further drying in an

oven for at least 48 hours. Ethanolic solutions are dried at 50°C, aqueous dispersions at 60°C to allow for curing of ERL.

During coating of the rate controlling membrane, samples of 10-15g were taken at different time points to measure the coating layer thicknesses, expressed as percentage weight gain, relative to the weight of the glass solution coated beads.

5.3.3 Drug diffusion

Drug diffusion through a rate controlling membrane is tested with a diffusion cell set up, represented in Figure 5.1.

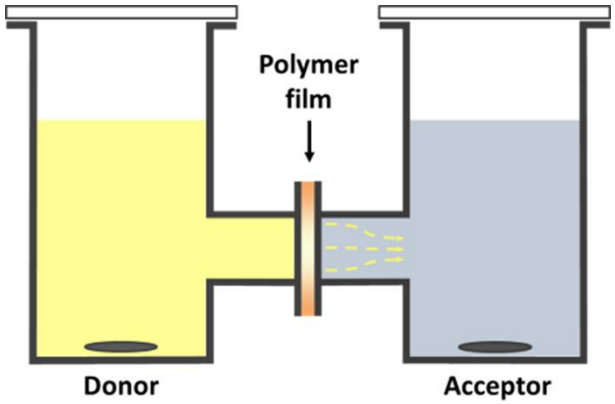

Figure 5.1: Schematic representation of the diffusion cell set-up.

The polymer film was clamped between a donor and acceptor compartment. The diameter of polymer film in contact with donor and acceptor compartment is 18 or 25mm depending on the used cells. The diffusion medium used was a 100mM phosphate buffer solution of pH 6.8 with 15% propylene glycol to enhance INDO solubility in the donor compartment. For the donor solution 1.00mg/ml INDO was dissolved in the diffusion medium, the acceptor solution contained the blank medium. Volume of both donor and acceptor compartment was 100ml. During diffusion experiments, both compartments were also sealed from the air and constantly stirred with magnetic stirrers to ensure homogeneous distribution.

Controlling rate membranes, tested in the diffusion experiments, were prepared by film casting from an ethanol solution or aqueous dispersion onto a Teflon plate and drying it for 24 h at room temperature under a funnel. After this, they were put into an oven and dried for an additional 24h at 50°C for the solutions and for 48h at 60°C for the dispersions. Eudragit RL and ethyl cellulose are used as controlled release polymers (ERL100% and EC 100%), PVP K25 is optionally added as a pore former in 10 or 25% (w/w) based on the total solid content

(ERL-PVP 90-10%, ERL-PVP 75-25%, EC-PVP 90-10% and EC-PVP 75-25%). TEC was added as a plasticizer in all membranes in a 20% (w/w) concentration, based on the controlled release polymer mass. Ethanol solutions were prepared for ERL and EC based samples and aqueous dispersions for ERL based samples, both in a 10% w/v ratio.

Diffusion tests were performed with an automated sampling device, a Gilson Liquid Handler 215 (Gilson, Middleton, WI, USA). All rate controlling membranes were tested in triplicate, except for EC 100% and EC-PVP 90-10% which were tested in duplicate. At each sampling point, a 1ml sample was removed from the acceptor compartment and replaced with 1ml of blank medium. Samples are directly injected into the HPLC system for analysis.

Drug concentrations at different time points were used to calculate the permeability coefficient (P, cm/s) using following equation [22]:

$$\frac{2PS}{V}t = -ln\left(\frac{C_0 - 2C_a}{C_0}\right) \qquad \text{Eq. 5.1}$$

In this equation; S is the diffusion surface area (cm^2), V is the volume of donor and acceptor (ml), C_0 is the initial donor concentration and C_a the acceptor concentration (mg/ml) at time t (s).

5.3.4 High Performance Liquid Chromatography (HPLC)

Quantitative analysis of the samples was performed using a Merck-Hitachi Lachrom HPLC system consisting of a Merck Hitachi L-7100 pump, an L-7420 UV-VIS detector, an L-7200 autosampler and a D-7000 interface (Merck, Darmstadt, Germany). Injections were run through a Chromolith performance RP-18 column of 100mm x 4.6mm (Merck, Darmstadt, Germany). The mobile phase was 30% orthophosphoric acid solution (0.5% v/v), 40% acetonitrile and 30% methanol. Flow rate was set at 1.0 ml/min and injection volume at 20µl. INDO absorption was measured at 320nm and the retention time was approximately 3.3min. A calibration curve of area under the curve (AUC) vs. concentration was constructed using standard INDO solutions (0.125 mg/ml – 0.244 µg/ml) prepared by diluting a stock solution (1mg/ml in ethanol). Linearity was confirmed through linear regression analysis (R^2 >0.999). Limit of detection (LOD) and limit of quantification (LOQ) were determined and were lower than the smallest INDO concentration of the calibration curve.

5.3.5 Drug sorption tests

Powders or films of ERL, ERS and EC were added in a test tube filled with 5.0ml of either a 200µg/ml or 100µg/ml INDO solution (medium: phosphate buffer pH 6.8) and rotated for 48 hours in a rotary mixer. After 48 hours, a sample was taken from the solution, filtered and analyzed with HPLC . Drug sorption to the polymer was calculated from the INDO concentration decline. All conditions were tested 5 times.

5.3.6 Solid-state NMR

The ^{13}C-CP/MAS NMR spectra were recorded at room temperature on an Agilent VNMRS DirectDrive 400MHz spectrometer (9.4 T wide bore magnet) equipped with a T3HX 3.2 mm probe dedicated for small sample volumes and high decoupling powers. Magic angle spinning (MAS) was performed at 15 kHz with ceramic rotors of 3.2 mm (22 µl rotors). The aromatic signal of hexamethylbenzene was used to determine the Hartmann-Hahn condition ($\omega_{1H} = \gamma_H B_{1H} = \gamma_C B_{1C} = \omega_{1C}$) for cross-polarization and to calibrate the carbon chemical shift scale (132.1 ppm). Other acquisition parameters were: a spectral width of 50 kHz, a 90° pulse length of 2.5 µs, a spin-lock field for CP of 100 kHz, a contact time for CP of 1.0 ms, an acquisition time of 20 ms, a recycle delay time of 7.5 s and 350-45000 accumulations (350 scans for INDO, 2700 scans for Eudragit RL® and 45000 scans for the INDO-ERL solid dispersion from an ethanol solution (INDO-ERL EtOH) as well as for the INDO-ERL powder isolated from a phosphate buffer pH6.8 (INDO-ERL pH 6.8)). High power proton dipolar decoupling during the acquisition time was set to 100 kHz.

Two different INDO-ERL samples were prepared. The first one was prepared by dispersing ERL particles in a 200µg/ml INDO solution in phosphate buffer pH 6.8. After 48h of constant stirring, ERL particles were filtered and dried in an oven at 50°C. The second sample was prepared by spray drying an equivalent INDO-ERL ratio from an ethanol solution (10% w/v) using a Büchi Mini Spray Dryer B-191 (Flawil, Switzerland) and applying an inlet air flow rate of 0.56 m³/min, an inlet air temperature of 50°C, an atomizing air flow rate of 0.02 m^3/min and a feed rate of 4.8 cm^3/min. After collecting of the powder, it was additionally dried in an oven at 50°C.

5.3.7 Water permeation through isolated polymer films

Water permeation through isolated polymer films was tested using aluminium cups containing 5.0ml of water. A schematic representation is provided in Figure 5.2.

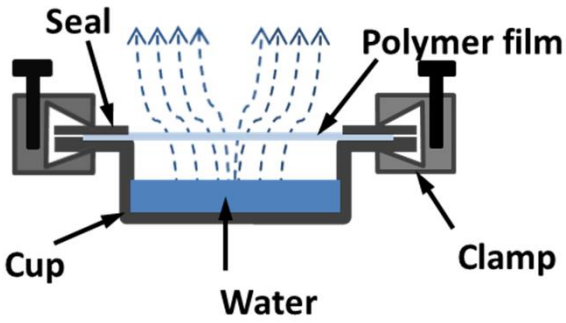

Figure 5.2/ Schematic representation of the diffusion cup set-up.

Films were prepared using the solvent casting method described in the drug diffusion section. Water evaporation was tested for the ERL 100%, ERL-PVP 90-10%, ERL-PVP 75-25%, EC-PVP 90-10% and EC-PVP 75-25% polymer films. Cups were stored at ambient conditions and weighed at fixed time intervals for at least 126 hours to constant mass. This allowed calculating the percentage loss of water at each weighing interval. Tests were performed in duplicate.

5.3.8 Drug release

Drug release tests of the different controlled release formulations were performed using a Hanson SR8PLUS dissolution station (SpectraLab Scientific Inc., Markham, Canada). The release medium was 500ml of a 100mM phosphate buffer pH6.8. Paddle speed was set at 120rpm and the temperature at 37.0 °C (±1.0). Samples were accurately weighed and were equivalent to an INDO dose of 75mg. At sampling time intervals, a 1ml sample was taken, filtered (pore size: 0.45µm) and put into an HPLC vial. The sample taken was replaced by 1ml of blank dissolution medium. Sampling times were 30, 60, 90, 120, 180, 240, 300 and 360 min. The quantitative analysis of the samples was performed with HPLC using the above described method. All formulations were tested in triplicate.

5.3.9 Content analysis

Accurately weighed formulations (with a theoretical INDO content of 3mg) were transferred into a test tube with 5.0ml of ethanol and rotated for 24h. Thereafter 1ml of ethanol solution was withdrawn, filtered (pore size 0.45µm) and analyzed with HPLC.

5.3.10 Statistical analysis

Differences between the permeability coefficients of the different membranes were evaluated using ANOVA and unpaired t-testing. Results were considered statistically significantly different if $p<0.05$.

The similarity factor *f2* was used to compare drug release profiles of different formulations[23]. Two profiles are considered not significantly different when the *f2* value is between 50 and 100.

5.4 Results

5.4.1 Indomethacin diffusion through rate controlling membranes

Permeability coefficients are calculated from the concentration change in the acceptor compartment. Values are shown in Figure 5.3.

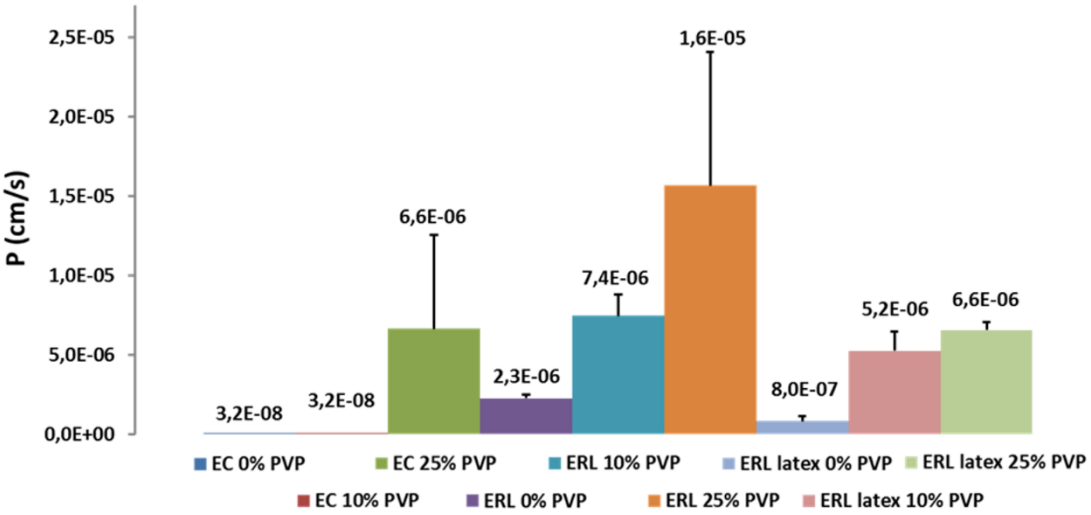

Figure 5.3: Permeability coefficients of INDO through different rate controlling membranes

In general, if the amount of PVP increases, the permeability of INDO increased as well. This is noticed for all three formulation groups, EC based films casted from an ethanol solution, ERL based films casted from an ethanol solution and ERL based samples casted from an aqueous dispersion (so-called 'latex').The differences in the permeability of the films when changing the PVP content are significant, except for ERL-PVP 90-10% and ERL-PVP 75-25% (p = 0,2371), ERL 100% and ERL-PVP 75-25% (p= 0,1104), and also, ERL-PVP 90-10% latex and ERL-PVP 75-25% latex (p= 0,1493). Apart from differences related to the amount of PVP incorporated, also differences related to the rate controlling polymer were observed. The permeability of INDO is always higher for ERL based formulations (solution or dispersion) as compared to EC based formulations (given the same amount of PVP). All these permeability differences are statistically significant, except for ERL-PVP 75-25% and EC-PVP 75-25% (p = 0,2035). Both of these films show a very large standard deviation in the value of P. Also ERL-PVP 75-25% latex and EC-PVP 75-25% do not show a significant difference since they have the same P-value. Films casted from a solution show higher P-values compared to films prepared from an aqueous dispersion, but the difference was only statistically significant for films of ERL 100% and ERL latex 100%; for films containing10% and 25% PVP the difference was not significant (p = 0,1052 and p = 0,2027).

5.4.2 Indomethacin sorption to rate controlling polymers

Because the rate controlling polymers EC, ERL and ERS are not soluble in aqueous media, INDO can sorb onto or into the swollen polymer particles. Figure 5.4 shows the amount (µg) of INDO that was sorbed into/onto the polymer particles (A) or the films (B) per milligram of CR polymer. These graphs clearly show that ERL powder and films incorporated the largest amount of INDO, irrespective of the INDO concentration in the medium. Moreover, INDO sorption in ERL doubled when the INDO concentration doubled, from 22.4µg/mg to 44.9µg/mg for the powder and from 20.4µg/mg to 44.0µg/mg for the film. EC showed the second largest INDO sorption in powders but lowest in the films, where it almost didn't sorb any INDO (0.0394µg/mg and 0.186µg/mg for 100 and 200µg/ml INDO concentration, respectively). INDO sorption in EC powder also almost doubled when the concentration doubled (8.76µg/mg and 16.4µg/mg). INDO sorption on ERS only slightly increased with increasing INDO concentration in films (from 4.74µg/mg to 6.71µg/mg) and powders (from 4.63µg/mg to 5.51µg/mg). Sorption in films was also slightly higher than sorption in powders.

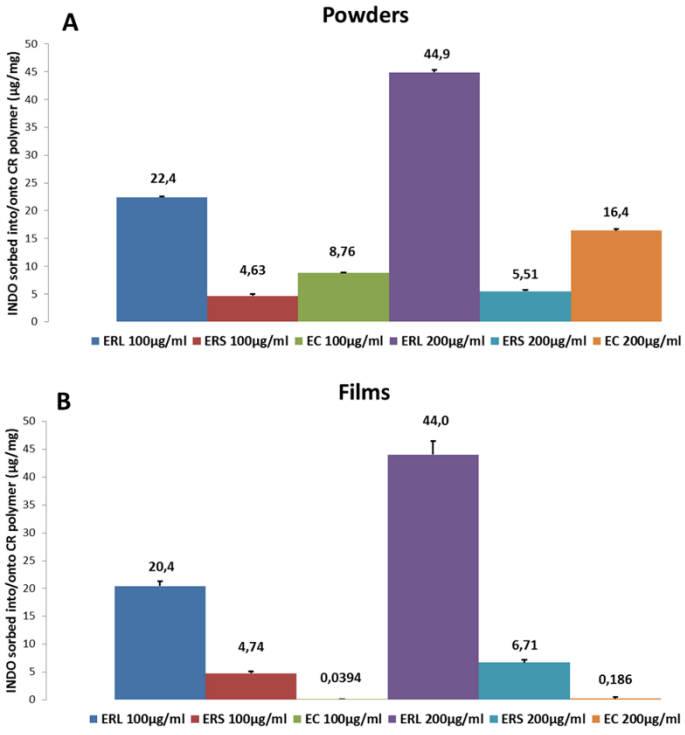

Figure 5.4: Sorption of INDO into/onto different controlling rate polymers in the form of powder (A) or a film (B) in phosphate buffer medium pH 6.8

5.4.3 ^{13}C-CP/MAS solid-state NMR investigation into drug-polymer interactions

INDO and ERL reference spectra, together with the spectra of INDO-ERL solid dispersion from an ethanol solution (INDO-ERL EtOH) and INDO-ERL powder isolated from phosphate buffer pH6.8 (INDO-ERL pH 6.8) are shown in Figure 5.5.

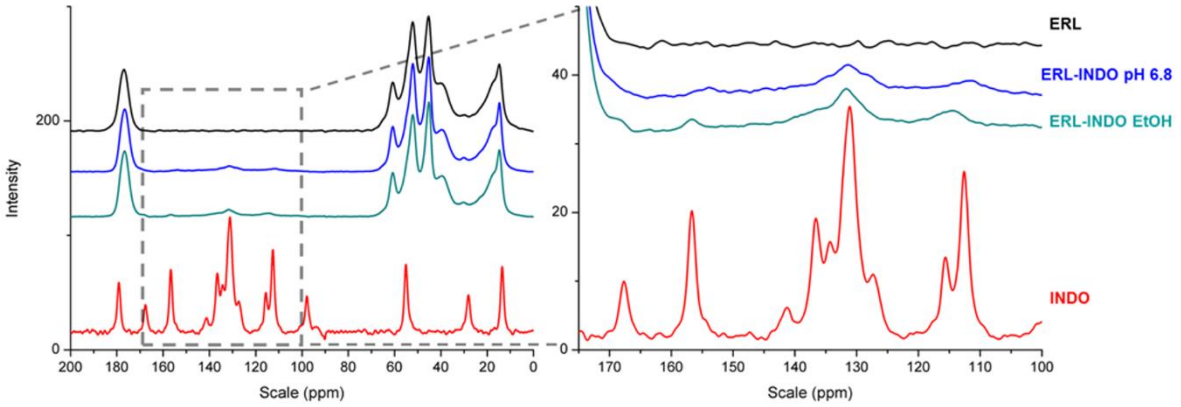

Figure 5.5: ^{13}C-CP/MAS NMR spectra of INDO (red), ERL (black), INDO-ERL solid dispersion from ethanol solution (green) and INDO-ERL powder isolated from phosphate buffer pH6.8 (blue). In the detailed view on the right, INDO intensity is reduced by factor 3.

Each INDO carbon nucleus shows a single signal without splitting, indicative for the stable γ -form[24]. Specially the signal at 156.7 ppm, attributed to the aromatic carbon bearing the methoxy group, is highly specific and confirms that the INDO starting material was γ -indomethacin[24, 25] (other peak assignments can be found in these references as well). The spectrum of INDO-ERL EtOH still shows the characteristic INDO peak at 156.7 ppm next to other INDO signals around 114.5 ppm, 131.5 ppm and 167.7 ppm. These peaks are situated at exactly the same position as for the INDO reference. The spectrum of the material prepared by soaking ERL in an INDO solution above its pKa (INDO-ERL pH 6.8) however shows clearly two significant chemical shift changes, i.e. an upfield shift of the signal at 156.7 ppm to 153.9 ppm, and an upfield shift of the signal at 114.5 ppm to 111.5 ppm. Moreover, the 167.7 ppm signal is shifted downfield and so coincides with the intense signal of the ERL carbonyl carbon. These changes point to an electrostatic interaction between INDO and ERL.

5.4.4 Water vapour diffusion through rate controlling membrane

The permeation of water through the polymer films (expressed as percentage water loss) was measured over time and plotted in Figure 5.6. The evaporation rate increased with increasing pore former concentration for both ERL based and EC base rate controlling films. The time to lose 50% of water was calculated according to the equation of the trendline and was found to be 68h for ERL-PVP 75-25%, 80h for ERL-PVP 90-10% and 97h for ERL 100%. The time to reach 50% water content was 83h for EC-PVP 75-25% and 103h for EC-PVP 90-10%. In case the same amount of pore former is present in the films, ERL based films have faster mass loss compared to EC based samples.

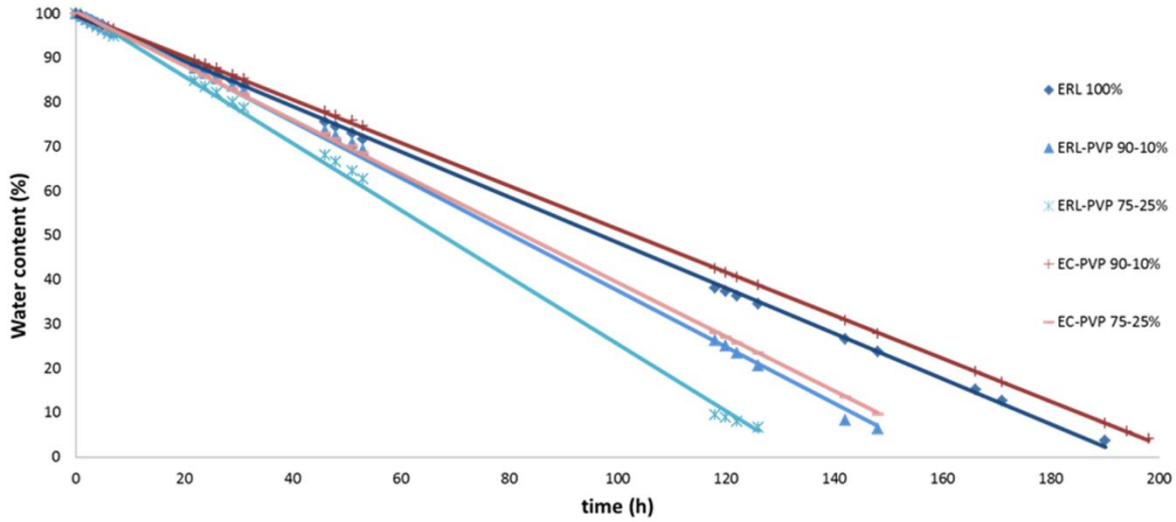

Figure 5.6: Water evaporation (in content %) through rate controlling membranes as a function of time.

5.4.5 Drug release

Crystalline indomethacin and INDO-PVP glass solutions

The dissolution of crystalline indomethacin and the release from INDO-PVP 30-70% (w/w) glass solutions coated onto sucrose beads is shown in Figure 5.7. Already at the first time point (60 min), INDO-PVP glass solutions showed full release. Glass solutions were considered to have an immediate release profile. Crystalline INDO on the other hand, only gradually reached a plateau of 95% release after 5 hours.

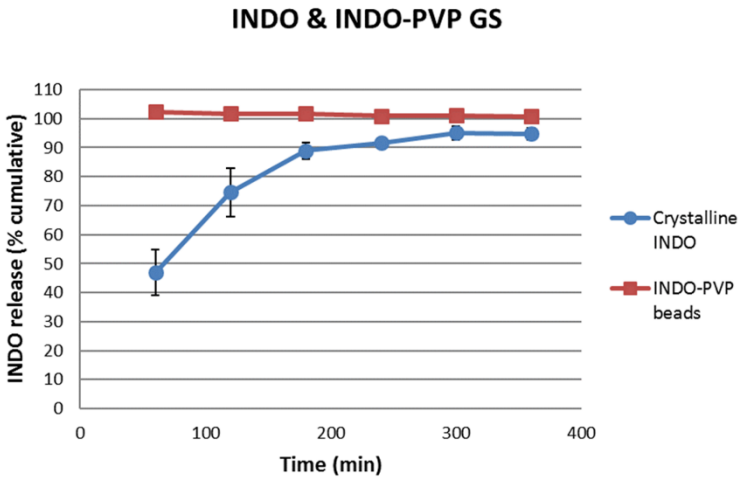

Figure 5.7: INDO release in function of time for crystalline INDO (blue dots) and INDO-PVP 30-70% (w/w) glass solution coated around inert carriers (red squares).

EC rate controlling membranes

INDO release was tested for EC-PVP 90-10% and EC-PVP 75-25% coatings on top of INDO-PVP glass solutions. Figure 5.8 shows the INDO release (cumulative %) in function of time for beads coated with an EC-PVP 90-10% rate controlling outer membrane. The coating thickness was varied from 9.7% to 36.6%. Increasing coating layer thicknesses showed decreased and slower INDO release. Maximum release after 6h was 96% for 9.7% coating, 38% INDO release for 19.1% coating, 3% for 28.0% coating and 9% for 36.6% coating. The profiles were different. Initial release is slow and shows a lag time, which increases with increasing coating layer thickness. This is followed by a period of high release rate for the 9.7% (between 60 and 180 min) and 19.1% (between 180 and 360 min) coating level. The lowest coating level shows a decreased INDO release between 180 and 360 min. The release profiles of the formulations with the highest coating levels (28.0 and 36.6%) were still in a lag phase which lasted for the entire 6 hours. All release profiles are significantly different, except for 28.0 and 36.6% (f_2=81.2), which explains why 36.6% coating level has a higher mean release compared to 28.0% coating level.

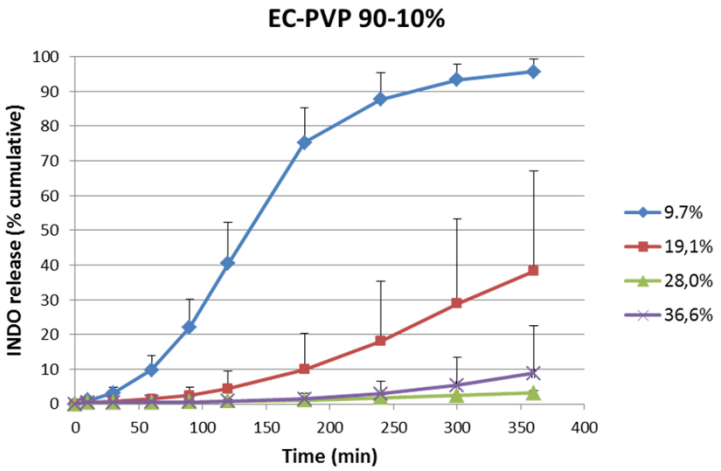

Figure 5.8: INDO release in function of time for INDO-PVP 30-70% (w/w) glass solution and an EC-PVP 90-10% (w/w) rate controlling membrane. Different coating levels were tested: 9.7% (blue), 19.1% (red), 28.0% (green) and 36.6% (purple).

INDO release from EC-PVP 75-25% beads was quasi immediate. All beads reach their maximum release after 60-100min and this irrespective of the coating layer thickness, which varied from 9.5% to 35.8% (a release profile has been provided in the Supplementary Data of this chapter, Figure A).

ERL rate controlling membranes

The INDO release from INDO-PVP glass solutions was tested with ERL-PVP 90-10% (coated from either an ethanol solution or an aqueous dispersion) and 75-25% rate controlling membranes on top of the glass solutions. The release profiles of ERL-PVP 90-10% rate controlling membranes, coated from a solution are shown in Figure 5.9. Also in this case, increasing the coating layer thickness resulted in slower and decreased INDO release. While a 11.2% coating layer still shows 84% release after 6h, the release drops to 75% for 21.7% coating level, to 55% for 31.7% coating level and, ultimately, to a mere 50% for the highest coating level (36.3%). ERL-PVP 90-10% beads showed initial high drug release rate (burst release) followed by a slower INDO release for the lowest coating level. Formulations having higher coating levels showed an initial slow release followed by an increased release rate up until 90 minutes followed by a decreased release rate. All release profiles are significantly different from each other except for 31.7% and 36.6% (f_2=66.2).

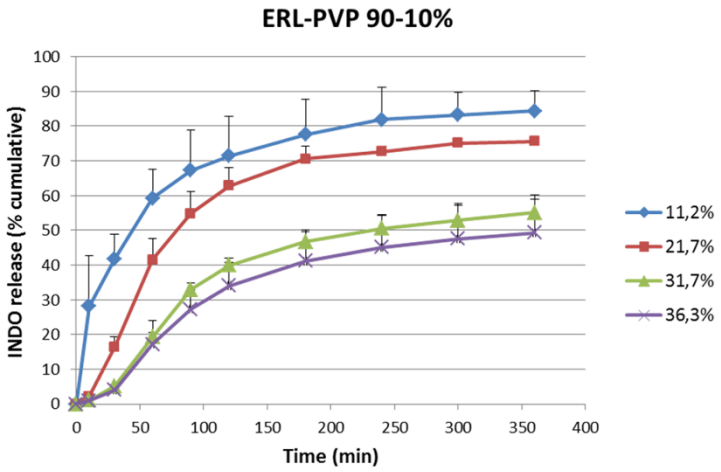

Figure 5.9: INDO release in function of time for INDO-PVP 30-70% (w/w) glass solution and an ERL-PVP 90-10% (w/w) rate controlling membrane. Different coating levels were tested: 11.2% (blue), 21.7% (red), 31.7% (green) and 36.3% (purple).

ERL-PVP 75-25% coated beads also showed an INDO release which was highest (93%) and fastest from beads with the smallest coating amount (11.3%). Similar to the other formulations, this decreased to 68% and 57% with an increasing coating level of 21.9% and 32.0% respectively. The release profiles are shown in Figure 5.10. Formulations having the lowest coating level showed a high release rate during 180min, followed by a quasi-plateau level for the remaining 3 hours. The higher coating levels both showed a lag phase for 10min followed by an enhanced release for 50min and a decreased release rate for the remaining 5 hours. All curves with different coating layer thicknesses are significantly different.

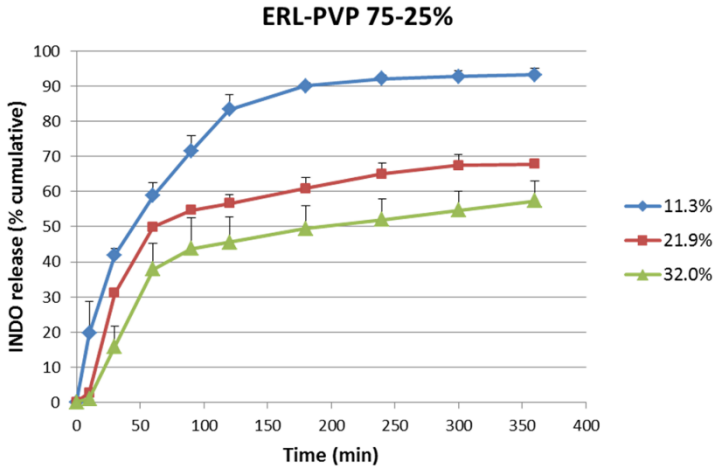

Figure 5.10: INDO release in function of time for INDO-PVP 30-70% (w/w) glass solution and an ERL-PVP 75-25% (w/w) rate controlling membrane. Different coating levels were tested: 11.3% (blue), 21.9% (red) and 32.0% (green).

Finally in Figure 5.11, the ERL-PVP 90-10% rate controlling membrane, coated from an aqueous dispersion, also showed a decreased and slower release with increasing coating level.

After 6 hours the release was 87% for 8.7% coating level and 69% for 17.1% coating level. Beads with 8.7% coating level showed high initial release (68% after 120min) followed by a slower release for the remaining 4 hours. After an initial (90min) high release for the beads having 17.1% coating level, INDO release approached zero-order release kinetics for the remainder of the release experiment. Both profiles showed to be significantly different from one another.

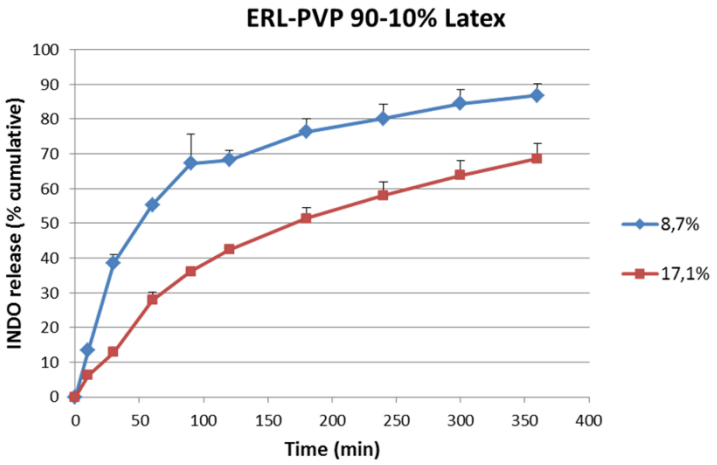

Figure 5.11: INDO release in function of time for INDO-PVP 30-70% (w/w) glass solution and an ERL-PVP 90-10% (w/w) rate controlling membrane, coated from an aqueous dispersion (latex). Different coating levels were tested: 8.7% (blue) and 17.1% (red).

5.5 Discussion

The difference of INDO diffusion through the different rate controlling membranes can be calculated based on the permeability coefficient. The applied equation has the benefit of being independent of membrane thickness. It is, however, important when calculating from a slope, that only the linear part of the plot is used. In other words, steady-state diffusion has to be reached to be able to calculate the permeability coefficient.

For EC-based as well as ERL-based samples, it is clear that an increased amount of PVP, which is added as a pore former, led to an increased permeability coefficient. This is to be expected because PVP is a hydrophilic polymer which is expected to leach out of the rate controlling membrane. This allows for a higher permeation of the drug because the EC or ERL polymer chains are not as closely packed as they would be in absence of a pore former. In the ERL based samples, the permeability coefficient increases gradually from 0% over 10% to 25% PVP; in the EC based samples P is very small when 0% and 10% of PVP is added but increases significantly when 25% of PVP is added. This can be explained by the miscibility of both

polymers, which has been reported in the companion paper. Because PVP and EC are completely immiscible, PVP is not able to interpenetrate the EC polymer chains as much as in ERL. So while the amount of PVP in EC-PVP 90-10% is not sufficient for an adequate pore former functionality (similar P-value with EC 100%), EC-PVP 75-25% led to the formation of weak spots in the rate controlling membrane with a higher permeability as a result. The partial miscibility of ERL and PVP allowed for a more gradual increase of the rate controlling membrane permeability with increasing pore former concentration.

Increasing pore former concentration also led to a higher variability of the permeability coefficient in case films were casted from an ethanol solution. This can also be explained by the (partial) immiscibility of the rate controlling polymer and the pore former. Increasing pore former concentration increased the heterogeneity of the films, resulting in a larger variation in permeability coefficients. When EC-based films are compared to ERL-based samples, a lower permeability coefficient was noticed for the same pore former concentration. This was most noticeable for the 0% and 10% pore former concentrations. Although there is a difference in the 25% PVP samples, this difference is not statistically significant due to the large standard deviation. When ERL films from an ethanolic solution are compared to films from an aqueous dispersion with equal pore former concentration, the second ones tended to have lower permeability coefficients. The main difference between film casting from a solution versus casting from a dispersion is that the latter requires a curing step. The polymer disposes itself as a small polymer particle (instead of spread out polymer chains in the solution) and needs to be stored at a temperature above the minimal film forming temperature for a certain amount of time to allow optimal coalescence of the dispersed polymer particles and polymer chain inter-diffusion for efficient film formation.

INDO sorption studies showed clear differences in the amount of INDO incorporated into the insoluble controlled release polymers ERL, ERS and EC. ERL showed the highest INDO sorption in all conditions, being different concentrations and form (powder or film). INDO sorption is the lowest in the case of ERS powder and second lowest in case of the films. As with ERL, the sorption into powders or films doesn't differ much, indicating that sorption in this case is independent of the available surface area. There is no relationship between ERS sorption and the INDO concentration in the medium. This observation also justifies the inclusion of ERS into this test as to show that the sorption of INDO in these polymers is independent upon the amount of quaternary ammonium groups present in these polymers (the part in the ter-co-polymer mainly responsible for the swelling). This is evidenced by the

fact that ERS has half of the quaternary ammonium groups compared to ERL and shows less than half of the amount of INDO sorbed. The link between the quaternary ammonium groups and INDO sorption also shows that an interplay of different forces is responsible for the sorption; not only a charge interaction, but also a decreased swelling of these particles because of the decreased amount of quaternary ammonium groups. Since these particles or films swell upon contact with the medium, INDO has a certain affinity for the hydrophobic environment of the polymers and will diffuse in them. This diffusion does not seem to be dependent on a charge interaction because it is also observed in the neutral EC polymer. Here, INDO sorption into/onto EC showed the second highest amount sorbed for the powders and lowest for the films. In the films almost no INDO is sorbed, which could be an indication for the dependence on the available surface area for INDO sorption. It can be presumed that the films have less surface area in contact with the medium compared to the powder. In the test with EC powder, INDO sorption is doubled when the INDO concentration in the medium is doubled. This can be in a direct way, pointing to sorption into or onto the available surface area or in an indirect way, meaning that the available surface area relates to the swelling of the polymer and that swelling has an impact on the diffusion into the polymer. The sorption of the active pharmaceutical ingredient into or onto the controlled release polymer can have certain implications towards incomplete drug release. These implications will only be enhanced when the coating layer thickness increases or if ERL should be used as part of the matrix of a different formulation.

To confirm the electrostatic charge interaction between INDO (above its pKa at pH 6.8) and ERL during drug diffusion through the controlled release membrane, solid-state NMR experiments were performed. The significant changes in chemical shift (3ppm) observed for INDO-ERL pH 6.8 are undeniably the result of an interaction between INDO and the cationic quaternary ammonium groups of the polymer. Moreover, this was not observed for the INDO-ERL solid dispersion prepared from EtOH in which INDO was not present in its ionic form. Thus, the observed interaction is only present when INDO and ERL are both in their ionic form. Due to this interaction, the electron density (chemical environment) of some of the INDO carbons is affected, leading to the observed changes in chemical shift [24, 25].

Diffusion through the rate controlling membranes was not only measured for INDO molecules in solution, also water vapor diffusion was monitored. Because of the uncharged nature of water molecules, the diffusion through the rate controlling membranes is not affected by possible charge interactions. The results of the water vapor diffusion tests were

along the same lines as INDO diffusion tests, i.e. diffusion of ERL-based membranes is always higher compared to EC-based samples with the same amount of PVP pore former. ERL-PVP 90-10% and EC-PVP 75-25% have comparable water mass losses in function of time, which is in accordance with INDO diffusion results. Water vapor diffusion tests confirm that diffusion is generally higher for ERL-samples compared to EC-samples (given an equal amount of pore former), and this is irrespective of a possible charge interaction between the diffusing molecules (INDO) and (part of) the rate controlling membrane (ERL). This leads to conclude that ERL is more hydrophilic, compared to EC.

When comparing the release from INDO-PVP coated beads and crystalline INDO in Figure 7, it can be seen that release from the glass solutions is faster and more uniform, opposed to crystalline INDO (larger standard deviation). This shows the poor dissolution characteristics of the pure crystalline drug, and the need to formulate INDO into a glass solution prior to sustaining the release.

INDO release from coated beads is dependent on the coating layer thickness in all formulations, except for those with a top-coating made up of EC-PVP 75-25% where all INDO is released immediately irrespective of the coating layer thickness. Increasing the coating layer thickness slows down and decreases the release of INDO from the coated beads, which can be attributed to the longer diffusion pathways for the drug[26] and diffusion through a somewhat denser polymer network. Hydrophobic drugs have also been reported to have slower release profiles compared to hydrophilic drugs[27]. The decrease in release can also be attributed to the increasing presence of rate controlling polymer which will not dissolve into the medium and sorb INDO as observed in the this study. A combination of these effects will lead to a decreased drug release rate and amount with increasing rate controlling membrane thickness. There is also an increase in lag-time with increasing coating thickness, which is also explained by the increased diffusion path for the drug [26].

Large differences are observed concerning the influence of the pore former depending on the rate controlling polymer used. When 10% and 25% PVP are compared in ERL-based samples with similar coating levels, the former led to a slightly faster and higher release compared to the latter, but the observed differences are never significant. In EC-PVP 90-10% and EC-PVP 75-25% on the other hand, differences could not be more remarkable. While 10% pore former is able to slow down the INDO release (given an appropriate coating level), EC-PVP 75-25% does not slow down the release for any coating level. This inability to control the

release points to a defect in the coating layer which can originate from a too high pore former concentration. The reason behind the coating defect could be explained by results obtained in the first part of this study (details are provided in the companion paper). Here, differences in polymer miscibility and, subsequently, pore former distribution along the surface were observed. The immiscibility between EC and PVP resulted in more isolated PVP presence along the surface which could lead to local coating defects when leached out in early stages of release experiments. When using 10% pore former concentrations, the isolated PVP regions are smaller and the dissolving pore former can still be replaced by the swelling EC polymer, successfully slowing down the release. The partial miscibility between ERL and PVP explains why the PVP is more homogeneously spread along the rate controlling membrane surface and why no coating defects are observed when using a 25% pore former concentration. Miscibility studies between rate controlling polymer and pore former can indicate formation of isolated pore former regions in the rate controlling membrane and may thus give an idea about the success rate in formulating rate controlling membranes.

Different release profiles are observed when different rate controlling polymers with equal coating levels and an equal pore former concentration (10% w/w) are compared. Only the lowest coating level shows a higher INDO release for EC after 6 hours (ERL: 84%, EC 90%). With higher coating levels, INDO release is always higher after 6 hours from ERL based samples. This difference becomes larger with increasing coating levels up to a point where, at ca. 36% coating level, INDO release for EC-PVP 90-10% is 3% and for ERL-PVP 90-10% it is 49%. All release profiles with comparable coating level have significantly different release profiles. Not only the release after 6 hours is smaller for EC, these formulations also show an extended lag time. For example, after 120 minutes, beads with coating levels of ca. 20% show an INDO release of 6% in EC-PVP 90-10% and 63% in ERL-PVP 90-10%. The burst release in the lower coating levels of ERL-PVP 90-10% could point to INDO release before complete swelling of the ERL coating. When 25% pore former concentration is applied, the situation is quite different. Because of the quasi immediate release (60-90 min) in case of EC-PVP 75-25%, these controlling rate membranes are not considered suitable for controlled release purposes. ERL-PVP 75-25% is, on the other hand, able to slow down the release in a way similar to ERL-PVP 90-10%. The reason for this difference is polymer miscibility as discussed in the previous paragraph.

Lastly, a comparison is made between identical rate controlling membranes coated from either an ethanol solution or an aqueous dispersion. While release profiles at 10% coating

levels are not significantly different (f_2: 63,0), at 20% coating level, the rate controlling membrane coated from a dispersion shows a slower and lower (after 6h: 69% for latex and 76% for solution) INDO release compared to the membrane coated from a solution. The release curves are significantly different from each other. Already 63% of INDO has been released after 120 min from the formulation coated from a solution. In the following 4 hours, an additional 13% INDO was released. In the formulation with the latex membrane the release after 120 minutes is 42% INDO and in the following 4 hours an additional 27%. This shows that the beads with a latex top layer show less burst release which allows for higher release after the initial phase. Indeed, after 90 minutes quasi-zero order release kinetics are observed, and from linear regression it can be calculated that all INDO will be released (given continuation of zero-order) at 10 hours and 42 minutes.

5.6 Conclusions

The pharmaceutical performance of a glass solution coated onto inert carriers with an additional rate controlling membrane was assessed. Firstly, diffusion through rate controlling membranes showed influence of pore former concentration, rate controlling polymer used and coating process, i.e. from a solution or a dispersion. Drug release experiments generally showed similar influences of formulation parameters and an additional influence of coating layer thickness. A link can be made between permeability coefficients and release behavior which shows, on one hand, that diffusion through the rate controlling membrane is the rate limiting step during drug release, and on the other hand, that drug diffusion results can be used as indicative values when screening for an appropriate controlled release dosage form.

Although INDO and ERL are an interacting system, this has no negative effect on drug release. On the contrary, ERL generally shows higher diffusion rates and faster release, but this can be mainly attributed to its more hydrophilic nature, compared to EC.

5.7 References

1. Sekiguchi, K.; Obi, N. Studies on absorption of eutectic mixture. I. A comparison of the behavior of eutectic mixture of sulfathiazole and that of ordinary sulfathiazole in man. *Chem. Pharm. Bull.* **1961**, 9, 866-872.

2. Chiou, W. L.; Riegelman, S. Pharmaceutical applications of solid dispersion systems. *J. Pharm. Sci.* **1971**, 60, 1281-1302.

3. Baghel, S.; Cathcart, H.; O'Reilly, N. J. Polymeric Amorphous Solid Dispersions: A Review of Amorphization, Crystallization, Stabilization, Solid-State Characterization, and Aqueous Solubilization of Biopharmaceutical Classification System Class II Drugs. *J. Pharm. Sci.* **2016**, 105, 2527-2544.

4. Van Duong, T.; Van den Mooter, G. The role of the carrier in the formulation of pharmaceutical solid dispersions. Part I: crystalline and semi-crystalline carriers. *Expert Opin. Drug Deliv*. **2016**, 13, 1583-1594.

5. Van Duong, T.; Van den Mooter, G. 2016. The role of the carrier in the formulation of pharmaceutical solid dispersions. Part II: amorphous carriers. *Expert Opin. Drug Deliv*. **2016**, http://dx.doi.org/10.1080/17425247.2016.1198769

6. Van den Mooter, G. The use of amorphous solid dispersions: A formulation strategy to overcome poor solubility and dissolution rate. *Drug Discov. Today Technol.* **2012**, 9, e79-e85.

7. Six, K.; Daems, T.; de Hoon, J.; Van Hecken, A.; Depre, M.; Bouche, M. P.; Prinsen, P.; Verreck, G.; Peeters, J.; Brewster, M. E.; Van den Mooter, G. Clinical study of itraconazole prepared by hot-stage extrusion. *Eur. J. Pharm. Sci.* **2005**, 24, 179–186.

8. Augustijns, P.; Brewster, M. E. Supersaturating drug delivery systems: fast is not necessarily good enough. *J. Pharm. Sci*. **2012**, 101,7-9.

9. Lang, B.; McGinity, J. W.; Williams, O. W. Hot-melt extrusion – basic principles and pharmaceutical applications. *Drug Dev. Ind. Pharm.* **2014**, 40, 1133-1155.

10. Crowley, M. M.; Zhang, F.; Repka, M. A.; Thumma, S.; Upadhye, S. B.; Battu, S. K.; McGinity, J. W.; Martin, C. Pharmaceutical Applications of Hot-Melt Extrusion: Part I. *Drug Dev. Ind. Pharm.* **2007**, 33, 909-926.

11. Tran, P. H. L.; Tran, T. T. D.; Park, J. B.; Lee, B. J. Controlled release systems containing solid dispersions: strategies and mechanisms. *Pharm. Res.* **2011**, 28, 2353-2378.

12. Nguyen, D. N.; Palangetic, L.; Clasen, C.; Van den Mooter, G. One-step production of darunavir solid dispersion nanoparticles coated with enteric polymers using electrospraying. *J. Pharm. Pharmacol.* **2016**, 68, 625-633.

13. Beten, D. B.; Amighi, K.; Moës A. J. Preparation of controlled-release coevaporates of dipyridamole by loading neutral pellets in a fluidized-bed coating system. *Pharm. Res.* **1995**, 12, 1269-1272.

14. Thakral, S.; Thakral, N. K.; Majumdar, D. K. Eudragit: a technology evaluation, *Expert Opin. Drug Deliv.* **2013**, 10, 131-149.

15. Yoshida, T.; Lai, T. C.; Kwon, G. S.; Sako, K. pH- and ion-sensitive polymers for drug delivery, *Expert Opin. Drug Deliv*. **2013**, 10, 1497-1513.

16. Bodmeier, R.; Guo, X.; Sarabia, R. E.; Skultety, P. F. The influence of buffer species and strength on diltiazem HCl release from beads coated with the aqueous cationic polymer dispersions, Eudragit RS, RL 30D. *Pharm. Res.* **1996**, 13, 52-56.

17. Narisawa S., Nagata M., Hirakawa Y., Kobayashi M., Yoshino H. An organic acid-induced sigmoidal release system for oral controlled-release preparations. 2. Permeability enhancement of Eudragit RS coating led by the physicochemical interactions with organic acid. *J. Pharm. Sci.* **1996**, 85, 184-8.

18. Narisawa, S.; Nagata, M.; Danyoshi, C.; Yoshino, H.; Murata, K.; Hirakawa, Y.; Noda, K. An organic acid-induced sigmoidal release system for oral controlled-release preparations. *Pharm. Res.* **1994**, 11, 111-116.

19. Pignatello, R.; Spadaro, D.; Vandelli, M. A.; Forni, F.; Puglisi, G. Characterization of the mechanism of interaction in ibuprofen-Eudragit RL100 coevaporates. *Drug Dev. Ind. Pharm.* **2004**, 30, 277-288.

20. Mollica, G.; Geppi, M.; Pignatello, R.; Veracini, C. A. Molecular properties of flurbiprofen and its solid dispersions with Eudragit RL100 studied by high- and low-resolution solid-state nuclear magnetic resonance. *Pharm. Res.* **2006**, 23, 2129-2140.

21. Geppi, M.; Guccione, S.; Mollica, G.; Pignatello, R.; Veracini, C. A. Molecular properties of ibuprofen and its solid dispersions with Eudragit RL100 studied by solid-state nuclear magnetic resonance. *Pharm. Res.* **2005**, 22, 1544-1555.

22. Van den Mooter, G.; Samyn, C.; Kinget, R. Characterization of colon-specific azo polymers: A study of the swelling properties and the permeability of isolated polymer films. *Int. J. Pharm.* **1994**, 111, 127-136.

23. FDA, S. Guidance for Industry: SUPAC-MR: Modified Release Solid Oral Dosage Forms; Scale-Up and Post-Approval Changes: Chemistry, Manufacturing and Controls. In Vitro Dissolution Testing, and In Vivo Bioequivalence Documentation **1997**.

24. Masuda, K.; Tabata, S.; Kono, H.; Sakata, Y.; Hayase, T.; Yonemochi, E.; Terada, K. Solid-state 13C NMR study of indomethacin polymorphism. *Int. J. Pharm.* **2006**, 318, 146-153.

25. Ukmar, T.; Kaucic, V.; Mali, G. Solid-state NMR spectroscopy and first-principles calculations: a powerful combination of tools for the investigation of polymorphism of indomethacin. *Acta Chim. Slov.* **2011**, 58(3), 425-433.

26. Kranz, H.; Gutsche, S. Evaluation of the drug release patterns and long term stability of aqueous and organic coated pellets by using blends of enteric and gastrointestinal insoluble polymers. *Int. J. Pharm.* **2009**, 380, 112-119.

27. Mehta, R.; Teckoe, J.; Schoener, C.; Workentine, S.; Ferrizzi, D.; Rajabi-Siahboomi, A. Investigation into the Effect of Ethylcellulose Viscosity Variation on the Drug Release of Metoprolol Tartrate and Acetaminophen Extended Release Multiparticulates-Part I. *AAPS PharmSciTech.* **2016**, DOI: 10.1208/s12249-015-0465-z

Chapter 6: Eudragit® RL as a stabilizer for supersaturation and a substrate for nanocrystal formation

Results of this chapter are based on:

Dereymaker, A.; Cinghia, G.; Van den Mooter, G. Eudragit® RL as a stabilizer for supersaturation and a substrate for nanocrystal formation. Eu J Pharm Biopharm ***xxxx****, (manuscript accepted for publication:* http://dx.doi.org/10.1016/j.ejpb.2017.02.002*).*

Abstract

In order to optimize supersaturation levels and avoid early drug precipitation, Eudragit® RL was tested as a carrier in solid dispersions, either alone or in combination with a hydrophilic polymer (PVP K25). In vitro dissolution performance of the spray dried solid dispersions was tested. The phase behavior of the produced solid dispersions was analyzed as well as dissolution precipitates. In case of weak acid model compounds (indomethacin and naproxen), the incorporation of Eudragit® RL resulted in a prolongation of supersaturation. A combination of PVP and Eudragit® RL led to high and stable drug concentrations. Eudragit® RL was only suited as a carrier in combination with higher drug loadings. Phase behavior analysis of the produced solid dispersions showed that Eudragit® RL could form glass solutions, and precipitate analysis showed that these drug-polymer combinations remained amorphous after in vitro dissolution for 24 hours. Surprisingly, indomethacin and naproxen also formed nanocrystals in presence of Eudragit® RL. These nanocrystals were formed by a dynamic interplay of dissolution, sorption and desorption. A charge interaction between anionic drugs and a cationic polymer provided a high driving force for sorption, which was necessary for nanocrystal formation and supersaturation stabilization.

6.1 Introduction

Solid dispersions are one of the go-to strategies when formulation scientists are confronted with poor solubility and dissolution rate of active pharmaceutical ingredients (API). These active substances have evolved over the years into increasingly potent but also structurally complex molecules. The growing complexity can be mainly explained by advances made in computer aided drug design [1], high throughput screening and combinatorial chemistry [2, 3], leading to decreased aqueous solubility of newly developed drug substances, with estimations ranging from 40-77% of new drug candidates displaying poor solubility, depending on the development stage of the drug candidates [4], and 30-35% of marketed drugs [5]. To estimate poor solubility, one needs to define solubility and this has been done by the introduction of the biopharmaceutics classification system (BCS) by Amidon *et al.* in 1995 [6]. The U.S. Food and Drug Administration (FDA) has adopted this classification system in their biowaiver guidelines [7]. The BCS classification divides drugs or drug candidates in 4 categories according to their high/low solubility and high/low permeability. A drug is considered highly soluble when its highest dose dissolves in less than 250ml of medium with a pH range of 1-7.5.

The increasing number of poorly soluble drug candidates created a vast array of enabling formulation strategies to overcome poor solubility and dissolution rate [8]. Among the enabling strategies, amorphous solid dispersions are very promising and intensively investigated [9-11]. However, 50+ years of research and development of solid dispersion has led to the marketing of ca. 20 products [12, 13].

Solid dispersions are able to create supersaturated drug concentrations. However, the fast and high increase in drug concentrations will lead to fast nucleation, crystal growth and eventually precipitation of the active substance, which results in a loss of the solubility and bio-availability advantage created. The emerging awareness of this disadvantage has come to attention in recent years [14, 15]. Moreover, it has also been shown that in vitro dissolution data cannot be readily transposed to the in vivo situation [16, 17].

The vast majority of carriers used in solid dispersions are polymers, early on mostly crystalline or semi-crystalline [18], later on mostly amorphous [19]. Only recently, a shift has been seen from the traditional hydrophilic polymers, to polymers used for controlled release purposes [20]. A recent study from Sun & Lee suggests that medium insoluble carriers exhibit a

more gradual generation of supersaturation, as a result of a diffusion-controlled release as opposed to a dissolution-controlled release, generated by medium soluble carriers [21].

The goal of this study is to further develop the concept of solid dispersions with altered, i.e. decreased dissolution rate properties. More in particular, we will exploit the possibility of using the model polymer, Eudragit® RL (ERL) as a carrier for solid dispersions, either by itself or in combination with a model hydrophilic polymer, polyvinylpyrrolidone K25 (PVP). The research question here is to what extent ERL, being an insoluble but swellable polymer, can, as (part of) the solid dispersion carrier, slow down or stabilize the drug precipitation which is typically observed in solid dispersions that are only made up of a hydrophilic carrier. The combination of ERL with the hydrophilic PVP should potentially allow for sufficiently high initial drug concentrations, which is lacking when only a hydrophobic polymer is used as a solid dispersion carrier. ERL is a ter-copolymer of ethyl acrylate, methyl methacrylate and trimethylammonioethyl methacrylate with chloride as a counterion. ERL is practically insoluble in water, but the quaternary ammonium groups are responsible for the swelling and permeability of the polymer. Indomethacin (INDO), naproxen (NAP) and cinnarizine (CINN) are used as model drugs, with the former two being weak acids which can form a charge interaction with ERL above their respective pKa values. Cinnarizine is a weak base, unable to form charge interactions with ERL. Spray drying, a well-established solvent evaporation method for the production of amorphous solid dispersions [22] was used to prepare all formulations starting from an ethanolic solution. The potential of using ERL as a carrier is tested by investigating its phase behavior on one hand, and its influence on drug dissolution behavior on the other hand, with special emphasis on supersaturation generation. Another unexpected property of ERL will be discussed, namely its ability to form drug nanocrystals in solution.

6.2 Materials and Methods

6.2.1 Materials

Indomethacin and cinnarizine were purchased from Fagron Ltd. (Waregem, Belgium), naproxen from CERTA Ltd (Braine l'Alleud, Belgium). Eudragit® RL was obtained from Evonik (Darmstadt, Germany) and PVP K-25 (Kollidon®25) was kindly donated by BASF SE (Ludwigshafen, Germany). Sodium acetate and phosphoric acid were obtained from Chemlab (Zedelgem, Belgium), sodium hydroxide from Merck (Darmstadt, Germany), acetic acid from VWR chemicals (Fontenay-sous-Bois, France) and potassium phosphate monobasic from Sigma-Aldrich (Steinheim, Germany), acetonitrile from Fisher Scientific (Leicestershire, UK) and methanol from Acros Organics (Geel, Belgium). Ultrapure water was produced with an Elga® Maxima system (Elga Ltd. High Wycombe Bucks, United Kingdom). All solvents used were of analytical grade.

6.2.2 Methods

Spray drying

Solid dispersions of drug and polymer(s) were spray dried using a Buchi mini spray-dryer B191 (Buchi, Flawil, Switzerland). An accurate amount of drug and polymer(s) was dissolved in ethanol (10% solution w/v) and this solution was spray dried using an inlet temperature of 50°C, an atomizing air flow rate 0.02 m^3/min, a drying air flow rate 0.56 m^3/min and a feed rate of 4.8 cm^3/min using a peristaltic pump. All spray-dried samples were additionally dried in a vacuum oven (Mazzali Systems, Monza, Italy) at 25°C for at least 2 days.

Modulated differential scanning calorimetry (mDSC)

mDSC was used to investigate the phase behavior of the spray dried solid dispersions and precipitates, obtained after *in vitro* dissolution. The analysis was carried out using a Q2000 Differential scanning calorimeter (TA Instruments, Leatherhead, UK) purged with a nitrogen flow rate of 50 ml/min during analysis. The mDSC was equipped with a Refrigerated Cooling System (RCS 90) (TA Instruments, Leatherhead, UK). The software used for data processing was TA instruments Universal Analysis 2000 (version 4.4, Leatherhead, UK). TA Instruments standard aluminum pans (Brussels, Belgium) were used for all measurements. A sample mass of 5-6 mg was accurately weighed into the pans and crimped together with a lid. All samples were measured in triplicate. Samples were heated from 0 to 180°C. A heating rate of 2°C/min

was applied with a temperature modulation of 0.636°C every 40s. Glass transition temperatures were measured at half height in the reversing heat flow. The step jump in heat capacity observed in the reversing heat flow signal was further examined in the corresponding derivative signal after Savitsky-Golay smoothing with points of window set at 10°C. n-Octadecane and indium were used to calibrate and validate the DSC temperature scale. Indium was also used to calibrate and validate the enthalpic response. The heat capacity was calibrated and validated using sapphire disks.

X-ray powder diffraction (XRPD)

The precipitate samples from *in vitro* dissolution studies (analyzed immediately after the filtration from the dissolution medium) were analyzed at room temperature using an automated X'pert PRO diffractometer (PANalytical, Almelo, the Netherlands). The precipitate samples were clamped between Kapton foil and placed in sample holders. Analysis was performed in transmission mode using a Cu tube (λ (Kα) 1.5418 Angstrom; generator at 45kV and 40mA). The analysis was performed in a continuous scan mode in a 2θ range from 4° to 40° with 0.0167° step size and 200 seconds step time. The X'pert Data Collector and X'pert Data Viewer (PANalytical, Almelo, The Netherlands) were used to collect and analyze the data.

Scanning electron microscopy (SEM)

Solid dispersion and precipitate morphology was analyzed using a Phillips XL30 ESEM-FEG (Philips, Eindhoven, The Netherlands) equipped with a Schottky field emission electron gun. Powders were fixed on an aluminum stub using double-sided carbon tape. The samples were coated with gold by sputtering for 45 s at 20 mA. The SEM instrument was used with an acceleration voltage of 10.00 kV, a spot size of 3 and a secondary electron detector.

Dynamic light scattering (DLS)

DLS measurements were performed in a CGS-3 spectrometer (Malvern Instruments, Worcestershire, UK) equipped with a goniometry, auniphase 22 mV He-Ne laser operating at 632.8 nm, an avalanche photodiode and detector and an ALV-5000/EPP multi-angle tau correlator. Light scattering was monitored at 90°.

***In vitro* dissolution studies**

In vitro dissolution performance of the solid dispersions was evaluated using an SR8PLUS dissolution test station (Hanson Research, Chatsworth, USA). The dissolution medium was either an acetate buffer at pH 4.5 or a hydrochloric acid solution at pH 1.2. The dissolution

volume was 500 ml, maintained at 37 ±0.5 °C. A dose of 150mg API was calculated for each sample and weighed accurately. Samples were taken at different time intervals by withdrawing 2ml of dissolution medium and filtering this medium using a PTFE filter with a pore size of 0.45 µm (Macherey Nagel, Duren, Germany). The first 1ml was discarded for filter saturation, the other 1ml was transferred to a test tube. 0.5 ml of sample was diluted 1:1 with acetonitrile (ACN) to avoid sample precipitation. All experiments were performed in triplicate. Drug concentrations were assessed using HPLC. At the end of experiment, the vessel content (dissolution precipitate) was filtered using a vacuum pump and a cellulose acetate filter with a pore size of 0.45 µm. One part of the precipitates was analyzed immediately with XRPD; the other part was further dried in the oven at 40°C for two days and analyzed with mDSC.

Solubility determination

Falcon™ 50ml conical centrifuge tubes were filled with 50.0 ml of medium (acetate buffer pH 4.5 or HCl solution pH 1.2) and rotated (3rpm) at 37 °C until constant API concentration. Optionally, an accurate amount of polymer(s) was weighed and added to the oversaturated API solution. At each withdrawal, 2 ml of sample was taken, filtered and diluted with ACN. Samples were again analyzed using HPLC. All experiments were performed in triplicate.

Sorption testing

Falcon™ 50ml conical centrifuge tubes were filled with 50.0 ml of an API solution in acetate buffer pH 4.5 and rotated (3 rpm) at 37 °C. The following API concentrations were chosen: CINN 0.03 mg/ml, NAP 0.08 mg/ml 0.02 mg/ml. At time zero an accurate amount of ERL (25 mg, 50 mg, 100mg, 200mg) was added to the test tubes and at several time points, samples were collected (1h, 2h, 4h, 6h, 24h, 48h) until constant concentration was reached. Samples were filtered using a PTFE filter (pore size 0.45 µm), diluted with ACN and analyzed with HPLC.

To construct sorption isotherms, 5 solutions with varying concentrations of NAP or INDO were prepared and 50.0 ml of this solution was transferred in Falcon™ 50ml conical centrifuge tubes. An accurately weighed amount of ERL was introduced and the tubes were rotated (3 rpm) at 37°C until constant concentration. Sorption isotherms were analyzed using the Langmuir adsorption model:

$$\frac{c}{y} = \frac{1}{y_m b} + \frac{c}{y_m} \qquad \text{(Eq. 6.1)}$$

In this equation c is the equilibrium concentration of the adsorbed drug in solution, y is the amount of adsorbed material (expressed per unit of mass of adsorbent), y_m is the amount of adsorbed material per mass unit of adsorbent when a monolayer is formed, and b is the ratio of the adsorption rate constant to the desorption rate constant.

High performance liquid chromatography (HPLC)

Drug concentrations were measured using HPLC. The set-up consisted of a pump L-7100, an autosampler L-7200, a UV-detector L-7420 and an interface D7000 (all from Merck, Darmstadt, Germany). The column used was a Chromolith® Performance RP-18e (100-4.6mm) from Merck kGaA (Darmstadt, Germany). Naproxen (retention time ~ 2.5 min) and Indomethacin (retention time ~ 3.2 min) were detected at a wavelength of 320 nm and the mobile phase composition was made up of 50% v/v of a 0.5% v/v orthophosphoric acid solution in ultrapure H_2O and 50% v/v of ACN. Cinnarizine (retention time ~ 5.50 min) was detected at a wavelength of 252 nm and the mobile phase was made up of a 35% v/v buffer (potassium phosphate 0.05M pH 6.0) and 65% v/v of ACN. All samples were analyzed in duplicate. A calibration curve of area under the curve (AUC) vs. concentration was constructed using standard drug solutions (0.125 mg/ml – 0.244 µg/ml) prepared by diluting a stock solution (1mg/ml). Linearity was confirmed through linear regression analysis (R^2 >0.999). Limit of detection (LOD) and limit of quantification (LOQ) were determined and were lower than the smallest drug concentration of the calibration curve.

6.3 Resuts

6.3.1 Solid state characterization of solid dispersions

Topography

The topography of spray dried solid dispersions was determined by SEM. Representative micrographs of the different solid dispersions containing INDO are shown in Figure 6.1.

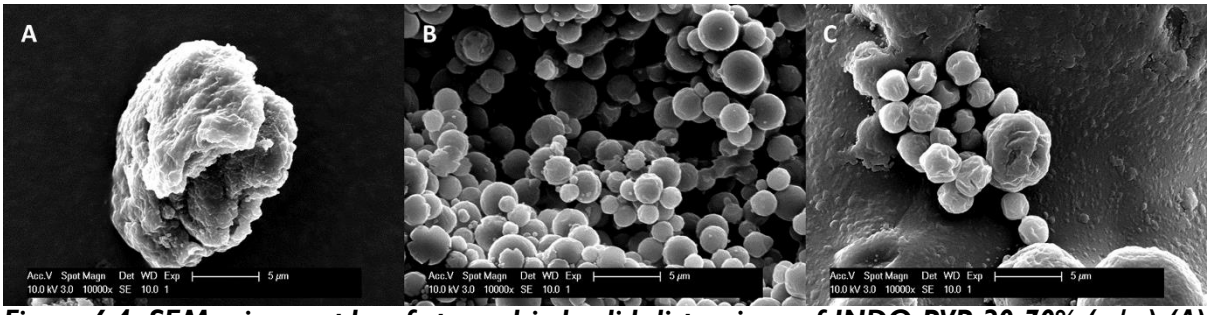

Figure 6.4: SEM micrographs of spray dried solid dispersions of INDO-PVP 30-70% (w/w) (A), INDO-ERL-PVP 30-35-35% (w/w) (B) and INDO-ERL 30-70% (w/w) (C)

INDO-PVP 30-70% (Figure 1A), INDO- ERL-PVP 30-35-35% (Figure 1B) and INDO-ERL 30-70% (Figure 1C) show different outer surface morphologies. Spray dried powder particles consisting of INDO and PVP showed a more irregular surface and shape, compared to particles containing ERL. INDO-PVP particles also appeared to be the largest. Spray drying INDO-ERL-PVP solid dispersion generated spherical particles with a smooth surface. These were also smaller compared to INDO-PVP particles and about the same size as INDO-ERL particles. INDO-ERL particles are also spherical but slightly less smooth than INDO-ERL-PVP particles.

Thermal analysis

Indomethacin solid dispersions

Spray dried solid dispersions were assessed on their phase behavior using modulated differential scanning calorimetry (mDSC). All formulations containing INDO are presented in Figure 6.2.

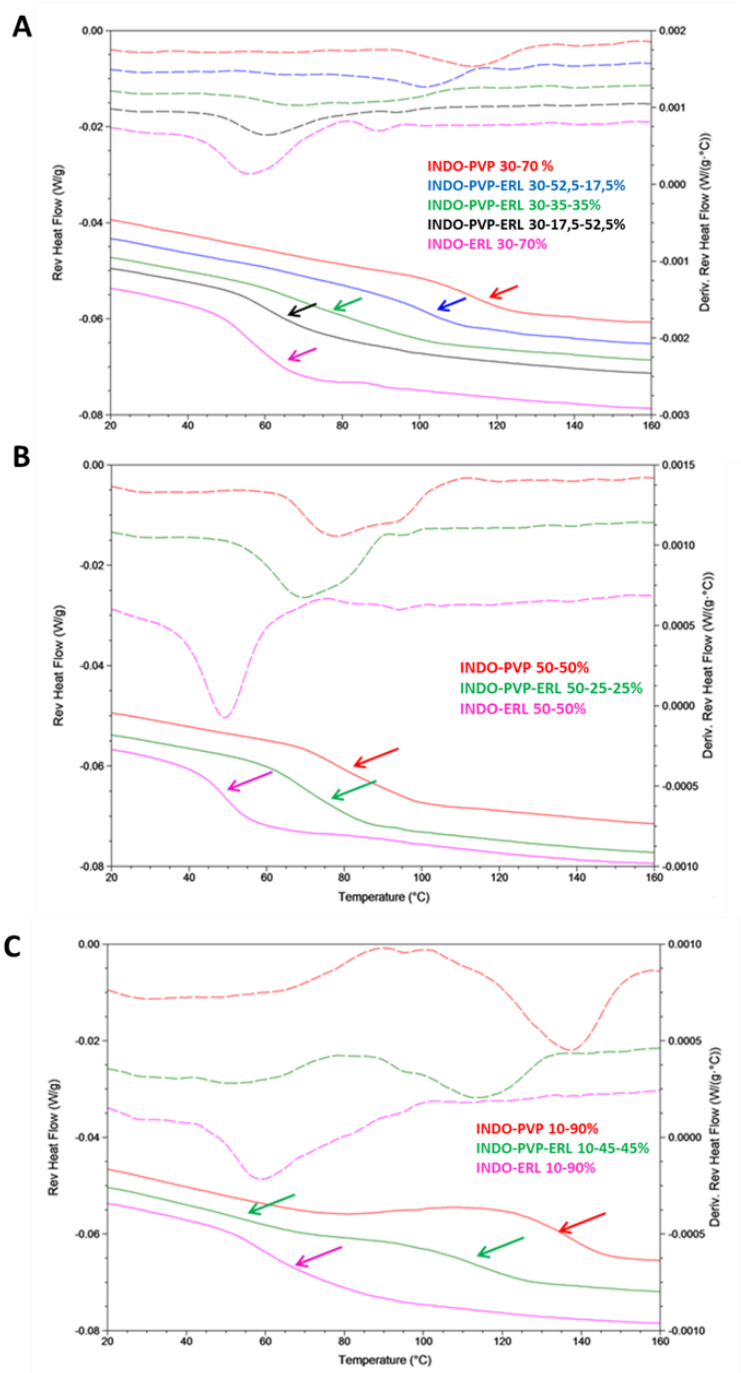

Figure 6.2: mDSC thermograms of spray dried solid dispersions of INDO with different polymers (or combinations) and INDO contents of 30% (A), 50% (B) and 10% (C). In panel A, INDO-PVP 30-70% is represented in red, INDO-PVP-ERL 30-52.5-17.5% in blue, INDO-PVP-ERL 30-35-35% in green, INDO-PVP-ERL 30-17.5-52.5% in black and INDO-ERL 30-70% in pink. In panel B, INDO-PVP 50-50% is represented in red, INDO-PVP-ERL 50-25-25% in green and INDO-ERL 50-50% in pink. In panel C, INDO-PVP 10-90% is represented in red, INDO-PVP-ERL 10-45-45% in green and INDO-ERL 10-90% in pink. Reversing heat flows are given in full lines, the 1st derivative of the reversing heat flows in dotted lines. Arrows indicate glass transitions.

All formulations containing 30% INDO formed glass solutions, i.e. a one phase system were the drug is molecularly dispersed into the polymer matrix. Please note that the term 'glass solution' does not indicate a thermodynamically stable system since the drug can be

oversaturated in these systems. Mean glass transitions ranged from 113.3°C (INDO-PVP 30-70%) to 57.1°C (INDO-ERL 30-70%). In glass solutions with a PVP-ERL mixture, mean glass transition temperatures were 90.9°C, 76.4°C and 62.5°C for INDO-PVP-ERL 30-52.5-17.5%, 30-35-35% and 30-17.5-52.5%, respectively.

In solid dispersions containing 50% INDO loadings (Figure 6.2B), single glass transitions were still observed at 79.9°C, 81.4°C and 49.8°C for INDO-PVP 50-50%, INDO-PVP-ERL 50-25-25% and INDO-ERL 50-50% respectively. Although these formulations could still be categorized as glass solutions, INDO-PVP 50-50% showed a very wide T_g, and from the shape of the derivative heat flow signal, 2 minima could be observed, which pointed to a phase separated system.

At 10% INDO loading (Figure 6.2C), both INDO-PVP and INDO-ERL are glass solutions with a mean glass transition at 134.3°C and 64.1°C respectively. INDO-PVP-ERL 10-45-45% on the other hand showed 2 glass transitions with means at 64.8°C and 113.6°C. This formulation clearly was a phase separated system.

Naproxen solid dispersions

In Figure 6.3, mDSC analysis of NAP solid dispersions (30% drug loading w/w) showed single glass transitions (Figure 6.3A) with a mean at 33.0°C, 56.3°C and 64.8°C for NAP-ERL 30-70%, NAP-PVP-ERL 30-35-35% and NAP-PVP respectively. NAP-ERL 30-70% also showed a NAP melting peak at 121°C (Figure 6.3B). NAP-ERL could not be considered as a true glass solution because it contained a crystalline NAP fraction.

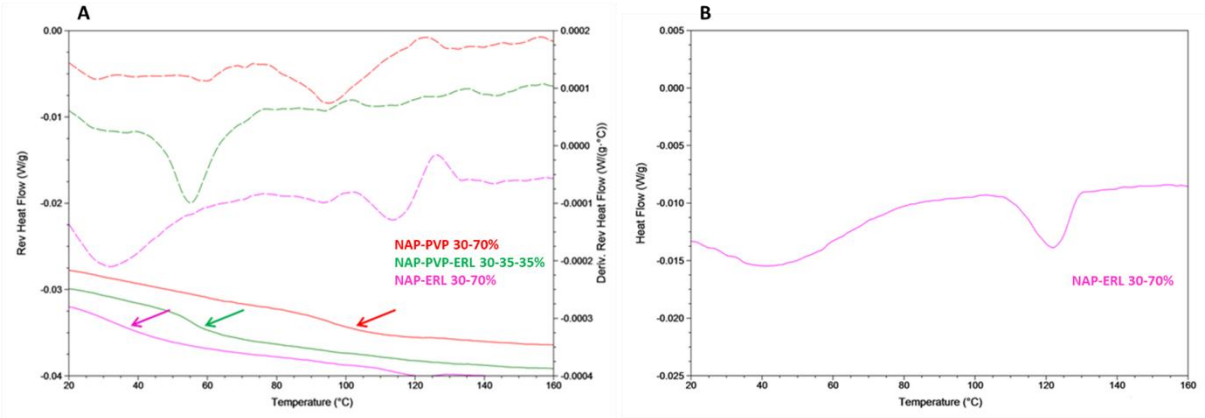

Figure 6.3: mDSC thermograms of spray dried solid dispersions of NAP with different polymers (or combinations). In panel A, NAP-PVP 30-70% is represented in red, NAP-PVP-ERL 30-35-35% in green, and NAP-ERL 30-70% in pink. Reversing heat flows are given in full lines, the 1st derivative of the reversing heat flows in dotted lines. Panel B represents the total heat flow of NAP-ERL 30-70. Arrows indicate glass transitions.

Cinnarizine solid dispersions

Thermograms of solid dispersions with CINN (30% drug loading w/w) are represented in Figure 6.4.

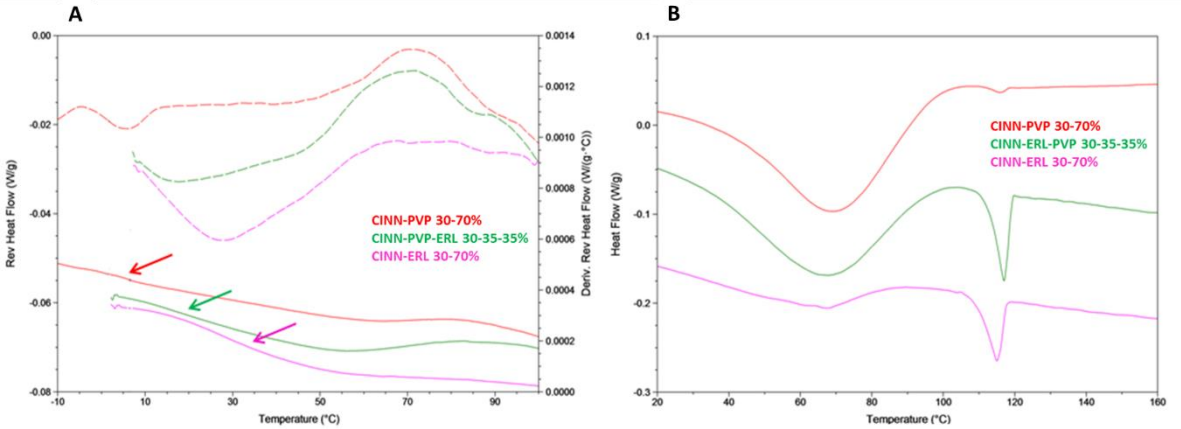

Figure 6.4: mDSC thermograms of spray dried solid dispersions of CINN with different polymers (or combinations). In panel A, CINN-PVP 30-70% is represented in red, CINN-PVP-ERL 30-35-35% in green, and CINN-ERL 30-70% in pink. Reversing heat flows are given in full lines, the 1st derivative of the reversing heat flows in dotted lines. Panel B represents the total heat flow of CINN-ERL 30-70 (red), CINN-PVP-ERL 30-35-35% (green), and CINN-ERL 30-70% (pink). Arrows indicate glass transitions.

Figure 6.4A shows the reversing heat flow signals of CINN solid dispersions. Mean glass transitions were observed at 5.5°C, 6.7°C and 31.9°C for CINN-PVP 30-70%, CINN-PVP-ERL 30-35-35% and CINN-ERL formulations respectively. Since all formulations showed CINN melting peaks in the total heat flow signals (Figure 6.4B), none of these solid dispersions could be categorized as a true glass solution.

Structural composition

To confirm the semi-crystalline composition of the NAP-ERL 30-70% formulation, the spray dried powder was analyzed by XRPD. The diffractogram, shown in Figure 6.5, showed characteristic NAP Bragg peaks in the NAP-ERL 30-70% sample.

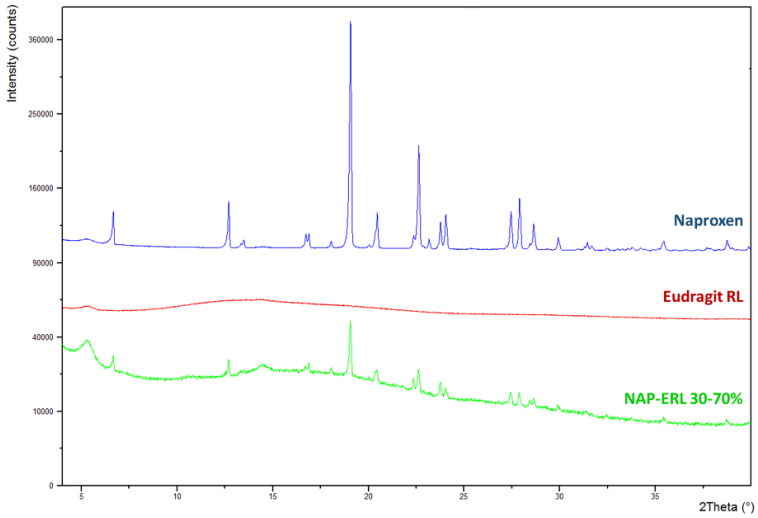

Figure 6.5: XRPD diffractogram of NAP (blue), ERL (red) and spray dried NAP-ERL 30-70% (green).

6.3.2 In vitro dissolution

Indomethacin solid dispersions

Dissolution testing was performed on spray dried solid dispersions containing INDO in different drug loadings (Figure 6.6).

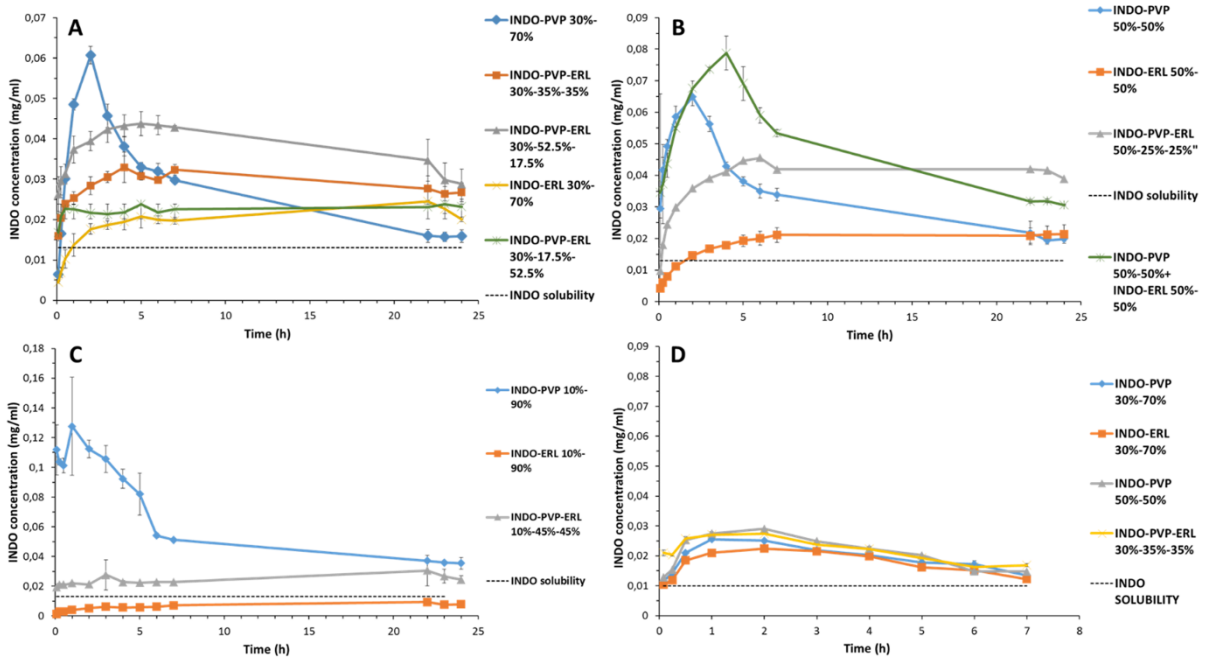

Figure 6.6: INDO concentrations in function of time of spray dried solid dispersions of INDO with different polymers (or combinations) and INDO contents of 30% (A), 50% (B) and 10% (C). In panel A, INDO-PVP 30-70% is represented in blue, INDO-PVP-ERL 30-52.5-17.5% in grey, INDO-PVP-ERL 30-35-35% in orange, INDO-PVP-ERL 30-17.5-52.5% in green and INDO-ERL 30-70% in yellow. In panel B, INDO-PVP 50-50% is represented in blue, INDO-PVP-ERL 50-25-25% in grey, INDO-ERL 50-50% in orange and a physical mixture of INDO-PVP 50-50% and INDO-ERL 50-50% in green. In panel C, INDO-PVP 10-90% is represented in blue, INDO-PVP-ERL 10-45-45% in grey and INDO-ERL 10-90% in orange. In panel A-C, dissolution is performed in an acetate buffer pH 4.5. In panel D dissolution is performed in an HCl solution pH 1.2. INDO-PVP 30-70% is represented in blue, INDO-PVP 50-50% in grey, INDO-PVP-ERL 30-35-35% in yellow and INDO-ERL 30-70% in orange. In all dissolution profiles, INDO solubility in the respective medium is represented by a black dashed line.

Concentrations in function of time of INDO 30% formulations are shown in Figure 6.6A. All formulations showed concentration levels above the INDO solubility level (0.013 mg/ml). All formulations reached a concentration level above INDO solubility within the first sampling time (5 min), except for INDO-PVP 30-70% (between 5 and 15 min) and INDO-ERL 30-70% (after 1h). INDO-PVP 30-70% shows the highest concentration level, 0.06 mg/ml after 2h, but also shows a steep concentration decline hereafter with concentrations approaching INDO solubility at 22h (0.016 mg/ml). Glass solutions where ERL is incorporated as a (co-)carrier on the other hand, did not reach the concentration level of INDO-PVP 30-70%. Depending on

the polymer composition, the highest concentration levels reached were 0.044 mg/ml for INDO-PVP-ERL 30-52.5-17.5% after 5h, 0.033 mg/ml for INDO-PVP-ERL 30-35-35% after 4h, 0.024 mg/ml for INDO-PVP-ERL 30-17.5-52.5% after 4h and 0.021 mg/ml for INDO-ERL 30-70% after 5h. However, in contrast to INDO-PVP 30-70%, no steep concentration decrease was observed. Concentrations at 24h only marginally declined or inclined, compared to the peak concentrations.

Similar observations could be made at 50% INDO drug loadings as shown in Figure 6.6B. INDO-PVP 50-50% showed a steep concentration incline to 0.065 mg/ml at 2h, with a concentration decline to 0.020 mg/ml at 24h. INDO-PVP-ERL 50-25-25% reached a maximum concentration of 0.045 mg/ml at 5h, which declined to 0.039mg/ml at 24h. INDO-ERL 50-50% reached its highest concentration of 0.021 mg/ml at 24h. Finally, a 1:1 physical mixture of INDO-PVP 50-50% and INDO-ERL 50-50% was tested. This formulation reached a peak concentration of 0.078 mg/ml at 4h and a concentration of 0.031 mg/ml after 24h dissolution.

At 10% INDO drug loading, shown in Figure 6.6C, INDO-PVP 90-10% reached the highest concentration (0.128 mg/ml) at 1h. This concentration declined to 0,035 mg/ml at 24h. INDO-PVP-ERL 10-45-45% reached a maximum concentration of 0.030 mg/ml at 22h. INDO-ERL 10-90% remained below INDO solubility for 24h. The maximum concentration reached was 0.009 mg/ml at 22h.

When INDO glass solutions with different polymer (mixtures) and drug loadings were tested in an HCl solution (pH 1.2), all formulations had similar release profiles (Figure 6.6D). Maximum concentrations reached were between 0.02 and 0.03 mg/ml at maximum 2h. After 7h of dissolution, all formulations approached INDO solubility (0.010 mg/ml).

Naproxen solid dispersions

Dissolution tests on spray dried solid dispersions with NAP at 30% w/w drug loading were performed in an acetate buffer pH 4.5. NAP concentrations in function of time are shown in Figure 6.7.

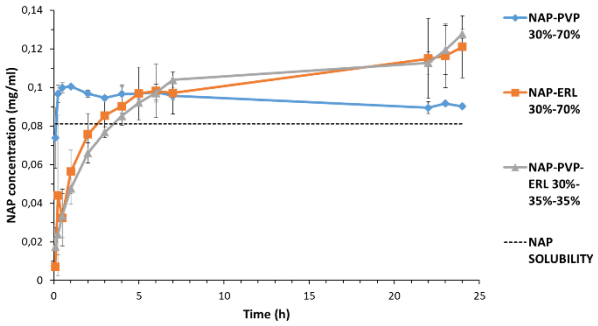

Figure 6.7: NAP concentrations in function of time of spray dried solid dispersions of NAP 30% with different polymers (or combinations). NAP-PVP 30-70% is represented in blue, NAP-PVP-ERL 30-35-35% in grey and NAP-ERL 30-70% in orange. Dissolution is performed in an acetate buffer pH 4.5. NAP solubility is represented by a black dashed line.

All tested formulations reached concentrations above NAP solubility (0.08 mg/ml). NAP-PVP 30-70% formulation showed a rapid concentration increase to a maximum of 0.100 mg/ml at 1h. This concentration showed a limited decrease at 24h to a concentration of 0.090 mg/ml. NAP-PVP-ERL 30-35-35% and NAP-ERL 30-70% reached concentrations higher than NAP solubility after 2h and 3h respectively. Highest NAP concentrations were only measured at 24h. NAP-PVP-ERL 30-35-35% reached a concentration of 0.128 mg/ml and NAP-ERL 30-70% a concentration of 0.121 mg/ml.

Cinnarizine solid dispersions

Spray dried solid dispersions of CINN, again at 30% w/w, showed very similar dissolution behavior when formulations with PVP, ERL, or a combination of both was applied (Figure 6.8).

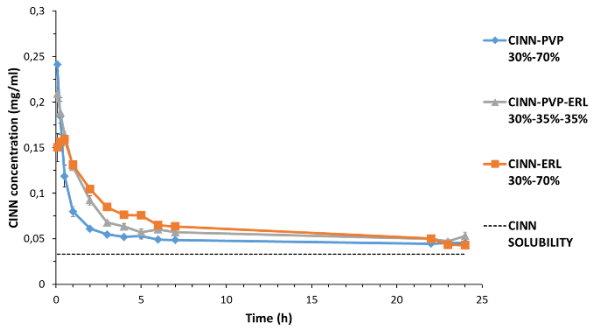

Figure 6.8: CINN concentrations in function of time of spray dried solid dispersions of CINN 30% with different polymers (or combinations). CINN-PVP 30-70% is represented in blue, CINN-PVP-ERL 30-35-35% in grey and CINN-ERL 30-70% in orange. Dissolution is performed in an acetate buffer pH 4.5. CINN solubility is represented by a black dashed line.

All formulations gave rise to concentrations above CINN solubility (0.033 mg/ml). Highest drug concentrations were measured immediately (at 5 min) for CINN-PVP 30-70% and CINN-PVP-ERL 30-35-35 % and were 0.241 mg/ml and 0.209 mg/ml respectively. In CINN-ERL 30-

70% the highest drug concentration (0.159 mg/ml) was reached after 30min. All formulations showed a steep concentration decline and reached concentrations of about 0.043-0.053 mg/ml at 24h, which is close to CINN solubility.

6.3.3 Solid state characterization of dissolution precipitates

Topography

Dissolution precipitates were analyzed by SEM, after filtering and drying. Figure 6.9 represents micrographs of INDO-PVP 30-70% (Figure 6.9A), INDO-PVP-ERL 30-35-35% (Figure 6.9B) and INDO-ERL 30-70% (Figure 6.9C) precipitates. The INDO-PVP precipitate clearly showed needle shaped structures which could represent crystalline INDO. The needle shaped crystals were clustered in a group of particles of around 30 µm. INDO-PVP-ERL and INDO-ERL did not show needle shaped structures, but spherical shaped particles which were more (INDO-PVP-ERL) or less (INDO-ERL) agglomerated into bigger particles.

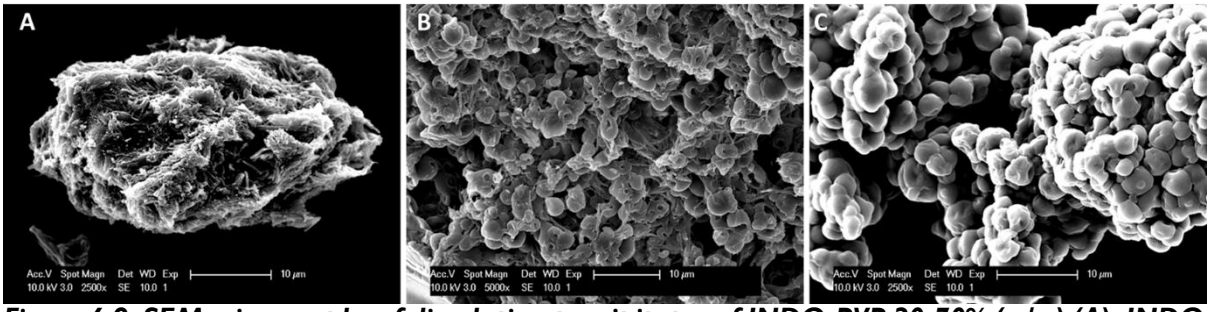

Figure 6.9: SEM micrographs of dissolution precipitates of INDO-PVP 30-70% (w/w) (A), INDO-ERL-PVP 30-35-35% (w/w) (B) and INDO-ERL 30-70% (w/w) (C)

Thermal analysis

Precipitates from INDO solid dispersions

After dissolution, filtered and dried precipitates of all INDO formulations were analyzed by mDSC. Thermograms are displayed in Figure 6.10.

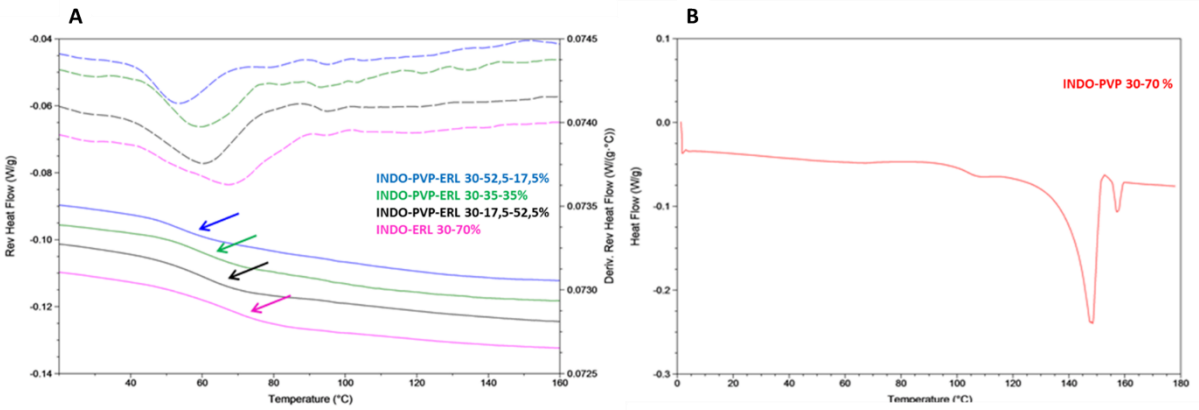

Figure 6.10: mDSC thermograms of dissolution precipitates of 30% INDO. In panel A, INDO-PVP-ERL 30-52.5-17.5% is represented in blue, INDO-PVP-ERL 30-35-35% in green, INDO-PVP-ERL 30-17.5-52.5% in black and INDO-ERL 30-70% in pink. Reversing heat flows are given in full lines, the 1st derivative of the reversing heat flows in dashed lines. Panel B represents the total heat flow of INDO-PVP 30-70% (red). Arrows indicate glass transitions.

Figures 6.10 A and 6.10 B represent 30% INDO loading. Here all precipitates from formulations containing ERL showed to be single phase amorphous. Mean glass transition temperatures were 55.1 °C, 58,6°C, 57,3°C and 67.6°C for INDO-PVP-ERL 30-52.5-17.5%, INDO-PVP-ERL 30-35-35%, INDO-PVP-ERL 30-17.5-52.5% and INDO-ERL 30-70% respectively (Figure 6.10 A). INDO-PVP 30-70% showed 2 melting peaks (Figure 6.10 B). The largest peak was at 148.1°C and the smallest one at 157.7°C.

INDO-ERL 50-50% showed a single glass transition temperature at 49.5°C, while INDO-PVP-ERL 50-25-25% showed a double glass transition. The first T_g was at 52.8°C, the second at 77.1°C. INDO-PVP 50-50% showed 2 melting peaks The largest peak was at 146.8°C and the smallest one at 157.4°C. The thermograms of this analysis are displayed in the Supplementary data (Supp. Figures A1 and A1').

Both INDO-ERL 10-90% and INDO-PVP-ERL 10-45-45% showed one glass transition at 52.9°C and 53.0°C respectively. INDO-PVP 10-90% showed 2 melting peaks of which the largest was at 145.4°C and the smallest at 155.9°C. These thermograms are shown in the supplementary data section (Supp. Figure A2 and A2').

Precipitates from NAP solid dispersions

In the mDSC precipitate analysis of NAP formulations, surprisingly, all total heat flow signals showed melting peaks at 154.7°C, 141.5°C and 150.9°C for NAP-PVP 30-70%, NAP-PVP-ERL 30-35-35% and NAP-ERL 30-70% respectively. NAP-PVP 30-70% showed the largest peak and this was closest to the melting point of NAP (156°C). Formulations containing ERL showed significant melting point depression and were the smallest melting peaks. Thermograms concerning NAP precipitate analysis are presented in the supplementary data (Supp. Figure B).

Precipitates from CINN solid dispersions

Reversing heat flow signals of CINN-PVP-ERL 30-35-35% and CINN-ERL 30-70% showed single glass transitions at 48.8°C and 50.5°C respectively. All formulations showed a melting peak situated at 119.2°C, 118.2°C and 115.2°C for CINN-PVP 30-70%, CINN-PVP-ERL 30-35-35% and CINN-ERL 30-70% respectively. The higher the amount of ERL in the formulation, the smaller and more depressed the precipitate melting peak was. Thermograms of precipitates of CINN formulations are presented in the supplementary data (Supp. Figure C1 and C2).

Presence of drug crystals

INDO and NAP precipitates were analyzed by XRPD. Diffractograms of INDO precipitates, together with the γ - and α - polymorphic form of INDO, are shown in the supplementary data (Supp. Figure D). All solid dispersion precipitates consisting of (a mixture with) ERL were amorphous since Bragg peaks were not observed. Precipitates of INDO-PVP 30-70%, INDO-PVP 50-50% and a physical mixture of INDO-PVP and INDO-ERL 50-50% all generated Bragg peaks matching the ones from α -INDO.

Diffractograms of NAP precipitates are shown in the supplementary data (Supp. Figure E). Precipitates of NAP-PVP-ERL 30-35-35%, either filtered and dried before measurement or analyzed immediately after filtering generated Bragg peaks characteristic of crystalline NAP. In the former, the amorphous halo of ERL is visible.

6.3.4 Drug Sorption

In a first set of experiments, NAP and CINN sorption onto/into ERL was tested. NAP (0.083mg/ml) and CINN (0.019 mg/ml) were tested in a concentration close to their solubility. A second NAP concentration (0.027 mg/ml) was tested close to CINN solubility. Figure 6.11 A shows API concentrations in function of ERL concentration.

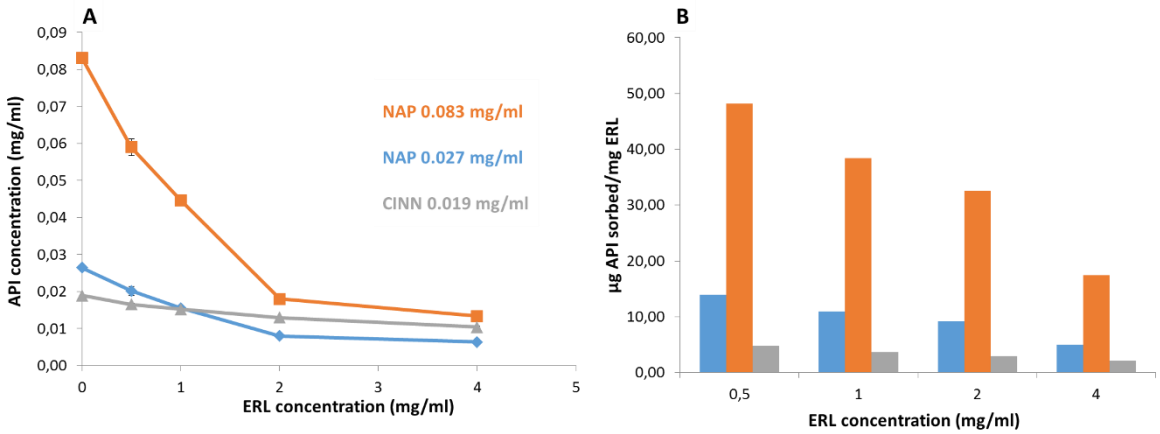

Figure 6.11: Sorption plots of NAP and CINN in presence of ERL in acetate buffer pH 4.5. Orange line and bars represent a 0.083 mg/ml NAP concentration, Blue line and bars a 0.027 mg/ml NAP concentration and grey line and bars a 0.019 mg/ml CINN concentration. Panel A plots API concentrations in function of ERL concentration. Panel B plots the amount of API sorbed per amount of ERL present in function of ERL concentration.

Up until an ERL concentration of 2 mg/ml, NAP concentrations decreased greatly. The concentration decrease of the highly-concentrated NAP solution was higher than that from the low concentrated solution. CINN concentrations on the other hand only marginally decreased. In figure 6.11 B, the amount of API sorbed (µg) per amount of ERL (mg) is plotted in function of ERL concentration for all 3 solutions. The amount of API sorbed per amount ERL decreased in function of increasing ERL concentration for all solutions, although only marginally for the CINN solution. The decrease was largest for the highest NAP concentration.

The sorption behavior was determined for INDO and NAP (Figure 6.12). The slope of the regression line represents $1/y_m$ according to Eq.1. The y_m value of the INDO sorption was 1.14 mg INDO per mg ERL, and 1.51 mg NAP per mg ERL for the NAP sorption.

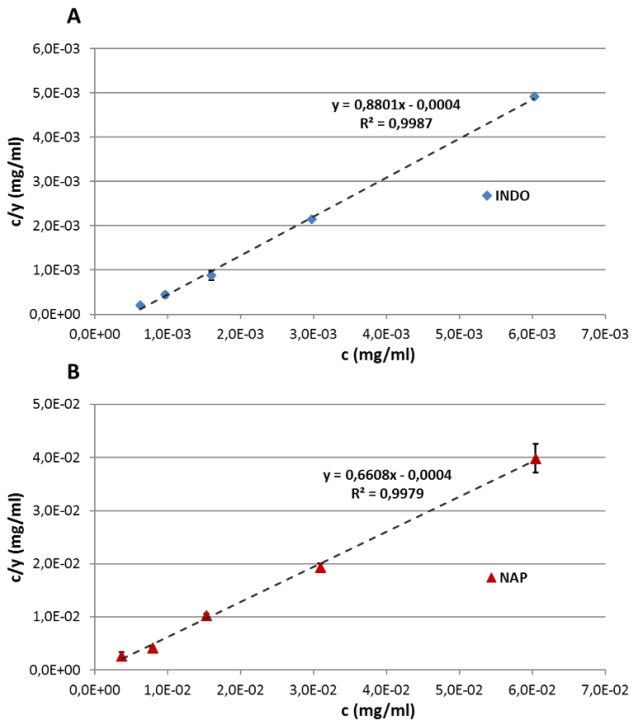

Figure 6.12: INDO (A) and NAP (B) sorption isotherms in presence of ERL in acetate buffer pH 4.5, modelled to the Langmuir model

6.3.5 Nanocrystal formation

During solubility testing of INDO and NAP in presence of ERL, nanocrystal formation was observed after ca. 48h in case of NAP and after ca. 240h in case of INDO. Particle size were measured using DLS and size distributions are shown in Figure 6.13 for INDO and NAP nanocrystals.

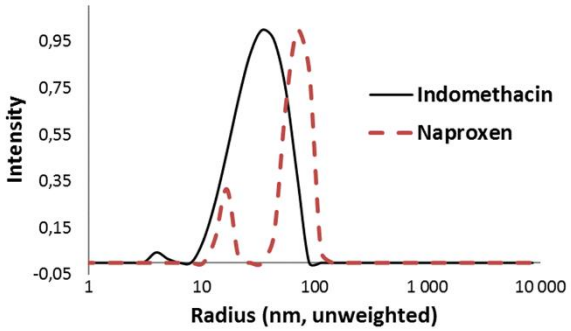

Figure 6.13: DLS particle size measurement of INDO (black full line) and NAP (red dashed line) nanocrystals in presence of 0.5 mg/ml ERL.

Both API's showed two particle size distributions. INDO nanocrystals showed two peaks with a mean peak position at 4.2 nm for the peak with the smallest intensity and at 32.0 nm for the peak with the largest intensity. For NAP nanocrystals, the smallest intensity peak had

a mean peak position of 16.1 nm and the largest intensity peak a mean peak position of 71.0 nm. Nanocrystal formation was not observed for CINN.

6.4 Discussion

The rationale for the current study was to find an answer to the question to what extent ERL, being an insoluble but swellable polymer, can, as (part of) the solid dispersion carrier slow down or stabilize the drug precipitation which is hampering the full exploitation of the potential of amorphous solid dispersions to increase the oral bioavailability. Precipitation in the gastrointestinal tract is often observed after administration of solid dispersions that are only made up of a hydrophilic carrier. The combination of ERL with the hydrophilic PVP should also potentially allow for sufficiently high initial drug concentrations, which is lacking when only a hydrophobic polymer is used as a solid dispersion carrier.

6.4.1 Phase behavior of solid dispersions containing ERL

SEM images of INDO solid dispersions showed topographical differences as different polymers or combinations of polymers were used. When PVP was used as a carrier, the largest particles were generated which also had the most irregular surface. Spray drying a 10% ethanol solution of INDO-PVP-ERL 30-35-35% generated particles of roughly 1-4 µm. These particles were spherical and had a smooth surface. INDO-ERL particles had similar size and shape, but the surface was somewhat more irregular. Shape and size differences can be attributed to the different drying kinetics of the different formulations during spray drying. Polymers made up 70% of all formulations, hence their properties will have a considerable influence on the final size, shape and topography of the produced particles.

mDSC analysis showed that spray drying INDO-polymer 30-70% (w/w) combinations generated glass solutions, irrespective to the fact that the polymer fraction was ERL, PVP or a combination of both. All glass transitions were found between the T_g's of the single components of INDO (47 °C), ERL (60.8 °C) and PVP K25 (156.8 °C) with 30% INDO loading. Moreover, glass transitions of all formulations corresponded well to theoretical glass transition temperatures calculated with the Gordon-Taylor (G-T) equation [22]. Measured T_g of INDO-PVP 30-70% showed the highest deviation compared to the G-T temperature, being 5°C lower. This was due to the hygroscopic properties of PVP, and hence the plasticization effect of water. When the INDO loading was changed to 50%, glass solutions were also formed in all carrier compositions. It was noted though, that T_g width was increased to 27,7°C for INDO-PVP 50-50% and 21,2°C for INDO-PVP-ERL 50-25-25%. INDO-ERL 50-50% had the narrowest T_g width of 15.9 °C. INDO-PVP 50-50% also showed to have 2 minima in the

thermogram of the 1st derivative of the reversing heat flow (Figure 6.2B). This, together with the wide T_g is the consequence of a more heterogeneous system [23]. INDO-ERL, on the other hand, still showed a homogeneous glass solution at 50% drug loading. When INDO loading was reduced to 10% (Figure 6.2C), glass solutions were still formed for INDO-PVP 10-90% and INDO-ERL 10-90% with glass transition temperatures moving closer to pure polymer T_g's. INDO-ERL 10-90% even has a higher Tg (64.1°C) than the one of pure ERL, this can point to strong drug-polymer interactions. INDO-PVP-ERL 10-45-45% showed 2 T_g's, one close to the T_g of ERL and one closer to the T_g of PVP. This formulation showed to be a phase separated system. This is understandable since the proportion of polymers in the system is the highest with only 10% drug loading and we recently showed that ERL and PVP as such are only partially miscible [24]. Hence, when the drug loading was high enough (>10% w/w), INDO could make a partially miscible polymer system fully miscible and thus acts as a blending agent for PVP and ERL.

Spray dried NAP solid dispersions presented different phase behavior (Figure 6.3 and 6.5). NAP-ERL 30-70% showed a melting peak pointing to the presence of a crystalline phase, as confirmed by XRPD where NAP-ERL 30-70% Bragg peaks matched the ones of crystalline naproxen. This solid dispersion was partly crystalline and partly amorphous since it still had a T_g at 33.0°C, which is between that of pure ERL and NAP (ca. 6°C [25]). Contrary to NAP-ERL 30-70%, NAP-PVP 30-70% and NAP-PVP-ERL 30-35-35% did form glass solutions.

CINN based solid dispersions all showed a melting peak in the total heat flow (Figure 6.4B) and a glass transition in the reversing heat flow (Figure 6.4A). None of the formulations was a glass solution, as they were partly amorphous and partly crystalline. It should be noted though that the melting peak in CINN-PVP 30-70% was much smaller compared to that in the other two formulations.

Having tested different API's and API ratios, it can be concluded that ERL can be used as a polymeric carrier for solid dispersions, either alone or in combination with a hydrophilic polymer like PVP K25.

6.4.2 In vitro dissolution and supersaturation of solid dispersions containing *ERL*

All formulations containing 30% INDO reach concentrations well above the INDO solubility level (Figure 6A). While the conventional solid dispersion using PVP as a carrier showed a fast concentration increase and a fast-subsequent precipitation of INDO, solid

dispersions containing ERL adequately retained elevated concentration levels (i.e. supersaturation). This hardly decreased during 24h. The higher the PVP ratio in carriers with PVP and ERL, the more the concentration dropped at 24h, but all were higher than the INDO-PVP solid dispersion. Although INDO-ERL reached concentrations above INDO solubility, as already shown in the past [21], a mixture of ERL and PVP combined the higher concentration levels observed with PVP with the supersaturation stabilization observed with ERL. An ERL ratio of merely 17.5% could already effectively stabilize supersaturation level for 24h, which translated in an area under the curve (AUC) which was 42% higher compared to that of INDO-PVP. It is well known that generation of supersaturated drug concentrations in the gastrointestinal tract can lead to enhanced flux across the intestinal wall and hence increased drug absorption[27, 28]. The higher AUC value observed with ERL based solid dispersions suggests their potential as supersaturation maintaining drug delivery systems and it may be worthwhile to explore this further in vivo. It has to be noted as well that initial drug dissolution is highest in glass solutions containing an ERL-PVP mixture as carrier. This effect, which is visible in the first 30 minutes of the in vitro drug dissolution (Figure 6A), can be attributed to a smaller particle size (Figure 1) and a the ability to avoid agglomeration of powder particles due to the presence of the hydrophobic ERL. These higher initial drug concentrations can be put forward as an additional advantage of incorporating ERL in these glass solutions (although this effect is only visible in 30% drug loading).

At 50% INDO loading, similar observations could be made (Figure 6.6B), although INDO-ERL 50-50% concentration never went above the INDO-PVP 50-50% concentration level. Interestingly, a 1:1 physical mixture of these two formulations generated a profile similar in shape to INDO-PVP, but at consistently higher concentration levels from 2 hours on. This is a large difference from the INDO-PVP-ERL 50-25-25% formulation, which has the same composition, but was spray dried as a single powder. In the physical mixture, it can be argued that INDO-PVP could immediately dissolve, resulting in higher concentrations, but there was also the stabilizing effect of INDO-ERL.

When the INDO content in solid dispersions was further decreased to 10% (Figure 6.6C), INDO-PVP outperformed both INDO-PVP-ERL 10-45-45% and INDO-ERL 10-90%, with this last formulation not even surpassing the INDO solubility level. Because ERL is an insoluble polymer, its ratio in these formulations is simply too high. INDO cannot sufficiently diffuse out of the ERL matrix within reasonable time frames. Although a higher amount of carrier usually results in higher solubilization or stabilization during dissolution in case hydrophilic polymers

are used as carrier, a low drug content in the insoluble ERL containing solid dispersions leads to the opposite effect since the drug cannot diffuse out of the matrix.

While formulations were previously tested in an acetate buffer pH 4.5, they were also tested in an HCl solution of pH 1.2 (Figure 6.6D). In this environment, INDO was completely unionized, which lowers its solubility. In this medium, all formulations performed equally, despite having different polymer compositions or drug loadings. A reason for this difference is the decreased solubility, and/or the inability of a charge interaction between INDO and ERL which has been shown previously [29].

NAP solid dispersions performed slightly different (Figure 6.7). NAP-PVP had a much less pronounced solubility increase (above NAP solubility) with subsequent precipitation. But here a similar benefit of ERL as a carrier can be observed. While dissolution is not as fast as in case of NAP-PVP, the solubility increase after 24h is clearly higher than NAP-PVP. What is also noticeable is that NAP-ERL and NAP-PVP-ERL have similar dissolution profiles, while both clearly show different phase behavior with NAP-PVP-ERL being a glass solution and NAP-ERL being partly crystalline. It should be noted as well that NAP has a pKa of 4.15, so part of it will be ionized, with a possibility of a charge interaction with ERL.

CINN solid dispersions have similar dissolution profiles with the different carriers tested. Drug concentrations start off high, but drug precipitation happens fast for all formulations. CINN as a fast crystallizer, does not seem to be suited to be formulated as a solid dispersion. There is also no possibility for a charge interaction between ERL and CINN, since it has a pKa of 8.4. This interaction seems to be beneficial for the performance of solid dispersions containing ERL.

6.4.3 Phase behavior of dissolution precipitates

The precipitation formed in the dissolution vessels was analyzed at the end of the in vitro dissolution tests (24h). From the SEM analysis, it can be clearly noticed that INDO-PVP precipitates contained INDO crystals (Figure 6.9A). In INDO-PVP-ERL (Figure 6.9B) and INDO-ERL (Figure 6.9C) these crystals are not visible. Moreover, the spherical particles seem to be preserved, although they have agglomerated to some extent. These findings were confirmed with mDSC. INDO-PVP 30-70% was crystalline as can be seen from the total heat flow curve (Figure 6.10B), where two melting peaks are visible, suggesting a polymorphic transition. All ERL containing precipitates remained completely amorphous (Figure 6.10A).

When a combination of ERL and PVP was used as a carrier, T_g's of precipitates were lower than the T_g's of the corresponding solid dispersions. This is because the PVP fraction dissolved and is not found in the precipitates. INDO-ERL 30-70% precipitate has a higher T_g, compared to the corresponding solid dispersion. Since solid dispersions are sprayed from an ethanol solution, no charge interaction could have taken place during the production of the solid dispersions. During dissolution on the other hand, INDO is partly ionized in the medium, allowing for a charge interaction with ERL. This strong interaction is the reason for a higher T_g in the precipitate. These amorphous precipitates can be beneficial in the situation were a poorly soluble drug has a high permeability. If the API is permeated through the gastro-intestinal barrier easily, this could create a situation where amorphous drugs can be released from an ERL 'reservoir' system and this could lead to higher release than a crystalline precipitate that should overcome the crystal lattice energy to dissolve. The amorphous precipitate can also be the reason why no crystalline precipitation is observed during in vitro dissolution of INDO-(PVP-)ERL solid dispersions. Since INDO has to diffuse out of the ERL matrix, a more gradual release is achieved and the propensity for nucleation and crystallization is not as high as when all INDO is dissolved into the medium directly [21].

In 50% and 10% INDO loadings, similar observations could be made (Supp. Figure A). Precipitates from PVP solid dispersions showed a double melting peak and solid dispersions containing ERL remained amorphous. T_g's were generally lower because of the absence of PVP in ERL-PVP precipitates. INDO-PVP-ERL 50-25-25% precipitate showed to be a phase separated system (double T_g). It cannot be ruled out that a fraction of PVP was trapped in the ERL matrix or only part of ionized INDO formed a charge interaction with ERL, leading to a higher second T_g

The double melting peak suggested a polymorphic transition of crystalline INDO. This was confirmed by XRPD analysis where crystalline precipitates showed Bragg peaks corresponding to the α -form of INDO (Supp. Figure D). This is a well-known and identified polymorphic transition during dissolution of amorphous INDO [30, 31]. No Bragg peaks of the γ -form of INDO can be seen in XRPD results, so the double melting peak can be attributed to a polymorphic transition during heating in mDSC. XRPD also did not show Bragg peaks in precipitates containing ERL, confirming the presence of amorphous INDO in these carriers.

NAP and CINN precipitates all showed melting peaks in the total heat flow signal (Supp. Figures B and C respectively). This shows that the crystallization of a drug in the medium is

highly dependent on its physicochemical properties like crystallization behavior [32]. The crystallinity of NAP-PVP-ERL precipitates was confirmed in XRPD (Supp. Figure D). To exclude phase transformations during drying, the precipitates were analyzed after filtration (wet) and after filtration and drying (dry). Since the Bragg peaks can be observed in both samples, the crystallinity was not induced during drying.

6.4.4 Sorption of drugs onto/into ERL

INDO sorption has been extensively studied in a previous publication from our group [29]. NAP sorption was confirmed for 2 starting concentrations. In the highest initial NAP concentration, the decrease in concentration was the highest with increasing ERL concentration (Figure 6.11A). On the other hand, the amount of NAP sorbed into/onto ERL decreased with increasing ERL concentration (Figure 6.11B), this leads to the identification of two driving forces for sorption into/onto ERL: the initial drug concentration and the concentration of ERL in the medium. By maximizing the former and minimizing the latter, optimal sorption can be achieved. CINN sorption was generally low which can be attributed to the absence of a charge interaction between drug and polymer, reducing the driving force for sorption. In a second sorption experiment, sorption of INDO and NAP was modelled to the Langmuir model (Figure 6.12). A higher y_m value for NAP was observed, indicating its higher sorption potential, compared to INDO.

6.4.5 Nanocrystal formation in presence of ERL

Surprisingly, the formation of nanocrystals was observed during solubility measurements of INDO and NAP in presence of ERL in acetate buffer (pH 4.5). This nanocrystal formation was not observed in solubility measurements of pure INDO or NAP, or in presence of PVP. The difference in time it took to observe the nanocrystals varied between NAP and INDO, and this can most likely be attributed to their different crystallization behavior [32]. It was also shown that the size of the formed nanocrystals is in the lower part of the nanometer range. It has to be noted that no stabilizer is added here, although this is generally recognized as an absolute necessity to produce stable nanosuspensions [33]. The mechanism of formation of the nanocrystals is schematically explained in Figure 6.14.

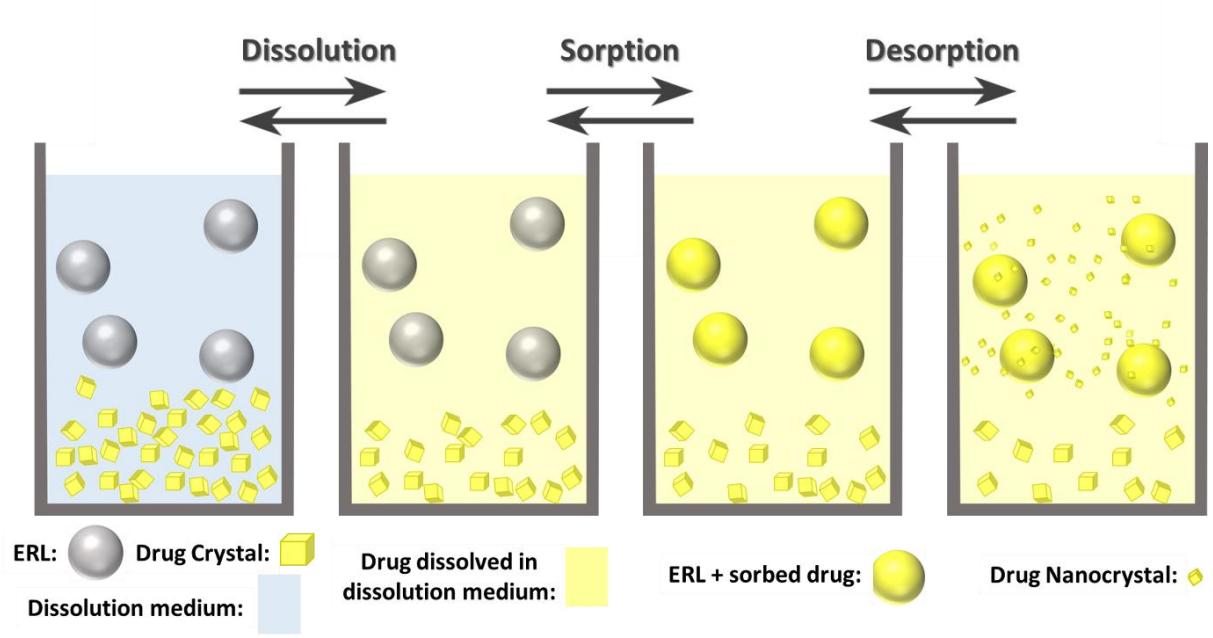

Figure 14: Schematic representation of nanocrystal formation in presence of ERL.

There are 3 steps in the formation of nanocrystals: dissolution of native drug crystals in the medium, sorption of the drug in or on (hydrated) ERL particles and desorption into the release medium. The desorption into the medium will result in nucleation and nanocrystal formation because the drug solubility has already been reached in the medium. It also means that an oversaturated drug solution is necessary to obtain nanocrystals, because the drug solubility has to be maintained at every moment, also when part of the drug in solution is sorbed into the ERL particles. Because sorption and desorption are dynamic processes, the desorbed drugs arrive in a saturated dissolution medium and crystallize upon arrival. This particular formation of nanocrystals can be seen as a start to develop new production methods for nanosuspensions. Moreover, not only has this method the potential to be further developed as a new method to produce nanocrystals, if drug and ERL are simultaneously introduced in the gastro intestinal tract in appropriate ratios, ERL could form nanocrystals 'in-situ'. The main challenge will be the adjustment of nanocrystal formation within pharmaceutically relevant time scales. Since CINN did not form nanocrystals, high sorption into ERL and/or a charge interaction seem to be necessary requirements for this kind of nanocrystal formation.

6.5 Conclusions

The feasibility of Eudragit® RL as a carrier for solid dispersions was assessed in this paper. Phase behavior studies showed that ERL can form glass solutions, either alone or as part of a binary polymer mixture with a hydrophilic polymer (PVP K25). In vitro dissolution tests showed that ERL can form and stabilize supersaturated drug concentration levels. Optimal concentration profiles however, are observed in combination with PVP, where an ideal combination of high concentration and prolongation of these concentration levels are achieved. Dissolution precipitates of INDO formulations with ERL remained amorphous, which can be beneficial to obtain high drug permeability.

The unexpected formation of INDO and NAP nanocrystals was observed in presence of ERL. Nanocrystals were on the lower end of the nanometer scale and were stable without addition of stabilizers. An interplay of dissolution, sorption and desorption is hypothesized as responsible for nanocrystal formation. Sorption of the drug into/onto ERL is a necessary condition for nanocrystal formation. Charge interactions between drug and ERL can enhance or promote sorption. Nanocrystal formation in presence of ERL can be further investigated as a potential new manufacturing method and/or can be exploited for 'in-situ' nanonization.

6.6 References

1. Marshall, G. R., Computer-Aided Drug Design. *Annual Review of Pharmacology and Toxicology* **1987**, 27 (1), 193-213.

2. Lipinski, C. A.; Lombardo, F.; Dominy, B. W.; Feeney, P. J., Experimental and computational approaches to estimate solubility and permeability in drug discovery and development settings. *Advanced Drug Delivery Reviews* **1997**, 23 (1), 3-25.

3. Lipinski, C. A., Drug-like properties and the causes of poor solubility and poor permeability. *Journal of Pharmacological and Toxicological Methods* **2000**, 44 (1), 235-249.

4. Elder, D.; Holm, R., Aqueous solubility: Simple predictive methods (in silico, in vitro and bio-relevant approaches). *International Journal of Pharmaceutics* **2013**, 453 (1), 3-11.

5. Takagi, T.; Ramachandran, C.; Bermejo, M.; Yamashita, S.; Yu, L. X.; Amidon, G. L., A Provisional Biopharmaceutical Classification of the Top 200 Oral Drug Products in the United States, Great Britain, Spain, and Japan. *Molecular Pharmaceutics* **2006**, 3 (6), 631-643.

6. Amidon, G. L.; Lennernas, H.; Shah, V. P.; Crison, J. R., A theoretical basis for a biopharmaceutic drug classification: the correlation of in vitro drug product dissolution and in vivo bioavailability. *Pharm Res* **1995**, 12 (3), 413-20.

7. Food and Drug, A., Guidance for industry: waiver of in vivo bioavailability and bioequivalence studies for immediate-release solid oral dosage forms based on a biopharmaceutics classification system. Food and Drug Administration, Rockville, MD **2000**.

8. Williams, H. D.; Trevaskis, N. L.; Charman, S. A.; Shanker, R. M.; Charman, W. N.; Pouton, C. W.; Porter, C. J. H., Strategies to Address Low Drug Solubility in Discovery and Development. *Pharmacological Reviews* **2013**, 65 (1), 315.

9. Newman, A.; Nagapudi, K.; Wenslow, R., Amorphous solid dispersions: a robust platform to address bioavailability challenges. *Therapeutic Delivery* **2015**, 6 (2), 247-261.

10. He, Y.; Ho, C., Amorphous Solid Dispersions: Utilization and Challenges in Drug Discovery and Development. *Journal of Pharmaceutical Sciences* **2015**, 104 (10), 3237-3258.

11. Baghel, S.; Cathcart, H.; O'Reilly, N. J., Polymeric Amorphous Solid Dispersions: A Review of Amorphization, Crystallization, Stabilization, Solid-State Characterization, and Aqueous Solubilization of Biopharmaceutical Classification System Class II Drugs. *Journal of Pharmaceutical Sciences* **2016**, 105 (9), 2527-2544.

12. Van den Mooter, G., The use of amorphous solid dispersions: A formulation strategy to overcome poor solubility and dissolution rate. *Drug Discovery Today: Technologies* **2012**, 9 (2), e79-e85.

13. Newman, A., *Pharmaceutical Amorphous Solid Dispersions*. **2015**: Wiley. 504.

14. Sun, D. D.; Lee, P. I., Haste Makes Waste: The Interplay Between Dissolution and Precipitation of Supersaturating Formulations. *The AAPS Journal* **2015**, 17 (6), 1317-1326.

15. Augustijns, P.; Brewster, M. E., Supersaturating Drug Delivery Systems: Fast is Not Necessarily Good Enough. *Journal of Pharmaceutical Sciences* **2012**, 101 (1), 7-9.

16. Van Speybroeck, M.; Mellaerts, R.; Mols, R.; Thi, T. D.; Martens, J. A.; Van Humbeeck, J.; Annaert, P.; Van den Mooter, G.; Augustijns, P., Enhanced absorption of the poorly soluble drug fenofibrate by tuning its release rate from ordered mesoporous silica. *European Journal of Pharmaceutical Sciences* **2010**, 41 (5), 623-630.

17. Six, K.; Daems, T.; de Hoon, J.; Van Hecken, A.; Depre, M.; Bouche, M.-P.; Prinsen, P.; Verreck, G.; Peeters, J.; Brewster, M. E.; Van den Mooter, G., Clinical study of solid dispersions of itraconazole prepared by hot-stage extrusion. *European Journal of Pharmaceutical Sciences* **2005**, 24 (2–3), 179-186.

18. Van Duong, T.; Van den Mooter, G., The role of the carrier in the formulation of pharmaceutical solid dispersions. Part I: crystalline and semi-crystalline carriers. *Expert Opinion on Drug Delivery* **2016**, 13 (11), 1583-1594.

19. Van Duong, T.; Van den Mooter, G., The role of the carrier in the formulation of pharmaceutical solid dispersions. Part II: amorphous carriers. *Expert Opinion on Drug Delivery* **2016**, 1-14.

20. Tran, P. H.-L.; Tran, T. T.-D.; Park, J. B.; Lee, B.-J., Controlled Release Systems Containing Solid Dispersions: Strategies and Mechanisms. *Pharmaceutical Research* **2011**, 28 (10), 2353-2378.

21. Sun, D. D.; Lee, P. I., Probing the mechanisms of drug release from amorphous solid dispersions in medium-soluble and medium-insoluble carriers. *Journal of Controlled Release* **2015**, 211, 85-93.

22. Paudel, A.; Worku, Z. A.; Meeus, J.; Guns, S.; Van den Mooter, G., Manufacturing of solid dispersions of poorly water soluble drugs by spray drying: Formulation and process considerations. *International Journal of Pharmaceutics* **2013**, 453 (1), 253-284.

23. Van den Mooter, G.; Wuyts, M.; Blaton, N.; Busson, R.; Grobet, P.; Augustijns, P.; Kinget, R., Physical stabilisation of amorphous ketoconazole in solid dispersions with polyvinylpyrrolidone K25. *European Journal of Pharmaceutical Sciences* **2001**, 12 (3), 261-269.

24. Song, M.; Hammiche, A.; Pollock, H. M.; Hourston, D. J.; Reading, M., Modulated differential scanning calorimetry: 4. Miscibility and glass transition behaviour in poly(methyl methacrylate) and poly(epichlorohydrin) blends. *Polymer* **1996**, 37 (25), 5661-5665.

25. Dereymaker, A.; Scurr, D. J.; Steer, E. D.; Roberts, C. J.; Van den Mooter, G., Controlling the release of indomethacin from ‚glass solutions layered with a rate controlling membrane using fluid-bed processing. Part 1: Surface and cross-sectional chemical analysis. *Molecular Pharmaceutics* **2017**, xx (xx), Submitted.

26. Paudel, A.; Van Humbeeck, J.; Van den Mooter, G., Theoretical and Experimental Investigation on the Solid Solubility and Miscibility of Naproxen in Poly(vinylpyrrolidone). *Molecular Pharmaceutics* **2010**, 7 (4), 1133-1148.

27. Brouwers, J., M.E. Brewster, and P. Augustijns, *Supersaturating drug delivery systems: the answer to solubility-limited oral bioavailability?* J Pharm Sci, 2009. **98**(8): p. 2549-72.

28. Stillhart, C. and M. Kuentz, *Trends in the Assessment of Drug Supersaturation and Precipitation In Vitro Using Lipid-Based Delivery Systems.* J Pharm Sci, 2016. **105**(9): p. 2468-76.

29. Dereymaker, A.; Pelgrims, J.; Engelen, F.; Adriaensens, P.; Van den Mooter, G., Controlling the release of indomethacin from glass solutions layered with a rate controlling membrane using fluid-bed processing. Part 2: The influence of charge interactions on drug release. *Molecular Pharmaceutics* **2017**, xx (xx), Submitted.

30. Greco, K.; Bogner, R., Crystallization of amorphous indomethacin during dissolution: effect of processing and annealing. *Mol Pharm* **2010**, 7 (5), 1406-18.

31. Andronis, V.; Yoshioka, M.; Zografi, G., Effects of Sorbed Water on the Crystallization of Indomethacin from the Amorphous State. *Journal of Pharmaceutical Sciences* **1997**, 86 (3), 346-351.

32. Van Eerdenbrugh, B.; Raina, S.; Hsieh, Y. L.; Augustijns, P.; Taylor, L. S., Classification of the crystallization behavior of amorphous active pharmaceutical ingredients in aqueous environments. *Pharm Res* **2014**, 31 (4), 969-82.

33. Tuomela, A.; Hirvonen, J.; Peltonen, L., Stabilizing Agents for Drug Nanocrystals: Effect on Bioavailability. *Pharmaceutics* **2016**, 8 (2), 16.

Chapter 7: General Discussion

During this project, attempts were undertaken to tackle some of the shortcomings or disadvantages of amorphous solid dispersions, or more specifically, glass solutions. Some stability issues are caused by residual solvent presence or additional processing steps like milling or compression [1, 2]. Fluid bed coating as a manufacturing method of solid dispersions can address these issues since efficient drying can be achieved during and post formation without additional transfer steps. While the solubility/dissolution rate of solid dispersions, produced with fluid bed coating has been investigated previously [3-5], not much is known about the phase behaviour of these coated solid dispersions around an inert carrier.

Secondly, glass solution formulations can suffer from fast precipitation of supersaturated drug concentrations [6]. In this context, an additional coating layer can be applied on top of the glass solution through fluid bed coating providing controlled drug release kinetics, to transform fast dissolving but fast precipitating delivery systems into sustained release formulations, effectively enhancing the window for absorption. Different formulation parameters can influence drug release. These complex coated systems do not generate formulations with a straight forward phase behaviour, therefore a combination of bulk and surface characterization methods was applied.

Lastly, instead of using an additional coating layer to control the release of glass solutions, an aqueous insoluble but swellable polymer was incorporated as (part of) the carrier of a glass solution, prepared by spray drying. The influence of different formulation parameters on the phase behaviour and the generation and maintenance of supersaturation was tested.

7.1 mDSC method development for glass solutions coated on inert carriers

To investigate the phase behaviour of coated glass solutions on inert carriers, mDSC analysis was performed (chapter 3). Since previously published research did not use mDSC, or sample preparation was not explicitly mentioned or discussed, in a first set of experiments beads were loaded as such into the DSC sample pans without any success. The very small contact area between the spherical beads and the surface of the sample pan resulted in undetectable phase transitions apart from the sucrose melting peak of the inert carriers. Softly grinding the beads to enhance the contact area did not result in visible glass solution transitions either. What did result in detectable glass transitions, was grinding and sieving the beads to obtain particles with different size ranges. From the resulting derivatives of the reversing heat

flows, it could be observed that the T_g decreased and broadened when particles increased in size. Because simply grinding the beads generates a collection of these particles with different sizes, all these glass transitions would be overlapping and less pronounced, hence resulting in a very broad and shallow glass transition which would be undetectable. The T_g shifting and broadening was confirmed in glass solution films prepared by rotary evaporation. Later, different API's and even different solvents (or solvent mixtures) showed similar phenomena. The T_g shift and broadening was attributed to different residual solvent mass losses below and above the T_g of the sample, due to large differences in surface area to mass ratios.

These findings highlight that it is tricky to analyse glass solutions which have high variations in particle size range. Because of the solvent involvement, the particle size influence on the T_g will only be a factor to take into consideration when analysing glass solutions prepared by rapid solvent evaporation. Some glass solutions, like KETO-PVP prepared from an ethanol solution or INDO-PVP prepared from DCM or DCM-MeOH solutions even showed double glass transitions in particles with an intermediate particle size range. This could be wrongly interpreted as a phase separated system since a double T_g is normally an indicator for different drug-polymer domains.

It is very useful to take these findings into consideration when using different solvent based manufacturing methods as well. Since in spray drying, the particle size distribution is normally smaller, the effect will be less pronounced within one batch of spray dried glass solution. But since it is known that process and formulation parameters can influence the resulting particle size of spray dried powders[7], varying these parameters or even using different spray dryers (e.g. in scaling up development), can result in unwanted shifting and broadening of glass transitions due to residual solvent mass loss. Often, small scale glass solution preparation by solvent evaporation is used for screening purposes. Here, glass solution films are prepared to have a quick idea about the feasibility of the preparation method and the phase behaviour of the produced glass solutions. When analysing these films by DSC, it is also possible that they are crushed, generating particles with a large size range and encountering these phenomena which can lead to false exclusion of the formulation for further research or development.

Attention should be drawn as well to the use of TGA in this study. While a linear heating regiment provided residual solvent contents, which were comparable for particles with different size ranges, a differentiation between sub-T_g and above-T_g solvent loss allowed to correlate the (lack of) sub-T_g solvent loss to the observed glass transition shifting and

broadening. It is advised, when performing TGA analysis, to measure solvent mass loss below and above the glass transition of the glass solution. By doing this, more specific information is provided about the kinetic phenomena of solvent loss, and not just the total amount of residual solvent present in the sample, also providing possible links with observed thermal events or differences in thermal events of different samples.

Is this mDSC method now the ideal method for characterizing the phase behaviour of glass solutions, coated on inert carriers? The answer to this question is twofold. First of all, the instrument set-up doesn't allow to analyse the coated beads as such, due to the very small contact area between spherical beads and the flat bottom of the aluminium pans, so sample manipulations for mDSC analysis will always be necessary. Grinding and sieving the beads requires external forces to be applied to the glass solution which can potentially be detrimental to the system since solid state transformations can be provoked. To exclude crystallization of the system for example, XRPD analysis can be performed together with mDSC analysis. Here, beads can be analysed as such, and grinding or sieving induced crystallization can be excluded. Kovacevic *et al.* recently published an alternative mDSC method to analyse drug-polymer coated beads. They were able to perform mDSC experiments by analysing free films with identical composition to the layered beads [8]. While this method doesn't require external forces to be applied to the system, the film formation process is not identical compared to the film formation process in fluid bed coating. In the formation of free films, a different substrate, drying environment (temperature, pressure difference) and drying time are all different which can lead to films with different physicochemical properties.

Instead of adjusting the sample to the needs of the analysis technique, the opposite can be done as well. When looking at alternative techniques that can cope with the coated bead geometry in a better way, microthermal analysis (MTA) techniques come into the picture [9]. Because of the 'scanning' or spatially resolved nature of these techniques, not the whole sample is analysed, but a surface on the sample with micrometer dimensions by heating an AFM probe tip. This could be easily performed on the surface of a bead. It would be very interesting to compare one of these localized techniques to the mDSC method to investigate if differences in phase behaviour can be observed between the two techniques. On the other hand, it could also provide an alternative analysis technique to measure the solvent poor surface and the solvent rich bulk of the glass solution described in this chapter.

7.2 Surface and cross-sectional chemical analysis of multilayer coated beads

By adding an additional coating layer on top of the INDO-PVP glass solution to control the drug release, bulk characterization methods like mDSC were insufficient to investigate the physical structure of the obtained coated beads. To have an idea about the composition and distribution of the different compounds in these coated beads, imaging (or spatially resolved) techniques were applied. ToF-SIMS is very well suited to accommodate these needs, since it has a very low detection limit, and high spatial resolution. Furthermore, because the primary ion beam only removes the first few monolayers of a sample, the very limited penetration depth (1-2 nm)[10] makes it an ideal method to even detect distributional changes at the upmost surface layer or within a coating layer when analysing cross sections, without possible blurring effects due to sample curvature. ToF-SIMS was also recently successfully applied in different studies concerning spray dried solid dispersions to form sustained release injectables [10-15].

From the results described in chapter 4 it can be concluded that ToF-SIMS proved to be very useful in the characterization of complex coated beads. The analysis of the surface and cross-sections of the beads allowed for a complete chemical analysis of the presence and the distribution of all compounds. High specificity could be achieved through specific marker ions of all compounds, which were five in total in case of the cross sections. Even chemically similar compounds like EC and sucrose from the inert carriers could be successfully distinguished from one another. Because of the size and spherical shape of the beads, only the upmost part of the sample could be analysed with ToF-SIMS. Therefore, the entire 200×200 µm analysis area was not covered in the surface analysis. The available spectra and images could still provide an accurate compositional and distributional analysis of the surface. All surfaces were also analysed in triplicate to exclude artefacts on the surface.

The presence of the PVP marker on the surface of the beads with an ERL or EC top coating can be explained by a coating contamination since both the glass solution and controlled release layer are coated consecutively without unloading the beads and cleaning the device in between the spraying cycles. It is highly unlikely to assume that the entire INDO-PVP solution was sprayed onto the beads. Some of the spraying solution was also sprayed on either the coating chamber walls or the inside of the Würster cylinder. Since the coated beads do not follow exactly the same patterns inside of the fluidized bed device, it is quite possible that they

collide with a dried glass solution powder particle residing inside of the coating device. This can explain the presence of PVP on the outer surface of the beads. The presence of the INDO marker ion of these outer surfaces is also seen but less clear compared to the PVP marker presence. This could be explained by the fact that in the glass solution, the ratio between INDO and PVP is 30% to 70% (w/w) of the respective compounds. Furthermore, the maker ion intensity in the control sample of PVP ($5.2*10^{-2}$) is more than double compared to the intensity of the INDO marker in the control sample ($2.37*10^{-2}$), hence the lower intensity and detection of this marker ion on the surface. ToF-SIMS analysis of the cross sections showed that there are no PVP channels being formed in the outer coating layer, excluding the possibility of polymer migration to the surface.

Cross-section analysis showed a very limited migration of PVP and mainly INDO across controlled release membranes, irrespective of their constitutions, through a gradient in marker intensity from the inner part to the outer part of the membrane. The fact that this migration was most prominent in the ERL latex formulation, was explained by a combination of a higher coating temperature, additional curing and/or the slower evaporation of water compared to ethanol in the controlled release membranes sprayed from a solution. These factors lead to a limited migration which also disproves the PVP presence on the surface as a result of polymer migration. It does, however, point to the influence of the spraying liquid (water vs. ethanol) on this migration. It would be very interesting to further investigate the influence of different formulation and process parameters on this migration and to possibly correlate this to drug release phenomena.

Another interesting observation made with ToF-SIMS was the distribution of INDO and PVP in the glass solution layer of the coated beads. In chapter 3 it was already established by mDSC that INDO-PVP 30-70% (w/w) forms glass solutions when layered on sucrose beads. When analysing the surface and cross-section of INDO-PVP coatings, clear moieties of both components are observed together with their distribution along the surface and cross-section, which results in an image of drug-polymer mixing. It would be interesting to analyse a solid dispersion that is simultaneously analysed with mDSC as a phase separated or crystallized system with ToF-SIMS to investigate distributional changes in the image. The link between phase separation/crystallization with distributional changes in ToF-SIMS images could result in a more profound understanding of this phenomenon The relatively large size of the coated beads (compared to spray dried powder particles) lends itself ideally to this kind of investigation.

7.3 Polymer miscibility in controlled release coatings

The importance of polymer miscibility in the release controlling outer membrane of the complex coated beads is demonstrated in chapter 4 and 5. The partial miscibility between ERL and PVP proved to be advantageous in the attachment of the controlled release membrane to the glass solution layer, the more homogeneous distribution of PVP along the surface when incorporated as a pore former and, finally, its influence on INDO release. When PVP was added as a pore former to EC in a ratio of 25% (w/w), this resulted in immediate release of INDO because of coating defects in the controlled release layer. These coating defects are isolated PVP domains in the controlled release layer, formed due to the immiscibility of both polymers. In ERL based rate controlling membranes, a 25% PVP incorporation as a pore former does not lead to such coating defects and the subsequent immediate release of INDO. This shows the impact of pore former miscibility on the ability of the controlled release coating layer to stay intact during dissolution and thus maintain its modified release properties.

7.4 Influence of formulation changes on the sustained in vitro release of INDO

Coating layer thickness increase leads to slower and decreased INDO release with an increased lag time in all formulations (except a defective coating), irrespective of their constitution. This can be attributed to increased diffusion pathways[16], a denser polymer network and sorption to the controlled release polymer. The influence of pore former concentration on the release of INDO was dependent on the controlled release polymer used. When ERL was applied there was little difference between 10% and 25% PVP, but in case that EC was used, there is a large difference in release. This can again be brought back to the difference in miscibility discussed in the previous section. Coating from an ethanol solution or an aqueous dispersion showed release differences at higher coating levels such as a lower level of burst release and quasi-zero order release after 90 minutes. Lastly, when comparing both controlled release polymers, ERL generally showed higher and faster release compared to EC samples, ERL also showed burst release while EC samples showed an extended lag time. In general, when choosing appropriate formulation parameters, adding a membrane to control or sustain drug release from glass solutions is a viable option to possibly extend the absorption window of solid dispersions. More extensive (in vivo) release studies, where direct and controlled release solid dispersions are compared, might elucidate this option even further.

Diffusion tests through rate controlling membranes generally show similar trends when varying formulation parameters compared to release tests, which lead to the conclusion that drug diffusion is the rate limiting step for drug release. On the other hand, it would also provide a good screening method for selecting the ideal controlled release coating formulation, depending on the requirements and needs of the drug delivery system.

Another objective investigated in this chapter is the possibility of a charge interaction between the drug and rate controlling polymer influencing the release. When INDO is introduced in an aqueous medium with a pH above its pKa (4.5), it is ionized. ERL on the other hand possesses quaternary ammonium groups which give the polymer its swelling capacity in aqueous media [17]. It has already been shown that drug release from ERL formulations can be sensitive to the presence of anionic species in the release buffer[18] or organic acids [19]. For this reason, it was hypothesized that INDO release would be altered by this charge interaction as well. While the interaction between both components was confirmed with solid-state NMR and drug sorption onto or into ERL particles and films was observed as well, no major influence could be seen on drug release. When comparing to the release from the neutral EC rate controlling membrane, it was found that the release through ERL membranes was generally faster. The same observation could be made from diffusion tests. However, because water vapour diffusion was also higher through ERL membranes, the higher diffusion rates can mainly be ascribed to the more hydrophilic nature of the polymer. It is very difficult to investigate the influence of a charge interaction on drug release. No comparison can be made for instance with other drugs that are not ionisable because these drugs would have different physicochemical properties, just like the difference in drug release through both polymers proved to be mainly due to their hydrophilic behaviour or swelling capacity instead of whether or not being ionic in nature.

7.5 Eudragit® RL as a carrier for solid dispersions

Controlling drug release from solid dispersions was not only attempted from complex coated systems, the potential of ERL as a carrier for solid dispersions was also investigated through its phase behaviour and the generation and maintenance of supersaturated drug concentrations from spray dried formulations. ERL could be applied alone as a carrier or in combination with a hydrophilic polymer (in this case PVP). mDSC studies showed that ERL as a carrier could form glass solutions even in higher drug loadings (up to at least 50% w/w) or

with different ratios of PVP. Glass solution formation largely depended on the physicochemical characteristics of the drug and the ratio of this drug incorporated into the solid dispersion. Drug dissolution studies showed that drugs which formed solid dispersions with ERL as a carrier could remain in a supersaturated state for a longer time compared to solid dispersions with PVP as a carrier. However, when a combination of ERL and PVP were tested, this generated higher drug concentrations compared to pure ERL and these higher drug concentrations were far better maintained over the course of 24 hours compared to pure PVP as a carrier. Highest stabilized drug concentrations were even seen in a physical mixture of spray dried INDO-PVP and INDO-ERL, so when there was no interaction or mixing between both polymers. INDO-(PVP-)-ERL precipitates also proved to remain completely amorphous when analysed after 24 hours of dissolution. This could be seen as a 'reservoir' system of amorphous INDO.

The potential of this approach seems to be enormous. The generality of these findings however, still needs to be further investigated. Weak acidic drugs for example seem to give the best results (in part) due to the charge interaction with ERL, but CINN which is a neutral compound in the tested conditions quickly precipitated to its thermodynamic solubility. Since this was also the case with the hydrophilic polymer PVP, the inability to maintain the supersaturated state could be entirely due to the characteristics of the drug. A large screening study of different API's with different physicochemical properties could potentially clarify the necessary properties of a drug candidate to be formulated in a solid dispersion together with ERL. Furthermore, the combination of ERL with PVP showed to give the best compromise in high drug concentration with stabilization of this concentration. But it is still unclear if this would work for all hydrophilic polymers. A comparative study incorporating different hydrophilic polymers in combination with ERL, could shed some light on this matter. Also, it is believed that the more gradual drug release would somehow be responsible for the stabilisation of the supersaturated drug concentrations. A mechanistic study into the exact role of ERL into the stabilization of supersaturated states is necessary to fully understand the potential and possible pitfalls of this approach. The influence of the manufacturing technique could also be further investigated. Currently spray drying was chosen over, for example, fluid bed coating because the latter doesn't create a high enough surface area for sufficiently fast diffusion out of the insoluble ERL matrix. Other technologies like electrospraying can create even smaller particles which could be beneficial for supersaturation generation. Other manufacturing methods like ball milling could prove to have some advantages as well. Lastly,

glass solutions have always been the class of solid dispersions showing the highest dissolution enhancing potential. However, for solid dispersions using an insoluble but swellable matrix this doesn't necessarily have to be the case. Creating a one phase system of a drug and ERL means intimate mixing between both components which could result in a slower drug release (see comparison between INDO-PVP-ERL 50-25-25% and the physical mixture of INDO-PVP and INDO-ERL 50-50%).

7.6 Eudragit® RL as a substrate for nanocrystal formation

The unexpected formation of INDO and NAP nanocrystals was observed during solubility studies in presence of ERL. The man size of the nanocrystals was smaller than 100nm for both drugs and did not need an additional stabilizer to avoid agglomeration. The proposed mechanism of nanoparticle formation is a combination of equilibrium dissolution, sorption and desorption of drug molecules which shifts into the formation of nanocrystals after desorption from ERL in a saturated solution. Sorption does seem to be a necessary condition to form nanocrystals and a charge interaction between drug and polymer enhances the driving force for this sorption. This is the reason why no CINN nanocrystals were observed.

This novel way of forming stable nanocrystals could be exploited in a production technique or be used for 'in situ' nanocrystal formation, given the time scale of the formation can be shortened. Again here, the full potential of the nanocrystal formation has not been investigated yet. Is sorption a sufficient condition for the nanocrystal formation or is a charge interaction absolutely necessary? If it is, can this approach be inversed as a cationic drug forming nanocrystals with an anionic polymer as a substrate? Can the polymer be chemically modified to speed up the nanocrystal formation? Clearly ERL has never been envisioned or developed as a substrate for nanocrystal formation, so could its structure be improved to better accommodate this nanocrystal formation? Long term stability investigation of the nanocrystals could make or break the ERL substrate method as a viable alternative to current nanosizing methods.

7.7 References

1. Descamps, M.; Willart, J. F., Perspectives on the amorphisation/milling relationship in pharmaceutical materials. *Adv Drug Deliv Rev* **2016**, 100, 51-66.

2. Ayenew, Z.; Paudel, A.; Van den Mooter, G., Can compression induce demixing in amorphous solid dispersions? A case study of naproxen-PVP K25. *Eur J Pharm Biopharm* **2012**, 81 (1), 207-13.

3. Sun, N.; Wei, X.; Wu, B.; Chen, J.; Lu, Y.; Wu, W., Enhanced dissolution of silymarin/polyvinylpyrrolidone solid dispersion pellets prepared by a one-step fluid-bed coating technique. *Powder Tech* **2008**, 182 (1), 72-80.

4. Li, J.; Liu, P.; Liu, J.-P.; Zhang, W.-L.; Yang, J.-K.; Fan, Y.-Q., Novel Tanshinone II A ternary solid dispersion pellets prepared by a single-step technique: In vitro and in vivo evaluation. *Eu J Pharm Biopharm* **2012**, 80 (2), 426-432.

5. Mahmoudi, Z. N.; Upadhye, S. B.; Ferrizzi, D.; Rajabi-Siahboomi, A. R., In vitro characterization of a novel polymeric system for preparation of amorphous solid drug dispersions. *AAPS J* **2014**, 16 (4), 685-97.

6. Augustijns, P.; Brewster, M. E., Supersaturating Drug Delivery Systems: Fast is Not Necessarily Good Enough. *J Pharml Sci***2012**, 101 (1), 7-9.

7. Paudel, A.; Worku, Z. A.; Meeus, J.; Guns, S.; Van den Mooter, G., Manufacturing of solid dispersions of poorly water soluble drugs by spray drying: Formulation and process considerations. *Int J Pharm* **2013**, 453 (1), 253-284.

8. Kovacevic, J.; Ibric, S.; Djuris, J.; Kleinebudde, P., Application of the design of experiments in optimization of drug layering of pellets with an insight into drug polymer interactions. *Int J Pharm* **2016**, 506 (1–2), 312-319.

9. Baird, J. A.; Taylor, L. S., Evaluation of amorphous solid dispersion properties using thermal analysis techniques. *Adv Drug Deliv Rev* **2012**, 64 (5), 396-421.

10. Meeus, J.; Chen, X.; Scurr, D. J.; Ciarnelli, V.; Amssoms, K.; Roberts, C. J.; Davies, M. C.; van Den Mooter, G., Nanoscale surface characterization and miscibility study of a spray-dried injectable polymeric matrix consisting of poly(lactic-co-glycolic acid) and polyvinylpyrrolidone. *J Pharm Sci* **2012**, 101 (9), 3473-85.

11. Meeus, J.; Scurr, D. J.; Amssoms, K.; Davies, M. C.; Roberts, C. J.; Van den Mooter, G., Surface characteristics of spray-dried microspheres consisting of PLGA and PVP: relating the influence of heat and humidity to the thermal characteristics of these polymers. *Mol Pharm* **2013**, 10 (8), 3213-24.

12. Meeus, J.; Scurr, D. J.; Chen, X.; Amssoms, K.; Davies, M. C.; Roberts, C. J.; Van den Mooter, G., Combination of (M)DSC and surface analysis to study the phase behaviour and drug distribution of ternary solid dispersions. *Pharm Res* **2015**, 32 (4), 1407-16.

13. Meeus, J.; Scurr, D. J.; Amssoms, K.; Wuyts, K.; Annaert, P.; Davies, M. C.; Roberts, C. J.; Van den Mooter, G., In vivo evaluation of different formulation strategies for sustained release injectables of a poorly soluble HIV protease inhibitor. *J Control Release* **2015**, 199, 1-9.

14. Meeus, J.; Scurr, D. J.; Appeltans, B.; Amssoms, K.; Annaert, P.; Davies, M. C.; Roberts, C. J.; Van den Mooter, G., Influence of formulation composition and process on the characteristics and in vitro release from PLGA-based sustained release injectables. *Eur J Pharm Biopharm* **2015**, 90, 22-9.

15. Meeus, J.; Lenaerts, M.; Scurr, D. J.; Amssoms, K.; Davies, M. C.; Roberts, C. J.; Van Den Mooter, G., The influence of spray-drying parameters on phase behavior, drug distribution, and in vitro release of injectable microspheres for sustained release. *J Pharm Sci* **2015**, 104 (4), 1451-60.

16. Kranz, H.; Gutsche, S., Evaluation of the drug release patterns and long term stability of aqueous and organic coated pellets by using blends of enteric and gastrointestinal insoluble polymers. *Int J Pharm* **2009**, 380 (1-2), 112-9.

17. Thakral, S.; Thakral, N. K.; Majumdar, D. K., Eudragit: a technology evaluation. *Expert Opin Drug Deliv* **2013**, 10 (1), 131-49.

18. Bodmeier, R.; Guo, X.; Sarabia, R. E.; Skultety, P. F., The influence of buffer species and strength on diltiazem HCl release from beads coated with the aqueous cationic polymer dispersions, Eudragit RS, RL 30D. *Pharm Res* **1996**, 13 (1), 52-6.

19. Narisawa, S.; Nagata, M.; Hirakawa, Y.; Kobayashi, M.; Yoshino, H., An organic acid-induced sigmoidal release system for oral controlled-release preparations. 2. Permeability enhancement of Eudragit RS coating led by the physicochemical interactions with organic acid. *J Pharm Sci* **1996**, 85 (2), 184-8.

Chapter 8: Summary/Samenvatting

SUMMARY

A general introduction concerning the research topics is provided in chapter 1. It provides a brief historical overview of drug discovery and the evolution towards poor solubility in drug candidates. Different enabling strategies are discussed which can address poor solubility and dissolution rate. The amorphous state of drugs is introduced together with its application in solid dispersions. More detailed information about different carriers, manufacturing techniques and characterization methods is provided.

The objectives of this thesis are given in chapter 2. Because of the different challenges still faced in solid dispersion research today, an alternative manufacturing approach was investigated in the form of fluid bed coating, which enables efficient drying and the omission of additional processing steps which can destabilize solid dispersions. Also, alternative formulation approaches are exploited by incorporating controlled release polymers into solid dispersions, either as a rate controlling membrane or as (part of) the solid dispersion carrier.

Chapter 3 describes the search for an mDSC sample preparation method for the analysis of INDO-PVP glass solutions coated onto inert sucrose beads using fluid bed coating. The spherical shape of these beads compromises the contact area with the bottom of a DSC sample pan. Grinding the coated beads and separating the resulting particles into different particle size ranges, resulted in a visible glass transition signal. This glass transition, however, shifted and broadened in particle samples with increasing size range. This phenomenon was confirmed in glass solutions prepared as isolated films by rotary evaporation, with different API's and from different solvent systems. Resulting from TGA analysis, where a difference was made between sub-T_g and above-T_g residual solvent evaporation, it could be concluded that the observed T_g shift and broadening could be ascribed to the differences in residual solvent mass loss from the bulk of the particles and from the surface. Since particles with a smaller size range exhibit a higher surface to mass ratio, they possess more solvent poor surface, as compared to particles with a larger size range, which possess more solvent rich bulk. These findings were confirmed by a correlation between the deviation from the Gordon-Taylor derived T_g and solvent mass loss from the T_g on.

In order to control the release of INDO from coated glass solutions, an additional rate controlling coating was applied on top of the glass solution. This can be done consecutively using fluid bed coating. The resulting multilayer coated beads require a combination of surface and bulk characterization to understand the phase behaviour. Different rate controlling

membranes were applied on INDO-PVP glass solutions comprising two possible controlled release polymers, different amounts of pore former can be added and the rate controlling membrane can be applied from an ethanol solution or an aqueous dispersion. The investigation of these different formulations on the phase behaviour of the drug delivery system is described in chapter 4. Surface and cross-sectional topography was investigated by SEM. Chemical composition and distribution analysis of these surfaces and cross-sections was performed using ToF-SIMS. Polymer miscibility was assessed with mDSC and crystallinity with XRPD. Topography differences observed on the surface or in the cross-sections of the coated beads can be ascribed to polymer miscibility differences or coating from a solution or a dispersion. PVP presence at the surface of pure ERL or EC coatings is the result of a coating contamination. The distributional changes of PVP, when incorporated as a pore former can also be explained by polymer miscibility differences. Limited INDO and PVP migration into the rate controlling membrane can be evidenced from cross-sectional ToF-SIMS analysis. Lastly, XRPD analysis shows that INDO remains amorphous after application of a rate controlling membrane, even if it is coated from an aqueous dispersion.

The influence of the above described formulation changes and rate controlling membrane thickness on the release of INDO was investigated in chapter 5. In addition to this, the role of a charge interaction between drug and controlled release polymer on the release of the former was investigated as well. Diffusion experiments showed a clear influence of the controlled release polymer used, pore former concentration and coating from a solution or suspension on the permeability of rate controlling membranes. These findings could be readily translated to their influence on drug release, pinpointing diffusion through the rate controlling membrane as the rate limiting step for drug release and showing the potential of these diffusion experiments for screening purposes of rate controlling membranes. A charge interaction between INDO and ERL was confirmed by ss-NMR but no clear influence of this interaction on the drug release was observed. The diffusion and release differences through ERL and EC coatings are mainly the result of the higher hydrophilicity of the former.

In chapter 6, the use of ERL as a solid dispersion carrier is investigated, either alone or in combination with the hydrophilic polymer PVP. The solid dispersions are produced by spray drying and analysed with respect to their phase behaviour and in vitro drug dissolution. After in vitro dissolution, precipitates are collected and analysed again with mDSC. ERL solid dispersions with INDO and NAP showed extended supersaturated drug concentrations, when compared to the hydrophilic polymer PVP. Combinations of PVP and ERL as a carrier

combined this extended supersaturation with higher drug concentrations compared to ERL alone. Phase behaviour analysis showed that ERL can form glass solutions and, in the case of INDO, one phase systems are found after 24h dissolution as well. Low drug loadings in combination with ERL as a carrier resulted in slow diffusion out of the carrier making this approach unfavourable. Oversaturated INDO and NAP solutions formed stable nanocrystals in presence of ERL. This formation can be explained by a dynamic interplay of dissolution, sorption and desorption. High sorption levels are necessary for this nanocrystal formation, and a charge interaction between INDO/NAP and ERL provide the necessary driving force for sorption.

An overall discussion on all these findings together with prospects of future studies are provided in chapter 7 of this thesis.

SAMENVATTING

Een algemene introductie over de verschillende deelaspecten van dit onderzoek wordt weergegeven in hoofdstuk 1. Deze introductie behandelt een kort historisch overzicht omtrent de ontdekking van geneesmiddelen en de evolutie naar slechte wateroplosbaarheid van recente geneesmiddelkandidaten. Verscheidene strategieën worden besproken die deze slechte oplosbaarheid en oplossnelheid kunnen verhelpen. Een inleiding over de amorfe toestand van geneesmiddelen wordt gegeven, samen met zijn mogelijke toepassing in vaste dispersies. Vervolgens wordt er ook verder ingegaan op de verschillende carriers voor vaste dispersies, productietechnieken en mogelijkheden tot karakterizering.

De doelstellingen van deze thesis worden besproken in hoofdstuk 2. Daar het onderzoek naar vaste dispersies tegenwoordig nog te maken heeft met verschillende uitdagingen, wordt een alternatieve productietechniek voorgesteld, namelijk wervelbed coating. Deze methode staat een efficiënte droging van de vaste dispersies toe en hoeft geen bijkomende behandelingsstappen te ondergaan die zouden kunnen leiden tot instabiliteit van deze vaste dispersies. Naast een alternatieve productiemethode wordt ook een alternatieve formuleringsstrategie onderzocht, die gebruik maakt van polymeren gebruikt voor gecontroleerde afgifte. Deze polymeren worden aangewend als een regulerend membraan of als (een deel) van de vaste dispersie carrier.

Hoofdstuk 3 beschrijft de zoektocht naar een geschikte mDSC staalvoorbereidingsmethode voor de analyse van INDO-PVP glasoplossingen, gecoat op inerte sucrose pellets door middel van wervelbed coating. De sferische vorm van deze pellets zorgt voor een zeer beperkt contactoppervlak met de platte bodem van DSC monsterhouders. Het verbrijzelen van deze gecoate pellets en scheiding naargelang partikelgrootte zorgde voor een zichtbaar glastransitiesignaal. De glastransitie verschoof en verbreedde echter bij partikels met een grotere partikelgrootte. Dit fenomeen werd bevestigd in geïsoleerde glasoplossingsfilmen, gemaakt door rotavaporisatie, met verschillende geneesmiddelen en verschillende solventen of mengsels van solventen. TGA maakte het mogelijk om een onderscheid te maken tussen solventverdamping onder en boven de Tg van de vaste dispersie. Deze aanpak leidde uiteindelijk tot de conclusie dat de glastransitie verschuiving en verbreding terug te brengen is tot verschillen in solventverdamping aan het oppervlak of vanuit de bulk van de partikels. Kleinere partikels hebben meer oppervlak per massa en bezitten dus meer solventarm oppervlak. Grotere partikels daarentegen bezitten dan weer meer solventrijke bulk. Deze

bevindingen werden bevestigd door een correlatie tussen de afwijking van de Tg, bepaald door de Gordon-Taylor vergelijking en het massaverlies door solventverdamping vanaf de glastransitie.

Om een controle te hebben over de afgifte van INDO werd een bijkomende coatinglaag over deze glasoplossingen aangebracht. Deze handeling kan worden uitgevoerd direct na het coaten van de glasoplossing in hetzelfde coating toestel. Om het fasegedrag van deze veellagige coating ten volle te kunnen onderzoeken is een combinatie nodig van oppervlakte- en bulkkarakterizering. Verschillende van deze gecontroleerde afgifte membranen werden aangebracht op de INDO-PVP glasoplossing met verschillende polymeren voor gecontroleerde afgifte, verschillende concentraties aan porievormer en deze membranen kunnen worden gecoat uit een ethanol oplossing of uit een waterige dispersie. Het onderzoek naar de invloed van deze formuleringsmogelijkheden op het fasegedrag van deze systemen wordt beschreven in hoofdstuk 4. De topografie van het oppervlak en de dwarsdoorsnedes wordt onderzocht met SEM. De chemische samenstelling en verdeling op het oppervlak en langs de dwarsdoorsnedes wordt geanalyseerd door middel van ToF-SIMS. Tenslotte wordt polymeermengbaarheid onderzocht met mDSC en de aanwezigheid van kristallen met XRPD. Topografieverschillen konden worden verklaard door verschillen in polymeermengbaarheid of door het feit dat er werd gecoat vanuit een oplossing of dispersie. De aanwezigheid van PVP aan het oppervlak van coatings die enkel zouden mogen bestaan uit ERL of EC was het resultaat van een coating contaminatie. De verdeling van PVP, wanneer toegevoegd als porievormer, aan het oppervlak was eens te meer te wijten aan polymeermengbaarheidsverschillen. Er werd ook een zeer beperkte migratie van INDO en PVP vastgesteld in de coatinglaag voor gecontroleerde afgifte door analyse van de dwarsdoorsneden. De analyse door middel van XRPD gaf aan dat INDO volledig amorf blijft na toevoeging van een gecontroleerde vrijgave membraan, zelfs wanneer deze laatste wordt aangebracht vanuit een waterige dispersie.

De invloed van voorgenoemde formuleringsvariaties, en de invloed van de dikte van de coatinglaag op de vrijgave van INDO wordt onderzocht in hoofdstuk 5. Ook wordt de rol nagegaan van een ladingsinteractie tussen geneesmiddel en gecontroleerde vrijgave polymeer op de vrijgave van het geneesmiddel. Diffusie experimenten duiden op een duidelijke invloed van het gebruikte gecontroleerde vrijgave polymeer, de porievormer concentratie en het coaten vanuit oplossing of dispersie op de permeabiliteit van gecontroleerde vrijgave membranen. Deze invloeden kunnen makkelijk worden doorgetrokken naar de geneesmiddelvrijgave, wat wijst op het feit dat diffusie de snelheidsbepalende stap is in de

vrijgave van het geneesmiddel, en dat deze diffusietesten potentieel hebben in screeningtesten van gecontroleerde vrijgave membranen. Een ladingsinteractie tussen INDO en ERL werd bevestigd door middel van ss-NMR, maar er werd geen duidelijke invloed van deze interactie gevonden op de vrijzetting van het geneesmiddel. Het grootste verschil tussen ERL en EC coatings ligt waarschijnlijk in het feit dat deze eerste hydrofieler is dan de tweede.

In hoofdstuk 6 werd het gebruik van ERL als carrier in vaste dispersies nagegaan. Ofwel alleen of in combinatie met het hydrofiel polymeer PVP. Vaste dispersies werden geproduceerd door middel van sproeidrogen en geanalyseerd op hun fasegedrag en in vitro dissolutie. Na de dissolutie wordt de gevormde neerslag in het dissolutiemedium verzameld en opnieuw geanalyseerd met mDSC. Vaste dispersies, bestaande uit ERL en INDO of NAP vertonen verlengde supersaturatie in vergelijking met PVP als carrier. Wanneer ERL en PVP gecombineerd werden als carrier werden hogere geneesmiddelconcentraties bekomen (t.o.v. ERL alleen). Deze verhoogde concentraties konden gedurende langere tijd worden aangehouden. Analyse van het fasegedrag toont aan dat ERL glasoplossingen kan vormen en dat, in geval van combinatie met INDO, een éénfasig systeem nog steeds wordt gevormd na dissolutie gedurende 24 uur. Lage geneesmiddelconcentraties in combinatie met ERL zorgen voor een trage diffusie uit de carrier en zijn bij deze toepassing dan ook ongewenst. Een interessante en eerder onverwachte bevinding was dat oversaturatie van INDO of NAP oplossingen in combinatie met de aanwezigheid van ERL leidt tot vorming van stabiele nanokristallen wat kan worden verklaard door een dynamische wisselwerking van dissolutie, sorptie en desorptie. Hoge sorptie is nodig voor de vorming van nanokristallen en een ladingsinteractie tussen INDO/NAP en ERL kan zulke sorptie in de hand werken.

Een algemene discussie over al deze bevindingen, samen met mogelijkheden voor toekomstig onderzoek worden besproken in hoofdstuk 7 van deze thesis.

Chapter 9: Supplementary Data

SUPPLEMENTARY DATA CHAPTER 4

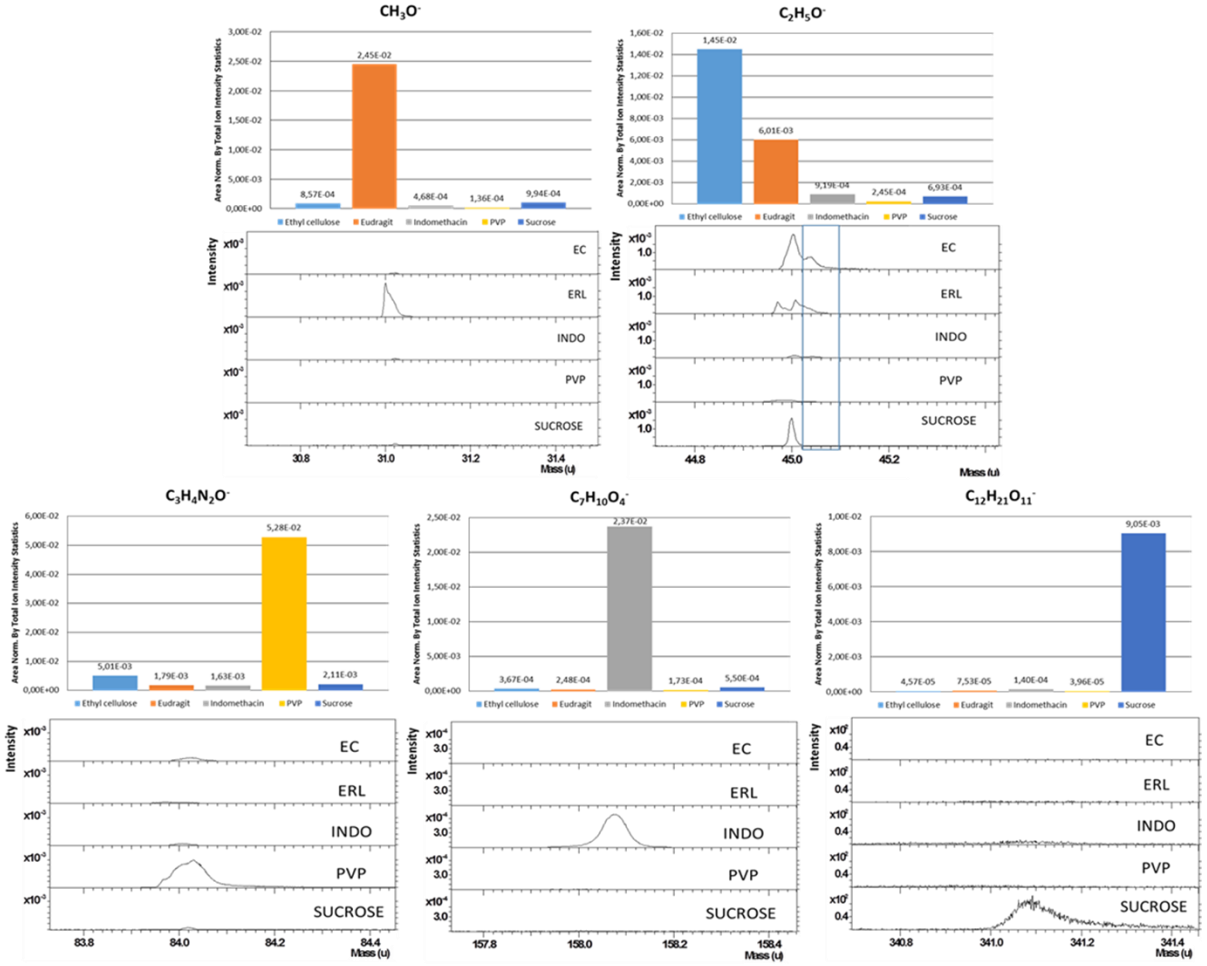

Figure A: Ion intensities and spectra of the component selective ion markers opposed to the other compound controls.

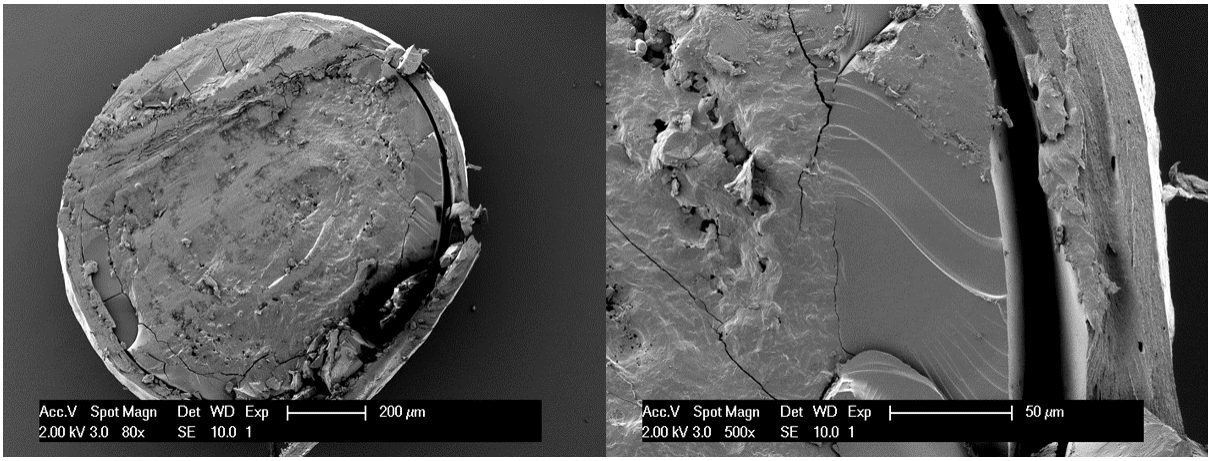

Figure B: SEM micrograph of a bead with INDO-PVP glass solution and EC-TEC top coating (left) and a detailed view on the coating layers (right).

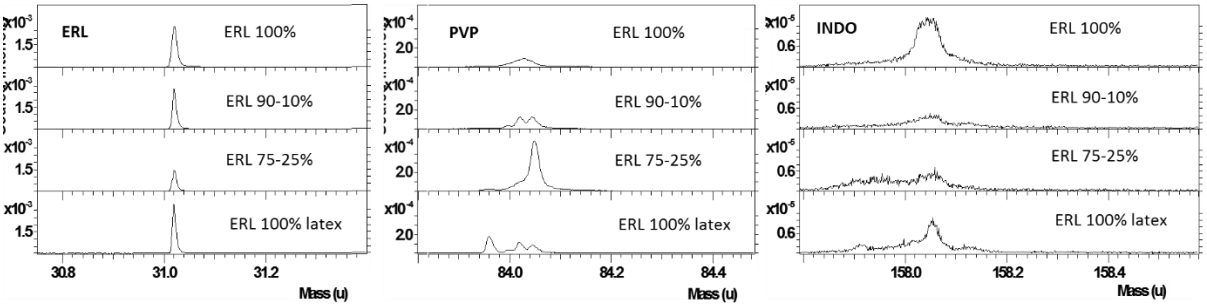

Figure C: ToF-SIMS ion spectra of ERL based outer layer coatings at the marker ion masses of ERL, PVP and INDO

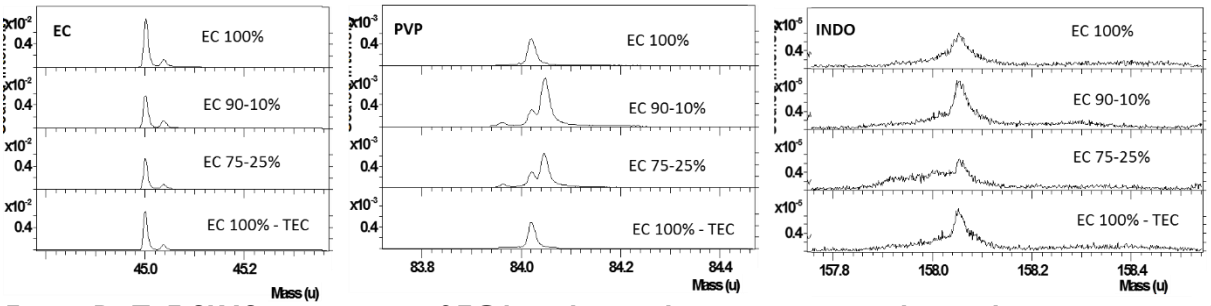

Figure D: ToF-SIMS ion spectra of EC based outer layer coatings at the marker ion masses of EC, PVP and INDO

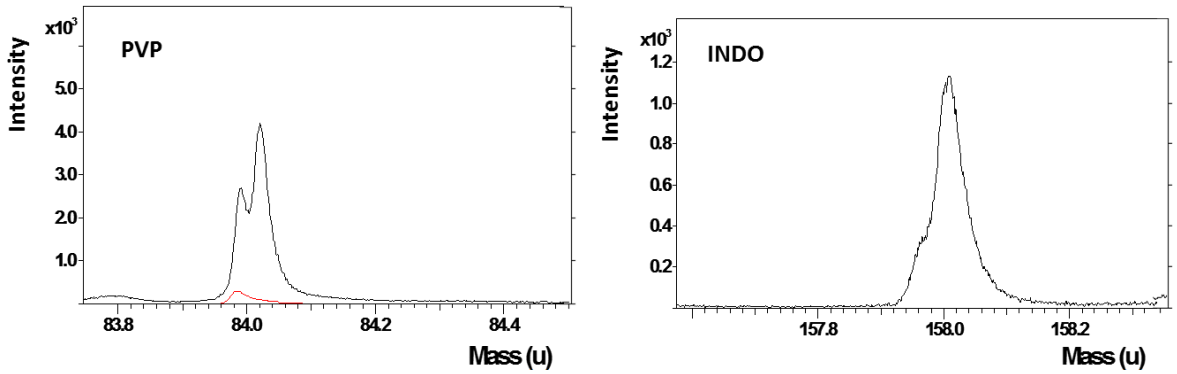

Figure E: ToF-SIMS ion spectra of INDO-PVP glass solution coating cross-sections at the marker ion masses of PVP, INDO and sucrose.

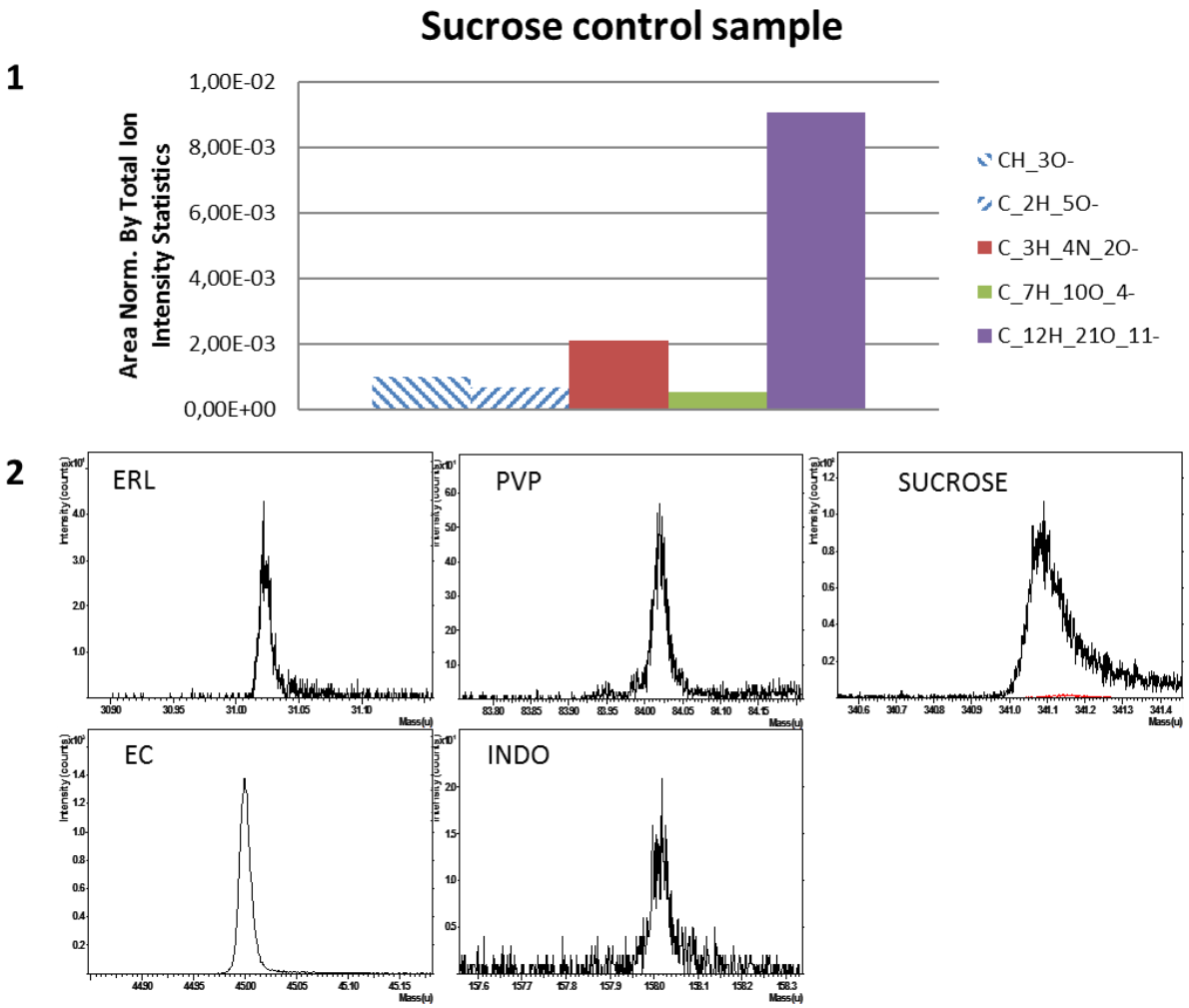

Figure F: Secondary ion spectra (1) and intensities (2) for the sucrose control sample. EC and ERL marker intensity is represented in striped blue bars, PVP marker intensity is a red bar, INDO marker intensity is a green bar and sucrose marker intensity is a purple bar. Ion intensities area is normalized by total ion statistics.

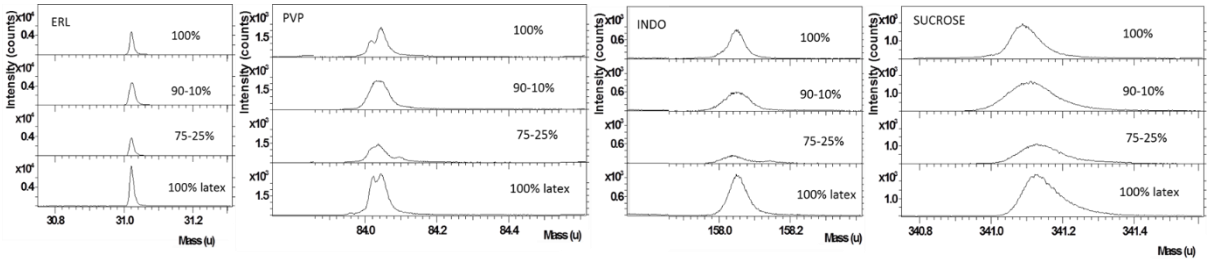

Figure G: ToF-SIMS ion spectra of ERL based outer layer coating cross-sections at the marker ion masses of ERL, PVP, INDO and Sucrose

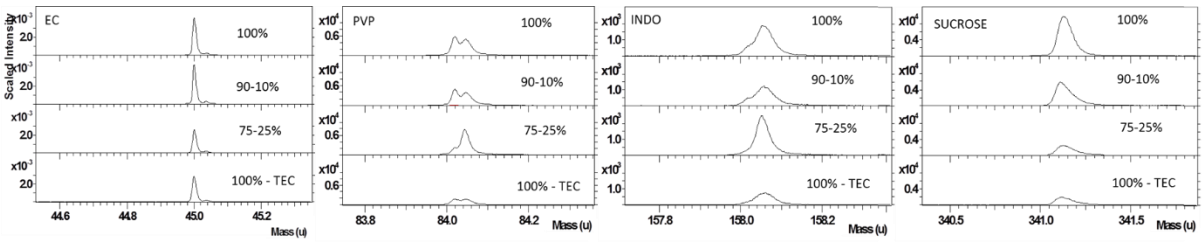

Figure H: ToF-SIMS ion spectra of EC based outer layer coating cross-sections at the marker ion masses of EC, PVP, INDO and Sucrose

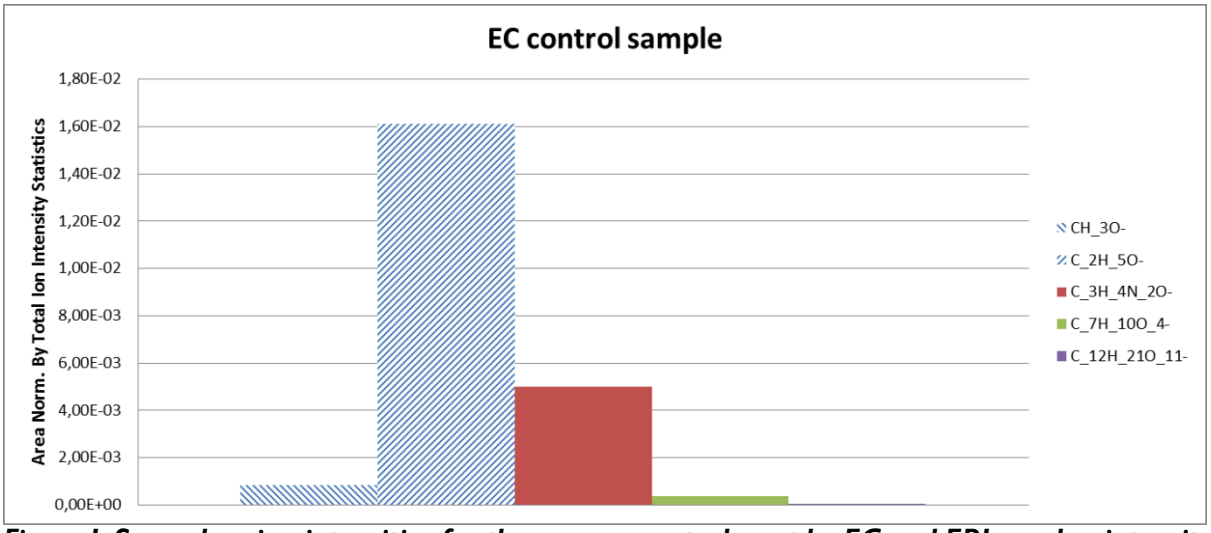

Figure I: Secondary ion intensities for the sucrose control sample. EC and ERL marker intensity is represented in striped blue bars, PVP marker intensity is a red bar, INDO marker intensity is a green bar and sucrose marker intensity is a purple bar. Ion intensities area is normalized by total ion statistics.

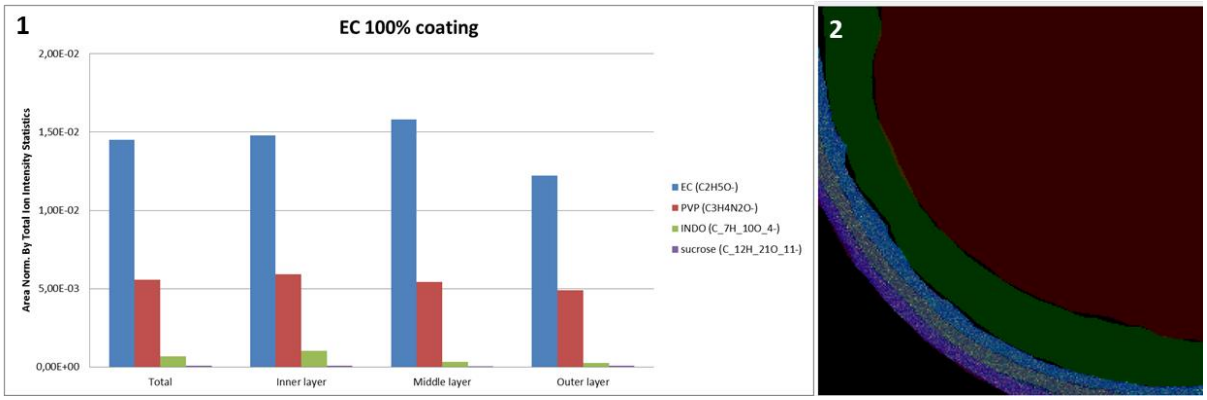

Figure J: Secondary ion intensities (1) of the EC marker intensity is represented in blue bars, PVP marker intensity in red bars, INDO marker intensity in green bars and sucrose marker intensity in purple bars. Ion intensities area is normalized by total ion statistics. The region of interest creation (2), the purple colored region represents the outer layer of the EC 100% coating, the yellow colored region the middle layer and the blue colored region the inner layer.

SUPPLEMENTARY DATA CHAPTER 6

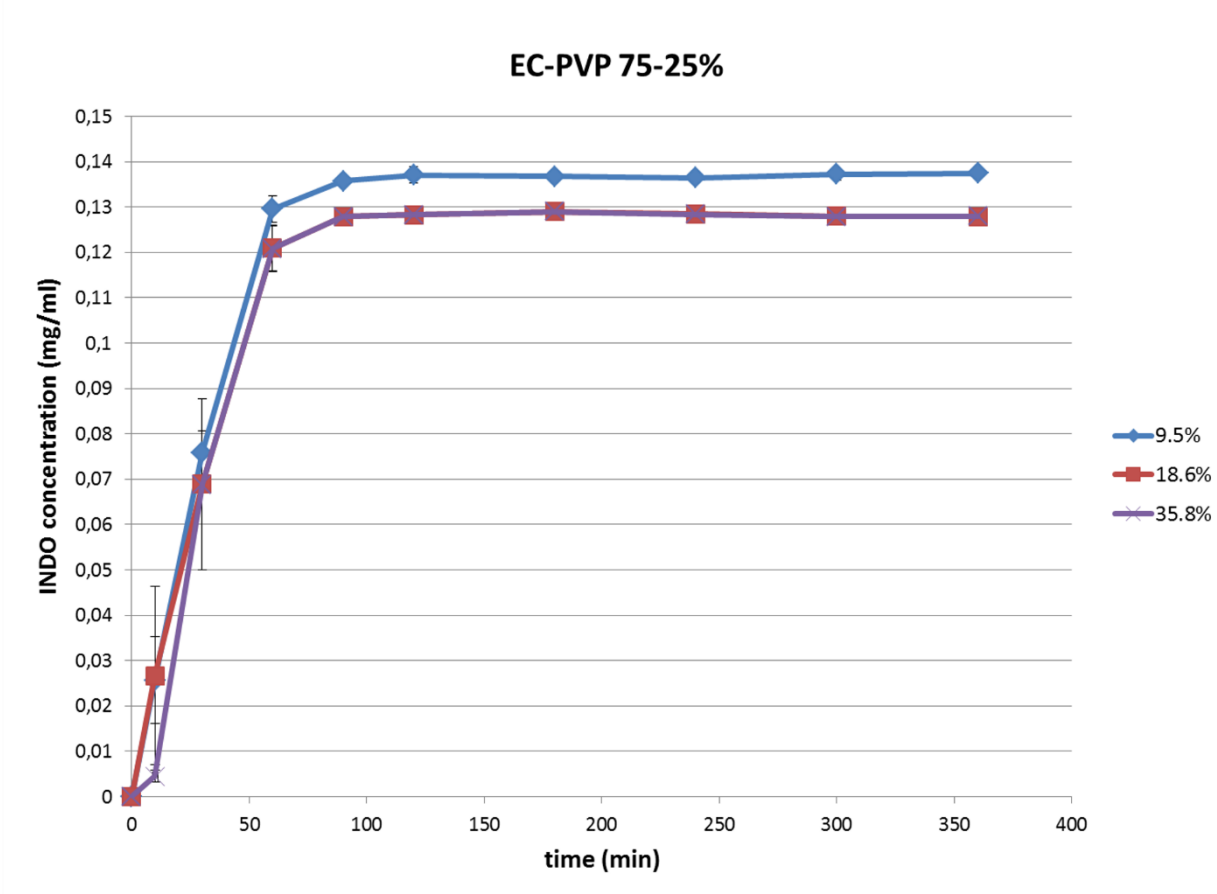

Figure A: . INDO concentration in function of time for INDO-PVP 30-70% (w/w) glass solution and an EC-PVP 75-25% (w/w) rate controlling membrane. Different coating levels were tested: 9.5% (blue), 18.6% (red) and 35.8% (purple).

SUPPLEMENTARY DATA CHAPTER 6

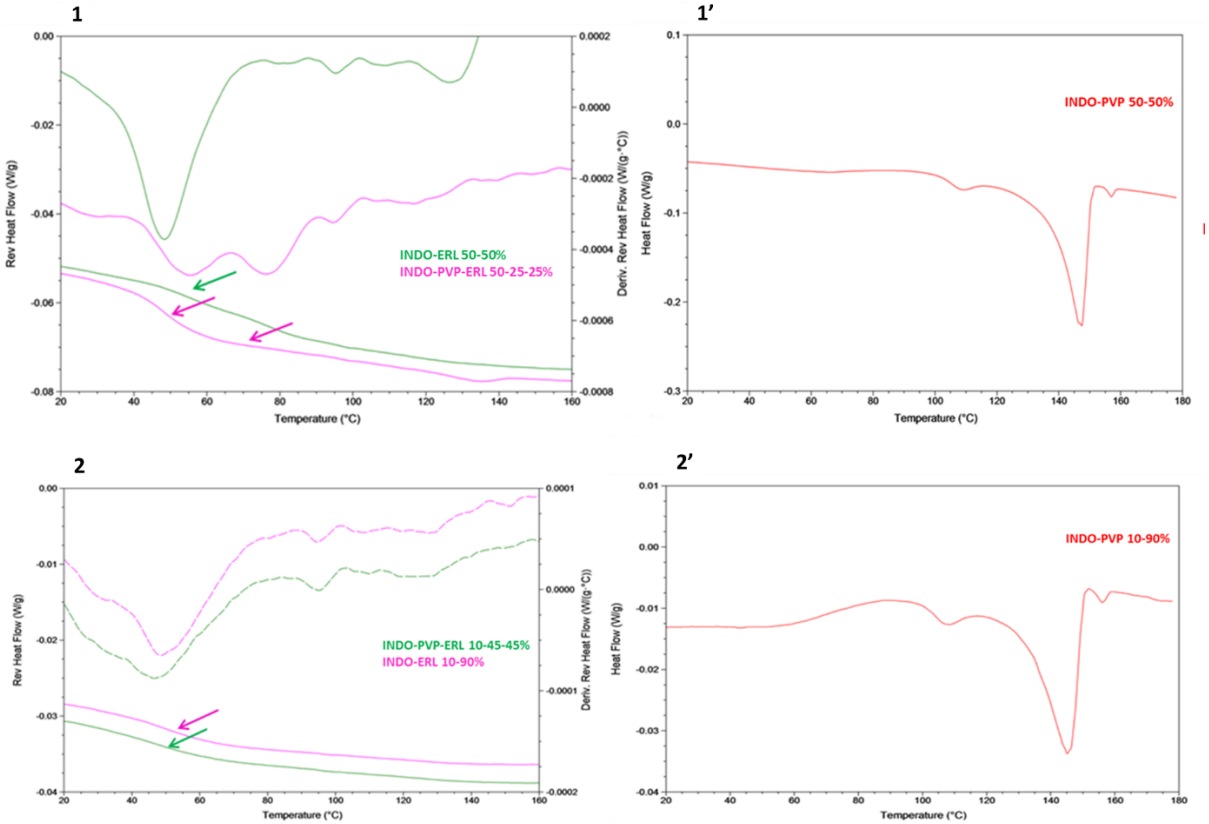

Figure A: mDSC thermograms of dissolution precipitates of INDO formulations with different polymers (or combinations) and INDO contents of 50% (1, 1') and 10% (2, 2'). In panel 1, INDO-PVP-ERL 50-25-25% is represented in green and INDO-ERL 50-50% in pink

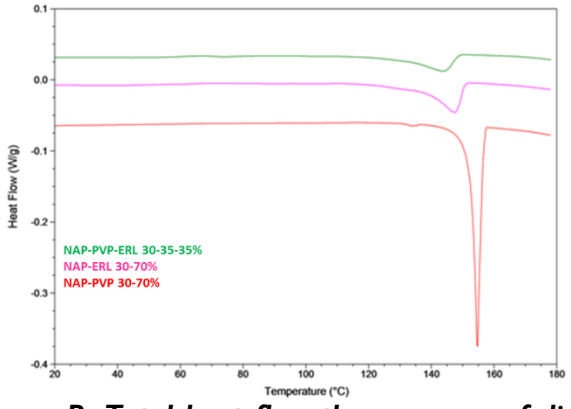

Figure B: Total heat flow thermograms of dissolution precipitates of 30% NAP formulations with different polymers (or combinations). NAP-PVP-ERL 30-35-35% is represented in green, NAP-ERL 30-70% in pink and NAP-PVP 30-70% in red.

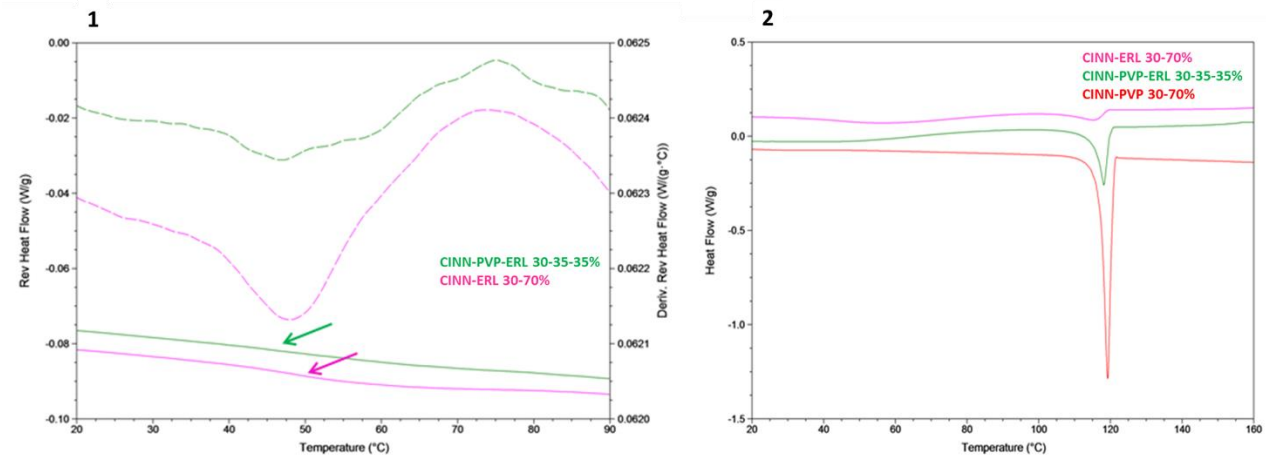

Figure C: mDSC thermograms of dissolution precipitates of 30% NAP formulations with different polymers (or combinations). In panel 1 CINN-PVP-ERL 30-35-35% is represented in green and CINN-ERL 30-70% in pink. Full lines represent the reversing heat flow

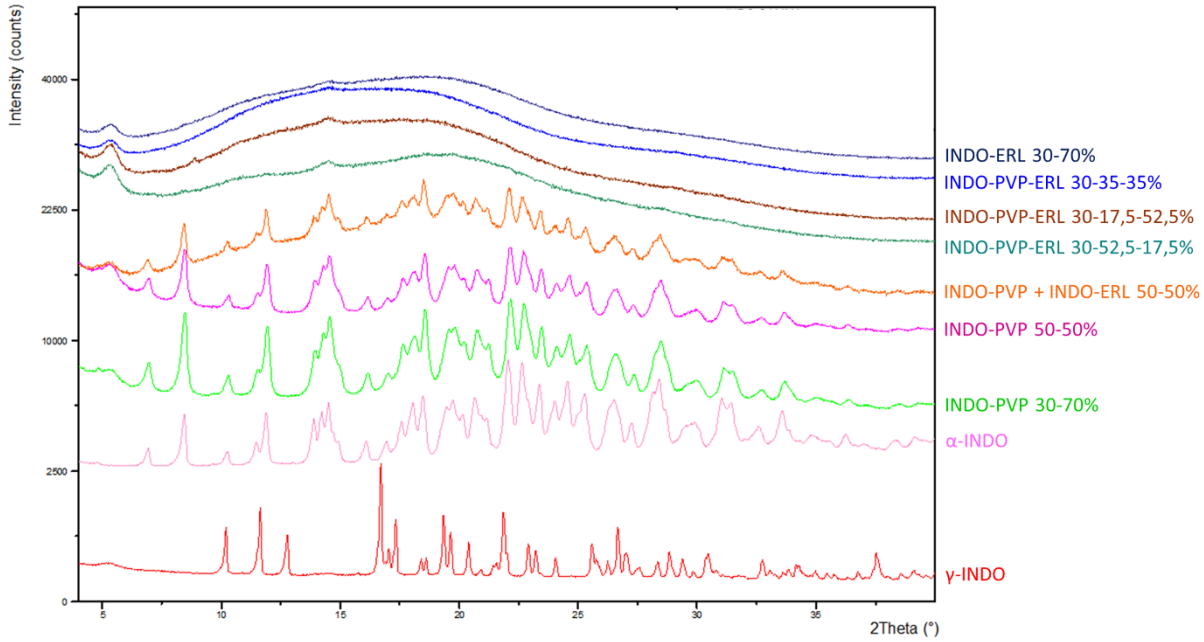

Figure D: XRPD diffractogram of γ -INDO (red) and α -INDO (light pink) together with dissolution precipitates of INDO formulations with varying drug loadings and polymer compositions. INDO-PVP 30-70% diffractogram is in green, INDO-PVP 50-50% in dark pink, a physical mixture of INDO-PVP and INDO-ERL 50-50% in orange, INDO-PVP-ERL 30-52.5-17.5% in teal, INDO-PVP-ERL 30-17.5-52.5% in brown, INDO-PVP-ERL 30-35-35% in blue and INDO-ERL 30-70% in dark blue

Curriculum Vitae

DEREYMAKER ASWIN

Education

2013-2017:Phd in Pharmaceutical Sciences, Katholieke Universiteit Leuven, Belgium

2009-2011: MSc in Drug Development, Katholieke Universiteit Leuven, Belgium

2004-2010: BSc in Pharmaceutical Sciences, Katholieke Universiteit Leuven, Belgium

Projects

PhD thesis: **"Broadening the scope of amorphous solid dispersions: alternative manufacturing and formulation approaches."** Promotor: Prof. dr. Guy Van den Mooter, co-promotor: Prof. dr. Johan Martens., Drug delivery and disposition, KU Leuven, Belgium

Master thesis: ***'Influence of the manufacturing process of solid dispersions of miconazole and poly(ethyleneglycol-g-vinylalcohol) on the phase behavior: comparison between spray-drying and hot-melt extrusion'*** Promotor: Prof. dr. Guy Van den Mooter, Supervisor: Dr. Sandra Guns Drug delivery and disposition, KU Leuven Belgium

Professional Experience

2/2013 – 2/2017: PhD in Pharmaceutical Sciences

2/2012 – 2/2013: Research Project 'Uterine controlled release formulation development' supervisor: Prof. dr. Guy Van den Mooter, Denali Medical II (Minnesota, USA) in collaboration with Drug Delivery and Disposition, KU Leuven, Belgium

7/ 2011- 9/ 2011: Pharmacy Rotation Placement, Multipharma group

Collaborations

August 2015 - …: **Use of surface analysis techniques (Atomic Force Microscopy and Time-of-Flight Secondary Ion Mass Spectroscopy),** Dr. David J Scurr and Prof. dr. Clive J Roberts, Laboratory of Biophysics and Surface Analysis, School of Pharmacy, The University of Nottingham, United Kingdom

Scientific Publications

- Guns S, Dereymaker A, Kayaert P, Mathot V, Martens J, Van den Mooter G 2011. Comparison Between Hot-Melt Extrusion and Spray-Drying for Manufacturing Solid Dispersions of the Graft Copolymer of Ethylene Glycol and Vinylalcohol *Pharm Res* **28**: 673-682

- Dereymaker A, Van den Mooter G 2015. The Peculiar Behavior of the Glass Transition Temperature of Amorphous Drug–Polymer Films Coated on Inert Sugar Spheres. *J Pharm Sci* **104**: 1759-1766

- Dereymaker A, Scurr DJ, Roberts CJ, Van den Mooter G 2017. Controlling The Release of Indomethacin from Glass Solutions Layered with a Rate Controlling Membrane Using Fluid-Bed Processing. PART 1: Surface and cross-sectional chemical analysis. *Mol Pharm* (manuscript submitted)

- Dereymaker A, Pelgrims J, Engelen F, Adriaensens P, Van den Mooter G 2017. Controlling The Release of Indomethacin from Glass Solutions Layered with a Rate Controlling Membrane Using Fluid-Bed Processing. PART 2: The influence of formulation parameters on drug release. *Mol Pharm* (manuscript submitted)

- Dereymaker A, Cinghia G, Van den Mooter G 2017. Eudragit RL as a stabilizer for supersaturation and a substrate for nanocrystal formation. *Eu J Pharm Biopharm* (manuscript accepted for publication)
- Riekes MK, Dereymaker A, Berben P, Augustijns P, Stulzer HK, Van den Mooter G 2017. Development of enteric-coated fixed dose combinations of amorphous solid dispersions of ezetimibe and lovastatin: Investigation of formulation and process parameters. *Int J Pharm* **520:** 49-58

Oral presentations

- Surface and cross-sectional phase analysis of coated controlled release glass solutions: a ToF-SIMS approach. 19th Forum der Farmaceutische Wetenschappen Brussels (Belgium) October 17-18 2016

- Surface and cross-sectional phase analysis of coated controlled release glass solutions: a ToF-SIMS approach. 10th Annual Symposium of Pharmaceutical Solid State Research Cluster (PSSRC), Copenhagen (Denmark), July 6-8 2016

- Controlling the drug release of indomethacin glass solutions, prepared by fluid bed coating. 9th Annual Symposium of Pharmaceutical Solid State Research Cluster (PSSRC), Ghent (Belgium), September 16-18 2015

- Development of a controlled release formulation from glass solutions by fluid-bed coating. 18th Forum der Farmaceutische Wetenschappen Blankenberge (Belgium) May 28-29 2015

- The Peculiar Behavior of the Glass Transition Temperature of Amorphous Drug–Polymer Films Coated on Inert Sugar Spheres. TA Instruments Users Meeting and Symposium 2015, Bergen op Zoom (The Netherlands), May 20-22 2015

- Particle size dependent glass transition in pharmaceutical glass solution films and coatings. 8th Annual Symposium of Pharmaceutical Solid State Research Cluster (PSSRC), Ljubljana/Portoroz (Slovenia), September 16-18 2014

Poster presentations

- Dereymaker A, Engelen F, Van den Mooter G. (2015) Controlling the drug release of indomethacin glass solutions, prepared by fluid bed coating. Meeting of the Belgian-Dutch biopharmaceutical society, Leuven (Belgium), November 23
- Dereymaker A, Engelen F, Van den Mooter G. (2015) Controlling the drug release of indomethacin glass solutions, prepared by fluid bed coating. 2015 AAPS Annual Meeting and Exposition, Orlando, Florida (United States), October 25-29
- Dereymaker A, Van den Mooter G. (2015) Particle size dependent glass transition in pharmaceutical glass solution films and coatings. ULLA Summer School, Chatenay-Malabry, France July 4-9
- Dereymaker A, Van den Mooter G. (2014) Particle size dependent glass transition in pharmaceutical glass solution films and coatings. 2016 AAPS Annual Meeting and Exposition, San Diego, California (United States), October 2-4
- Dereymaker A, Van den Mooter G. (2014) Particle size dependent glass transition in pharmaceutical glass solution films and coatings. 11th European Symposium on Thermal Analysis and Calorimetry (ESTAC 11), Espoo (Finland), August 17-21

Meetings

- ULLA Summer School, Chatenay-Malabry (France) July 4-9 2015
- APGI 2nd Coating Workshop, Lille (France), April 17 2013
- Hüttlin seminar : Coating – fine particles, Granules, Pellets, Tablets, Schopfheim (Germany), June 18-20 2013

Undergraduate and graduate student supervision

- September 2013 - January 2014: Shari Kiekens (Influence Of Process Parameters On The Phase Behavior Of Glass Solutions Of Naproxen And PVP K 25 Prepared By Fluid Bed Coating)
- February 2015 - June 2015: Frederik Engelen (Development and characterization of a controlled release system of indomethacin from amorphous solid dispersions)
- September 2015 - December 2015: Jirka Pelgrims (Investigation of a controlled release formulation of indomethacin glass solutions, prepared with spray drying or fluid bed coating)
- March 2016 - August 2016: Giulia Cinghia (Supersaturation of glass solutions of poorly soluble drugs containing polymer mixtures of Eudragit RL and PVP K25)